UNIVERSITY OF LJUBLJANA
BIOTECHNICAL FACULTY

Marijan BAJIĆ

DEVELOPMENT OF MINIATURIZED PACKED BED REACTORS WITH IMMOBILIZED ENZYMES FOR BIOCATALYTIC PROCESSES

DOCTORAL DISSERTATION

Ljubljana, 2017

UNIVERSITY OF LJUBLJANA
BIOTECHNICAL FACULTY

Marijan BAJIĆ

DEVELOPMENT OF MINIATURIZED PACKED BED REACTORS WITH IMMOBILIZED ENZYMES FOR BIOCATALYTIC PROCESSES

DOCTORAL DISSERTATION

RAZVOJ MINIATURIZIRANIH REAKTORJEV S STRNJENIM SLOJEM ZA BIOKATALITSKE PROCESE Z IMOBILIZIRANIMI ENCIMI

DOKTORSKA DISERTACIJA

Ljubljana, 2017

The experimental work was performed within the Microprocess Engineering Research Group, established at the Chair of Chemical Process, Environmental and Biochemical Engineering of the Faculty of Chemistry and Chemical Technology, University of Ljubljana.

Based on the Statute of University of Ljubljana and the decision made by Senate of Biotechnical Faculty at the 22nd session of the Commission for the Doctoral Studies of University of Ljubljana held on November 10th 2015, it was confirmed that the PhD candidate Marijan BAJIĆ fulfills conditions for the matriculation at the Interdisciplinary doctoral study program of Biosciences, scientific field of Biotechnology. The same document designated Prof. Dr. Polona ŽNIDARŠIČ PLAZL as the supervisor of the doctoral dissertation.

The Senate of Biotechnical Faculty at the 16th session held on April 24th 2017 appointed the following commission for the assessment and defense of the doctoral dissertation:

President: Prof. Dr. Ines MANDIĆ-MULEC
University of Ljubljana, Biotechnical Faculty,
Department of Food Science and Technology

Member: Assoc. Prof. Dr. Aleš PODGORNIK
University of Ljubljana, Faculty of Chemistry and Chemical Technology,
Department of Chemical Engineering and Technical Safety

Member: Assoc. Prof. Dr. Bruno ZELIĆ
University of Zagreb, Faculty of Chemical Engineering and Technology,
Department of Reaction Engineering and Catalysis

Date of defense: June 16th 2017

I, the undersigned doctoral candidate declare that this doctoral dissertation is a result of my own research work and that the electronic and printed versions are identical. I am hereby non-paidly, non-exclusively, and spatially and timelessly unlimitedly transferring to University the right to store this authorial work in electronic version and to reproduce it, and the right to enable it publicly accessible on the web pages of Digital Library of Biotechnical Faculty.

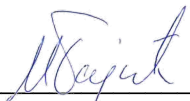

Marijan Bajić

KEY WORDS DOCUMENTATION

DN Dd
DC UDC 544.473:577.15:602.44(043.3)
CX biocatalysis/miniaturization/enzymes/immobilization/packed bed/scale-up
AU BAJIĆ, Marijan
AA ŽNIDARŠIČ PLAZL, Polona (supervisor)
PP SI-1000 Ljubljana, Jamnikarjeva 101
PB University of Ljubljana, Biotechnical Faculty, Interdisciplinary Doctoral Programme in Biosciences, Scientific field Biotechnology
PY 2017
TI DEVELOPMENT OF MINIATURIZED PACKED BED REACTORS WITH IMMOBILIZED ENZYMES FOR BIOCATALYTIC PROCESSES
DT Doctoral dissertation
NO XXIV, 147, [9] p., 14 tab., 55 fig., 2 ann., 453 ref.
LA en
AL en/sl

AB Miniaturized packed bed reactors applying LentiKats® and Novozym® 435 with immobilized ω-transaminase and *Candida antarctica* lipase B, respectively, were developed as tools for a continuous enzymatic process establishment. A systematic increase in reactors capacity was achieved by increasing the individual dimensions of rectangular and hexagonal channels, where lens-shaped poly(vinyl alcohol) and spherical acrylic resin particles were either uniformly or randomly distributed. Evaluation of reactors with volumes ranging from a few µL up to several mL revealed the benefits of using a single layer of LentiKats®, or up to two layers of Novozym® 435, packed between two plates forming a wide channel with triangular inlet and outlet parts containing pillars, where favorable flow conditions resulted in a good biocatalyst accessibility and high production rates. The reactors were also used to establish a temperature dependence of the immobilized ω-transaminase and lipase yielding 55 and 75 °C as the optimal temperatures, respectively. High operational stabilities at 24 °C were achieved, where more than 80% and 40% of the initial productivities were retained after 21 and 53 days in the reactors with ω-transaminase and lipase, respectively. Pressure drops of up to 88 kPa were measured at flow rates up to 1,800 µL min^{-1} within the tested microliter and milliliter-scale reactors. Moreover, measurements of the residence time distribution in miniaturized reactors with rectangular channels utilizing Novozym® 435 using an integrated glucose biosensor revealed small deviations from ideal plug flow. We might conclude that miniaturized reactors developed in this study were very efficient for the selected biotransformations. In addition, a microfluidic-based method was used for the immobilization of *E. coli* cells overexpressing ω-transaminase in alginate microparticles, thereby obtaining a biocatalyst with a high activity. Thus we have developed new approach for development of immobilized biocatalysts potentially applicable in miniaturized packed bed reactors.

KLJUČNA DOKUMENTACIJSKA INFORMACIJA

ŠD Dd
DK UDK 544.473:577.15:602.44(043.3)
KG biokataliza/miniaturizacija/encimi/imobilizacija/strnjen sloj/povečevanje naprav
AV BAJIĆ, Marijan
SA ŽNIDARŠIČ PLAZL, Polona (mentorica)
KZ SI-1000 Ljubljana, Jamnikarjeva 101
ZA Univerza v Ljubljani, Biotehniška fakulteta, Interdisciplinarni doktorski študij Bioznanosti, znanstveno področje Biotehnologija
LI 2017
IN RAZVOJ MINIATURIZIRANIH REAKTORJEV S STRNJENIM SLOJEM ZA BIOKATALITSKE PROCESE Z IMOBILIZIRANIMI ENCIMI
TD Doktorska disertacija
OP XXIV, 147, [9] str., 14 pregl., 55 sl., 2 pril., 453 vir.
IJ en
JI en/sl
AI Kot orodje za postavitev kontinuirnih encimskih procesov smo razvili miniaturizirane reaktorje s strnjenim slojem, ki smo jih preučevali na osnovi dveh encimskih pripravkov, LentiKats® z imobiliziranimi ω-transaminazami in Novozym® 435 z imobiliziranimi lipazami B iz kvasovke *Candida antarctica*. S sistematičnim povečanjem posameznih dimenzij pravokotnih in šesterokotnih kanalov smo dosegli povečevanje zmogljivosti reaktorjev, pri čemer smo delce enakomerno ali naključno porazdelili v kanale. Vrednotenje reaktorjev prostornin od nekaj μL do več mL je izkazalo prednost uporabe ene plasti pripravka LentiKats® ter dveh plasti pripravka Novozym® 435, polnjenih med dvema ploščama, ki tvorita širok kanal z vstopnim in izstopnim trikotnim delom, s stebri, s čimer smo zaradi ustreznega tokovnega režima dosegli dobro dostopnost biokatalizatorja in posledično relativno visoke produkcijske hitrosti. Reaktorje smo uporabili tudi za oceno temperaturne odvisnosti imobilizirane ω-transaminaze in lipaze, pri čemer se je za prvo kot optimalna temperatura izkazala 55 °C in za drugo 75 °C. Dosegli smo tudi visoko obratovalno stabilnost pri 24 °C, ki je znašala pri LentiKats® več kot 80 % začetne produktivnosti po 21 dneh, pri Novozym® 435 pa je znašala 40 % začetne produktivnosti po 53 dneh. V razvitih mikro- in mezoreaktorjih smo pri pretokih do 1800 μL min^{-1} izmerili padce tlaka do 88 kPa. Vrednotenje porazdelitve zadrževalnih časov na osnovi integriranega glukoznega senzorja v miniaturiziranih reaktorjih s pravokotnimi kanali, polnjenimi z Novozym® 435, je izkazalo majhna odstopanja od idealnega čepastega toka. Tako lahko zaključimo, da so bili miniaturizirani reaktorji, razviti v tej študiji, zelo učinkoviti za izbrani biotransformaciji. Poleg tega smo z metodo, ki smo jo razvili na osnovi uporabe mikrofluidike, uspešno imobilizirali celice *E. coli* z izraženo ω-transaminazo v alginatne mikrodelce, pri čemer je pridobljeni biokatalizator izkazal visoko aktivnost. Na ta način smo razvili nov pristop k pripravi imobiliziranih biokatalizatorjev za nadaljnjo uporabo v miniaturiziranih reaktorjih s strnjemim slojem.

TABLE OF CONTENTS

LISTS OF TABLES

LIST OF FIGURES

LIST OF ANNEXES

GLOSSARY

LentiKats®	Porous, lens-shaped poly(vinyl alcohol) hydrogel particles containing entrapped ω-transaminases.
Novozym® 435	Commercially available biocatalyst preparation with *Candida antarctica* lipase B immobilized on a hydrophobic macroporous acrylate-based polymeric resin by physical adsorption.
Systematic scale-up	Increasing the characteristic dimension of the reactor to achieve increased internal volume and therefore higher throughput, concomitantly keeping other two dimensions constant.

NOMENCLATURE

Latin symbols

A	cross-sectional area of the tube/channel [m^2]
a	radius of the LentiKats® circular base [mm]
Bo	*Bond number* [–]
BPN	biocatalyst productivity number [$\mu mol_{ACP}\ g_{ATA\text{-}wt}^{-1}$; $mmol_{BB}\ g_{CaLB}^{-1}$]
C	concentration [mol m^{-3}]
Ca	capillary number [–]
C_{ACP}	concentration of acetophenone [mol m^{-3}]
C_{ALA}	concentration of L-alanine [mol m^{-3}]
$C_{ATA\text{-}wt}$	concentration of ATA-wt [$g_{ATA\text{-}wt}\ L^{-1}$]
C_{alg}	concentration of alginate [g L^{-1}]
C_{BB}	concentration of butyl butyrate [mol m^{-3}]
C_{BUT}	concentration of 1-butanol [mol m^{-3}]
C_{BUTin}	inlet concentration of 1-butanol [mol m^{-3}]
C_{CaLB}	concentration of CaLB [$g_{CaLB}\ L^{-1}$; $g_{CaLB}\ m^{-3}$]
C_e	enzyme concentration expressed per reactor volume [g L^{-1}; g m^{-3}]
$C_{e,v}$	enzyme concentration expressed per reactor void volume [g L^{-1}]
C_{glu}	glucose concentration [mM]
C_{LK}	concentration of LentiKats® [$g_{LK}\ L^{-1}$]
C_{N435}	concentration of Novozym® 435 [$g_{N435}\ L^{-1}$]
C_{MBA}	concentration of (*S*)-(–)-α-methylbenzylamine [mol m^{-3}]
C_{Pout}	product outlet concentration [mM]
C_{PYR}	concentration of pyruvate [mol m^{-3}]
C_{Sin}	substrate inlet/initial concentration [mM; mol m^{-3}]
C_{Sout}	substrate outlet concentration [mM]
C_{VB}	concentration of vinyl butyrate [mM; mol m^{-3}]
C_{VBin}	inlet concentration of vinyl butyrate [mM; mol m^{-3}]
d	channel depth [µm; mm; m]
D	diffusion coefficient [$m^2\ s^{-1}$]
Da	*Damköhler number* [–]

D_{ACP}	diffusion coefficient of acetophenone in water [$m^2\ s^{-1}$]
D_{ALA}	diffusion coefficient of L-alanine in water [$m^2\ s^{-1}$]
Da_{I}	first *Damköhler number* [–]
Da_{II}	second *Damköhler number* [–]
D_{BB}	diffusion coefficient of of butyl butyrate in *n*-heptane [$m^2\ s^{-1}$]
D_{BUT}	diffusion coefficient of of 1-butanol in *n*-heptane [$m^2\ s^{-1}$]
D_e	effective diffusion coefficient [$m^2\ s^{-1}$]
d_e	equivalent particle diameter [m]
D_{eACP}	effective diffusion coefficient of acetophenone in LentiKats® [$m^2\ s^{-1}$]
D_{eALA}	effective diffusion coefficient of L-alanine in LentiKats® [$m^2\ s^{-1}$]
D_{eBB}	effective diffusion coefficient of butyl butyrate in Novozym® 435 [$m^2\ s^{-1}$]
D_{eBUT}	effective diffusion coefficient of 1-butanol in Novozym® 435 [$m^2\ s^{-1}$]
D_{eMBA}	effective diffusion coefficient of (*S*)-*α*-MBA in LentiKats® [$m^2\ s^{-1}$]
D_{ePYR}	effective diffusion coefficient of pyruvate in LentiKats® [$m^2\ s^{-1}$]
D_{eVB}	effective diffusion coefficient of vinyl butyrate in Novozym® 435 [$m^2\ s^{-1}$]
D_{MBA}	diffusion coefficient of (*S*)-(–)-*α*-methylbenzylamine in water [$m^2\ s^{-1}$]
d_{N435}	average diameter of Novozym® 435 [μm; m]
D_{PYR}	diffusion coefficient of pyruvate in water [$m^2\ s^{-1}$]
d_h	channel hydraulic diameter [m]
d_p	particle diameter [μm; m]
D_{VB}	diffusion coefficient of of vinyl butyrate in *n*-heptane [$m^2\ s^{-1}$]
d_{32}	Sauter mean diameter of LentiKats® [mm; m]
$\mathfrak{D}$	axial dispersion coefficient [$m^2\ s^{-1}$]
E	exit age distribution [min^{-1}]
g	gravitational acceleration [$m\ s^{-2}$]
h	height of LentiKats® [mm]
K_{BUT}	binding constant of 1-butanol [$mol\ m^{-3}$]
k_{cat}	turnover number [s^{-1}]
K_{iBUT}	inhibition constant of 1-butanol [$mol\ m^{-3}$]
K_{iVB}	inhibition constant of vinyl butyrate [$mol\ m^{-3}$]
K_{VB}	binding constant of vinyl butyrate [$mol\ m^{-3}$]
L	characteristic length [m]
l	channel length [mm; m]

logP	octanol/water partition coefficient [–]
M_B	molecular weight of the solvent [g mol^{-1}]
N	molar flux [mol m^{-2} s^{-1}]
$\vec{n}$	flux vector normal to the interfacial surface [–]
$\vec{N}_{ACP}$	molar flux of acetophenone normal to the interfacial surface [mol m^{-2} s^{-1}]
$\vec{N}_{ALA}$	molar flux of L-alanine normal to the interfacial surface [mol m^{-2} s^{-1}]
$\vec{N}_{MBA}$	molar flux of (*S*)-α-MBA normal to the interfacial surface [mol m^{-2} s^{-1}]
$\vec{N}_{PYR}$	molar flux of pyruvate normal to the interfacial surface [mol m^{-2} s^{-1}]
OD_{600}	optical density measured at a wavelength of 600 nm [–]
Oh	*Ohnesorge number* [–]
Pe	*Péclet number* [–]
Pe_p	*Péclet number* for inert particle [–]
PR	production rate [µmol$_{ACP}$ h^{-1}; mmol$_{BB}$ h^{-1}]
P_1	energy dissipation rate [kW m^{-3}]
Q	volumetric flow rate [µL min^{-1}; m^3 s^{-1}]
Q_c	volumetric flow rate of continuous phase [µL min^{-1}; m^3 s^{-1}]
Q_d	volumetric flow rate of droplet phase [µL min^{-1}; m^3 s^{-1}]
Q_P	volumetric productivity [mmol$_{ACP}$ L^{-1} min^{-1}; mmol$_{BB}$ L^{-1} min^{-1}]
r_a	reaction rate [mol m^{-3} s^{-1}]
Re	*Reynolds number* [–]
Re_p	particle *Reynolds number* [–]
s	skewness [–]
S_{LK}	area of the upper curved surface of LentiKats® [mm^2]
$S_{LKtotal}$	total surface area of LentiKats® [mm^2]
T	temperature [°C; K]
t	time [s; min; h; day]
t'	relative time with respect to when a particular volume enters the system [min]
U	voltage output [V]
U_d	moving velocity of aqueous microdroplets [m s^{-1}]
V	volume of empty reactor [µL]
v	mean superficial fluid velocity [m s^{-1}]
v_i	mean interstitial fluid velocity [m s^{-1}]

v_0	initial reaction rate [mol g^{-1} s^{-1}; mol g^{-1} min^{-1}]
$\vec{v}$	velocity vector [m s^{-1}]
V_A	molar volume of the solute [mL mol^{-1}]
V_f	maximum velocity of the forward reaction [mol g^{-1} s^{-1}]
V_{LK}	volume of LentiKats® [mm^3]
V_v	reactor void volume [µL]
v_x	average fluid velocity in *x*-direction [m s^{-1}]
w	channel width [µm; mm; m]
w_c	channel width for continuous phase [µm; m; mm]
w_d	channel width for droplet phase [mm; m]
X	conversion [%]
x	space co-ordinate/space co-ordinate in the direction of the channel length [m]

Greek symbols

γ	interfacial tension [mN m^{-1}; N m^{-1}]
γ_e	enzyme load [U μL^{-1}; U mL^{-1}]
δ_{CaLB}	thickness of shell containing *Candida antarctica* lipase B [µm; m]
Δp	pressure drop [P; kPa]
$\Delta p_{heptane}$	pressure drop when flowing *n*-heptane [Pa]
Δp_{water}	pressure drop when flowing water [Pa]
$\Delta \rho$	fluid density difference [kg m^{-3}]
ε	bed porosity [–]
ε_p	particle porosity [–]
ε_{LK}	porosity of LentiKats® [–]
ε_{N435}	porozity of Novozym® 435 [–]
ζ_p	particle tortuosity [–]
ζ_{LK}	tortuosity of LentiKats® [–]
ζ_{N435}	tortuosity of Novozym® 435 [–]
η	fluid dynamic viscosity [Pa s]
η_B	dynamic viscosity of the solvent [mPa s]
η_c	fluid dynamic viscosity of continuous phase [Pa s]
η_d	fluid dynamic viscosity of droplet phase [Pa s]

ρ	fluid density [kg m^{-3}]
ρ_c	fluid density of continuous phase [kg m^{-3}]
ρ_d	fluid density of droplet phase [kg m^{-3}]
σ^2	variance [s^2; min^2]
τ	mean residence time [min]
τ_p	diffusion time in a porous particle [s; min]
τ_r	reaction time [s; min]
τ_t	transport time [s; min]
$\tau_{t\text{-}diff}$	transport time by diffusion [s; min]
Φ_B	association factor of the solvent [–]
ψ	particle sphericity [–]

ABBREVIATIONS AND ACRONYMS

ACE	acetaldehyde
ACP	acetophenone
Asp	aspartate
ATA-wt	amine transaminase – wild-type
ATA-117	amine transaminase 117
BB	butyl butyrate
BUT	1-butanol
CaLB	*Candida antarctica* lipase B
CPBR	conventional packed bed reactor
CTAB	cetrimonium bromide
ePTFE	expanded polytetrafluoroethylene
FEP	fluorinated ethylene propylene
G	α-L-guluronate residue residue in alginate
GC	gas chromatography
GOx	glucose oxidase
His	histidine
HPLC	high-performance liquid chromatography
ID	inner diameter
IScPR	*in situ* co-product removal
ISPR	*in situ* product removal
LK	LentiKats®
Lys	lysine
L-ALA	L-alanine
M	β-D-mannuronate residue in alginate
MPBR	miniaturized packed bed reactor
MPPA	1-methyl-3-phenylpropylamine
N435	Novozym® 435
OD	outer diameter
PBS	phosphate buffered saline
PDMS	polydimethylsiloxane
PEEK	polyetheretherketone

PFA	perfluoroalkoxy
PLP	pyridoxal-5'-phosphate
PMMA	poly(methyl methacrylate)
PMP	pyridoxamine-5'-phosphate
PTFE	polytetrafluoroethylene
PVA	poly(vinyl alcohol)
PYR	sodium pyruvate
RTD	residence time distribution
Ser	serine
Tris	tris(hydroxymethyl)aminomethane
VB	vinyl butyrate
(*S*)-*α*-MBA	(*S*)-(–)-*α*-methylbenzylamine
α-TA	α-transaminase
ω-TA	ω-transaminase

1 INTRODUCTION

Chemical industry is facing with the high demands towards the implementation of the environment-friendly production. Such aspirations mostly involve processes capable of preventing waste generation already at an early stage of development as well as avoiding utilization of toxic or hazardous auxiliaries. This trend practically dates from the period before early 1990s, when Japan, Italy, and the United Kingdom launched major initiatives towards the production which is nowadays known as 'Green Chemistry' or alternatively 'Sustainable Technology' (Sheldon et al., 2007). Since then, the concept has been gaining importance rapidly and becoming a synonym for an innovative, modern and sustainable industrial manufacturing.

Biocatalysis has emerged as a technology which perfectly fits the above-mentioned concept, and because of that is becoming a very attractive complement or alternative to chemical catalysis (Bommarius and Riebel, 2004; Straathof and Adlercreutz, 2005; Buchholz et al., 2012). Its application in various industrial productions of chemicals is increasing due to several advantages, including high selectivity, diversity, and environment-friendly nature of biocatalytic processes (Wohlgemuth, 2010). Various enzymes and whole cells are powerful biocatalysts capable of catalyzing immense and diverse set of chemical reactions, which makes them very convenient for a broad application. Indeed, there are certain prognostics saying that in the following years a growth of the global market for industrial enzymes at a rate of about 5% annually will be driven by innovations in various areas of biotechnology as well as by replacing conventional chemical catalysis with biocatalysis (Grunwald, 2015). On the contrary, a relatively high price of isolated enzymes stemming from complicated production processes limits their potential in various applications, which might be overcome by their immobilization (Cao, 2005; Sheldon, 2007).

There is a strong need to find a reactor system capable of providing high productivities when using immobilized biocatalysts. Within this context, a synergy between biocatalysis and reactor/unit operation miniaturization has recently been shown to be a powerful tool for the rapid development of biocatalytic processes through both – process intensification (Marques and Fernandes 2011; Karande et al., 2016) and process design intensification (Hessel et al., 2012), as well as the possibility to explore novel process windows (Pohar and Plazl, 2009; Hessel et al., 2009, 2013). Such miniaturized systems have revealed numerous advantages over the conventional ones, primarily due to high surface-to-volume ratio stemming from their small dimensions, and consequently favorable mass and heat transfer (Bolivar et al., 2011). The fact that such devices can be of a modular type and operated in a continuous flow mode brings additional advantages in favour of the process efficiency and good spatial and temporal control (Wegner et al., 2011; Bieringer et al., 2013; Munirathinam et al., 2015; Wohlgemuth et al., 2015; Jensen, 2017), as well as ability to perform multi-step

bioconversions by consecutively coupling reactors with various enzymes (Matosevic et al., 2011a; Halim A. A. et al., 2013; Gruber et al., 2017).

Although biocatalytic processes performed in miniaturized reactors have gained increased attention over the last decade, they still can be treated as novel tools in comparison with the chemical miniaturized reactors which are about 20 years old (Matosevic et al., 2011b; Hessel et al., 2014; Žnidaršič-Plazl, 2014; Laurenti and dos Santos Vianna Jr., 2016). Accordingly, the literature review has revealed that miniaturized biocatalytic reactors are disproportionately less reported than their counterparts used in the chemical synthesis. Regarding the biocatalytic miniaturized reactors, those with surface immobilized biocatalysts (Stojkovič et al., 2011, 2014; Bolivar and Nidetzky, 2012; Stojkovič and Žnidaršič-Plazl, 2012), biocatalysts entrapped into monolithic structures (Krenkova and Svec, 2009) as well as packed bed reactors are the most frequently reported.

Continuously operated miniaturized packed bed reactors (MPBRs) with immobilized enzymes or whole cells are stemming from the conventional packed bed reactors (CPBRs) which have been occupying a meaningful place in the chemical industry, as well as in preparative and analytical chromatography over many decades, particularly due to their uncomplicated but concurrently convenient design (Ganetsos and Barker, 1991; Kolev, 2006; Sen et al., 2017). Despite the fact that MPBRs are endowed by many advantages compared to CPBRs, they are not fully commercialized yet. Therefore, finding the sustainable solution for an efficient scale-up of MPBRs and at the same time retaining the benefits of microscale reactors is the key point towards their implementation on the industrial scale.

Many important processes in the modern industrial production rely on mathematical modeling since it, among many other tasks, may be of a great importance in data collection, statistical analysis, as well as process planning, development and simulation (Bailey, 1998; Aris, 1999). Modeling of MPBRs with immobilized enzymes could be of great help in a practical facet of their development and design optimization (Azevedo et al., 2004a; Pohar et al., 2012; Denčić et al., 2013; Fischer et al., 2013; Tibhe et al., 2013).

In order to develop efficient MPBRs, adequate carriers for biocatalyst immobilization should be considered. For that purpose, natural and synthetic polymers are oftentimes used for the production of polymer particles, preferably with small dimensions in order to reduce mass transfer limitations (Wang J.-T. et al., 2011; Datta et al., 2012; Rathore et al., 2013). The use of miniaturized reactors for polymer microparticles generation could be a promising path towards the preparation of efficient porous carriers applicable in MPBRs (Kumacheva and Garstecki, 2011; Mazzitelli et al., 2013).

1.1 THE PURPOSE OF THE WORK

The purpose of the work was the development and characterization of MPBRs with immobilized biocatalysts, an ω-transaminase entrapped in the lens-shaped poly(vinyl alcohol) (PVA) particles (LentiKats®) and *Candida antarctica* lipase B adsorbed on acrylic resin (Novozym® 435). The systematic scale-up of the MPBRs for transaminase- and lipase-catalyzed processes was done with the objective of increasing the reactor capacity and at the same time to enable efficient biocatalyst use. Therefore, the influence of rectangular and hexagonal channel geometries with various lengths, widths, and depths on the reactor's performances were evaluated regarding the reactor productivity. Temperature effects on the immobilized enzymes and operational stability of the continuously operated MPBRs were evaluated as well. Moreover, pressure drop measurements and a residence time distribution analysis of MPBRs were among the aims.

A microfluidic-based method suitable for the entrapment of *E. coli* cells overexpressing ω-transaminase in alginate microparticles and applicability of resulting biocatalyst were shown as a proof-of-concept to pave the path towards the application of miniaturized devices in biocatalyst immobilization with a great potential to be used in MPBRs.

2 LITERATURE REVIEW

2.1 BIOCATALYSIS AND BIOCATALYTIC PROCESSES

The history of biocatalysis, as prominent part of much broader biotechnology field (Figure 1), is essentially related to the vinegar production, probably the most familiar example of microbial biotransformation throughout history (Vasic-Racki, 2006). Nowadays, biocatalysis is broadly applied in order to achieve desired transformations of many compounds into value-added products (Straathof and Adlercreutz, 2005; Liese et al., 2006; Fessner and Anthonsen, 2009). That can be achieved by using a biocatalyst – an enzyme, an enzyme complex, a cell organelle or a whole cell, either viable growing, non-growing or non-viable (Buchholz and Poulsen, 2005).

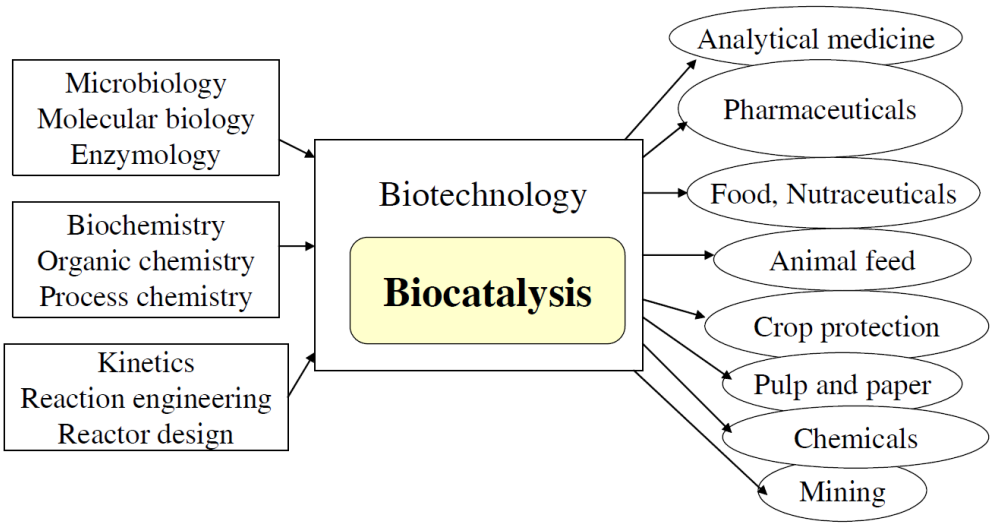

Figure 1: The role of biocatalysis and biotechnology between the interdisciplinary sciences and industries including other users (Bommarius and Riebel, 2004: 7).

Slika 1: Vloga biokatalize in biotehnologije med interdisciplinarnimi vedami in industrijo ter ostalimi uporabniki (Bommarius in Riebel, 2004: 7).

Enzymes are in the core of every biocatalytic process and may be reasonably considered as the cornerstone of industrially important processes (Choi J.-M. et al., 2015). They are remarkable and ubiquitous catalysts endowed by a distinct mechanism of action that allows them conversion of many important substances at a significant rate without being altered (Voet D. and Voet J. G., 2011). As any other catalysts, enzymes reduce the magnitude of the energy barrier needful to be overcome for a reaction to take place, and bring the reaction to equilibrium more quickly than would occur without their presence (Aehle, 2004; Illanes, 2008).

Enzymes differ from ordinary chemical catalysts in an advantageous way through several facets. They show greater specificity with respect to the substrate molecules than the

chemical catalysts, because their active site consists of an indentation or cleft in the molecule's surface and has a high geometric complementarity to the substrate's shape and size (Voet D. and Voet J. G., 2011). Enzymes are exclusively composed of L-amino acids and possess high regio-, chemo- and stereospecificity (Voet D. and Voet J. G., 2011). This is a unique property of enzymes because it usually means no side reactions and less pollution as well as easier downstream processing and lower production costs, which is particularly useful in the processes where the high purity of the final product is an imperative.

Unlike ordinary chemical catalysts, enzymes have been tailored *in vivo* and due to it, they express high activity under mild conditions, usually at nearly neutral pH values, temperatures below 100 ºC and atmospheric pressure. Enzymes are biodegradable, non-toxic, environment-friendly and generally considered as a natural product.

Natural origin of enzymes sometimes could be an obstacle for the industrial application because they have high molecular complexity, and thus the production and purification of isolated enzymes are often economically unfavorable. The enzymes' intrinsic fragility might be unsuitable for the applications under tough conditions occurring *in vitro* (Illanes, 2008). Therefore, in addition to their application in an isolated form, enzymes are applied in the form of whole cells, which is more convenient for the biotransformations that require presence of cofactors (Faber, 2011). *Pros* and *cons* of enzymes as biocatalysts are summarized in Table 1.

Table 1: Advantages and disadvantages of enzymes as biocatalysts (Illanes, 2008: 3).
Tabela 1: Prednosti in slabosti encimov kot biokatalizatorjev (Illanes, 2008: 3).

Advantages	**Drawbacks**
High specificity	High molecular complexity
High activity under moderate conditions	High production costs
High turnover number	Intrinsic fragility
Highly biodegradable	Long-term stability and activity
Generally considered as natural products	

Current trends in biocatalysis strive towards the application of non-conventional media (such as organic solvents, ionic liquids, deep eutectic solvents, supercritical fluids and fluorous solvents) in order to overcome potential problems of poorly water-soluble organic substrates (Žnidaršič-Plazl, 2014; Grunwald, 2015). New advances in the fields of functional metagenomics and *in vitro* evolution of enzymes may immeasurably contribute to the development of novel processes and generation of many value-added products (Yeh W.-K. et al., 2010).

2.1.1 Properties and application of ω-transaminases

The amino-acid breakdown in metabolic pathways ordinarily begins with the removal of α-amino groups (deamination). Most of the amino acids are deaminated in the process known as transamination, the reaction in which their amino group is transferred to an α-keto acid, concomitantly yielding the α-keto acid of the original amino acid and a new amino acid as product and co-product, respectively (Voet D. and Voet J. G., 2011).

This reaction is catalyzed by transaminases (EC 2.6.1.X), an enzyme subclass belonging to transferases whose occurrence is essential for the amino acid metabolism (Figure 2a). Transamination would be impossible without the presence of pyridoxal-5'-phosphate (PLP), a biologically important derivative of pyridoxine (vitamin B_6) which participates in the amino group accommodation (Figure 2b) by its conversion throughout different forms (Mukherjee et al., 2011; Voet D. and Voet J. G., 2011).

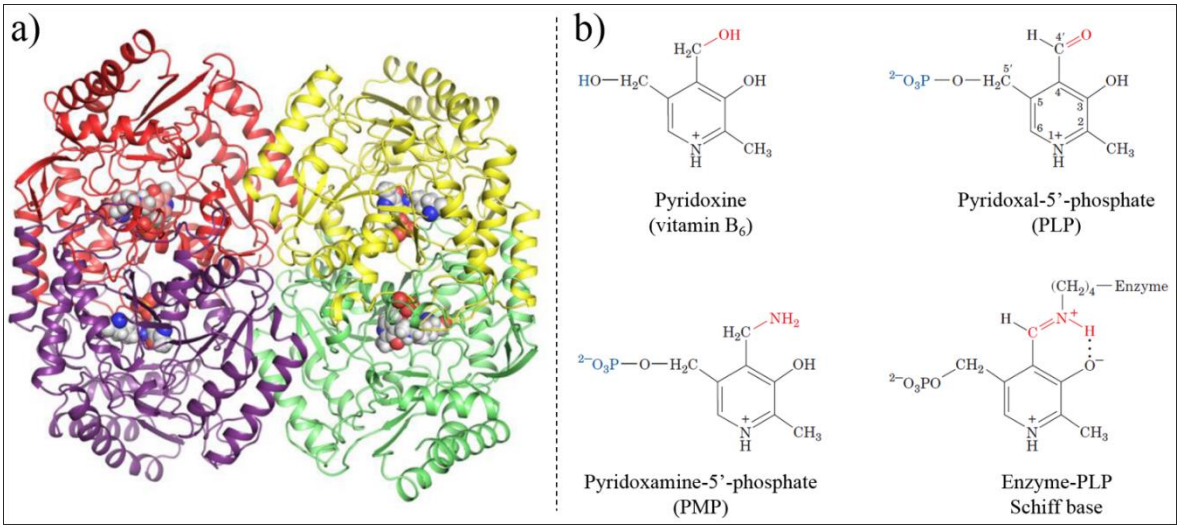

Figure 2: Transaminase and PLP: a) crystal structure of a wild-type transaminase in a complex with PLP (Börner et al., 2017a: 3, Supporting Information); b) biological forms of PLP (Voet D. and Voet J. G., 2011: 1020).

Slika 2: Transaminaza in PLP: a) kristalna struktura divjega tipa transaminaze v kompleksu s PLP (Börner in sod., 2017a: 3, priloga); b) biološke oblike PLP (Voet D. in Voet J. G., 2011: 1020).

Stemming from the amino-acid sequence alignment of 51 enzymes, transaminases are divided into groups I, II, III and IV (Mehta et al., 1993; Malik et al., 2012a), where transaminases from the second group exclusively transfer the amino functionality from an amino donor onto an amino acceptor, whereby at least one of the two substances is not an α-amino acid or an α-keto acid (Koszelewski et al., 2010a). Such transaminases are collectively named ω-transaminases (ω-TAs), opposite to other three groups denoted as α-transaminases (α-TAs) (Koszelewski et al., 2010a; Malik et al., 2012a).

ω-TAs (EC 2.6.1.18) have been gaining a significant attention as industrially desired biocatalysts because they utilize a broad range of substrates and have high enantioselectivity (Fuchs M. et al., 2015). This trend has been spurred during 1990s by the achievement of Celgene Corporation who applied ω-TAs for the preparation of chiral amines (Stirling et al., 1990; Matcham and Bowen, 1996). The chiral *prim*-, *sec*-, and *tert*-amines are pharmaceutically relevant as building blocks for many bioactive molecules, and their industrial-scale synthesis in the enantiomerically pure form is literally a driving force for ω-TAs application (Koszelewski et al., 2010a; Mathew and Yun, 2012; Kroutil et al., 2013; Kohls et al., 2014).

On a preparative scale, ω-TAs can be applied *via* three different reaction schemes which together stand for the transamination reaction run in forward and backward direction: kinetic resolution of racemic (*rac*) amines (Figure 3a), asymmetric synthesis from prochiral ketones (Figure 3b), and deracemization (Figure 3c) (Nestl et al., 2014).

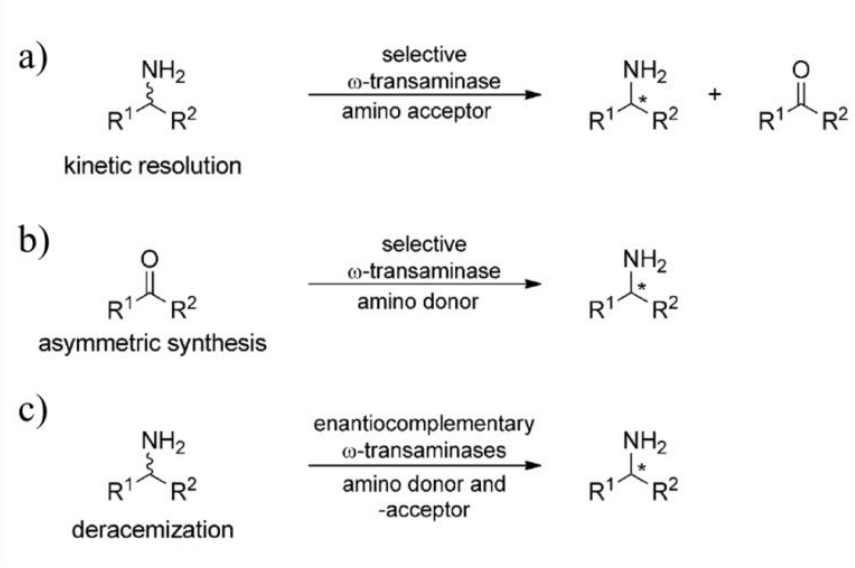

Figure 3: ω-TAs-catalyzed reactions: a) kinetic resolution; b) asymmetric synthesis and c) deracemization (Nestl et al., 2014: 3078).

Slika 3: Reakcije katalizirane z ω-transaminazo: a) kinetična resolucija; b) asimetrična sinteza in c) deracemizacija (Nestl in sod., 2014: 3078).

Kinetic resolution of *rac*-amines is commonly applied strategy, although it theoretically generates only 50% yield (Shin and Kim, 1997; Shin J.-S. et al., 2001a, 2001b; Malik et al., 2012b; Park E.-S. et al., 2014; Shin G. et al., 2015), in contrast to the asymmetric synthesis from prochiral ketones which allows a 100% yield of the optically pure target product (Shin and Kim, 1999a; Mutti et al., 2011; Mutti and Kroutil, 2012; Park E.-S. et al., 2013; Kroutil et al., 2013; Halim M. et al., 2014; Mallin et al., 2014). Deracemization is also able to achieve the theoretical yield of 100%, but it remains the least attractive strategy due to its complexity (Shin G. et al., 2013; Nestl et al., 2014; Park and Shin, 2014).

A broader utilization of (*S*)- and (*R*)-selective ω-TAs on the industrial scale is highly desirable, primarily through the strategy of direct asymmetric synthesis, which is seen as the state-of-the-art of the technology (Koszelewski et al., 2010a; Tufvesson et al., 2011). However, this is quite a challenging task due to several typical problems such as substrate and/or (co-)product inhibition, thermodynamic limitations mirrored in an unfavorable equilibrium position which is highly influenced by the choice of the amino donor/amino acceptor system (Tufvesson et al., 2012; Gundersen et al., 2015), as well as biocatalyst and substrates/products solubility limitations (Tufvesson et al., 2011; Green et al., 2014).

The strategies proposed for overcoming such problems mainly rely on shifting the equilibrium towards the product side by using stronger amino donor or its excess (Tufvesson et al., 2015), reducing the product or co-product inhibition by *in situ* product removal (ISPR) (Shin and Kim, 1999b; Shin J.-S. et al., 2001a; Rehn et al., 2014; Heintz et al., 2016a) or *in situ* co-product removal (IScPR) (Tufvesson et al., 2014) as well as using enzymatic cascade reactions (Simon et al., 2014), also possibly coupled to ISPR (Börner et al., 2015). Biocatalyst limitations are being solved by its improvement (Casablancas et al., 2013), by separation and recycling achieved by means of immobilization (Koszelewski et al., 2010b; Päiviö and Kanerva, 2013; Mallin et al., 2014; Neto et al., 2015) and by using the whole-cell biocatalysts (Cárdenas-Fernández et al., 2012), even those with surface expressed ω-TA (Gustavsson et al., 2014). Low substrate or product water-solubility is highly undesirable since the application of low substrate concentration leads to poor volumetric productivities and negatively affects the downstream step as well as economic feasibility of the process. Hence, the main strategies focus on the application of water-miscible solvents acting towards better substrate solubility in the water phase or water-immiscible solvents acting as a substrate reservoir (Mutti and Kroutil, 2012; Truppo et al., 2012; Fuchs C. S. et al., 2014).

The enzyme used in this study is a wild-type ω-TA (Figure 2a), a homotetramer with a high sequence identity to *Pseudomonas* sp. obtained from a metagenomic library (Börner et al., 2017a). Other widely applied ω-TAs originate from *Chromobacterium violaceum* DSM 30191 (Kaulmann et al., 2007; Smithies et al., 2009; Halim M. et al., 2014), *Vibrio fluvialis* JS17 (Shin J.-S. et al., 2001a, 2001b; Yi et al., 2007), *Bacillus thuringiensis* JS64 (Shin and Kim, 1999b; Shin J.-S. et al., 2001a), *Burkholderia vietnamiensis* (Jiang et al., 2014), *Mycobacterium vanbaalenii* (Shin G. et al., 2015), or from *Ochrobactrum anthropi* expressing an ω-TA reported to devoid the substrate and product inhibition (Park and Shin, 2013). Different strategies for improvements, such as redesigning the substrate specificity of ω-TAs (Cho et al., 2008), and the quest for wild-type microorganisms showing ω-TA activity (Koszelewski et al., 2010a), are in full swing.

2.1.1.1 Transaminase-catalyzed synthesis of acetophenone

The first selected model reaction studied in this work is the transamination of (*S*)-(–)-*α*-methylbenzylamine ((*S*)-*α*-MBA) using sodium pyruvate (PYR) as an amino acceptor, yielding acetophenone (ACP) and L-alanine (L-ALA) as the product and co-product, respectively (Figure 4). This reaction is used for testing alginate microparticles with immobilized recombinant *E. coli* cells overexpressing ω-TA (Section 4.1) as well as for evaluation of MPBRs with LentiKats® (Section 4.2).

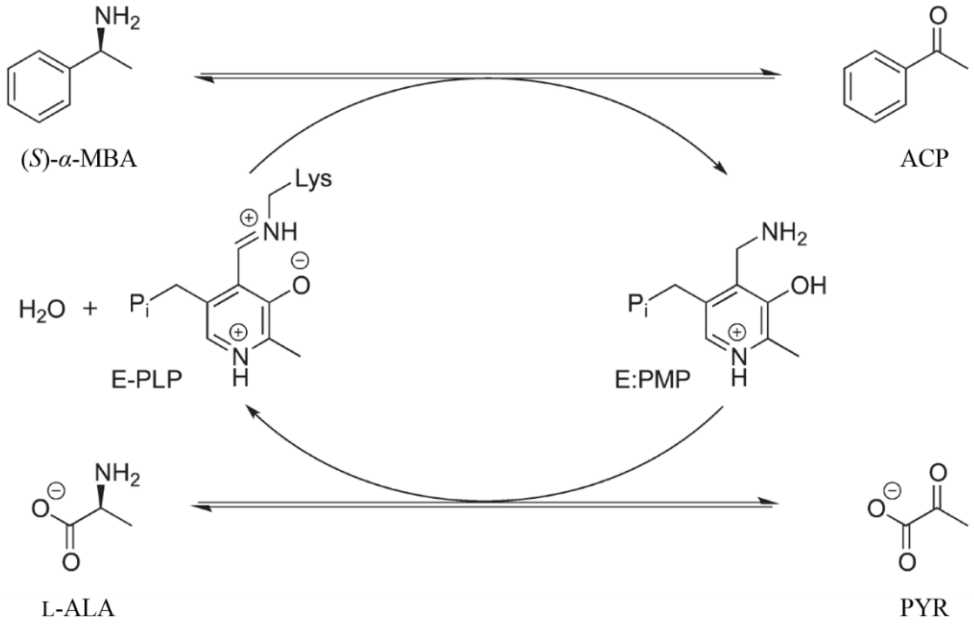

Figure 4: Reaction scheme of transamination using (*S*)-*α*-MBA as an amino donor and PYR as an amino acceptor, yielding ACP and L-ALA as the product and co-product, respectively (Engelmark Cassimjee et al., 2015: 3).

Slika 4: Reakcijska shema za transaminacijo z (*S*)-*α*-MBA kot amino donorjem in PYR kot amino akceptorjem, ki prinašata ACP in L-ALA kot produkt in stranski produkt (Engelmark Cassimjee in sod., 2015: 3).

In this ω-TA-catalyzed reaction, PLP is firstly bonded as a Schiff-base to a lysine (Lys) residue in the enzyme's active site, forming a stable intermediate enzyme-PLP complex (*internal aldimine*) (Engelmark Cassimjee et al., 2015). The mechanism of the *internal aldimine* formation could be found throughout the literature and stands for the most of PLP-dependent enzymes including ω-TAs (Oliveira et al., 2011). Further on, PLP reacts with (*S*)-*α*-MBA over the formation of a new intermediate complex (*external aldimine*), which consequently results in the formation of ACP with the consumption of a water molecule and simultaneous conversion of PLP to pyridoxamine-5'-phosphate (PMP), afterwards the amino acceptor PYR is converted to L-ALA to complete the catalytic cycle by regenerating the *internal aldimine* and the water molecule (Figure 4) (Toney, 2005; Engelmark Cassimjee et al., 2015). In sum, the amino donor (*S*)-*α*-MBA is bound first, and then the product ACP is

released before PYR is added, while the co-product L-ALA leaves the enzyme last. Such sequentially ordered interaction between the enzyme and substrate/product molecules is typical for transaminases, and can be described by a ping-pong bi-bi reaction mechanism (Bisswanger, 2002; Leskovac, 2003; Engelmark Cassimjee et al., 2015).

(*S*)-*α*-MBA has been reported to be a strong amino donor capable of displacing the resulting reaction thermodynamic equilibrium towards the product side whereby the generation of ACP and L-ALA is greatly favored (Fesko et al., 2013; Jiang et al., 2014; Tufvesson et al., 2015). The economic considerations of a process should not be neglected, because the price of the amino donor strongly affects the operating costs and the price of optically pure (*S*)-*α*-MBA is relatively low (100–150 € kg^{-1}), which could not be said for the cofactor PLP (1,000–2,115 € kg^{-1}) (Tufvesson et al., 2015). A potential drawback of this reaction is the low reaction yield, caused by the poor water solubility of ACP, which is cca. 9-, 38-, and 228-times lower than the solubility of (*S*)-*α*-MBA, L-ALA and PYR, respectively (Tufvesson et al., 2011). This problem may be solved by performing the reaction in organic solvents (Truppo et al., 2012), or using a two-liquid-phase reaction system (Shin J.-S. et al., 2001a).

Although the chosen reaction does not reflect an industrially relevant one for an attractive product, e.g. synthesis of 1-methyl-3-phenylpropylamine (MPPA) using a cheap amino donors, it is a frequently used as an assay/model reaction (Martin et al., 2007; Mallin et al., 2014; Rehn et al., 2014; Heintz et al., 2016b; Börner et al., 2016, 2017a; Miložič et al., 2017). Likewise, Börner et al. (2016) have reported that 40 mM equimolar concentrations of both substrates together with 0.1 mM PLP has been found as the optimal reaction conditions for the same enzyme as in this study. Besides, the reaction hardly affects the pH in sodium phosphate buffer where the enzyme had the highest relative activity at pH 8.0 (Börner et al., 2016).

2.1.2 Properties and application of *Candida antarctica* lipase B

Lipases or triacylglycerol ester hydrolases (EC 3.1.1.3) constitute a versatile, omnipresent, robust and highly promiscuous group of enzymes capable of catalyzing a broad range of hydrolytic and synthetic reactions under natural as well as unnatural conditions (Kapoor and Gupta, 2012; Stergiou et al., 2013; De Miranda et al., 2015; Salihu and Alam, 2015). Most lipases manifest the best catalytic activity when the reaction takes place in an organic solvent with some water activity present (Adlercreutz, 2013; Sharma and Kanwar, 2014; Kumar et al., 2016), or at an organic-aqueous interface due to the phenomenon of interfacial activation (Reis et al., 2009).

Yeast *Candida antarctica*, an extremophile originally isolated on Antarctica, produces two quite different lipases denoted as A and B (Goto et al., 1969; Nielsen et al., 1999). *Candida antarctica* lipase B (CaLB) is frequently discussed as an atypical lipase due to its specific

characteristic compared to other enzymes from the same group (Anderson et al., 1998). Such characteristics in the first instance imply an insignificant homology to other known lipase sequences, low activity towards the large triglyceride molecules and eventually lack of the interfacial activation (Uppenberg et al., 1994; Martinelle et al., 1995), albeit a recent study by Zisis et al. (2015) has provided arguments in favor of the interfacial activation of CaLB on highly hydrophobic surfaces.

CaLB is a globular, cofactor-independent, approximately 30 × 40 × 50 Å large, and α/β type-folded enzyme composed of 317 amino acid residues with a molecular weight of 33 kDa and pI of 6.0 (Uppenberg et al., 1994). Its active site, which is accessible through approximately 10 × 4 Å wide and 12 Å deep hydrophobic channel, is made of a Serine-Histidine-Aspartate (Ser^{105}-His^{224}-Asp^{187}) catalytic triad and has flexible α5 and α10 helix regions potentially acting as a lid (Uppenberg et al., 1994, 1995; Ganjalikhany et al., 2012; Stauch et al., 2015). The channel consists of an acyl and secondary alcohol binding 'pockets' (Trodler and Pleiss, 2008). The channel is spatially-limited which causes physical restriction for the substrate, and together with its hydrophobic nature lead to a high substrate selectivity (Uppenberg et al., 1995; Anderson et al., 1998). According to Pleiss et al. (1998), the pocket is large enough to accept substrate molecules with total carbon-chain length up to 13 –CH– moieties. Figure 5a shows the crystal structure of CaLB at 1.55 Å resolution (Uppenberg et al., 1994), where the active site was modified to represent an intermediate of an acetylation reaction (Klähn et al., 2011).

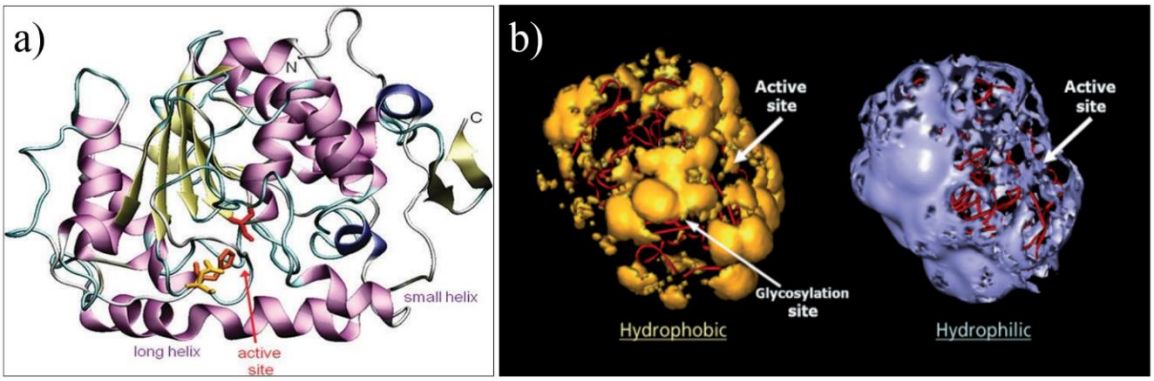

Figure 5: *Candida antarctica* lipase B: a) crystal structure with highlighted catalytic triad in the active site showing Ser^{105} (red), His^{224} (orange) and Asp^{187} (yellow) (Klähn et al., 2011: 1651); b) hydrophobic and hydrophilic surface areas (Basso et al., 2007: 882).

Slika 5: Lipaza B iz kvasovke *Candida antarctica*: a) kristalna struktura z poudarjeno katalitsko triado v aktivnem mestu, ki kaže aminokisline Ser^{105} (rdeče), His^{224} (oranžno) and Asp^{187} (rumeno) (Klähn in sod., 2011: 1651); b) hidrofobne in hidrofilne površine (Basso in sod., 2007: 882).

Many reactions with CaLB are performed in organic solvents, and therefore molecular dynamic simulations are frequently used for investigation of CaLB conformational stability and activity in both polar (logP < 2) and non-polar (logP > 4) solvents (Trodler and Pleiss, 2008; Li C. et al., 2010; Adlercreutz, 2013). It has been shown that CaLB has lower activity

in polar solvents, because solvent's molecules intensively interact with the enzyme's active site and lead to its conformational change by destroying the hydrogen bonds between Ser^{105} and His^{224} (Li C. et al., 2010; Park H. J. et al., 2013). On the other side, the enzyme's overall conformation remains stable in organic solvents, but its flexibility is affected compared to that in an aqueous environment mainly due to the creation of a spanning water network on the protein's surface, changing the ratio between hydrophilic and hydrophobic areas shown in Figure 5b (Trodler and Pleiss, 2008; Li C. et al., 2010). Therefore, it may be concluded that CaLB would have the highest activity when used in a non-polar solvent with a low water content.

CaLB was immobilized in many different ways (Kramer et al., 2010; Idris and Bukhari, 2012; Nicoletti et al., 2015; Jakovetić Tanasković et al., 2016), but the best known is immobilized on acrylic resin, a preparation commercially available under the trademark Novozym® 435. It is widely used in the production of biodiesel (Casas et al., 2013; José et al., 2013), isoamyl acetate (Pohar et al., 2009; Žnidaršič-Plazl and Plazl, 2009; Cvjetko et al., 2012), butyl butyrate (De los Ríos et al., 2008; Pohar et al., 2012; Denčić et al., 2013), polycaprolactone (Kundu et al., 2011), propyl caffeate (Wang J. et al., 2013), caffeic acid phenethyl ester (Wang J. et al., 2014), and several other chemicals.

2.1.2.1 Lipase-catalyzed synthesis of butyl butyrate

Transesterification of vinyl butyrate (VB) and 1-butanol (BUT) to butyl butyrate (BB) and acetaldehyde (ACE) was selected as the model reaction with immobilized CaLB (Figure 6a).

As seen from the general transesterification scheme (Figure 6b), after entering the enzyme's active site, the first substrate undergoes a nucleophilic attack by the catalytic Ser^{105} and covalently binds to its oxygen atom, forming the first tetrahedral intermediate and releasing the first product. Consequently an acylated enzyme is created, which further undergoes the nucleophilic attack by the second substrate resulting in the creation of the second tetrahedral intermediate and releasing the second product, whereby the enzyme is regenerated eventually (Ferrario et al., 2015). Such reaction scenario obeys a ping-pong bi-bi mechanism (Bisswanger, 2002; Leskovac 2003, Ferrario et al., 2015).

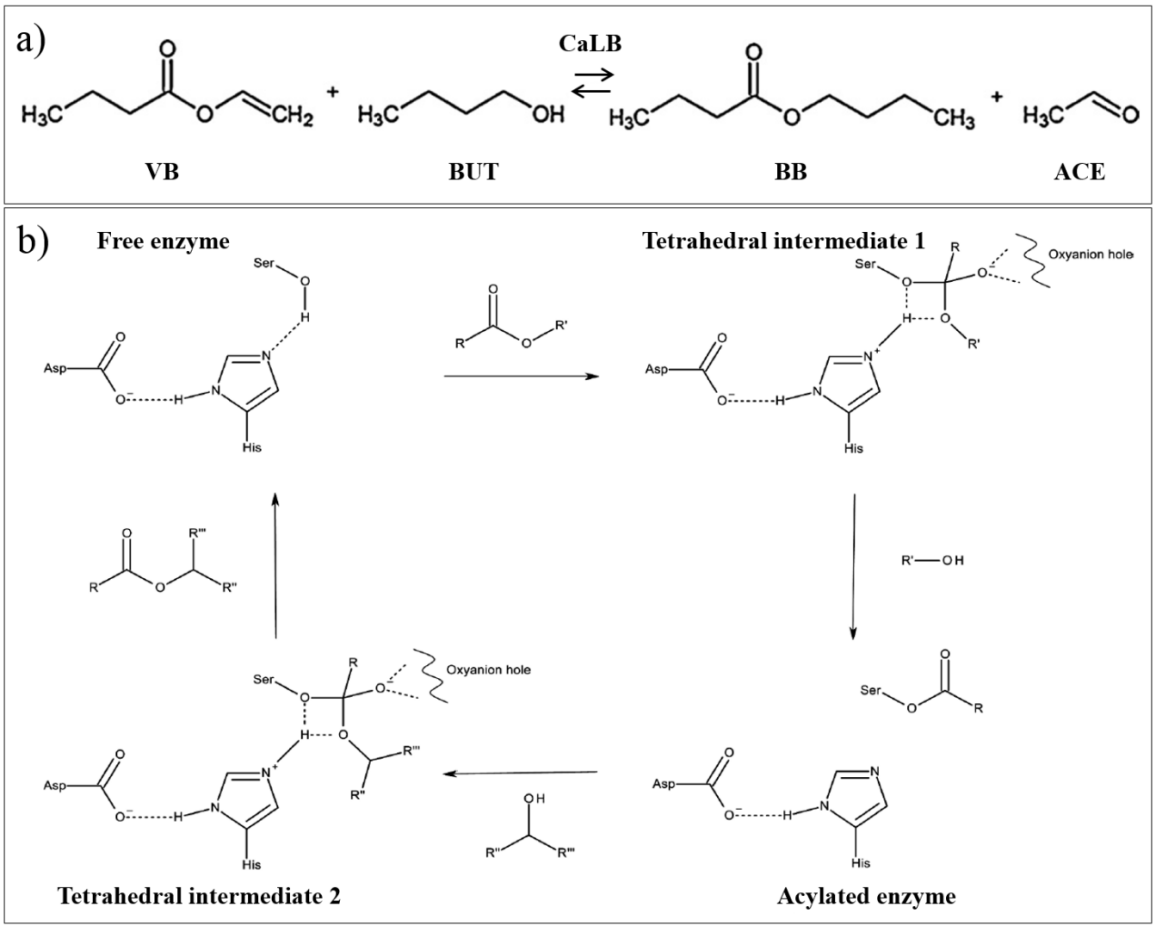

Figure 6: Transesterification of VB and BUT to BB and ACE: a) an overall reaction scheme; b) schematic illustration of the reaction catalytic mechanism (Ferrario et al., 2015: 88).

Slika 6: Transesterifikacija VB in BUT v BB in ACE: a) splošna shema reakcije; b) shematski prikaz katalitskega mehanizma reakcije (Ferrario in sod., 2015: 88).

The synthesis of BB from VB and BUT is commonly performed by CaLB, because it is a highly demanded industrial fragrance that resembles a pineapple (Santos and De Castro, 2006; De los Ríos et al., 2007, 2008; Pohar et al., 2012). Furthermore, VB is easily accepted by the enzyme's active site as a short-chain vinyl ester. CaLB is also remarkably stable towards ACE, an inevitable co-product of acyl transfer reactions with vinyl esters (Weber et al., 1995). Inhibition by both substrates was determined for this reaction using an ionic liquid as a solvent (Pohar et al., 2012). Among various solvents, *n*-heptane presents a good choice primarily due to its non-polarity (logP > 4) and low water content (0.004%) (Sangster, 1989 and ref. therein; KEM Kyoto Electronics).

2.2 BIOCATALYST IMMOBILIZATION

According to the International Union of Pure and Applied Chemistry, immobilization is defined as "the technique used for the physical or chemical fixation of cells, organelles, enzymes, or other proteins onto a solid support, into a solid matrix or retained by a membrane, in order to increase their stability and enable their repeated or continuous use" (Nagel et al., 1992).

Modern industrial production is routinely using immobilized biocatalysts (Cantone et al., 2013; DiCosimo et al., 2013), either isolated enzymes (Cao, 2005) or whole cells (Nedović and Willaert, 2004). Immobilization offers improved catalytic and non-catalytic functions, including enhanced solvent and high temperature resistance, stability, and selectivity of the biocatalyst as well as its facilitated separation, purification and reuse, which altogether lead to an efficient biocatalytic process (Eş et al., 2015). A lower risk of contamination caused by the presence of biocatalyst residues in the final product is also expected when using immobilized systems (Sheldon and van Pelt, 2013). However, mass transfer limitations potentially occurring in a heterogeneous biocatalyst could present a significant problem (Adlercreutz, 2013).

Every immobilization process actually includes an interplay between the biocatalyst and carrier, and hence a careful choice of support material is required together with a suitable immobilization technique. Support material strongly depends on the reactor configuration and must provide a high biocatalyst load and sufficient chemical and mechanical stability (Eş et al., 2015). Hanefeld et al. (2009) have highlighted important parameters related to the biocatalyst, carrier and specific factors of the reaction system which have to be considered when planning an immobilization.

The most commonly applied immobilization methods are entrapment in a carrier, immobilization *via* ionic interactions, carrier-free immobilization (cross-linking), covalent attachment (tethering) and non-covalent adsorption on a carrier, whereby the last two methods often use a different kind of short or long spacers to enhance stability and conformational flexibility of immobilized enzymes (Hanefeld et al., 2009). The effectiveness of immobilization methods can be assessed regarding the immobilization yield and efficiency, activity recovery and biocatalyst load (Sheldon and van Pelt, 2013). Immobilization by entrapment and adsorption on a carrier are the methods used for the preparation of biocatalysts applied in this study, and hence *pros* and *cons* of these two approaches will be more thoroughly considered in the following subchapters.

2.2.1 Immobilization by entrapment

Entrapment refers to the procedure by which a biocatalyst is embedded in a matrix (a three-dimensional polymer network) chemically or physically formed by means of cross-linking or gelation (Cao, 2005). The biocatalyst is pre-mixed with the components for matrix formation, where the cross-linking or gelation is performed during the immobilization process. Entrapment is preferably used for immobilization of whole cells rather than free enzymes, because they are larger and could be easily retained within the formed matrix (Sheldon and van Pelt, 2013). However, there are numerous examples of enzyme immobilization by this method throughout the literature (Rebroš et al., 2007; Fernandes et al., 2009; Nunes et al., 2012).

Immobilization by entrapment is carried out under mild conditions by using harmless chemical agents, concomitantly preventing biocatalyst denaturation and activity loss, so that possible damage caused by immobilization can be minimized. The biocatalyst is also protected from the shear stress in the matrix (Eş et al., 2015). In the case of enzymes as immobilization subject, an additional advantage is that they are not chemically bonded to the carrier, and disruption of the enzyme native configuration is less likely to occur. But sometimes enzyme leakage from the matrix may happen and an additional covalent attachment is required (Sheldon and van Pelt, 2013).

On the other side, possible diffusion limitations in the matrix could be pronounced by using whole cells due to hampered transport of reactive species through the cell membrane (Willaert et al., 2004). Relatively low mechanical strength of the carrier could be another potential problem for application in robust processes. Therefore, a high attention should be devoted to physical (pore size, particle size, nature of the pore, morphology, shape and mechanical stability) and chemical (hydrophilicity and hydrophobicity, nature of the active and inactive functionality) requirements of the carrier (Cao, 2005; Cantone et al., 2013).

The most commonly used materials for the immobilization by entrapment are synthetic and natural polymers (Riddle and Mooney, 2004), especially highly hydrophilic which are capable of forming hydrogels, three-dimensional networks with a large amount of water (Ahmed, 2015). For the purpose of this study two polymers were used for the immobilization of biocatalysts, namely alginate as a representative of the natural group of polymers, and poly(vinyl alcohol) as a representative of the synthetic group of polymers in the form of commercially available preparation LentiKats®.

2.2.1.1 Alginate

Alginate is an ubiquitous, highly exploited and extensively studied biopolymer broadly used for biocatalyst immobilization (Melvik and Dornish, 2004). The main source for alginate extraction are brown algae members of the class *Phaeophyceae*, including *Laminaria hyperborea*, *Laminaria digitata*, *Laminaria japonica*, *Ascophyllum nodosum* and *Macrocystis pyrifera* (Smidsrød and Skjåk-Bræk, 1990).

This is highly biocompatible, non-toxic and relatively inexpensive polyelectrolyte, composed of unbranched blocks of copolymers containing (1,4)-glycosidically linked *β*-D-mannuronate (M) and *α*-L-guluronate (G) residues interconnected in such manner to form consecutive G-residues (GGGGGG), consecutive M-residues (MMMMMM), and alternating M- and G-residues (GMGMGM), respectively (Figure 7a) (Lee and Mooney, 2012). Such structure is capable of gelling under mild conditions and yielding a porous hydrogel, usually in the form of spherical particles (Melvik and Dornish, 2004; Manojlovic et al., 2008). Gelation takes place between G-blocks and divalent cations (mostly Ca^{2+}), which replace monovalent cations (Na^{+}) in alginate structure, forming in that way cross-linked regions (so-called 'egg-box' model) which are the basis of the matrix (Figure 7b) (Braccini and Pérez, 2001; Lee and Mooney, 2012).

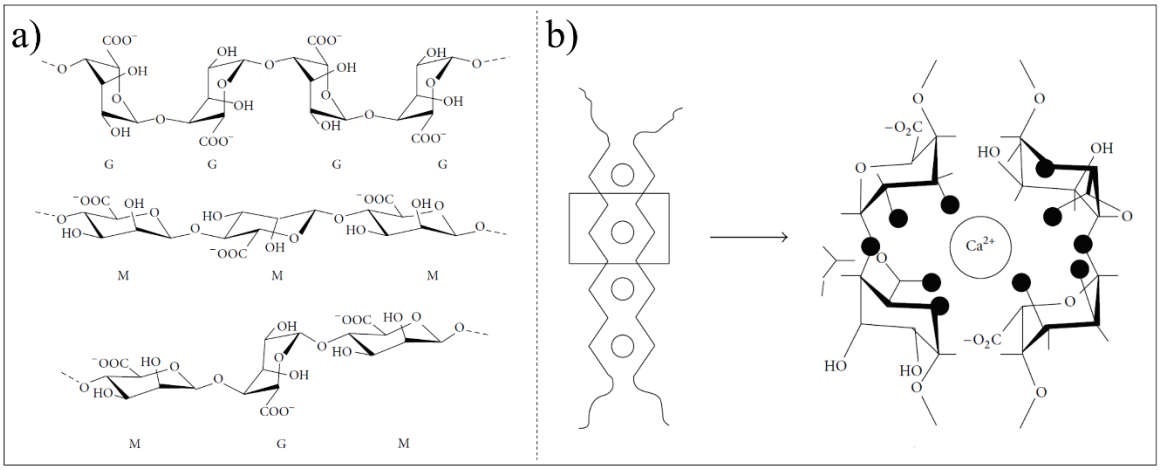

Figure 7: Structure of alginate and resulting hydrogel: a) G-block, M-block, and alternating block (Lee and Mooney, 2012: 108); b) schematic drawing of the 'egg-box' model (Braccini and Pérez, 2001: 1090).

Slika 7: Struktura alginata in nastalega hidrogela: a) G-blok, M-blok in izmenični blok (Lee in Mooney, 2012: 108); b) shematski prikaz modela 'škatla za jajca' (Braccini in Pérez, 2001: 1090).

It has been found that the rate of gelling in 50 mM $CaCl_2$ solution is around 100 µm min^{-1}, so a hypothetical spherical particle with a diameter of 500 µm is gelled in cca. 2.5 min, which is close to the rate of freely diffusing Ca^{2+} (Gåserød 1998; Melvik and Dornish, 2004). Additionally, an electron microscopic observation of a 2% Ca-alginate hydrogel particle has revealed that the pore size is between 5 and 200 nm (Buchholz et al., 2012). However, the

physicochemical and functional properties of resulting hydrogel highly depend on the concentration of gelling agent and biological material to be immobilized as well as concentration of alginate, its M/G ratio, G-block length and molecular weight, which in turn depends on the origin of alginate (Melvik and Dornish, 2004; Lee and Mooney, 2012). In general, bacterial biosynthesis is foreseen to provide more chemically- and structurally-defined alginate than that which could be obtained by extraction from brown algae (Hay et al., 2013). Alginate is sometimes used to make copolymers as immobilization matrixes, for instance with PVA (Levic et al., 2013). The main disadvantage of alginate hydrogels is their instability in the presence of chelating compounds and cations such as phosphate, lactate, citrate, Na^+ and Mg^{2+} (Smidsrød and Skjåk-Bræk 1990; Melvik and Dornish, 2004).

A vast number of different macro-scale methods including emulsification, spray drying, coaxial bead generator, jet cutter and electrostatic droplet generation have been applied to produce alginate microparticles with immobilized biocatalysts (Rathore et al., 2013; Kang et al., 2014). Robustness and relatively high price of the used equipment which usually generates highly polydisperse particles sometimes present a serious deficiency in their application. Miniaturized devices have appeared as an alternative to such equipment because they provide better control over size, shape and composition of resulting microparticles (Xu S. et al., 2005; Kumacheva and Garstecki, 2011; Mazzitelli et al., 2013). Production of alginate microparticles in that way mostly relies on the integration of two steps: emulsification in a microfluidic device resulting in the generation of aqueous alginate droplets as a semi-product, and *in situ* or *ex situ* gelation of generated droplets into solid alginate microparticles (Zhang et al., 2007; Dang and Joo, 2013; Hu et al., 2015).

Different biological materials have been immobilized in alginate microparticles of various sizes by microfluidic-based methods (Table 2). According to author's best knowledge, with the exception of an assay in alginate microparticles containing immobilized glucose oxidase (Um et al., 2008), none of the studies listed in Table 2 has considered the application of alginate microparticles as a biocatalyst support in a continuous biotransformation process.

Table 2: Biological materials immobilized in alginate microparticles obtained by microfluidic devices.
Tabela 2: Biološki material imobiliziran v alginatne mikrodelce pridobljene z uporabo mikrofluidnih naprav.

Immobilized biological material	**Reference**
Human embryonic kidney cells	(Sugiura et al., 2005; Workman et al., 2007, 2008)
Yeast cells expressing green fluorescence protein	(Choi C.-H. et al., 2007)
Mouse erythroleukaemia cells	(Shintaku et al., 2007)
Jurkat cells	(Tan and Takeuchi, 2007; Hong et al., 2010; Onoe et al., 2014)
Human osteosarcoma cells; Cells derived from a rat pheochromocytoma	(Workman et al., 2008)
Glucose oxidase	(Um et al., 2008)
Chlamydomonas	(Morimoto et al., 2009)
Human breast cancer cells	(Kim C. et al., 2009)
Chondrocytes	(Huang S.-B. et al., 2010; Wu and Pan, 2010)
Breast tumor cells	(Yu et al., 2010)
Sertoli cells	(Capretto et al., 2010)
Bovine serum albumin	(Yeh C.-H. et al., 2011)
Mouse embryonic carcinoma cell	(Kim C. et al., 2009, 2011, 2014; Kim C., 2015)
Mouse myeloma NS0	(Cheng et al., 2011)
Saccharomyces cerevisiae	(Martinez et al., 2012)
Pancreatic islets cells	(Tendulkar et al., 2012)
Anti-*Mycobacterium tuberculo*sis and Anti-*Escherichia coli* antibody	(Chen W. et al., 2013)
Dental-derived mesenchymal stem cells	(Moshaverinia et al., 2013)
Antibody-secreting hybridoma cells; Mouse breast cancer cells	(Akbari and Pirbodaghi, 2013)
Human liver cancer cells	(Um et al., 2008; Kim C. et al., 2009)

2.2.1.2 LentiKats®

LentiKats® refers to PVA lens-shaped hydrogel particles typically used for biocatalysts immobilization (Wittlich et al., 2004; Bouškova et al., 2011; Cárdenas-Fernández et al., 2012; Schenkmayerová et al., 2014; Krasňan et al. 2016). PVA is a hydrophilic polymer whose aqueous solutions spontaneously form hydrogen bonds between hydroxyl groups of the adjacent polymer chains over time, resulting in the creation of a non-covalent matrix (Figure 8a) (Wittlich et al., 2004). Thus produced porous hydrogel is stable to above 60 ºC and possesses excellent physico-mechanical characteristics, such as high elasticity and low

abrasion that provide for robustness and long lifetimes (Wittlich et al., 2004; Schenkmayerová et al., 2014). Besides, PVA is biologically non-degradable and has zero toxicity without any negative effect on the biochemical process, which makes it a desirable material for biocatalyst immobilization (Bouškova et al., 2011).

Difficulties with PVA application in biotechnology lay in the fact that a spontaneous gelation at temperatures above 0 ºC is a long-term process and the resulting hydrogels are too weak and inappropriate (Wittlich et al., 2004). The mechanical characteristics of PVA hydrogels were improved when the PVA solution was subjected to cryogelation (Lozinsky, 1998), or to gelation with boric acid (Wang H.-H. et al., 1999), but all procedures lead to the significant loss of immobilized biocatalyst activity (Wittlich et al., 2004; Krasňan et al., 2016). These problems were neutralized by Ding and Vorlop who developed a method based on the gelation under mild temperature and pH conditions, using non-toxic and inexpensive mixture of PVA and polyethylene glycol, and sodium sulfate as a stabilizing solution (Ding and Vorlop, 1995; Krasňan et al., 2016). Such gentle conditions allow the immobilization of any enzyme or microorganism and offer relatively simple production procedure and high retention of biocatalyst activity (Ding and Vorlop, 1995; Rebroš et al., 2007).

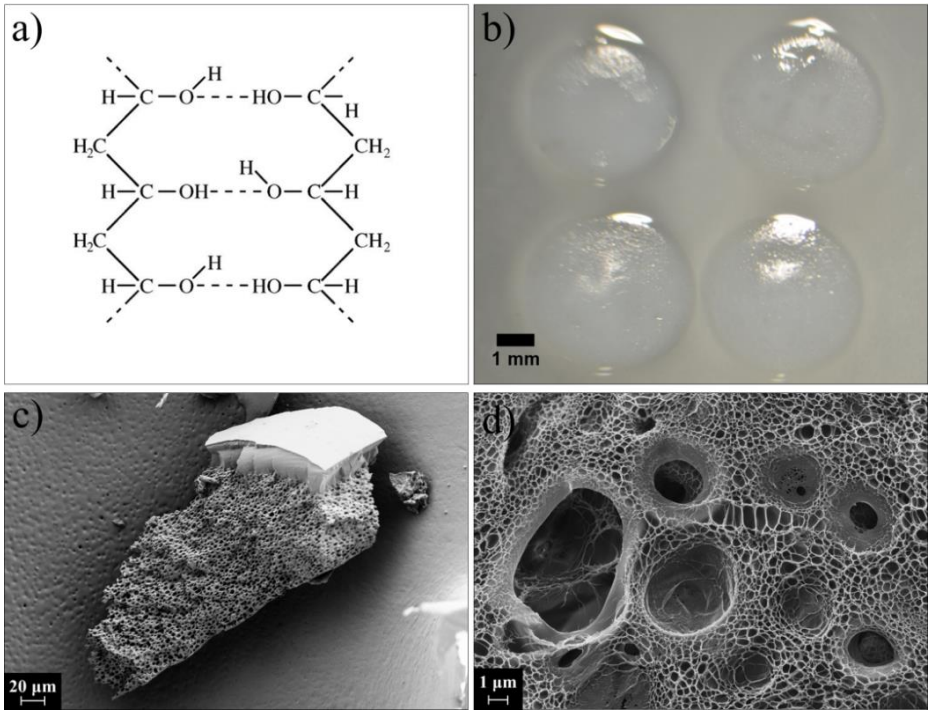

Figure 8: LentiKats®: a) chemical structure of PVA gel (Wittlich et al., 2004: 54); b) lens-shaped hydrogel particles; c) micrograph of fractured particle showing the outer layer and porous internal structure (photo: LentiKat's a.s., 2016; internal company's material); d) micrograph showing a detail of the internal porous structure (photo: LentiKat's a.s., 2016; internal company's material).

Slika 8: LentiKats®: a) kemijska struktura PVA gela (Wittlich in sod., 2004: 54); b) delci hidrogela v obliki leče; c) mikrograf odlomljenega delca, ki prikazuje zunanjo plast in porozno notranjo strukturo (slika: LentiKat's a.s., 2016; interni material podjetja); d) mikrograf, ki podrobno prikazuje notranjo porozno strukturo (slika: LentiKat's a.s., 2016; interni material podjetja).

Resulting PVA lens-shaped hydrogel particles, namely LentiKats® (Wittlich et al., 2004), are presented in Figure 8b. Controlled drying of particles enables the formation of a thin layer on the surface shown in Figure 8c, acting as a membrane with the molecular weight cut-off for polysaccharides and proteins of 7.6 and 14.2 kDa, respectively (Schenkmayerová et al., 2014). The particles have a porous 'sponge-like' internal structure with a pore size ranging between 1 and 10 µm (Figures 8c and 8d), and a lens shape that combines the advantages of small and large particles and favors diffusion due to the high surface-to-volume ratio (Wittlich et al., 2004). Diverse application of LentiKats® in biotechnology is distinctly featured in the review article by Krasňan et al. (2016).

2.2.2 Immobilization by adsorption on a carrier

Immobilization of a biocatalyst onto the surface of a carrier could be obtained *via* physical adsorption that includes non-specific (van der Waals forces), biospecific (using immobilized ligands), affinity (using immobilized dyes or metals), electrostatic (ionic) and hydrophobic interactions (Cao, 2005). This is probably the simplest method initiated only by the biocatalyst-carrier contact (Adlercreutz, 2013), and therewith it was among the first methods used for the enzyme immobilization (Nelson and Griffin, 1916).

Advantages of the immobilization by adsorption encompass the possibility for carrier reuse and potentially high retention of enzyme activity compared to the covalent attachment, which implies chemical modifications. Disadvantages include relative weakness of the interactions involved in the adsorption which may cause enzyme leakage from the support as well as change of the enzyme microenvironment leading to undesirable disruption of the forces that maintain the enzyme's native conformation (Cao, 2005).

Numerous carriers such as organic and inorganic polymers or mesoporous silica have been applied for immobilization by adsorption (Adlercreutz, 2013; Sheldon and van Pelt, 2013). The selected carrier has to meet certain physical and chemical requirements essential for an efficient immobilization. The physical requirements mainly relate to the particle size, i.e. indirectly sufficient surface area for immobilization (> 100 m^2 g^{-1}), capable of achieving high enzyme loads with an even monolayer distribution, as well as pore size large enough to be accessed by the enzyme and to avoid diffusion constraints (e.g. > 100 nm based on lipases) (Bosley, 1997; Cantone et al., 2013). Chemical requirements relate to the composition of the carrier, i.e. the nature of functionality that directly interacts with the enzyme (Cao, 2005).

2.2.2.1 Novozym® 435

Novozym® 435 represents one of the most popular catalysts available on the market. In this preparation, CaLB is immobilized on a hydrophobic macroporous polymeric resin (Lewatit VP OC 1600), which is based on methyl and butyl methacrylic esters cross-linked with divinylbenzene (Heinsman et al., 2003; Poojari and Clarson, 2013). Although the main enzyme-carrier interactions in Novozym® 435 are van der Waals forces, the immobilization is rather entropy driven, because the enzyme displaces a large number of water molecules from the carrier and its own surface. Such gain in entropy is also known as hydrophobic interaction (Hanefeld et al., 2009). However, these forces are relatively weak, and CaLB tends to leak from the carrier in the aqueous environments, which is the biggest problem to be solved in order to enhance the stability of Novozym® 435 (Wiemann et al., 2009a, 2009b; Saunders and Brask, 2010).

Observation of Novozym® 435 by infrared microspectroscopy has revealed that the radial distribution of CaLB is uneven, whereby the enzyme is localized in an outer shell of the particle (thickness 80–100 μm) in a non-uniform density throughout it, as depicted in Figure 9 (Mei et al., 2003). It has also been reported that the average pore size of Novozym® 435 is 100 nm, which is large enough to allow an unhindered diffusion of macromolecules with molecular masses up to 46 kDa (Mei et al., 2003; Wiemann et al., 2009a).

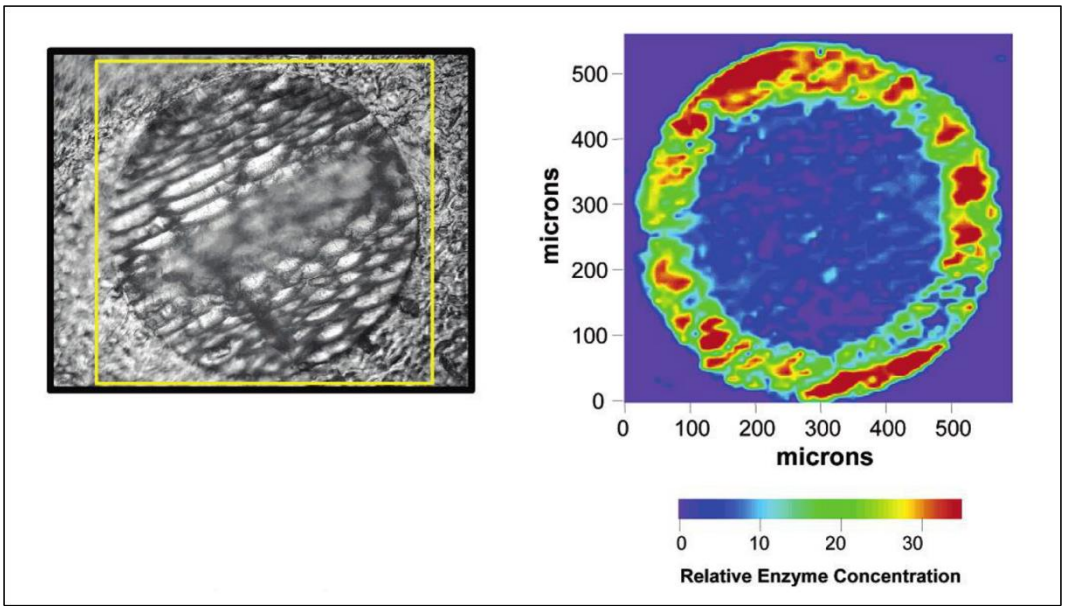

Figure 9: Visible light image (left) of a Novozym® 435 together with the area imaged by the infrared microscope (the yellow box), and the enzyme distribution (right) throughout the center section of the Novozym® 435 (Mei et al., 2003: 72).

Slika 9: Slika delca Novozym® 435 v vidnem spektru (levo) skupaj z površino, ki je posneta z infrardečim mikroskopom (rumeni kvadrat, levo) in porazdelitev encima po preseku Novozym® 435 delca (desno) (Mei in sod., 2003: 72).

Application of Novozym® 435 is widely discussed in the part considering CaLB (Section 2.1.2). The most important physical characteristics of commercial preparation Novozym® 435 are listed in Table 3.

Table 3: The most important physical characteristics of commercial preparation Novozym® 435.
Tabela 3: Najpomembnejše fizikalne lastnosti komercialnega pripravka Novozym® 435.

Characteristic	**Value**	**Reference**
Amount of CaLB	0.1 mg_{CaLB} mg_{N435}^{-1}	(Kundu et al., 2011)
Shell thickness	80–100 μm	(Mei et al., 2003)
Density	0.555 mg_{N435} μL^{-1}	(Denčić et al., 2013)
Diameter	315–1,000 μm	(Chen B. et al., 2008)
Moisture content	1%–2% (w/w)	(Chen H.-C. et al., 2011)
Specific surface area	130 m^2 g_{N435}^{-1}	(Chen B. et al., 2008)
Pore size	100 nm	(Mei et al., 2003)
Tortuosity	6	(Dong et al., 2010)
Porosity	0.5	(Dong et al., 2010)

2.3 MINIATURIZATION AND MICROSYSTEMS

The main feature of miniaturized reactors is their micro scale. Such reactors present a wide spectrum of devices fabricated predominantly by microengineering, with at least one characteristic dimension below 1 mm and surface-to-volume ratio much higher than traditional reactors, typically from 10,000 to 50,000 m^2 m^{-3} (Ehrfeld et al., 2001; Hessel et al., 2004; Renken and Kiwi-Minsker, 2010; Wirth, 2013). Continuous flow processing occurring under laminar flow conditions allows nearly gradientless mass and heat transfer leading to the process intensification (Kockmann, 2008; Pohar and Plazl, 2009; Wegner et al., 2011; Hessel et al., 2012). Good spatial and temporal control, as well as possibilities for building mobile manufacturing plants with reduced environmental, financial and safety burdens, are additional advantages of miniaturization (Wohlgemuth et al., 2015).

2.3.1 Transport phenomena at small scale

Miniaturized devices are endowed by reduced and precisely defined transport paths, and therefore momentum and mass transport occur in a very efficient manner and within short times (Kockmann, 2008). The ratio between surface and volume forces changes in favor of the first ones by switching to the small scale, whereby the relative importance of such forces

is represented by a set of dimensionless numbers. Some of the most important dimensionless numbers will be presented below, while the others could be found throughout the literature (Green and Perry, 2008; Berthier and Silberzan, 2010).

2.3.1.1 Fluid dynamics

The *Reynolds number* (*Re*) arises from the non-dimensionalization of the Navier-Stokes equation and reflects the relative importance of the inertial and viscous forces (Kumacheva and Garstecki, 2011; Marques and Fernandes, 2011). The three distinct parameters that *Re* (Equation 1) relies on are channel geometry, fluid properties embodied in its density (ρ) and dynamic viscosity (η), and flow conditions embodied in the mean superficial (or empty channel) fluid velocity (v), which is obtained when the volumetric flow rate is divided by the channel cross-sectional area. In the case of a fluid flow through the tubular channel, characteristic length (L) stands for the tube internal diameter, while in the case of a fluid flow through the rectangular channel L stands for the hydraulic diameter (d_h), as demonstrated by Equation 2.

$$Re = \frac{\text{inertial forces}}{\text{viscous forces}} = \frac{\rho\, v\, L}{\eta} \quad \text{... (1)}$$

$$L = d_h = \frac{4\, d\, w}{(2\, d + 2\, w)} \quad \text{... (2)}$$

Re	*Reynolds number [–]*
ρ	*fluid density [kg m^{-3}]*
v	*mean superficial fluid velocity [m s^{-1}]*
L	*characteristic length [m]*
d_h	*channel hydraulic diameter [m]*
η	*fluid dynamic viscosity [Pa s]*
d	*channel depth [m]*
w	*channel width [m]*

Values of *Re* in miniaturized devices are ordinarily small which implies laminar flow with typically parabolic velocity profile governed by the dominance of viscous forces over inertial ones (Atencia and Beebe 2005; Žnidaršič-Plazl and Plazl, 2011). Application of highly viscous fluids in miniaturized devices is therefore disadvantageous because it may cause a large friction between the fluid and channel surface that leads to the high pressure drop and consequently high energy dissipation.

Another significant dimensionless number is the *capillary number* (*Ca*), which compares viscous and interfacial forces and allows a distinction between two-phase flow patterns and the mechanism of droplet break-up (Equation 3) (Kumacheva and Garstecki, 2011; Zhao and Middelberg, 2011).

$$Ca = \frac{\text{viscous forces}}{\text{interfacial forces}} = \frac{\eta\, v}{\gamma} \quad \text{... (3)}$$

Ca *capillary number [–]*
γ *interfacial tension [N m^{-1}]*

In the case of droplet formation, the calculation of *Bond number* (*Bo*) could tell us if the droplets will adopt a flattened shape (*Bo* > 1) determined mostly by the gravitational effects, or the shape of a sphere (*Bo* < 1) determined mostly by the interfacial forces (Equation 4) (Kumacheva and Garstecki, 2011; Zhao and Middelberg, 2011).

$$Bo = \frac{\text{gravitational force}}{\text{interfacial forces}} = \frac{\Delta\rho\, g\, L^2}{\gamma} \quad \text{... (4)}$$

Bo *Bond number [–]*
$\Delta\rho$ *fluid density difference [kg m^{-3}]*
g *gravitational acceleration [m s^{-2}]*

Finally, the relative importance of the inertial and viscous forces on the motion of an interface between two immiscible fluids is given by the *Ohnesorge number* (*Oh*) (McKinley and Renardy, 2011), which is oftentimes also called "the *Reynolds number* for free surface flows" (Equation 5) (Kumacheva and Garstecki, 2011; Zhao and Middelberg, 2011).

$$Oh = \frac{\text{viscous forces}}{\text{inertial forces}} = \frac{\eta}{(\rho\, \gamma\, L)^{1/2}} = \left(\frac{Ca}{Re}\right)^{1/2} \quad \text{... (5)}$$

Oh *Ohnesorge number [–]*

The hydrodynamic behavior of flowing systems is extensively characterized using the residence time distribution (RTD) analysis (Levenspiel, 1999). Briefly, a given volume of fluid entering the system at time t_0 can be partitioned into fractional volumes that exit the system after t_0. The fractional volumes could take various paths through the reactor causing different lengths of time to pass through it, and hence creating a distribution that can be plotted *versus* time. Such obtained distribution of times is a density function denoted as $E(t')$ which is in continuous form described by the convolution integral (Equation 6) (Levenspiel, 1999).

$$C_{out}(t) = \int_0^t C_{in}(t - t')\, E(t')\, \mathrm{d}t' \qquad \text{... (6)}$$

$C_{out}(t)$	*output signal*
$C_{in}(t-t')$	*input signal*
t	*time [min]*
t'	*relative time with respect to when a particular volume enters the system [min]*
E	*exit age distribution [min^{-1}]*

Although the four moments of distribution may be calculated (mean, variance, skewness and kurtosis), the mean and variance are particularly useful in the analysis, since they present the average age of the fluid exiting the system and variation of fluid age or dispersion, respectively (Levenspiel, 2012; Coblyn et al., 2016). The easiest way for obtaining the RTDs is to inject a known concentration of a non-reactive tracer as a pulse or step input and to follow its outlet concentration (Levenspiel, 1999, 2012).

In practical terms, RTD analysis helps in detection of possible presence of stagnant flow regions or flow maldistribution (channeling, bypassing and recirculation) in the reactor. The method has been used to study hydrodynamic behavior of miniaturized reactors in general (Trachsel et al., 2005; Bošković et al., 2011; Cantu-Perez et al., 2011; Georget et al., 2013; Kashid et al., 2015; Coblyn et al., 2016), as well as MPBRs (Tang et al., 2004; Márquez et al., 2008; Faridkhou et al., 2013).

2.3.1.2 Mass transfer

Transport of reactant species at small scale occurs merely by molecular diffusion defined by Fick's law, as demonstrated by Equation 7 (Cussler, 2009).

$$N = -D\,\frac{\partial C}{\partial x} \qquad \text{... (7)}$$

N	*molar flux [mol m^{-2} s^{-1}]*
D	*diffusion coefficient [m^2 s^{-1}]*
C	*concentration [mol m^{-3}]*
x	*space coordinate [m]*

Although molecular diffusion coefficient (D) can be determined by different experimental methods (Fate and Lynn, 1990; Delgado et al., 2005; Miložič et al., 2014), in the practical work one often uses an appropriate empirical correlation from several of them that have been proposed for a quick estimation of this constant (Scheibel, 1954; Wilke and Chang, 1955; Reddy and Doraiswamy, 1967; Lusis and Ratcliff, 1968; Hayduk and Laudie, 1974). Certainly one of the most commonly used correlations is the empirically modified Stokes-

Einstein equation proposed by Wilke and Chang (1955) (Equation 8). This correlation is employed for the estimation of diffusivity of a solute in a solvent, usually in the liquid binary mixtures of non-electrolytic and low molecular weight chemical species and has an estimated error up to 20% (Li and Carr, 1997).

$$D = \frac{7.4 \times 10^{-8} \, (\Phi_B \, M_B)^{0.5} \, T}{\eta_B \, V_A^{0.6}} \quad \text{... (8)}$$

Φ_B *association factor of the solvent [–]*
M_B *molecular weight of the solvent [g mol^{-1}]*
T *temperature [K]*
η_B *dynamic viscosity of the solvent [mPa s]*
V_A *molar volume of the solute [mL mol^{-1}]*

Mass transfer limitations at small scale are stated to be less pronounced when compared to the large-scale reactors, but they are still present and have to be taken into consideration (Walter et al., 2005; Roy et al., 2011). They are especially important in miniaturized biocatalytic reactors where an integrated approach addressing biocatalyst features, reaction kinetics, mass transfer, and reactor engineering is required (Marques and Fernandes, 2011; Karande et al., 2016). Renken and Kiwi-Minsker (2010) have defined a time scale showing that the physical processes (mixing, heat and mass transfer) occur within the characteristic times roughly spanning from 10 to 10^{-3} s for conventional and from 10^{-2} to 10^{-5} s for microstructured reactors. Therefore, it is essential that the reaction time scales are within the same time window as the time scales of physical processes, i.e. preferably one order of magnitude higher, in order to completely eliminate mass transfer limitations (Kiwi-Minsker, 2010; Hartman et al., 2011). Stemming form this, it would be meaningful to merge microstructured reactors only with very fast reactions having a time scale in the range of 10^{-3} to 10^{-5} s (Kiwi-Minsker, 2010; Karande et al., 2016). For example, Karande et al. (2016) have calculated that a poorly soluble (< 20 mM) organic compound would require 20 to 0.2 s for the conversion in an aqueous environment assuming the presence of an enzyme (1 mM) with the average turnover number (k_{cat}) estimated to be between 1 and 100 s^{-1}.

Dimensionless *Damköhler number* (*Da*) is also very convenient tool for the time-scale analysis because it relates transport time of reacting species (τ_t) and reaction time (τ_r), as shown in Equation 9 (Berthier and Silberzan, 2010).

$$Da = \frac{\text{transport time}}{\text{reaction time}} = \frac{\tau_t}{\tau_r} \quad \text{... (9)}$$

Da *Damköhler number [–]*
τ_t *transport time [s]*
τ_r *reaction time [s]*

There are two *Damköhler numbers* that correlate the reaction rate with convective (Da_{I}) or diffusive (Da_{II}) transport (Kockmann, 2008). It is considered that the mass transfer is the rate limiting step of the overall process if $Da >> 1$, whereas for $Da << 1$ the overall process is limited by reaction rate (Marques and Fernandes, 2011). However, a generic model-based methodology for evaluation of mass transfer limitations in micro devices could give better predictions for the reactor design (Van Daele et al., 2016).

Characteristic diffusion ($\tau_{t\text{-}diff}$) and reaction times are given by Equations 10 and 11, respectively (Swarts et al., 2010; Hartman et al., 2011; Bolivar and Nidetzky, 2013).

$$\tau_{t\text{-}diff} = \frac{x^2}{D} \quad \text{... (10)}$$

$$\tau_r = \frac{C_{Sin}}{v_0 \, C_e} \quad \text{... (11)}$$

$\tau_{t\text{-}diff}$ *transport time by diffusion [s]*
C_{Sin} *substrate inlet/initial concentration [mol m^{-3}]*
v_0 *initial reaction rate [mol g^{-1} s^{-1}]*
C_e *enzyme concentration expressed per reactor volume [g m^{-3}]*

In the flow reaction concepts, the ratio embodied in the dimensionless *Péclet number* (Equation 12) should be used to quantify the dominance of convective ($Pe > 1$) or diffusive ($Pe < 1$) mass transport in the system (Kockmann, 2008; Hartman et al., 2011).

$$Pe = \frac{\text{convective transport}}{\text{diffusive transport}} = \frac{v \, l}{D} \quad \text{... (12)}$$

Pe *Péclet number [–]*
l *channel length [m]*

2.3.2 Droplet generation in miniaturized devices

High-throughput microfluidic devices with different channel geometries capable of performing diverse 'digital fluidic' operations are widely applied for generation of monodispersed droplets (Teh et al., 2008; Kumacheva and Garstecki, 2011; Mashaghi et al., 2016). The most commonly used geometry is a T-junction (Figure 10), firstly introduced by Thorsen et al. (2001), in which the mechanism of droplet formation has recently been extensively studied (Bai et al., 2016; Chen S. et al., 2016; Pang et al., 2016; Soh et al., 2016; Prileszky et al., 2016; Yagodnitsyna, et al., 2016).

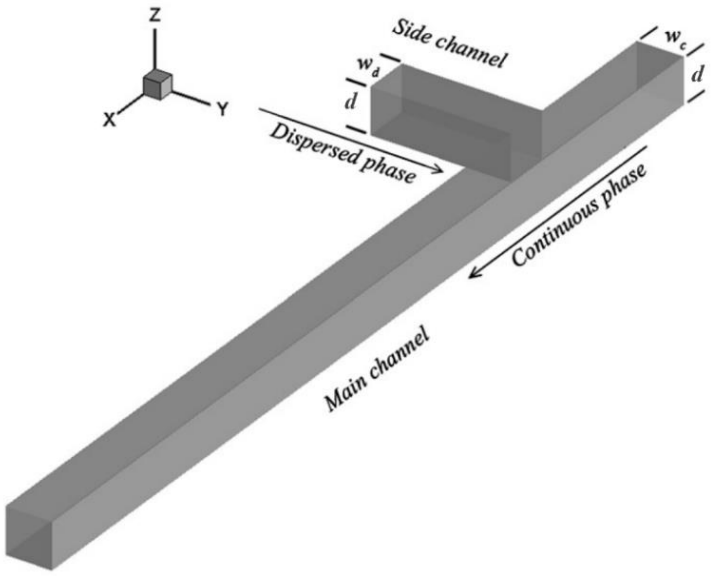

Figure 10: An example of a microfluidic T-junction presented in 3D geometry (Yang et al., 2013: 103).
Slika 10: Primer mikrofluidnega T-stičišča, predstavljenega v 3D geometriji (Yang in sod., 2013: 103).

Generation of droplets in a T-junction is based on an emulsification of two immiscible fluids, e.g. an oil and water, resulting in an inverted water-in-oil emulsion (Xu J. H. et al., 2006a). The fluid with higher viscosity (oil) enters the main channel as the continuous phase, while the fluid of less viscosity that is to be dispersed (water) enters the side channel (Figure 10). The system dynamics is determined by three groups of parameters (Bai et al., 2016). The first group involves the structural parameters specified by the channel aspect ratio (d/w_c) and the ratio of inlet channels widths (w_d/w_c), where the subscripts d and c denote droplet (discontinuous/dispersed) and continuous phase, respectively (Figure 10). The second group involves the operating conditions, i.e. the flow rates of a droplet (Q_d) and a continuous (Q_c) phase, as well as their flow ratio (Q_d/Q_c). Finally, in the third group are parameters related to the fluids' physical properties like viscosities and their ratio (η_d/η_c), densities and their ratio (ρ_d/ρ_c) and the interfacial tension between them (γ). The channel wall wettability and possible application of surfactants also play a big role in this process (Dreyfus et al., 2003; Kumacheva and Garstecki, 2011).

When *Ca* decreases below a certain limiting value, the dominant surface tension forces break the fluid into droplets and minimize the interfacial area, which is a phenomenon known as Rayleigh-Plateau instability (Kumacheva and Garstecki, 2011). Four different flow patterns have been observed during the droplet formation in a T-junction using highly viscous fluids: laminar, squeezing, dripping and jetting (Figure 11) (Bai et al., 2016).

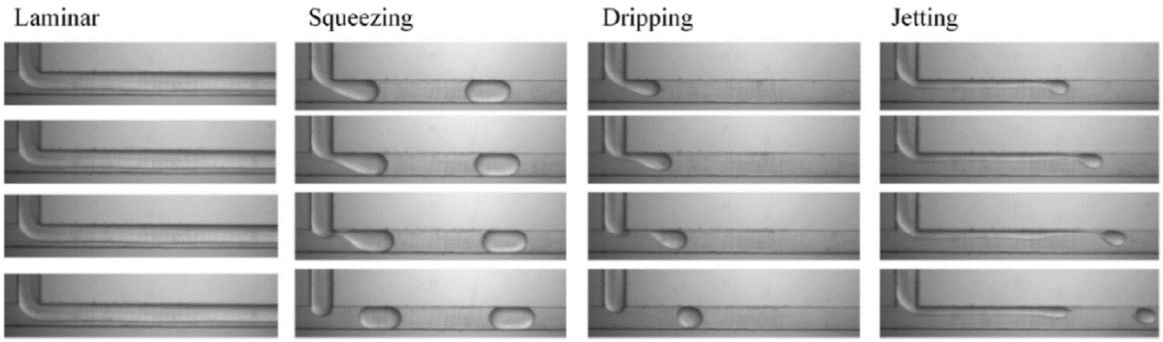

Figure 11: Micrographs of typical flow patterns in a T-junction (Bai et al., 2016: 145).
Slika 11: Mikrografi tipičnih tokovnih režimov tekočine v T-stičišču (Bai in sod., 2016: 145).

2.3.2.1 Production of alginate microparticles using miniaturized devices

The principles of droplet-based microfluidics can bring enormous benefit in the production of various polymeric microparticles (Xu S. et al., 2005; Dendukuri and Doyle, 2009; Wang J.-T. et al., 2011; Wan, 2012; Zamora-Mora et al., 2014; Marquis et al., 2015). Monodisperse droplets generated by means of microfluidic devices are usually subjected to solidification in order to obtain mechanically and chemically stable as well as advanced and multipurpose microparticles (Zhang et al., 2007; Dendukuri and Doyle, 2009; Huang K.-S. et al., 2011; Wan, 2012).

Alginate, as well as other biopolymers, are widely used to produce microparticles and therefore the routes for its production in microfluidic systems are widely explored (Zhang et al., 2007). If an aqueous solution of alginate is used as a droplet phase and an oil as a continuous phase, then is possible to produce a stable emulsion resulting in the formation of monodispersed alginate droplets (Capretto et al., 2010; Chen W. et al., 2013). So far, alginate droplets formation was done using 'in-house' produced microfluidic devices with channel geometries such as flow-focusing (Zhang et al., 2006; Dang and Joo, 2013), or cross- (Huang K.-S. et al., 2006, 2007; Xu J. et al., 2008; Lin et al., 2013), Y- (Capretto et al., 2008, 2010), and T-junction (Tan and Takeuchi, 2007; Amici et al., 2008; Yeh C.-H. et al., 2009). Utilization of devices with even more complex manifold structure is also reported in the literature (Chuah et al., 2009; Kim C. et al., 2014).

Alginate droplets produced in this fashion were further solidified by applying internal (Tan and Takeuchi, 2007; Zhang et al., 2007; Liu L. et al., 2013; Akbari and Pirbodaghi, 2013) or external (Zhang et al., 2007; Capretto et al., 2008, 2010; Yeh C.-H. et al., 2009; Chuah et al., 2009; Hu et al., 2012; Chen W. et al., 2013) gelation procedure, done either *in situ* (Zhang et al., 2006; Choi C.-H. et al., 2007; Xu J. et al., 2008) or *ex situ* (Yeh C.-H. et al., 2009; Capretto et al., 2010; Dang and Joo, 2013; Lin et al., 2013). The latter one sometimes results in formation of tail-shaped (also 'teardrop-shaped' or 'tadpole-shaped') microparticles

(Capretto et al., 2008, 2010; Hu et al., 2012; Dang and Joo 2013; Lin et al., 2013; Wang Q. et al., 2015), which is undesirable in the most cases. Otherwise, alginate microparticles have a big potential as biocatalysts carriers and as such for successful application in packed bed reactors (Shin J.-S. et al., 2001b; Tepe and Dursun, 2008; Al-Mayah, 2012; Hussain et al., 2015).

2.3.3 Miniaturized packed bed reactors

System miniaturization has emerged as an efficient tool for biocatalytic processes development and intensification (Bolivar and Nidetzky, 2013; Krühne et al., 2014; Wohlgemuth et al., 2015; Laurenti and dos Santos Vianna Jr., 2016). Different types of miniaturized enzymatic bioreactors have been presented so far, including those with free biocatalyst in one phase (Tišma et al., 2009; Kolfschoten et al., 2011; Rosinha Grundtvig et al., 2017), in a two-phase system with parallel flow (Žnidaršič-Plazl and Plazl, 2009; Marques et al., 2012) and in a two-phase system with droplet or segmented flow (Pohar et al., 2009, Šalić et al., 2011; Novak and Žnidaršič-Plazl, 2013; Novak et al., 2016) (Figures 12a–12c). Besides, biocatalysts could be immobilized on a membrane placed in a microreactor (Honda et al., 2006; Machsun et al., 2010), on a microreactor inner surface by silanization (Stojkovič and Žnidaršič-Plazl, 2012; Stojkovič et al., 2014) or using Z_{basic2} tag (Bolivar et al., 2016; Miložič et al., 2017), on the inner surface and pillars (Koch et al., 2008), on nanosprings inserted in microreactors (Schilke et al., 2010; Fu et al., 2012), as well as immobilized into different particles packed in the reactor (Cvjetko et al., 2012; Pohar et al., 2012) (Figures 12d–12h). Magnetic field-assisted microreactors have also been reported as efficient biocatalytic systems (Šalić et al., 2013, 2016).

Generally, packed bed reactors (Figure 12h) have a simple but concurrently conducive design made of a column/channel packed with catalytic particles continuously perfused by medium (liquid, gas or both in the case of multiphase reactors) containing reactants (Obradovic et al., 2004; Warnock et al., 2005). MPBRs are capable of providing relatively small pressure drops, but also a large surface area for liquid-particle contact, biocatalyst reusability without prior separation, high biocatalyst load and long-term operational life (Pohar et al., 2012; Žnidaršič-Plazl, 2014; Wohlgemuth et al., 2015).

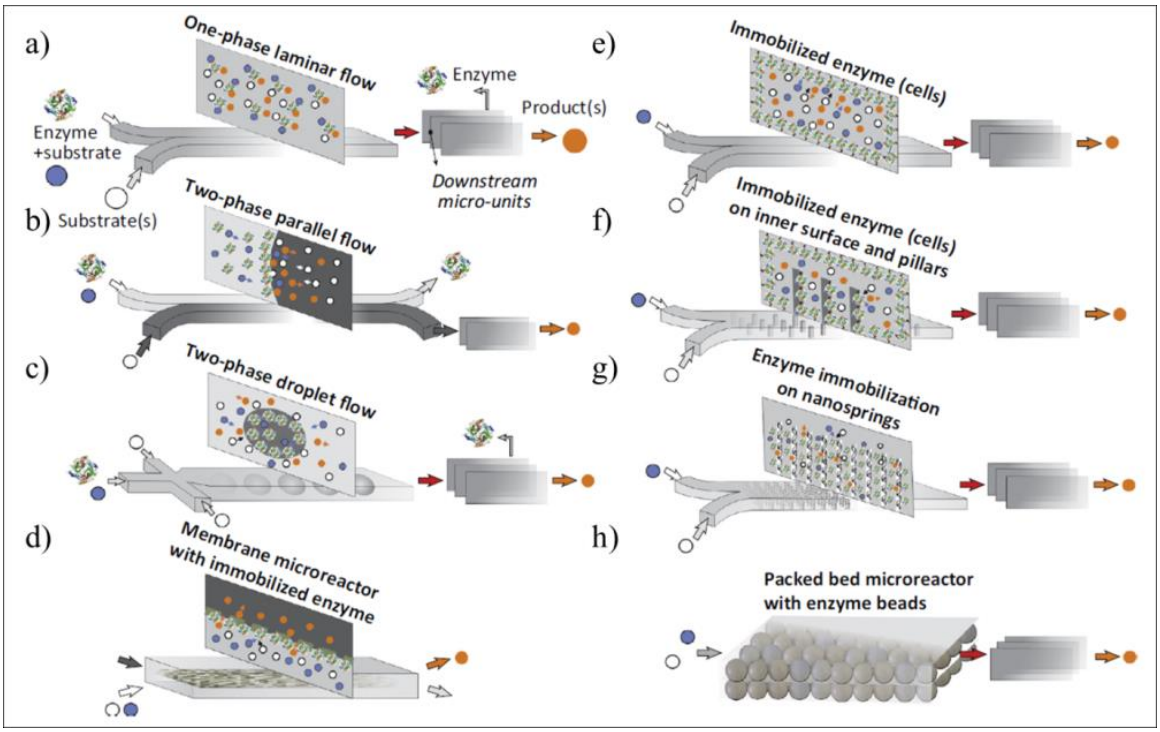

Figure 12: Types of miniaturized reactors for biocatalytic processes: a) reactor with free biocatalyst in an one-phase laminar flow; b) reactor with free biocatalyst in a two-phase parallel flow; c) reactor with free biocatalyst in a droplet flow; d) reactor with biocatalyst immobilized on the membrane; e) reactor with biocatalyst immobilized on the inner surface of a microchannel; f) reactor with biocatalyst immobilized on the inner surface and pillars; g) reactor with nanospring supports for biocatalyst immobilization and h) packed bed reactor with particles containing immobilized biocatalyst (Wohlgemuth et al., 2015: 309).

Slika 12: Vrste miniaturiziranih reaktorjev za biokatalitske procese: a) reaktor s prostim biokatalizatorjem v enofaznem laminarnem toku; b) reaktor s prostim biokatalizatorjem v dvofaznem vzporednem toku; c) reaktor s prostim biokatalizatorjem v kapljičastem toku; d) reaktor z biokatalizatorjem, ki je imobiliziran na membrano; e) reaktor s biokatalizatorjem, ki je imobiliziran na notranjo površino mikrokanala; f) reaktor s biokatalizatorjem, ki je imobiliziran na notranjo površino mikrokanala in stebre; g) reaktor z nanovzmetmi za imobilizacijo biokatalizatorja, in h) reaktor s strnjenim slojem, ki vsebuje delce z imobiliziranim biokatalizatorjem (Wohlgemuth in sod., 2015: 309).

2.3.3.1 Design and characteristics of miniaturized packed bed reactors

MPBRs are designed to act as an easily assembled, reusable, robust and chemically inert casing for performing processes under a wide range of operational conditions. They could be produced from materials such as glass (Azevedo et al., 2004a), stainless steel (Tomin et al., 2010), aluminium (Kundu et al., 2011), polydimethylsiloxane (PDMS) (Wang J. et al., 2014), fluorinated ethylene propylene (FEP) (Halim A. A. et al., 2013) and poly(methyl methacrylate) (PMMA) (Cvjetko et al., 2012; Pohar et al., 2012). Even an HPLC column could be used as an MPBR (Babich et al., 2012). However, the priority is given to glass and polymer-based materials due to their transparency, low-cost and facile processing (Pohar et al., 2012). A simple and efficient catalyst load could be achieved by using modular,

'sandwich-like' assembled MPBRs, but a special attention has to be devoted to an efficient sealing system in order to avoid fluid leakage (Kundu et al., 2011; Pohar et al., 2012).

The overall volumetric productivity represents the average reactor production capacity per unit of volume and time, and its maximization stands for minimization of the investment and operating costs (Cabral and Tramper, 2005). The amount of product that can be produced per mass of biocatalyst (biocatalyst productivity number, *BPN* (Valinger et al., 2014)) is another important parameter and its maximization is highly desirable for the favorable process economy (Tufvesson et al., 2015). The reactor efficiency is not limited only by biocatalyst concentration and its activity, but also by physical constraints such as hydrodynamics and mass transfer (Cabral and Tramper, 2005). Therefore, maximization of these parameters is expected in MPBRs, since they can provide facilitated mass transfer and more favorable hydrodynamics compared to their large-scale counterparts, which for the same purpose require an initial fluid distribution performed with various types of complex and usually very expensive fluid distributors (Bozzano et al., 2014a, 2014b).

In order to estimate the fluid flow characteristics in packed bed reactors, the *Reynolds number* has been modified into the particle *Reynolds number*, Re_p (Equation 13) which can be calculated based on the equivalent particle diameter (d_e) and the mean interstitial fluid velocity (v_i) that prevails in the spaces between the packing material, indicated by Equation 14 (Dwivedi and Upadhyay, 1977; Delgado, 2006).

$$Re_p = \frac{v_i \, d_e \, \rho}{\eta} \quad \text{... (13)}$$

$$v_i = \frac{v}{\varepsilon} \quad \text{... (14)}$$

Re_p	*particle Reynolds number [–]*
v_i	*mean interstitial fluid velocity [m s^{-1}]*
ε	*bed porosity [–]*
d_e	*equivalent particle diameter[m]*

Besides, there are two additional equations for Re_p, but Equation 13 is the most commonly used for the liquid-phase packed bed reactors (Dwivedi and Upadhyay, 1977). The flow regime is assumed to be laminar if $Re_p < 10$, transitional if $10 \leq Re_p \leq 300$ and turbulent if $Re_p > 300$ (Ribeiro et al., 2010). Re_p is also used to evaluate a friction factor caused by fluid flow, i.e. the pressure drop through the packed bed, which might be predicted by the Ergun equation (Equation 15) (Ergun and Orning, 1949; Ozahi et al., 2008).

$$\frac{\Delta p}{l} = 150\ \frac{(1-\varepsilon)^2}{\psi^2\ \varepsilon^3}\frac{\eta\ v}{{d_p}^2} + 1.75\ \frac{1-\varepsilon}{\varepsilon^3}\ \frac{\rho\ v^2}{\psi\ d_p} \qquad \text{... (15)}$$

Δp *pressure drop [Pa]*
ψ *particle sphericity [–]*
d_p *particle diameter [m]*

Particles' shape, size distribution and packing arrangement (e.g. loose, dense, uniform, random) in general determine the void size distribution and consequently play a significant role on the pressure drop and hydrodynamics in packed bed reactors (Allen et al., 2013; Faridkhou and Larachi, 2014; Koekemoer and Luckos, 2015; Du et al., 2016).

In heterogeneous liquid-solid (bio-)catalysis performed on meso and macro scales, the reactor effectiveness often depends on the rate of transport of reactant(s) to and product(s) from the biocatalyst particle (external mass transfer), as well as on the rate of transport inside the immobilized system (internal mass transfer) (Buchholz et al., 2012; Doran, 2013; Illanes et al., 2014). External transfer occurs in the bulk of the flow, where reactants have to exceed a certain pathway and to diffuse through a hypothesized stagnant hydrodynamic boundary layer surrounding the solid (bio-)catalyst, and imposing the most prominent mass transfer resistance (Doran, 2013). The mass transfer through this layer as the rate-limiting factor highly depends on the reactor hydrodynamics (applied flow rate/mixing speed and fluid viscosity), and is expected to appear in e.g. mixed batch reactors with submerged (bio-)catalytic particles or meso-scaled packed bed reactors whereby it can be diminished by increasing the agitation speed/fluid velocity (Trubiano et al., 2006; Halim S. F. A. et al., 2009; Dong et al., 2010). Many authors consider the hydrodynamic boundary layer as a significant mass transfer limitation factor in the MPBRs (Tidona et al., 2012; Denčić et al., 2013; Faridkhou et al., 2016), but more likely that is not the case because the layer should have to be enough thick (presumably in the length scale of μm) to cause a significant resistance. If we take into consideration the length scale of the MPBRs and the size of employed catalytic particles, the existence of the layer could be neglected. An overview of the most commonly used particles/carriers in MPBRs is given elsewhere in the literature (Bajić et al., 2017).

However, the MPBRs are not deprived of the internal mass transfer limitations caused by the nature and/or size and shape of the carrier. The movement of reactant molecules and possible mass transfer limitations in the interior of a porous particle (e.g. a hydrogel particle) is highly dependent on its structure that might impose a big resistance to molecular diffusion towards the interior. In that case the diffusion decreases and becomes lower than the diffusion in the aqueous phase without any limitations, which stands for so-called effective diffusivity (Willaert et al., 2004). This happens due to exclusion and obstruction effects caused by supporting material because a portion of the total volume is unapproachable for

diffusing molecules leading to longer diffusional path lengths (Amsden, 1998). The path length depends on the size of the (bio-)catalyst particle (a bigger particle leads to longer path of reactant to be surmounted in order to reach the (bio-)catalyst's active site), and its morphology (primarily porosity and tortuosity) (Willaert et al., 2004; Matyka et al., 2008). The effect of both particle porosity (ε_p) and tortuosity (ζ_p) on the effective diffusivity coefficient (D_e) can be represented by Equation 16 (Willaert et al., 2004).

$$D_e = \frac{\varepsilon_p}{\zeta_p} D \qquad \text{... (16)}$$

D_e *effective diffusion coefficient [$m^2\ s^{-1}$]*
ε_p *particle porosity [–]*
ζ_p *particle tortuosity [–]*

In heterogeneous biocatalysis the mass transfer phenomena occur simultaneously with the reaction, and due to it these two processes are interdependent and have to be observed as a whole (Doran, 2013). Instead of tedious estimation of the influence of external and internal mass transfer limitations using proposed dimensionless numbers (such as *Observable* and *Weisz's* modulus), one can perform an analysis of characteristic times pertinent to the overall process flow to see which phenomenon imposes the largest resistance (Bolivar and Nidetzky, 2013; Jovanovic et al., 2015; Miložič et al., 2017). Apropos the time-scale analysis, the characteristic diffusion time in a porous particle (τ_p) can be defined as demonstrated by Equation 17 (Jovanovic et al., 2015), and used for the analysis in packed bed reactors.

$$\tau_p = \frac{{d_e}^2}{4\, D_e} \qquad \text{... (17)}$$

τ_p *diffusion time in a porous particle [s]*

Quantification of the dominance of convective or diffusive transport in packed bed reactors is usually done using (equivalent) particle diameter as the characteristic length, which is defined by the *Péclet number* for inert particle (Pe_p), as indicated by Equation 18 (Delgado, 2006; Márquez et al., 2008).

$$Pe_\mathrm{p} = \frac{v_i\, d_e}{D} \qquad \text{... (18)}$$

Pe_p *Péclet number for inert particle [–]*

2.3.3.2 Biotransformations in miniaturized packed bed reactors

Trends in the application of miniaturized reactors have been striving towards broader utilization of MPBRs for continuous biocatalytic processes. The highest number of continuously operated MPBRs reported so far has been used for lipase-catalyzed biotransformations (Veny et al., 2014; Csajági et al., 2008; Falus et al., 2010; Tomin et al., 2010), especially those utilizing Novozym® 435 as a biocatalyst for ester synthesis (Woodcock et al., 2008). Very notable studies consider application of Novozym® 435 for synthesis of isoamyl acetate (Cvjetko et al., 2012), propyl caffeate (Wang J. et al., 2013), caffeic acid phenethyl ester (Wang J. et al., 2014), and butyl butyrate in a selected ionic liquid (Pohar et al., 2012) or in a solvent-free system using a high concentration of one substrate (Denčić et al., 2013). Solvent-free approach has also been applied for biolubricant production (Madarász et al., 2015). Furthermore, the first continuous enzyme-catalyzed polymerization reaction in a packed bed microreactor was performed with Novozym® 435 (Kundu et al., 2011). The chemo-enzymatic oxidation of alkenes in a borosilicate glass capillary with Novozym® 435 was also reported (Wiles et al., 2009).

Besides lipase-based processes, *E. coli* cells overexpressing ω-TA attached to methacrylate beads were used in an MPBR for the efficient and clean synthesis of chiral amines in methyl *tert*-butyl ether (Andrade et al., 2014). Alcohol oxidase (Azevedo et al., 2004a) and horseradish peroxidase (Azevedo et al., 2004b) covalently immobilized on a controlled pore glass were employed in an MPBR used for analytics. Removal of endocrine disrupting chemicals was reported in meso-scale packed bed reactors using laccase immobilized in a sol-gel matrix (Lloret et al., 2011) and on Eupergit® (Lloret et al., 2012). Furthermore, an immobilized β-galactosidase was broadly applied for various biotransformations using micro- and meso-scaled MPBRs (Sotowa et al., 2005; Fischer et al., 2013; Warmerdam et al., 2014; Sen et al., 2014).

Other reported biocatalytic processes with continuously operated enzymatic micro- and meso-scaled MPBRs encompass sucrose hydrolysis (Carvalho and Fernandes, 2015), steroid biotransformations (Marques et al., 2012), ellagic acid production (Buenrostro-Figueroa et al., 2014), synthesis of phenylserine (Tibhe et al., 2013), kinetic resolution of chiral amines (Shin J.-S. et al., 2001b) and *de novo* designed multi-step synthesis of a chiral amino alcohol (Halim A. A. et al., 2013). Meso- and micro-scaled MPBRs with immobilized enzymes have also found application as efficient analytical tools for determination of kinetic parameters providing low material consumption (Seong et al., 2003; Kerby et al., 2006; Özdural et al., 2008). In addition, magnetic field-assisted enzymatic MPBRs with trypsin immobilized on nano- and microparticles have been reported as an easily fabricated and efficient tool for protein digestion (Liu J. et al., 2007; Li Y. et al., 2007).

The MPBRs utilizing PVA particles with immobilized naringinase and ω-TAs were employed for naringin hydrolysis (Nunes et al., 2014) and asymmetric synthesis of MPPA (Heintz, et al., 2016b), respectively.

2.3.3.3 Mathematical modeling of miniaturized packed bed reactors

In the engineering practice, mathematical models and numerical simulations are prominent tools that could be of paramount importance for design and optimization of miniaturized devices at the expense of time and costs (Bodla et al., 2013; Jovanovic et al., 2015; Lubej et al., 2015; Miložič et al., 2017). *In silico* process data acquiring has been recently successfully performed for studying of various catalytic and non-catalytic packed bed reactors (Rong et al., 2013; Pohar et al., 2014; Tran et al., 2014; Boccardo et al., 2015; Dorn and Hekmat, 2016; Mohanty et al., 2016; Kashani et al., 2016; Singhal et al., 2016; Das et al., 2017). However, the exact mathematical description of a packed bed reactor is not an easy task due to complex physical and chemical phenomena simultaneously taking place in heterogeneous systems (Iordanidis, 2002; Froment et al., 2011; Petera et al., 2013). Diffusion-reaction dynamics in a (bio-)catalytic packed bed reactor with (bio-)catalysts immobilized in a porous carrier depends on many parameters, whereby the most of them can hardly be individually and independently evaluated, and hence more detailed models may suffer from a low accuracy (Iordanidis, 2002; Froment et al., 2011; Doran, 2013).

On this basis, it can be concluded that there is no a universal model, and different model simplifications capturing the most important features of the system under consideration are often applied to describe packed bed reactors (Iordanidis, 2002). One of the most common approaches involves a continuum-based heterogeneous model in which the physical domain is separated into two parts: the fluid phase comprising convective and diffusive transport of species around the particle, and solid (carrier) phase usually comprising only diffusive transport (if the biocatalyst is not immobilized on the carrier's surface, which implies the absence of the internal mass transfer) (Iordanidis, 2002; Allain and Dixon, 2010; Petera et al., 2013; Dixon et al., 2014). Anyhow, modeling of packed bed reactors was also discussed in another, simpler ways in the literature (Iordanidis, 2002).

In respect of the MPBRs with immobilized enzymes, there are several studies proposing different mathematical models (Azevedo et al., 2004a; Pohar et al., 2012; Denčić et al., 2013; Fischer et al., 2013; Tibhe et al., 2013). The study by Pohar et al. (2012) is particularly interesting because it basically can be applied to the MPBRs with Novozym® 435 developed in this work, and some conclusions stemming from the reported kinetic model are discussed in Section 4.3.5. On the other hand, a detailed mathematical model capable of predicting the performance of an MPBR with LentiKats® is lacking in the literature, and due to it a proposal on how the model could be developed is presented in Annex A. However, the proposed

model does not contain the kinetic parameters which are necessary in order to perform a simulation, but they could be obtained using one of the ways described for various ω-TAs (Shin and Kim, 1998; Tufvesson et al., 2014; Börner et al., 2016).

2.3.4 Scale-up of miniaturized devices

Successful scale-up of a biocatalytic process from lab to the industrial scale is the key point towards the practical, economically competitive and sustainable application of biocatalysis (Tufvesson et al., 2010). Nevertheless, this is not an easy task since the hydrodynamics and mass transfer which govern any biocatalytic process are scale dependent, and the scale-up of the reactor would typically lead to the reduced process performances (Marques et al., 2010; Duduković and Mills, 2015; Najafpour, 2015; Morchain, 2017). The main issue is how to efficiently scale-up devices that operate over the length scales spanning from micrometers to millimeters and corresponding time scales from microseconds onwards (Figure 13).

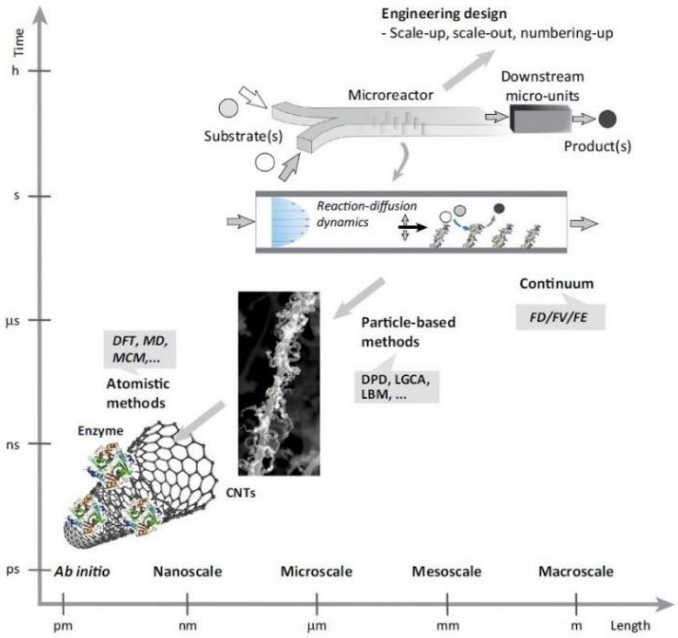

Figure 13: An example of the various time and space scales encountered in hierarchical multiscale modeling (Wohlgemuth et al., 2015: 311).

Slika 13: Primer različnih časovnih in prostorskih nivojev, ki se srečajo v hierarhičnem multinivojskem modeliranju (Wohlgemuth in sod., 2015: 311).

A powerful tool for addressing the scale-up is dimensional analysis based on the Buckingham's π-theorem (Delaplace et al., 2015; Zlokarnik, 2006). Stemming from that, Zlokarnik (2006) stated the following assertion: "Two processes may be considered completely similar if they take place in a similar geometrical space and if all the dimensionless numbers necessary to describe them have the same numerical value". This

statement is known as a theory of similarity and is the only way to generalize the results obtained from one scale to another (Delaplace et al., 2015). It practically implies the equality of the numerical value (= *idem*) of dimensionless numbers used to describe the system on both scales.

For increasing the capacity of microstructured devices, external and internal numbering-up (also called scale-out) have been proposed (Schenk et al., 2004; Kashid et al., 2010; Su et al., 2016), and a few studies on efficient parallelization of catalytic micro packed bed reactors have been reported (Losey et al., 2001; Murakami et al., 2012; Inoue et al., 2015). However, due to potential problems in providing a stable and evenly distributed fluid flow in parallel microchannels (Tonkovich and Daymo, 2009; Saber et al., 2010; Kashid et al., 2015), avoidance of numbering-up concept is advisable (Roberge et al., 2009; Kockmann et al., 2011). Instead, a scale-up by increasing the characteristic dimensions of the continuously operated reactors to achieve increased internal volume and therefore higher throughput has been suggested (Tonkovich et al., 2005; Jensen et al., 2014; Woitalka et al., 2014; Heintz et al., 2016b). Such systematic scale-up of a single reactor could be achieved by increasing only one characteristic dimension of the channel, simultaneously keeping other two dimensions constant as well as the initial (miniaturized) size of the reactor. Then such optimized 'full-scale' reactor, which would retain the advantages of miniaturization, may be considered for mutltiplication by numbering-up in order to reach desired commercial capacity spanning from a few to several tons per year (Tonkovich et al., 2005; Jensen et al., 2014) (Figure 14).

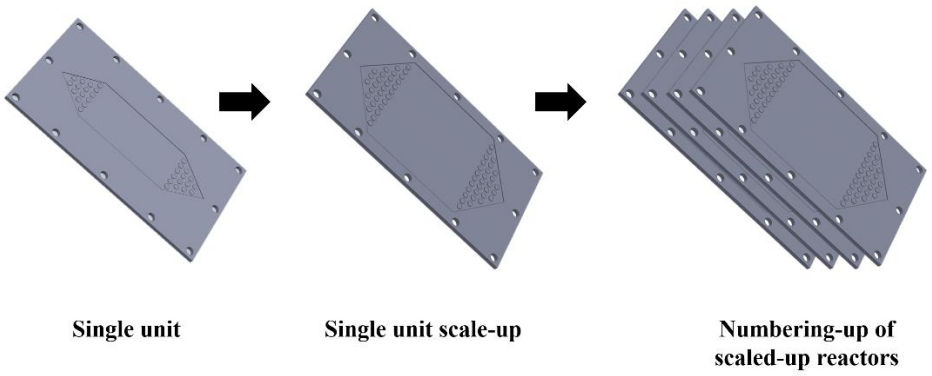

Figure 14: Illustration of the systematic process capacity increase.
Slika 14: Ilustracija sistematičnega povečevanja kapacitete procesa.

This approach is the core of the present study, and will be used for the scale-up of MPBRs with immobilized enzymes. Since the hydrodynamic conditions change with the scaling due to fluid maldistribution such as channeling and the formation of dead zones, typically observed within CPBRs (Fourati et al., 2012; Bozzano et al., 2014a), the limits of a single unit scale-up should be defined in order to retain the above listed advantages of miniaturized reactors.

3 MATERIALS AND METHODS

3.1 CHEMICALS

Sodium pyruvate, acetophenone, (*S*)-(–)-*α*-methylbenzylamine, pyridoxal-5'-phosphate, L-alanine, vinyl butyrate, 1-butanol, butyl butyrate, monobasic and dibasic sodium phosphate, monobasic potassium phosphate, ammonium chloride, magnesium sulfate, acetonitrile, glycerol, hydrochloric acid, sodium hydroxide solution (purity 50%), *n*-heptane, alginic acid sodium salt (M/G ratio of 1.56; molecular weight of 120,000–190,000 g mol^{-1}), D-(+)-glucose and kanamycin sulfate from *Streptomyces kanamyceticus* were all from Sigma-Aldrich (Steinheim, Germany) and were of analytical grade (except sodium hydroxide solution). Calcium acetate, sodium sulfate and tris(hydroxymethyl)aminomethane (Tris) were from Kemika (Zagreb, Croatia), while calcium chloride was purchased from Carlo Erba Reagents (Val de Reuil, France). Edible refined sunflower oil Floriol® was from Bunge (Budapest, Hungary). Yeast extract and peptone bacteriological were from Biolife (Milan, Italy) and isopropyl *β*-D-1-thiogalactopyranoside (IPTG) was from Gold Biotechnology (St. Louis, USA). Milli-Q® water was used throughout all experiments with ω-transaminases, except in the cultivation of *E. coli* cells where deionized water was used.

Chemical compounds used in this work are listed in Annex B, together with corresponding PubChem CID that can be used to extract all relevant information from the available database (NCBI, 2004).

3.2 IMMOBILIZATION OF *E. coli* CELLS IN ALGINATE MICROPARTICLES

3.2.1 Preparation of *E. coli* cells overexpressing ω-transaminase

3.2.1.1 Microorganism

Recombinant *E. coli* BL21(DE3) cells intracellularly overexpressing an ω-transaminase (wild-type amine transaminase, ATA-wt) were kindly provided by c-LEcta (Leipzig, Germany). The strain is a descendant of *E. coli* B and has known genome sequences (Daegelen et al., 2009; Jeong et al., 2009). Besides, it is a non-pathogenic laboratory strain which is not capable of colonizing or infecting human organism and therefore belongs to the Risk Group 1 of biohazardous agents (Kuhnert et al., 1997; Chart et al., 2000; NIH Guidelines 2016).

The gene coding expression of the enzyme ATA-wt was obtained from a metagenomic library by c-LEcta. Since the enzyme is a patent protected by the same company, the exact amino-acid sequence alignment is unknown, but it has been reported that the enzyme has a high sequence identity to a *Pseudomonas* sp. transaminase (Börner et al., 2017a, 2017b).

3.2.1.2 Preparation and composition of the culture medium

The culture medium ZYM-505 (Studier, 2005) was used for the cultivation of *E. coli* cells. All stock solutions for the culture medium were prepared using deionized water and autoclaved for 20 min at 121 °C (Table 4).

Table 4: Stock solutions for the preparation of the culture medium.
Tabela 4: Založne raztopine za pripravo gojišča.

Abbreviation	Component	Final concentration
ZY	yeast extract	5 g L^{-1}
	peptone	10 g L^{-1}
M	Na_2HPO_4	0.5 M
	KH_2PO_4	0.5 M
	NH_4Cl	1.0 M
	Na_2SO_4	0.1 M
505	glycerol	250 g L^{-1}
	glucose	25 g L^{-1}
$MgSO_4$	$MgSO_4$	2 mM

The culture medium ZYM-505 was freshly prepared by mixing the stock solutions as follows: ZY/1 with M/20, 505/50 and 2 mM $MgSO_4$. Kanamycin sulfate from *Streptomyces kanamyceticus* at the concentration of 50 µg mL^{-1} was added to the medium.

3.2.1.3 Cell cultivation and ω-transaminase induction

For intracellular expression of ATA-wt in *E. coli* cells, 50 mL of ZYM-505 culture medium containing 50 µg mL^{-1} of kanamycin sulfate from *Streptomyces kanamyceticus* in 250 mL Erlenmeyer flasks with baffles was inoculated with the preculture to give final OD_{600} of 0.1. The flasks were then shaken on the incubator shaker IKA® KS 4000 i control (IKA-Werke GmbH & Co. KG, Staufen, Germany) at 30 °C and 140 rpm until OD_{600} 0.6–1.0. IPTG in the final concentration of 0.1 mM was used for the induction and the flasks were shaken for the next 12–20 h under the same conditions. After harvesting by centrifugation on the refrigerated centrifuge Heraeus Contifuge 17RS (Marshall Scientific, Hampton, USA) at 3,000 rpm for 15 min, cells were washed twice with deionized water and then resuspended in 20 mM Tris-HCl buffer (AppliChem, 2008), adjusted with 1 M HCl to pH 8.0.

3.2.1.4 Determination of ω-transaminase activity in *E. coli* cells

ATA-wt activity in *E. coli* cells was determined using the initial rate method (Bisswanger, 2014). Measurements were carried out using 40 mM equimolar solution of (*S*)-*α*-MBA and PYR in 20 mM Tris-HCl buffer (pH 8.0) together with 0.1 mM PLP. The experiments were performed in batch runs using a jacketed glass vessel thermostated at 30 °C and stirred using a magnetic stirrer IKA® RCT (IKA-Werke GmbH & Co. KG, Staufen, Germany) at 200 rpm. The solution optical density OD_{600} was set to 0.1, where OD_{600} 1 was considered to equal 1×10^9 cells mL^{-1} or cell dry weight of 0.39 mg_{dry} mL^{-1} (Sezonov et al., 2007; Glazyrina et al., 2010).

During the sampling, the withdrawn aliquots were quickly diluted with 0.1 M NaOH (volume ratio 1:1) in order to stop the reaction, and centrifuged at 13,000 rpm for 5 min before the analysis. ACP concentration in the withdrawn samples was followed over the time and the activity was calculated from its linear increase. Specific activity was expressed per mass of dry cells [U mg_{dry}^{-1}], while U was defined based on the synthesis of 1 µmol of ACP per min under described conditions. All assays were performed in duplicates.

3.2.2 Preparation of alginate microparticles using a microflow system

A 22.5 mm long, 15.0 mm wide and 4.0 mm thick glass droplet junction microchip (Dolomite, Royston, UK) with maximal operating pressure of 3 MPa was used as a continuous droplet generator (Figure 15) (Dolomite Product Datasheet). The chip has a 105 µm wide and 100 µm deep T-junction which is a part of bigger 300 µm wide and 100 µm deep main and side channels with a hydrophobic coating (inset picture in Figure 15), suitable for production of inversed water-in-oil emulsions. The channel length and volume after the junction were 11.25 mm and 0.31 µL, respectively (Dolomite Product Datasheet).

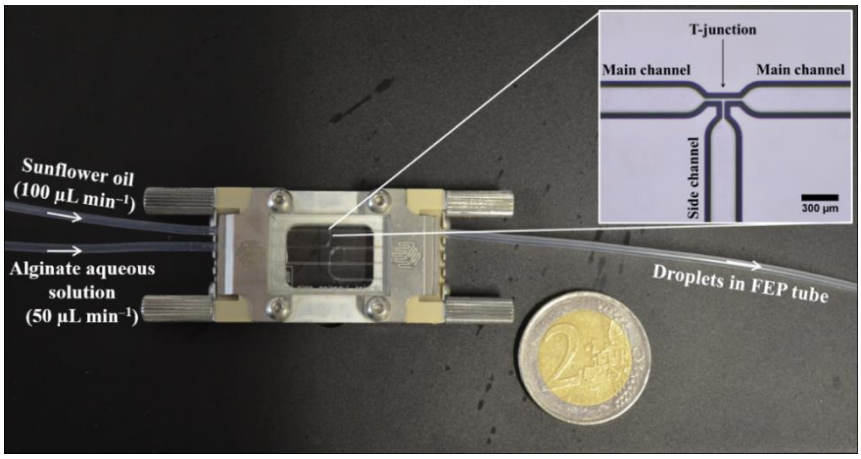

Figure 15: Experimental set-up for water-in-oil emulsification in the droplet junction microchip.
Slika 15: Eksperimentalna postavitev za emulgiranje vode v olju z uporabo mikročipa za tvorbo kapljic.

Edible sunflower oil used as a hydrophobic continuous phase and an aqueous solution of alginate (C_{alg} = 2 g L^{-1}) used as a hydrophilic droplet phase were supplied to the main and the side channel (Figure 15). Flow rates of the continuous (Q_c) and droplet (Q_d) phases were 100 µL min^{-1} and 50 µL min^{-1}, respectively. The fluid flows were driven by Harvard Apparatus PHD 4400 syringe pumps (Harvard Apparatus, Holliston, USA) equipped with stainless steel syringes connected to the microchip by FEP tubes (1.59 mm OD; 0.50 mm ID) from VICI AG International (Schenkon, Switzerland). The emulsification in the microchip was monitored by using a light microscope (Leica Microsystems, Wetzlar, Germany) equipped with a photo camera (Nikon D5100, Tokyo, Japan).

Solidification (gelation) of alginate-containing aqueous microdroplets was performed *ex situ*, by collecting them into a glass measuring cylinder with a volume of 100 mL (Brand® Silberbrand Eterna 100:2 mL; height 165 mm; Brand, Wertheim, Germany) containing aqueous and oil solution of Ca^{2+} ions (Capretto et al., 2008), continuously stirred at 300 rpm on a magnetic stirrer. Two phases constituted two layers, the upper one consisted of 30 mL of calcium acetate solution in oil (1 g L^{-1}), while the lower one consisted of 70 mL of calcium chloride aqueous solution (1.5 g L^{-1}). The FEP tube (30 cm length; 1.59 mm OD; 0.50 mm ID) coming from the microchip (Figure 15) was immersed slightly below the surface of the upper layer, just enough to allow the direct injection of the outflow (Dang and Joo, 2013). The gelation of alginate-containing aqueous microdroplets was triggered by the ion exchange reaction carried out according to Equation 19, afterwards the alginate microparticles moved slowly down towards the interface of the aqueous solution under the influence of gravity (Dang and Joo, 2013).

$$2\ \text{Na-alginate} + Ca^{2+} \rightarrow \text{Ca-alginate} + 2\ Na^{+} \quad \text{... (19)}$$

Upon collection in the aqueous phase, partly solidified alginate microparticles were left for further gelation during the next 15 min under the continuous stirring at 300 rpm. Thereafter, the gelling solution was carefully outpoured and the alginate microparticles were placed on a vacuum filter, quickly washed with 10 mL of *n*-heptane to remove the residual oil, additionally washed with 50 mL of water and stored in 20 mM Tris-HCl buffer (pH 8.0) until use. The experiment was performed at 24 ºC (in a temperature-controlled room), if not stated otherwise.

3.2.2.1 Characterization of droplet flow in the microflow system

In order to characterize droplet flow in the microflow system, the properties of the sunflower oil and aqueous solution of alginate (C_{alg} = 2 g L^{-1}), namely density, viscosity and interfacial tension were determined. All measurements were performed in triplicates at 24 ºC.

Densities of sunflower oil and aqueous solution of alginate were determined using a pycnometer, while the viscosities were determined using a Cannon-Fenske viscometer of size 300 (Figure 16a) (The Emil Greiner Co., New York, USA). The sample (10 mL) was allowed to freely flow through the right tube, and the efflux time (the time required for the meniscus of the fluid to pass from the mark A to mark B in Figure 16a) was measured using a stopwatch. The kinematic and dynamic viscosities of both fluids were then calculated using the efflux time, an associate viscometer constant and fluid density (Fan, 2001).

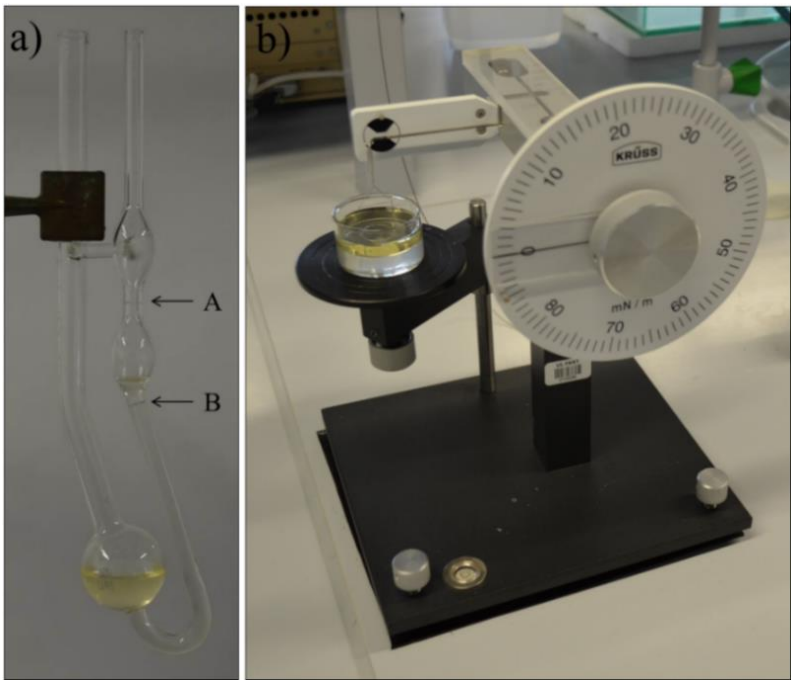

Figure 16: Determination of fluid properties: a) determination of viscosity using a Cannon-Fenske viscometer; b) determination of interfacial tension using a manual force tensiometer K6.

Slika 16: Določanje lastnosti tekočin: a) določanje viskoznosti pomočjo Cannon-Fenske viskozimetra; b) določanje medfazne napetosti pomočjo ročnega tenziometra.

The interfacial tension between sunflower oil and alginate solution (15 mL of each sample) was measured using a manual force tensiometer K6 (Krüss, Hamburg, Germany) shown in Figure 16b (Krüss user manual, 2002). The measurement is based on the principles of Du Noüy ring method (Du Noüy, 1919, 1925). The method in this case implies slowly lifting of the platinum ring through the interface of two immiscible liquids, whereby the force necessary to raise the ring through it is being measured and correlated to the interfacial tension (Krüss user manual, 2002; Butt et al., 2003).

3.2.2.2 Determination of alginate microparticles size and size distribution

Alginate microparticles were placed on a microscope slide and the images were captured using the light microscope equipped with the photo camera. The average diameter of alginate

microparticles was then estimated from the captured images using the image analysis software ImageJ (National Institutes of Health, Bethesda, USA). The data are expressed based on results obtained by measuring diameters of at least 80 microparticles, where a diameter of each microparticle was expressed as an average of three measurements obtained from three different directions.

3.2.3 Immobilization of *E. coli* cells in alginate microparticles

The immobilization of recombinant *E. coli* cells was done according to the procedure described in Section 3.2.2, just they were previously mixed with the aqueous solution of alginate (C_{alg} = 2 g L^{-1}) to achieve OD_{600}-specific concentration of *E. coli* cells of 1, i.e. the concentration of dry cells 0.39 mg_{dry} mL^{-1}.

3.2.3.1 Determination of ω-transaminase activity in immobilized *E. coli* cells

Determination of ATA-wt activity in *E. coli* cells immobilized in alginate microparticles was performed in a batch process using the same reaction system as described in Section 3.2.1.4. Assuming a 100% efficiency of immobilization (i.e. approximately 1×10^9 cells or 0.39 mg_{dry} per mililiter of alginate hydrogel), and taking into consideration the density of alginate aqueous solution (C_{alg} = 2 g L^{-1}) as stated in the results, the concentration of alginate microparticles was set to 0.1 g mL^{-1}, in order to give the final optical density OD_{600} of 0.1, which equals to 1×10^8 cells mL^{-1}, i.e. 0.039 mg_{dry} mL^{-1}. Other conditions were the same as described in Section 3.2.1.4.

Furthermore, alginate microparticles with immobilized *E. coli* cells were tested for the activity in a batch reactor using selected transamination reaction over the course of 47 h under the same conditions as described in Section 3.2.1.4.

3.2.3.2 Storage stability of immobilized *E. coli* cells

Storage stability of immobilized *E. coli* cells was evaluated by measuring their specific activity (according to the procedure explained in Section 3.2.3.1) during the time period of 6 days. Each time the predetermined amount of alginate microparticles containing immobilized *E. coli* cells was taken from the storage solution containing of 20 mM Tris-HCl buffer (pH 8.0) kept at 4 ºC. Storage stability was expressed as relative specific activity in comparison with that obtained immediately after the immobilization.

3.3 TRANSAMINATION WITH LENTIKATS®

3.3.1 Enzyme

ATA-wt was supplied by c-LEcta as a crude preparation in a powder form. Other information about the enzyme are given in Section 3.2.1.1.

3.3.2 Determination of non-immobilized ω-transaminase activity

The activity of non-immobilized ATA-wt was determined using the initial rate method, according to the procedure explained in Section 3.2.1.4. The assays were carried out using 40 mM equimolar solution of (*S*)-*α*-MBA and PYR in 20 mM sodium phosphate buffer (pH 8.0) together with 0.1 mM PLP, as optimized for the selected enzyme (Börner et al., 2016). The concentration of ATA-wt in the vessel, $C_{ATA\text{-}wt}$ was set to 0.16 $g_{ATA\text{-}wt}\ L^{-1}$. The experiments were performed in duplicates at 30 ºC.

ACP concentration in the withdrawn aliquots was followed over the time and the activity was calculated from its linear increase. The enzyme-specific activity was expressed per mass of enzyme [U $mg_{ATA\text{-}wt}^{-1}$], while U was defined based on the synthesis of 1 µmol of ACP per min under described conditions. Dilution with NaOH followed by centrifugation was required in order to stop the reaction. This procedure was done in the same way as explained in Section 3.2.1.4.

3.3.3 Preparation and characterization of LentiKats®

3.3.3.1 Preparation of LentiKats®

PVA particles with immobilized ω-TA were kindly prepared and provided by LentiKat's a.s. (Stráž pod Ralskem, Czech Republic) according to the standard procedure based on the patent of Ding and Vorlop (1995).

The enzyme ATA-wt in a form of powder (250 g) was added to 750 mL of 20 mM potassium phosphate buffer (pH 8.0) and mixed with 4 kg of PVA gel, printed by LentiPrinter® and dried to reach about 30% of the initial mass. Solid PVA matrix was swollen in the stabilizing solution according to standard manufacturing method (Ding and Vorlop, 1995). The final enzyme concentration expressed per mass of PVA gel was 50 $mg_{ATA\text{-}wt}\ g_{PVA}^{-1}$ (Heintz et al., 2016b). An immobilized enzyme in the form of lens-shaped PVA particles (LentiKats®) was stored at 4 °C in 20 mM potassium phosphate buffer (pH 8.0) until use.

For mass determination, the PVA particles were placed on a strainer in one layer, carefully wiped at the bottom side and weighed in a closed beaker using the analytical weighing

machine (Mettler-Toledo Ltd., Leicester, UK). The mass of ATA-wt was determined from the mass of particles (Heintz et al., 2016b).

3.3.3.2 Determination of LentiKats® size and size distribution

In calculations, LentiKats® were considered as a spherical cap (Polyanin and Manzhirov, 2007), and a schematic presentation of a particle together with the characteristic dimensions (radius of the circular base and height) is shown in Figure 17.

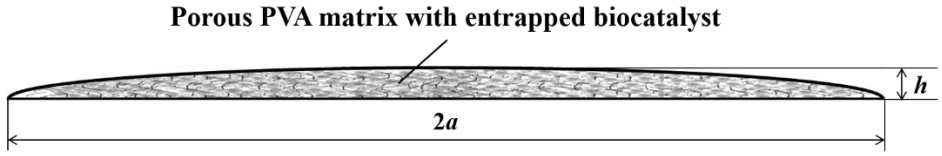

Figure 17: Schematic illustration and characteristic dimensions of LentiKats®.
Slika 17: Shematski prikaz in značilne dimenzije LentiKats® delca.

The average circular base diameter of LentiKats® was estimated from images of particles (cca. 1500 particles in total) using the image analysis software ImageJ, while the average particle height was estimated using a caliper. The volume (V_{LK}), the area of the upper curved surface (S_{LK}) and the total surface area of LentiKats® ($S_{LKtotal}$) were then calculated considering the shape of a spherical cap, according to Equations 20, 21 and 22, respectively (Polyanin and Manzhirov, 2007).

$$V_{LK} = \frac{\pi\, h}{6}\,(3\,a^2 + h^2) \quad \text{... (20)}$$

$$S_{LK} = \pi\,(a^2 + h^2) \quad \text{... (21)}$$

$$S_{LK_{total}} = \pi\,(h^2 + 2\,a^2) \quad \text{... (22)}$$

V_{LK}	*volume of LentiKats® [mm³]*
S_{LK}	*area of the upper curved surface of LentiKats® [mm²]*
$S_{LKtotal}$	*total surface area of LentiKats® [mm²]*
a	*radius of the LentiKats® circular base [mm]*
h	*height of LentiKats® [mm]*

Due to the non-sphericity of LentiKats®, Sauter mean diameter (d_{32}) was used as a suitable particle equivalent diameter. This parameter incorporates both volume and surface area of the particle, i.e. it is defined as the diameter of a sphere that has the same volume-to-surface area ratio as LentiKats® (Equation 23) (Wang D. and Fan, 2013).

$$d_{32} = \frac{6\ V_{LK}}{S_{LK_{total}}} \quad \text{... (23)}$$

d_{32} *Sauter mean diameter of LentiKats® [mm]*

3.3.3.3 Determination of ω-transaminase activity in LentiKats®

The activity of ATA-wt in LentiKats® was determined according to the procedure explained in Section 3.3.2. The concentration of LentiKats® in the vessel, C_{LK} was set to 3.20 $g_{LK}\ L^{-1}$ in order to give the final ATA-wt concentration $C_{ATA\text{-}wt}$ = 0.16 $g_{ATA\text{-}wt}\ L^{-1}$. The experiments were performed in duplicates at 30 ºC.

ACP concentration in the withdrawn aliquots was followed over the time and the activity was calculated from its linear increase (the withdrawn samples were not diluted with 0.1 M NaOH and centrifuged before the analysis because no enzyme leakage from the PVA matrix was assumed). Specific activity was expressed either per mass of LentiKats® [U mg_{LK}^{-1}], or per mass of enzyme [U $mg_{ATA\text{-}wt}^{-1}$], while U was defined based on the synthesis of 1 µmol of ACP per min under described conditions.

3.3.3.4 Effect of different mixing speeds on ω-transaminase activity in LentiKats®

The enzyme-specific activity was also determined at different stirring speeds of 400, 600, 800, and 1,000 rpm, according to procedure described in Section 3.3.3.3.

3.3.4 Design of miniaturized packed bed reactors with LentiKats®

The general microreactor assembly is shown in Figure 18. MPBR housing was made from two PMMA plates where the upper one had inlet and outlet holes connected to perfluoroalkoxy (PFA) tubes (1.59 mm OD; 0.50 mm ID) *via* high-pressure polyetheretherketone (PEEK) tube fittings (Vici AG International, Schenkon, Switzerland). The plates for the MPBRs with rectangular channels had dimensions of 10.0 cm × 5.0 cm × 1.5 cm, while the plates for the MPBRs with hexagonal channels were of 19.8 cm × 15.8 cm × 1.5 cm regarding length, width and depth, respectively. Channels of various dimensions were carved out from an expanded polytetrafluoroethylene (ePTFE) film GORE-TEX® (Gore & Associates, Inc., USA) of 0.5 mm thickness by means of a scalpel. An outer spacer providing fixed channel depth was carved in the same way from a non-compressible polytetrafluoroethylene (PTFE) stripe DASTAFLON® 1620 (Dastaflon, Medvode, Slovenia) of 0.3 mm thickness. In the case of hexagonal channels, ePTFE cylindrical pillars were cut out by a hole punch tool cutter (hole diameter 4 mm) and placed in the inlet and

outlet triangular regions by fixing them to the surface of PMMA plates, using a solvent-free glue (UHU GmbH & Co. KG, Bühl, Germany). Selected LentiKats® of cca. 4 mm diameter were then inserted in the channels by manual packing in one, two or three layers (for the latter two, particles were packed one on top of the other). For the random package, 2,725.1 mg of particles was placed and spread out within the channel.

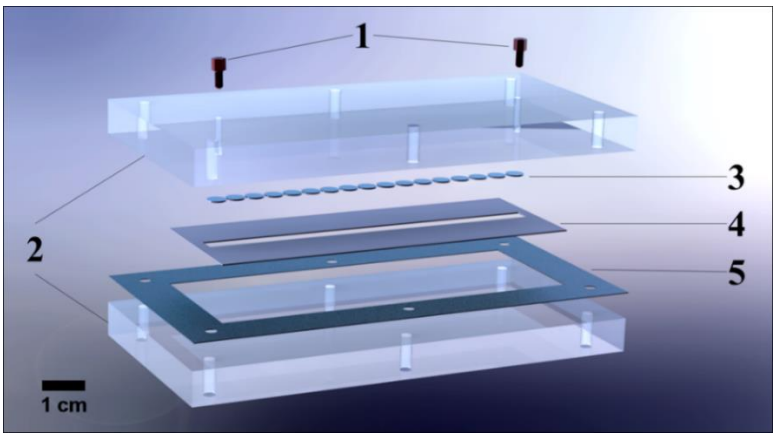

Figure 18: Assembling and the main parts of an MPBR with LentiKats®: 1) high pressure tube fittings; 2) PMMA plates; 3) LentiKats®; 4) ePTFE gasket; 5) 0.3 mm thick non-compressible PTFE spacer.

Slika 18: Sestava in glavni deli MPBR z LentiKats®: 1) tesnila za visokotlačni cevi; 2) PMMA plošči; 3) LentiKats®; 4) ePTFE tesnilo; 5) 0.3 mm debel nestisljiv PTFE distančnik.

After the insertion of particles, the upper PMMA plate was mounted on the spacer and assembled using bolts, nuts, and washers to provide essential sealing and to prevent fluid leakage. The volume of each channel was estimated by several measurements of the volume of water filling the channel by means of a Harvard Apparatus PHD 4400 high pressure pump. Furthermore, fluid flow distribution in the widest channel with triangular pre-chamber containing pillars was monitored by pumping a colored water using dye Amidoblau V (Simon & Werner GmbH & Co, Flörsheim am Main, Germany) at the flow rate of 1,000 µL min^{-1}.

3.3.5 Biotransformation in miniaturized packed bed reactors with LentiKats®

3.3.5.1 Continuous transamination

The transamination reaction was performed by pumping an equimolar 40 mM solution of (*S*)-α-MBA and PYR in 20 mM sodium phosphate buffer (pH 8.0) together with 0.1 mM PLP at flow rates ranging from 1.7 to 1,730.7 µL min^{-1} through the MPBRs with the channels of different size and shape by means of the high pressure pump equipped with a stainless steel syringe. Reactors were packed with various amounts of LentiKats® (from 19.5 to 2,725.1 mg) yielding enzyme loads (γ_e) from 40.57 to 167.45 U mL^{-1}, as specified in the results. After reaching the steady state, at least two consecutive samples were taken from the

outflow of the MPBR, collected in a closed vial in order to prevent ACP evaporation (Figure 19), and analyzed as described in Section 3.5.1. Experiments were performed at 24 ºC.

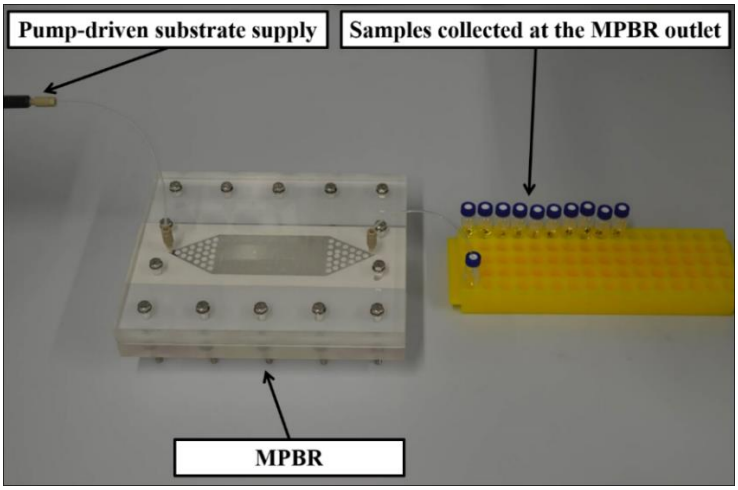

Figure 19: Experimental set-up of a continuous transamination in an MPBR.
Slika 19: Eksperimentalna postavitev za kontinuirno transaminacijo v MPBR.

The mean residence time (τ), conversion (X), volumetric productivity (Q_p), production rate (PR) and biocatalyst productivity number (BPN) (Valinger et al., 2014) were calculated using Equations from 24 to 28, respectively.

$$\tau = \frac{V_v}{Q} \quad \text{... (24)}$$

$$X = \frac{C_{Sin} - C_{Sout}}{C_{Sin}} \times 100 \quad \text{... (25)}$$

$$Q_p = \frac{C_{Pout}}{\tau} \quad \text{... (26)}$$

$$PR = Q_p \times V_v \quad \text{... (27)}$$

$$BPN = \frac{C_{Pout}}{C_{e,v}} \quad \text{... (28)}$$

τ	*mean residence time [min]*
V_v	*reactor void volume [µL]*
Q	*volumetric flow rate [µL min^{-1}]*
X	*conversion [%]*
C_{Sout}	*substrate outlet concentration [mM]*
Q_P	*volumetric productivity [mmol L^{-1} min^{-1}]*
C_{Pout}	*product outlet concentration [mM]*
PR	*production rate [µmol h^{-1}]*
BPN	*biocatalyst productivity number [mmol g^{-1}]*
$C_{e,v}$	*enzyme concentration expressed per reactor void volume [g L^{-1}]*

Reactor void volume (V_v) and bed porosity (ε) of MPBRs were calculated from volumes of the empty channels and particles (Equation 29). The latter was defined from the number of particles and their volume, defined in Section 3.3.3.2, except for the randomly packed MPBR, where the volume of particles was calculated from the particles' total mass and their average density.

$$\varepsilon = \frac{V_v}{V} \quad \text{... (29)}$$

V *volume of empty reactor [µL]*

3.3.5.2 Estimation of temperature effects

The temperature effect on the transamination process was evaluated by embedding the MPBR with a 81.61 mm long, 4.10 mm wide and 0.32 mm deep rectangular channel, packed with one layer of PVA particles with immobilized ATA-wt, yielding enzyme load of 43.28 U mL^{-1}, into a thermostated bath placed on a magnetic stirrer with temperature control IKA® RCT. The flow rate and thus the mean residence time were set to be constant, specifically 25 µL min^{-1} and 2.6 min, respectively, while the temperature varied from 30 to 75 (± 0.5) ºC. The reaction mixture was the same as described in Section 3.3.5.1. After reaching the steady state, samples were collected at the outlet of the reactor and analyzed as described in Section 3.5.1.

3.3.5.3 Estimation of operational stability

Transaminase-catalyzed biotransformation was continuously performed using the MPBR with rectangular 20 mm long, 4 mm wide and 0.23 mm deep channel, packed with one layer of PVA particles yielding enzyme load of 65.88 U mL^{-1}, at the flow rate of 0.5 µL min^{-1} (τ = 0.15 min) at 24 ºC over the period of 21 days. The reaction mixture was the same as described in Section 3.3.5.1. At selected time intervals, volumetric productivity was determined by increasing the flow rate to 50 µL min^{-1} and evaluating ACP concentration in the outflow after reaching the steady state. Operational stability was expressed as relative volumetric productivity in comparison with that obtained at the beginning of the experiment.

3.3.6 Hydrodynamics of miniaturized packed bed reactors with LentiKats®

3.3.6.1 Pressure drop measurements

The pressure drop in the MPBRs was measured at the reactor inlet by flowing water at different flow rates (from 10 to 1,000 µL min^{-1}), whereby the reactor outlet was opened and exposed to the atmospheric pressure. The measurements were performed using a silicon piezoresistive pressure sensor (with the operating range from 0 to 100 kPa) that works based on the piezoresistive effect (Fraga and Koberstein, 2012), shown in Figure 20a. The MPBR was placed laterally and the sensor coupled with the voltmeter was connected using a T-junction (Figure 20b). The experiments were performed at 24 ºC.

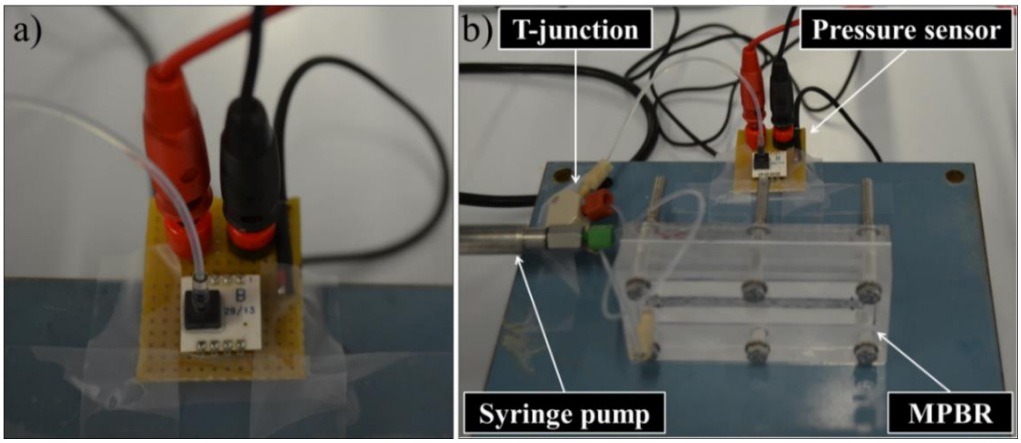

Figure 20: Experimental set-up for the pressure drop measurement (Q = 1–1,000 µL min^{-1} and T = 24 ºC).
Slika 20: Eksperimentalna postavitev za merjenje padca tlaka (Q = 1–1000 µL min^{-1} in T = 24 ºC).

The pressure drop was measured (the relation between applied pressure and output voltage is given by Equation 30) at each flow rate three times sequentially and the corresponding standard deviations were calculated thereof. The energy dissipation rate (the energy input per liquid volume), P_1 was then calculated from the measured pressure drop according to Equation 31.

$$\Delta p = \frac{U - 0.7}{0.03} \quad \text{... (30)}$$

$$P_1 = \frac{\Delta p\, Q}{V_v} \quad \text{... (31)}$$

Δp *pressure drop [kPa]*
U *voltage output [V]*
P_1 *energy dissipation rate [kW* m^{-3}*]*

3.4 TRANSESTERIFICATION WITH NOVOZYM® 435

3.4.1 Enzyme

CaLB in the form of commercially available immobilized preparation Novozym® 435 was used for transesterification. Novozym® 435 with a nominal catalytic activity of 10,000 PLU g^{-1} (propyl laureate units per gram) and 1–2% (w/w) of moisture (Chen H.-C. et al., 2011) was kindly donated by Novozymes A/S (Bagsværd, Denmark).

3.4.2 Characterization of Novozym® 435

3.4.2.1 Particles size and size distribution

To obtain the particles with narrow size distribution, Novozym® 435 was sieved through the system of sieves with different pore size, ranging from 500 to 300 µm (Figure 21a). Each fraction was then analyzed under the light microscope and the average particle diameter was determined based on images analysis of cca. 300 spherical particles (Figure 21b) using the ImageJ software.

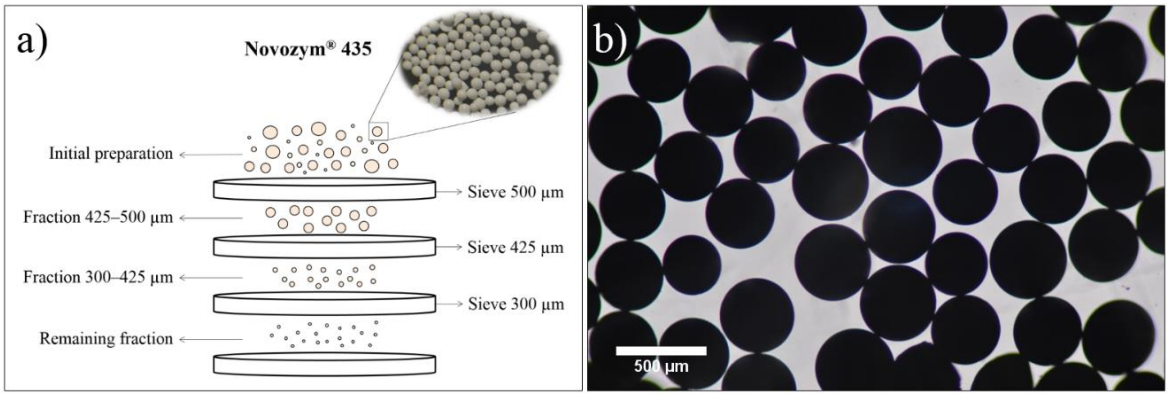

Figure 21: Characterization of Novozym® 435: a) sieving through the sieves of different pore size; b) particles under the light microscope (fraction 300–425 µm).

Slika 21: Karakterizacija pripravka Novozym® 435: a) sejanje skozi sita z različno velikostjo por; b) delci pod svetlobnim mikroskopom (frakcija 300–425 µm).

3.4.2.2 Determination of Novozym® 435 catalytic activity

The activity of immobilized CaLB was determined using the initial rate method. Measurements were carried out at 24 ºC in small test tubes with a ground glass stopper having the total volume of 9 mL, continuously stirred on a magnetic stirrer at 800 rpm. The reaction mixture (2 mL) was an equimolar 600 mM solution of VB and BUT in *n*-heptane. The concentration of Novozym® 435 in the vessel (C_{N435}) was set to 5 g_{N435} L^{-1} in order to

reach the final CaLB concentration (C_{CaLB}) of 0.5 $g_{CaLB}\ L^{-1}$. The assay was performed in duplicates.

BB concentration in the withdrawn samples was followed over the time and the activity was calculated from its linear increase. Specific activity was expressed either per mass of Novozym® 435 [U mg_{N435}^{-1}], or per mass of enzyme [U mg_{CaLB}^{-1}], while U was defined based on the synthesis of 1 µmol of BB per min under described conditions.

3.4.2.3 Effect of different mixing speeds and substrate concentrations on transesterification

The effect of different mixing speed (300, 500, 800 and 1,200 rpm) on transesterification was studied in a batch reactor. The reaction mixture (2 mL) was an equimolar 500 mM solution of VB and BUT in *n*-heptane.

Additionally, the effects of different substrate initial concentrations were studied in another batch process in order to verify the inhibition type reported in the literature (Pohar et al., 2012). The first set of experiments used the reaction mixture (2 mL) with fixed initial concentration of VB (600 mM) and varying concentrations of BUT (from 300 to 900 mM), whereby the second set of experiments used the reaction mixture (2 mL) with fixed initial concentration of BUT (700 mM) and varying concentrations of VB (from 400 to 1,100 mM).

The nominal concentration of Novozym® 435 in the vessel was set to C_{N435} = 12.5 $g_{N435}\ L^{-1}$ in both cases, in order to give the final CaLB concentration C_{CaLB} = 1.25 $g_{CaLB}\ L^{-1}$. Other reaction conditions (temperature, mixing speed) were the same as described in Section 3.4.2.2. The assays were performed in duplicates.

3.4.3 Design of miniaturized packed bed reactors with Novozym® 435

The MPBRs with rectangular channels packed with Novozym® 435 were assembled using two PMMA plates with dimensions of 10.0 cm × 5.0 cm × 1.5 cm, while the plates for the MPBRs with hexagonal channels were of 15.7 cm × 6.6 cm × 1.5 cm regarding length, width and depth, respectively. Two non-compressible (0.1 mm and 0.3 mm thick) PTFE stripes were placed as an outer spacer providing fixed channel depth. A thin polyester double-sided adhesive tape ARcare® 90445 (Adhesives Research, Inc., Glen Rock, USA) was placed at the lower PMMA plate in order to fix the particles and prevent their leaching from the reactor. Other reactor parts were the same as described in Section 3.3.4. The general microreactor assembly is shown in Figure 22.

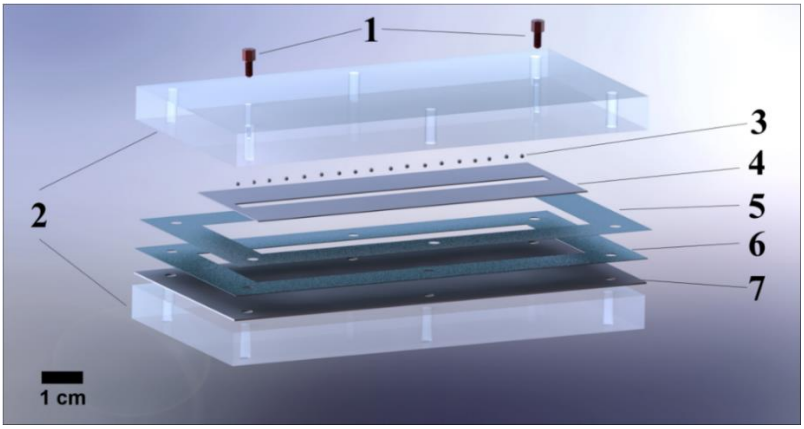

Figure 22: Assembling and the main parts of an MPBR with Novozym® 435: 1) high pressure tube fittings; 2) PMMA plates; 3) Novozym® 435; 4) ePTFE gasket; 5) 0.1 mm thick non-compressible PTFE spacer; 6) 0.3 mm thick non-compressible PTFE spacer; 7) thin polyester double-sided adhesive tape.

Slika 22: Sestava in glavni deli MPBR z Novozym® 435: 1) tesnila za visokotlačni cevi; 2) PMMA plošči; 3) Novozym® 435; 4) ePTFE tesnilo; 5) 0.1 mm debel nestisljiv PTFE distančnik; 6) 0.3 mm debel nestisljiv PTFE distančnik; 7) tanek poliesterski dvostranski lepilni trak.

Selected fraction of Novozym® 435 was then randomly inserted in the channels by manual packing in one or two layers. For the MPBR packed with two layers, the polyester double-sided adhesive tape was placed on both upper and lower PMMA plates and the particles were fixed on it. Packing more than two layers of Novozym® 435 would not be possible due to difficulties to retain the medium layers of particles within the reactor.

3.4.4 Biotransformation in miniaturized packed bed reactors with Novozym® 435

3.4.4.1 Continuous transesterification

The reaction was performed by pumping an equimolar 600 mM solution of VB and BUT in *n*-heptane at flow rates ranging from 12.2 to 3,756.3 µL min^{-1} through the MPBRs with channels of different size and shape. Reactors were randomly packed with various amounts of Novozym® 435 (from 7.1 to 148.4 mg), yielding final enzyme loads (γ_e) from 5.06 to 5.53 U μL^{-1}, as specified in the results. After reaching the steady state, at least two consecutive samples were taken from the outflow of the MPBR, collected in a closed vial in order to prevent evaporation, and analyzed as described in Section 3.5.2. The experiments were performed at 24 ºC.

The mean residence time, conversion, volumetric productivity, production rate and biocatalyst productivity number were calculated as described in Section 3.3.5.1. Void volume and bed porosity of MPBRs were calculated from the volume of the empty channels and volume of particles, where the latter was calculated from the particles mass and their density which is considered to be 0.555 mg μL^{-1} (Denčić et al., 2013).

3.4.4.2 Estimation of temperature effects

The temperature effect on the transesterification process was evaluated by embedding the MPBR with a 23.93 mm long, 3.12 mm wide and 0.40 mm deep rectangular channel, packed with 7.1 mg of Novozym® 435 in one layer, yielding final enzyme load of 5.53 U μL^{-1}, into a thermostated bath with automatic temperature control (Julabo, Seelbach, Germany). The flow rate and thus the mean residence time were set to be constant, specifically 170.72 µL min^{-1} and 0.1 min, while the temperature varied from 24 to 80 (± 0.5) ºC. The reaction mixture was the same as described in Section 3.4.4.1. After reaching the steady state, samples were collected at the outlet of the reactor and analyzed as described in Section 3.5.2. The experiments were performed in duplicates.

3.4.4.3 Estimation of operational stability

The lipase-catalyzed transesterification was continuously performed using the MPBR with rectangular 82.00 mm long, 2.92 mm wide and 0.40 mm deep channel, packed with 22.2 mg of Novozym® 435 in one layer yielding final enzyme load of 5.28 U μL^{-1}, at the flow rate of 559 µL min^{-1} (τ = 0.1 min) at 24 ºC over the period of 53 days. The reaction mixture was the same as described in Section 3.4.4.1. After each continuous-flow experiment, the flow through the microreactor was stopped and the system was stored at 24 ºC till the next evaluation (Cvjetko et al., 2012). Operational stability was expressed as relative volumetric productivity in comparison with that obtained at the beginning of the experiment.

3.4.5 Hydrodynamics of miniaturized packed bed reactors with Novozym® 435

3.4.5.1 Pressure drop measurements

The flow rates of water through the MPBRs were ranging from 30 to 1,800 µL min^{-1}, and the pressure drop was measured using a silicon piezoresistive pressure sensor. The sensor and experimental set-up were the same as described in Section 3.3.6.1.

3.4.5.2 Estimation of the residence time distribution

The hydrodynamic behavior of MPBRs randomly packed with Novozym® 435 in one layer was characterized by RTD analysis performed at 24 ºC by means of a stimulus-response experiment with a pulse input (Levenspiel, 2012), using glucose dissolved in phosphate buffered saline (PBS) as a non-reactive tracer. The instantaneous readings of glucose concentrations at various times were performed at the MPBRs outlet using a calibrated biosensor with immobilized glucose oxidase (GOx) from *Aspergillus niger* VII S (EC

1.1.3.4) integrated in the microfluidic chip. The sensor with the volume of 4 µL was developed and fabricated by Measurement Technology Unit of the University of Oulu, Finland, based on the work of Ricci et al. (2002, 2003). Potentiostat PalmSens (Houten, the Netherlands) was used as the signal converter.

The experimental test loop for the stimulus-response experiment with the pulse input is shown in Figure 23. Briefly, PBS was continuously supplied through the system interconnected with PFA tubes (1.59 mm OD; 0.50 mm ID) using a high pressure pump at the flow rate of 100 µL min^{-1}. At time t_0, 10 µL of 50 mM glucose solution (total load 5×10^{-4} mmol of glucose) in 100 mM PBS (pH 7.4) was instantaneously injected in the system using an HPLC injection valve connected to the pump (Márquez et al., 2008), and its concentration was followed at the reactor outlet using the GOx biosensor, whereby the output signal was read using the potentiostat. The experiments were performed in triplicates.

The frequency of measurement was 10 Hz. Due to the high quantity of data, the average for every second (10 measurements) was calculated, and the yielding values were used to generate the pulse-response curve.

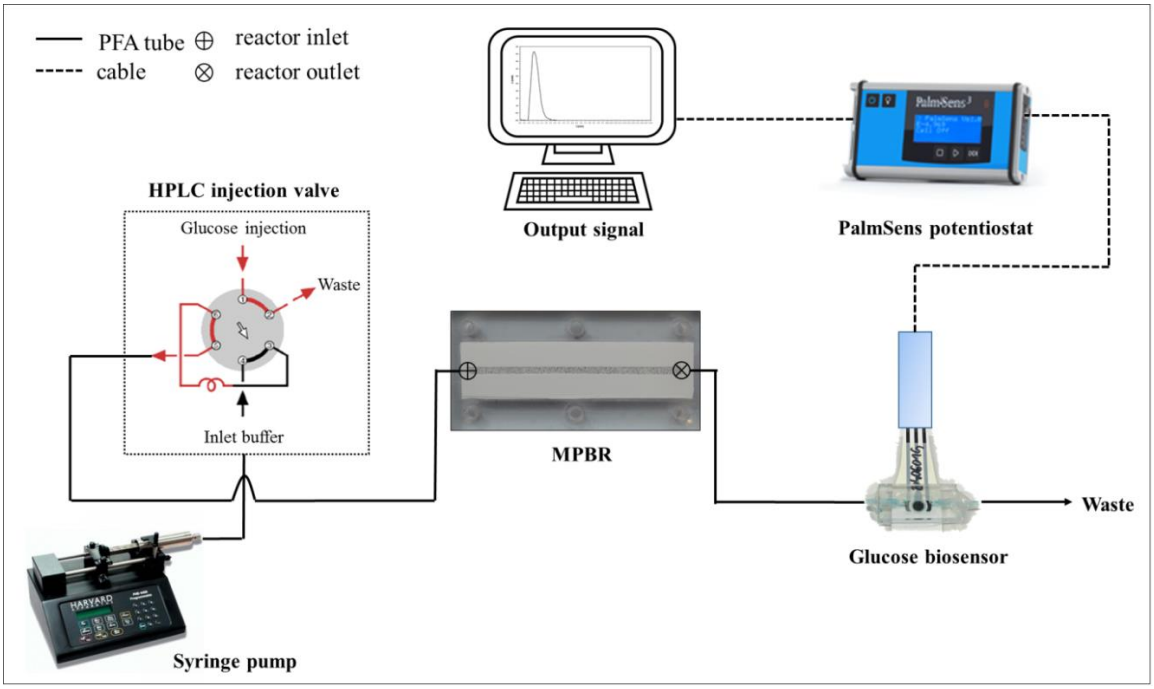

Figure 23: Schematic of the test loop for the stimulus-response experiment with the pulse input.

Slika 23: Shema eksperimentalne postavitve merjenja porazdelitve zadrževalnih časov s pulzno motnjo.

The mean residence time, variance (σ^2) and skewness (s) of the distribution $C_{glu}(t)$ were calculated from the pulse-response measurements using Equations 32 to 34 (Levenspiel, 2012; Coblyn et al., 2016).

$$\tau = \frac{\Sigma\, t\, C_{glu}}{\Sigma\, C_{glu}} \quad \text{... (32)}$$

$$\sigma^2 = \frac{\Sigma\, (t)^2 C_{glu}}{\Sigma\, C_{glu}} - \tau^2 \quad \text{... (33)}$$

$$s = \frac{\Sigma\, (t-\tau)^3\, C_{glu}}{\sigma^3\, \Sigma\, C_{glu}} \quad \text{... (34)}$$

C_{glu} *glucose concentration [mM]*
σ^2 *variance [min^2]*
s *skewness [–]*

The starting assumptions involved the closed boundary conditions (the fluid enters and leaves the reactor only once and there is no recirculation), steady state flow, homogeneous system, an inert tracer which does not disturb the flow, and isothermal conditions (Levenspiel, 1999; Coblyn et al., 2016).

3.5 ANALYTICAL METHODS

3.5.1 Evaluation of the transamination reaction

Concentrations of (*S*)-*α*-MBA and ACP were evaluated either by HPLC or GC analysis, where for the latter analytes were extracted in *n*-heptane as described below. Both analyses yielded the same results within the specified standard deviation.

3.5.1.1 HPLC analysis

An HPLC (Figure 24a) with a diode array detector (Shimadzu, Tokyo, Japan) equipped with Gemini®-NX 3µm C18 110Å (150 × 4.60 mm) column (Phenomenex, Torrance, USA) was used for the isocratic separation. The mobile phase consisted of 50% (v/v) acetonitrile and 50% (v/v) aqueous solution (pH 11.0) obtained by addition of NaOH solution (purity 50%), and was vacuum-filtered using S-Pak filters (pore size 0.22 µm; diameter 47 mm) made from mixed esters of cellulose (Merck Millipore, Billerica, USA). The flow rate through the column thermostated at 30 °C was 1 mL min^{-1}. Residence times for (*S*)-*α*-MBA and ACP, detected at 260 nm, were 2.5 and 3.6 min, respectively (Figure 24b). The concentrations of analytes were calculated from the calibration curves prepared from the standard solutions.

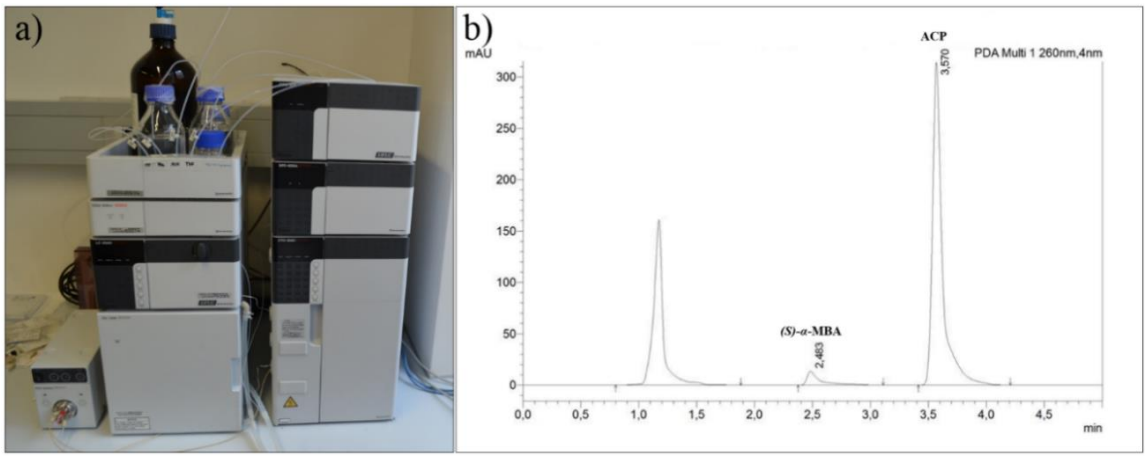

Figure 24: HPLC analytics: a) an HPLC used for measurements; b) an example of HPLC chromatogram showing peaks and residence times for (*S*)-*α*-MBA and ACP, respectively.

Slika 24: HPLC analitika: a) HPLC uporabljen za merjenje; b) primer HPLC kromatograma, ki prikazujen vrhove in zadrževalne čase za (*S*)-*α*-MBA in ACP.

3.5.1.2 GC analysis

Prior to analysis, 60 µL of an aqueous sample and 60 µL of *n*-heptane were contacted for 3 min on a vortex mixer Vibromix 204 EV (Tehtnica, Železniki, Slovenia) at 1,500 rpm at 24 °C. (*S*)-*α*-MBA and ACP concentrations in *n*-heptane were determined on a gas chromatograph HP 6890 (Hewlett-Packard, Palo Alto, USA) equipped with a hydrogen flame ionization detector and a fused silica (diphenyl dimethyl polysiloxane) Rtx®-35 (30 m length × 0.25 mm ID × 0.5 µm film thickness) column (Restek Corporation, State College, USA) (Figure 25a). Nitrogen was used as a carrier gas at the flow rate of 1 mL min^{-1}. The temperature of the oven at the injection was 100 °C and was kept constant for 1 min. The linear increase in temperature up to 180 °C was set to 50 °C min^{-1} and from 180 °C to 250 °C to 20 °C min^{-1}, while later the temperature was kept constant until the end of the analysis (7.1 min). Residence times for (*S*)-*α*-MBA and ACP were 3.7 and 3.9 min, respectively (Figure 25b).

In order to calculate the concentration in the original sample, the partitioning coefficients for both analyzed compounds in an *n*-heptane/aqueous buffer system were evaluated as described elsewhere (Cvjetko et al., 2012) and taken into account. Where it was required, dilution with 0.1 M NaOH was also taken into consideration.

The concentrations of analytes were calculated from the calibration curves prepared from the standard solutions. Preparation of calibration curves directly after contacting the aqueous standard solutions with *n*-heptane was also possible, and this option allowed avoidance of the partitioning coefficient utilization.

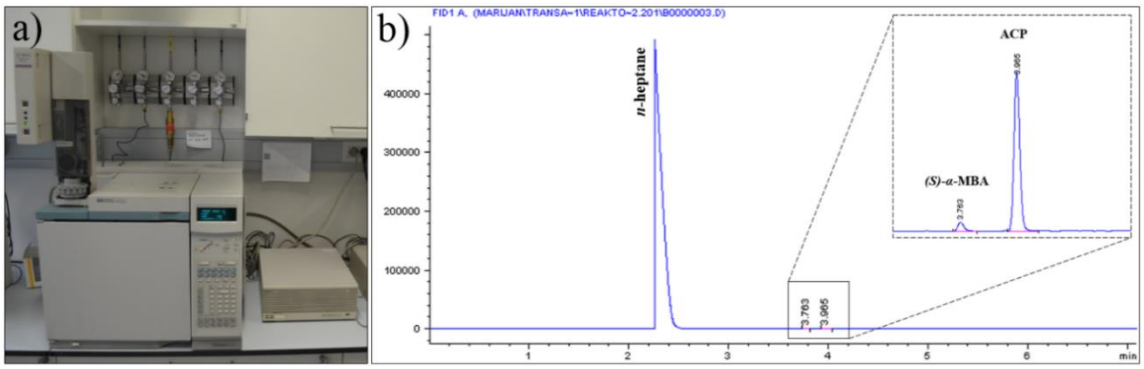

Figure 25: GC analytics: a) gas chromatograph used for measurements; b) an example of GC chromatogram showing peaks and residence times for *n*-heptane, (*S*)-*α*-MBA and ACP, respectively.

Slika 25: GC analitika: a) GC uporabljen za merjenje; b) primer GC kromatograma, ki prikazuje vrhove in zadrževalne čase za *n*-heptan, (*S*)-*α*-MBA in ACP.

3.5.2 Evaluation of the transesterification reaction

3.5.2.1 GC analysis

Gas chromatograph described in Section 3.5.1.2, equipped with an HP-INNOWAX (30 m length × 0.25 mm ID × 0.5 µm film thickness) column (Agilent Technologies, Santa Clara, USA) was used to determine the concentration of VB, BUT and BB in *n*-heptane. The used carrier gas was nitrogen, which was supplied at the flow rate of 29 mL min^{-1}. The temperature of the oven at the injection was 100 °C and was kept constant for 1 min. The linear increase in temperature to 200 °C was set by 35 °C min^{-1}, and was kept at this temperature till the end of the analysis. The temperature in the injector and detector was 250 °C (Žnidaršič-Plazl and Plazl, 2009). Residence times for VB, BUT and BB were 1.2, 1.4 and 1.7 min, respectively (Figure 26). The concentrations of analytes were calculated from the calibration curves prepared from the standard solutions.

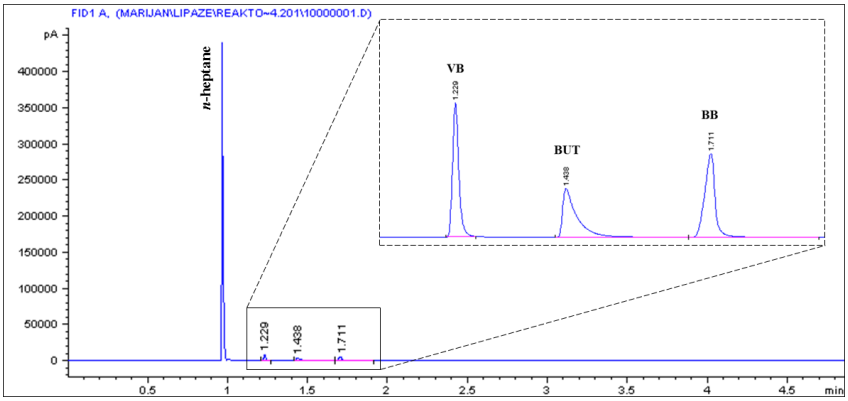

Figure 26: An example of a GC chromatogram showing peaks and residence times for *n*-heptane, VB, BUT and BB, respectively.

Slika 26: Primer GC kromatograma, ki prikazuje vrhove in zadrževalne čase za *n*-heptan, VB, BUT in BB.

4 RESULTS WITH DISCUSSION

4.1 IMMOBILIZATION OF *E. coli* CELLS IN ALGINATE MICROPARTICLES

4.1.1 Mechanism of microdroplets formation

A microfluidic-based approach for the production of alginate-containing aqueous microdroplets by emulsification in an oil phase and their further solidification by *ex situ* external cross-linking was investigated. The first part of the method, the formation of aforementioned microdroplets, was done in the microfluidic chip with a T-junction made of 105 µm wide and 100 µm deep channels (Section 3.2.2). Two immiscible fluids with an interfacial tension of 10.5 mN m^{-1}, namely an edible sunflower oil and an aqeous solution of alginate (C_{alg} = 2 g L^{-1}), were continuously supplying to the main and side (lateral) channel of the T-junction (both 300 µm wide and 100 µm deep) as a continuous and a droplet phase at flow rates of 100 and 50 µL min^{-1}, respectively (Figure 27a). The chosen flow rates enabled the instantaneous formation of a parallel flow of two immiscible phases (Figure 27a), resulting in the formation of stable microdroplets in the FEP outlet tube (Figure 27b).

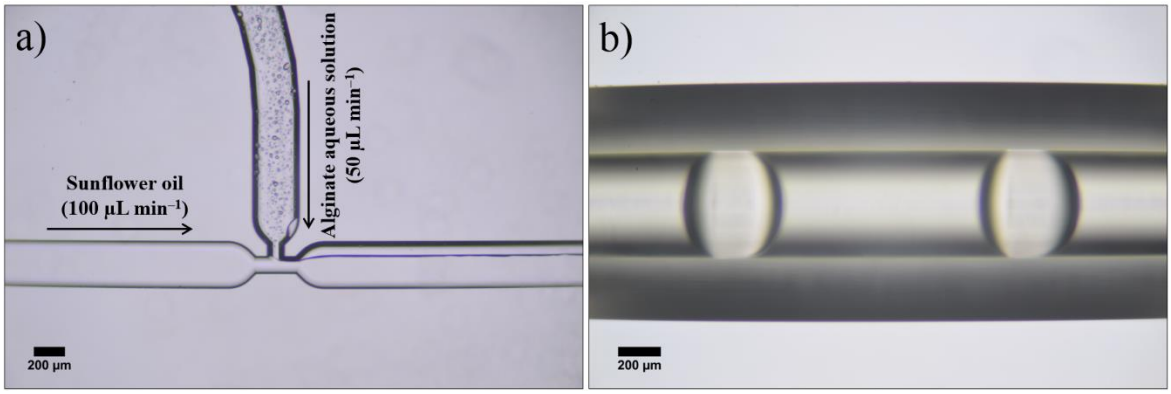

Figure 27: Droplet formation using microfluidics: a) parallel flow of sunflower oil and alginate aqueous solution in the T-junction microchip; b) outlet FEP tube with formed aqueous microdroplets containing alginate.

Slika 27: Tvorba kapljic pomočjo mikrofluidike: a) vzporedni tok sončničnega olja in vodne raztopine alginata v mikročipa z T-križiščem; b) izstopna FEP cevka z nastalimi mikrokapljicami z alginatom.

The microfluidic device was consisted of two integrated parts: a microfluidic chip with the T-junction connected to the manifold of three bigger channels (Figure 27a), and an outlet FEP tube connected in the extension (Section 3.2.2 and Figure 27b). Therefore, both fluids needed to pass through the channels of different geometries and dimensions, affecting the fluid flow formation. As can be observed from Figure 27a, under given conditions a parallel flow of two immiscible liquids was established along the 11.25 mm long channel positioned at the right side of the T-junction. Such parallel flow entered the outlet FEP tube of a different geometry and size than the channels on the microchip (30 cm length; 0.5 mm ID), resulting

in the formation of monodisperse spherical alginate-containing aqueous microdroplets which adopted the size of the tube, i.e. their diameter equalled to the tube diameter which was 500 μm (Figure 27b). Although it looks like that the aqueous microdroplets wet the inner wall of the tube (Figure 27b), it was not the case because there is a thin film of continuous oil phase that separates them. This is of the utmost importance for the formation of a stable and ordered droplet flow pattern. Otherwise, even a partial wetting of the tube wall by droplet aqueous phase would result in the appearance of an erratic, disordered and uncontrollable two-phase flow (Dreyfus et al., 2003; Xu J. H. et al., 2006b).

In order to describe the flow pattern in the FEP tube, the adequate dimensionless numbers were calculated from the operational conditions and fluid properties (Table 5) according to Equations 1, 3, 4 and 5, respectively, taking the tube internal diameter (0.5 mm) as the characteristic length.

Table 5: Fluid properties and dimensionless numbers used to describe the process of microdroplets formation.
Tabela 5: Lastnosti tekočin in brezdimenzijske številke uporabljene za opis procesa nastanka mikrokapljic.

	Fluid	η [mPa s]	ρ [kg m^{-3}]	γ [mN m^{-1}]
Fluid properties	Oil	70.19 ± 1.90	916.04 ± 1.20	10.5
	Alginate$_{(aq)}$	18.01 ± 0.10	1,008.70 ± 0.30	
Calculated dimensionless numbers[a)]	Re [–]	Oh [–]	Bo [–]	Ca [–]
	0.055	1.012	0.022	0.057

a) Calculated using the flow rate (Q = 100 μL min^{-1}) and properties of more viscous oil phase.

The dimensionless numbers presented in Table 5 have revealed laminar flow in the outlet tube which implies the dominance of viscous forces over inertial ones (Re = 0.055 and Oh > 1), as well as dominance of the interfacial over gravitational force (Bo << 1) (Kumacheva and Garstecki, 2011). Besides, Figure 27a revealed the laminar flow of two phases in the rectangular channels supplying T-junction, which was also confirmed with the calculated Re for the single flows of the alginate aqueous solution (Q_d = 50 μL min^{-1}) and oil (Q_c = 100 μL min^{-1}) occurring in these channels, which were 0.233 and 0.109, respectively. The most significant parameter relating the viscous and interfacial forces that determine the flow pattern in the microchannels, Ca number (Li X.-B. et al., 2012; Chen B. et al., 2015; Bai et al., 2016), was also calculated for the outlet FEP tube (Table 5).

The moving velocity of aqueous microdroplets in the tube (U_d) under given conditions, calculated according to Equation 35 (Chen B. et al., 2015), was 1.27 × 10^{-2} m s^{-1}, which further means that the alginate microdroplets were transferred from the outlet tube to the gelling bath at a rate of around 25 s^{-1}.

$$U_d = \frac{Q_c + Q_d}{A} \quad \text{... (35)}$$

U_d *moving velocity of aqueous microdroplets [m s^{-1}]*
Q_c *volumetric flow rate of continuous phase [m^3 s^{-1}]*
Q_d *volumetric flow rate of droplet phase [m^3 s^{-1}]*
A *cross-sectional area of the tube [m^2]*

No significant change in the process dynamics after the addition of *E. coli* cells in the aqueous alginate solution was observed.

4.1.2 Preparation and characterization of alginate microparticles

The alginate-containing aqueous microdroplets obtained in the microflow system (with or without recombinant *E. coli* cells) were cross-linked in a gelling bath to get water-insoluble hydrogel microparticles appropriate for further utilization. The microdroplets were first passing the upper (oil) phase with Ca^{2+} ions in order to attempt a partial solidification before they went across the interface (Figure 28), i.e. to the aqueous phase with Ca^{2+} ions.

Figure 28: Alginate-containing aqueous microdroplets (cca. 500 µm in diameter) in the external oil phase, where the gelation takes place.

Slika 28: Vodne mikrokapljice z alginatom (premer pribl. 500 µm) vstopajo v zgornjo (oljno) fazo zunanje kopeli, kjer poteka želiranje.

Resulting blank alginate microparticles had a spherical body and ‘tails’ (Figure 29a). The average diameter, measured for the spherical part (Dang and Joo, 2013), was 446.21 ± 36.54 µm (Figure 29b).

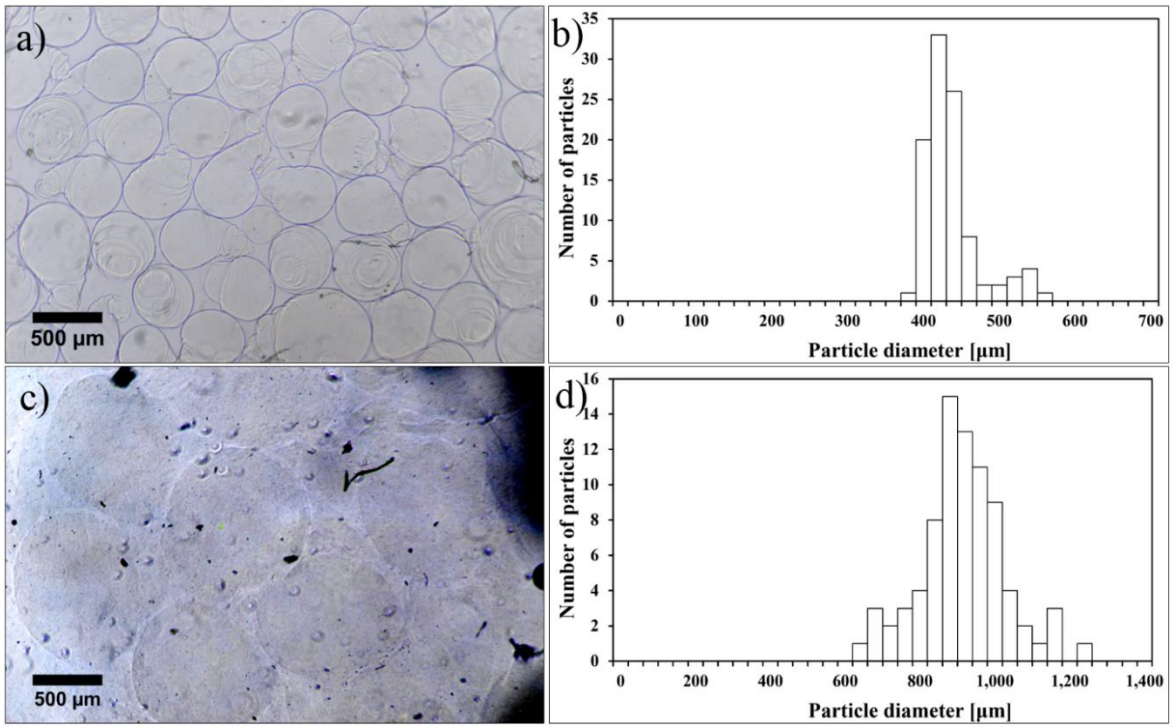

Figure 29: Characterization of alginate microparticles: a) blank microparticles; b) size distribution of blank microparticles (n = 100); c) microparticles with immobilized *E. coli* cells; d) size distribution of microparticles with immobilized *E. coli* cells (n = 80).

Slika 29: Karakterizacija alginatnih mikrodelcev: a) prazni mikrodelci; b) porazdelitev velikosti praznih mikrodelcev (n = 100); c) mikrodelci z imobiliziranimi *E. coli* celicami; porazdelitev velikosti mikrodelcev z imobiliziranimi *E. coli* celicami (n = 80).

The formation of tail-shaped alginate microparticles is frequently reported in the literature (Capretto et al., 2008; Hu et al., 2012; Dang and Joo, 2013; Lin et al., 2013). The tail is formed when the alginate spherical microdroplets sediment and pass the oil-aqeous interface in the gelling bath under the influence of gravity (Dang and Joo, 2013; Lin et al., 2013). The influence of the interfacial tension impels alginate microdroplets to occupy as smaller as possible space inside the oil phase, which corresponds to their spherical shape. As the microdroplets move to the aqueous phase, the interfacial forces change due to the difference in properties between the oil and aqueous phases. Besides, the lower part of a microdroplet in contact with the aqueous phase quickly undergoes cross-linking during its transport across the layer, causing an imbalance in the surface tension of the upper part of the microdroplets, which is still in the oil phase, resulting in the formation of tail-shaped alginate microparticles (Dang and Joo, 2013).

The gelation of alginate-containing aqueous microdroplets with *E. coli* cells (in the concentration of 1×10^9 cells mL^{-1} or 0.39 mg_{dry} mL^{-1}) resulted in the formation of more spherical and tail-free alginate microparticles (Figure 29c) with 2-times bigger average diameter of 932.72 ± 115.30 µm (Figure 29d) and ostensibly lower mechanical strength than in the case of blank microparticles (Figure 29b). It would be meaningful to presuppose that

there was a high amount of cells per mass of hydrogel (cca. 0.36 mg_{dry} $g_{hydrogel}^{-1}$) that hindered the interconnections between the neighbouring polymer chains resulting in the formation of mechanically weaker matrix capable of capturing a higher amount of water that eventually led to the swelling of microparticles. Furthermore, it could be hypothesized that the optimization regarding the cell amount per hydrogel mass would lead to the formation of smaller and more compact microparticles. Swelling of alginate microparticles after the addition of cells was also reported in the case of utilization of yeast *Saccharomyces cerevisiae* as model cells, where the concentrations higher than 2×10^7 cells mL^{-1} led to a significant increase in the microparticles' diameter (Manojlovic et al., 2006).

This method has a good potential in the production of alginate-based carriers for biocatalysts immobilization, but it has not been fully optimized yet and the addressing of several issues would be highly appreciated. It turned out that e*x situ* gelation presents a bottleneck in the production of spherical alginate microparticles, so further optimization of the parameters such as height of the upper oil phase (retention time of settling alginate microdroplets), speed of movement through the interface, stirring speed in the gelling bath, and concentration of Ca^{2+} ions would be necessary to achieve a method for the production of microparticles with spherical shape (Dang and Joo, 2013), which would be highly desirable for the application in MPBRs.

However, a genuine highlight of the method would be a successful generation of alginate-containing aqueous microdroplets directly on the junction that would give a possibility for their *in situ* (one-step) solidification and therefore avoidance of a tedious and time-consuming *ex situ* solidification. It usually implies the utilization of micromachining techniques for fabrication of microdevices with more complicated manifolds that fulfill the process requirements, but the result could be a rapid and efficient production of the appropriate polymer-based microparticles that potentially can be applicable as carriers for biocatalysts immobilization (Liu K. et al., 2006; Zhang et al., 2006; Xu J. et al., 2008; Amici et al., 2008; Fang and Cathala, 2011).

4.1.3 Batch biotransformation with immobilized *E. coli* cells

The specific activity of immobilized *E. coli* cells determined in a batch process (Figure 30) at the cell concentration of 0.039 mg_{dry} mL^{-1} was 4.46 ± 0.47 U mg_{dry}^{-1}. On the other hand, non-immobilized cells had more than twelve times lower specific activity (0.36 ± 0.01 U mg_{dry}^{-1}) as compared to immobilized cells. By comparison, the specific activity of non-immobilized *E. coli* cells containing ω-TAs determined in 20 mM sodium phosphate buffer (pH 8.0) was 0.60 U mg_{dry}^{-1} (unpublished results), which is more than 1.5-times higher than obtained in 20 mM Tris-HCl buffer.

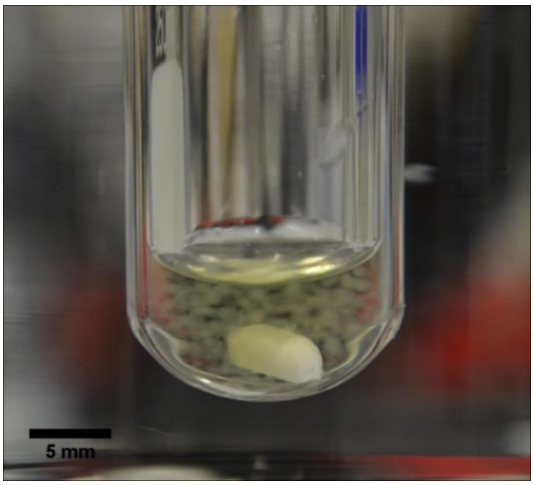

Figure 30: Alginate microparticles with immobilized *E. coli* cells in a reactor with a magnetic stirrer.
Slika 30: Alginatni mikrodelci z imobiliziranimi celicami *E. coli* v reaktorju z magnetnim mešalom.

Although a lower specific activity of immobilized *E. coli* cells was expected due to hampered mass transport within the hydrogel carrier, this was not the case, and a possible reason for that might be in the interaction between Tris and enzyme's cofactor. Namely, Tris is a primary amine which is able to interact with the enzyme-associated PLP under specific pH conditions, acting in that way as a competitive inhibitor (Han et al., 2004, 2009). So, it may be discussed that pH conditions in the interior of the hydrogel microparticles are such as to suppress possible negative effects of Tris-PLP interactions, which is not a case with non-immobilized cells. Anyway, a further screening of the optimal pH range for non-immobilized and immobilized cells would be necessary in order to accept or reject this hypothesis (Martin et al., 2007). The reason for Tris-HCl buffer application in this experiment as opposed to the sodium phosphate buffer that was commonly used in the transamination reaction throughout this study was in the instability of alginate hydrogel in the presence of Na^+ ions and phosphates (Smidsrød and Skjåk-Bræk 1990; Melvik and Dornish, 2004).

Further measurements of the specific activity of *E. coli* cells containing ω-TAs immobilized in alginate microparticles have shown that the activity decreased below 40% of the initial one after 4 days of storage in 20 mM Tris-HCl buffer (pH 8.0) at 4 °C (Figure 31).

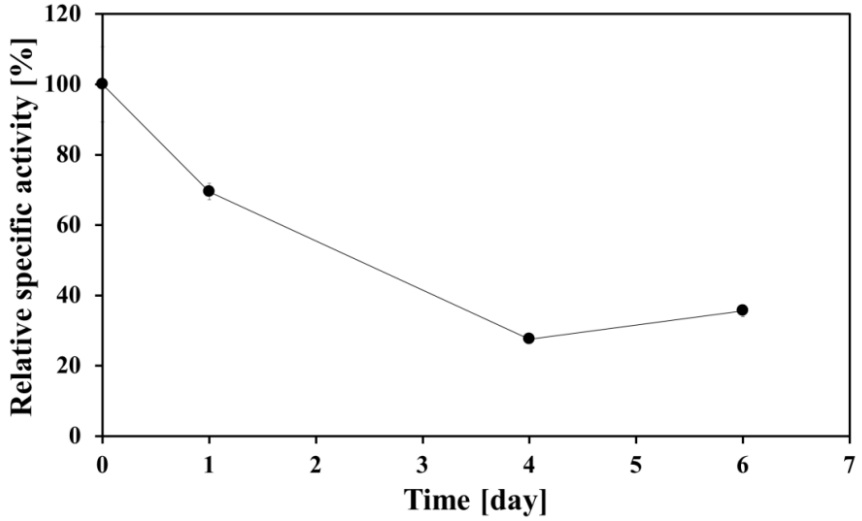

Figure 31: Storage stability of immobilized *E. coli* cells over the period of six days. The cell-containing alginate microparticles were stored in 20 mM Tris-HCl buffer at 4 °C between the activity measurements performed as described in Section 3.2.3.2. The trendline is only for data visualization.

Slika 31: Obstojnost imobiliziranih *E. coli* celic v obdobju šestih dni. Alginatni mikrodelci z imobiliziranimi celicami so bili med meritvami aktivnosti opisanih v poglavju 3.2.3.2, shranjeni v 20 mM Tris-HCl pufru pri 4 °C. Trendna črta je samo za vizualizacijo podatkov.

As evident from Figure 32, cca. 90% conversion was achieved within less than 30 h when immobilized *E. coli* cells (0.039 mg_{dry} mL^{-1}) were used for ω-TA-catayzed synthesis of ACP.

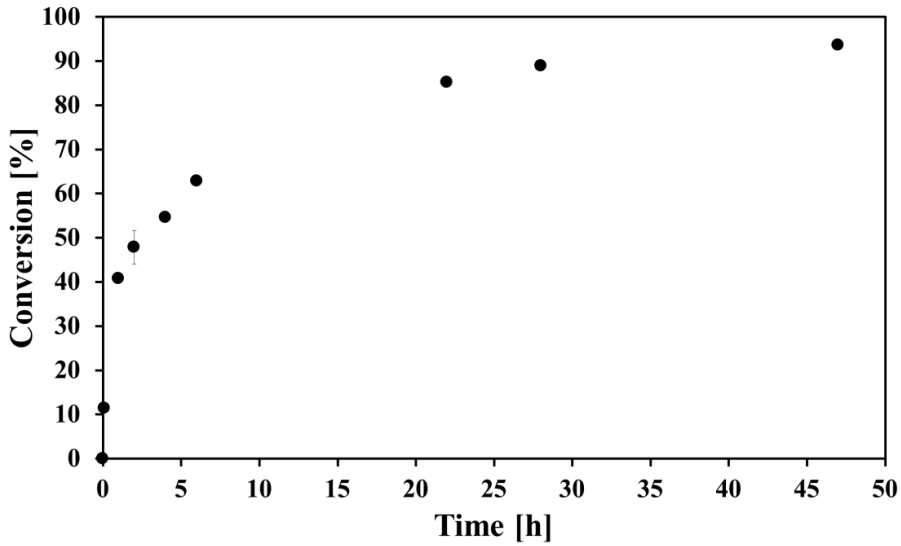

Figure 32: Conversion achieved in a batch process using *E. coli* cells immobilized in alginate microparticles. Concentration of alginate microparticles was 0.1 g mL^{-1}, which corresponds to the cell concentration of 0.039 mg_{dry} mL^{-1}. The reaction was performed using 40 mM equimolar concentration of both substrates in 20 mM Tris-HCl buffer (pH 8.0) together with 0.1 mM PLP, at 30 °C and stirring speed of 200 rpm.

Slika 32: Konverzija v šaržnem procesu z celicami *E. coli* imobiliziranimi v alginatne mikrodelce. Koncentracija alginatnih mikrodelcev je bila 0,1 g mL^{-1}, kar ustreza koncentraciji celic 0,039 mg_{dry} mL^{-1}. Reakcijo smo izvedli z uporabo 40 mM ekvimolarne koncentracije obeh substratov v 20 mM Tris-HCl pufru (pH 8,0) skupaj z 0,1 mM PLP, pri 30 °C in z vrtilno hitrostjo 200 min^{-1}.

The time necessary to achieve conversion higher than 90% was assumed to be a consequence of relatively small concentration of cells, but also a consequence of the internal diffusional limitations in alginate hydrogel (Shin J.-S. et al., 2001b; Martin et al., 2007). Mass transfer limitations through the cell membrane also play a significant role, but this problem might be partially solved by permeabilization of the cell membrane with cetrimonium bromide (CTAB) or ethanol. For instance, the observed reaction rate of the asymmetric synthesis of 1-phenylethylamine and 3-amino-1-phenylbutane was increased by 40% after the permeabilization of *E. coli* cells with 0.1% CTAB (Cárdenas-Fernández et al., 2012).

To sum up, the microfluidic-based system provided a convenient tool for the formation of monodisperse droplets that after further solidification produced stable submillimeter-sized alginate microparticles. Such produced microparticles have a high potential for biocatalyst immobilization and further implementation in continuous biocatalytic processes in MPBRs.

4.2 MINIATURIZED PACKED BED REACTORS WITH LENTIKATS®

4.2.1 Characterization of LentiKats®

The image-analysis based measurements of the selected LentiKats® which were tested in MPBRs with uniform packing revealed the average circular base diameter of 3.87 ± 0.33 mm (Figure 33), while the estimated height of particles was 0.35 ± 0.10 mm. Data are in accordance with the previous study on LentiKats®, where the average circular base diameter of 3.65 ± 0.38 mm and the average height of 0.341 ± 0.110 mm were reported (Schenkmayerová et al., 2014). Calculated Sauter mean diameter (Wang D. and Fan, 2013) of applied LentiKats® was 0.52 mm, while their average density was 1.78 ± 0.04 mg μL^{-1}.

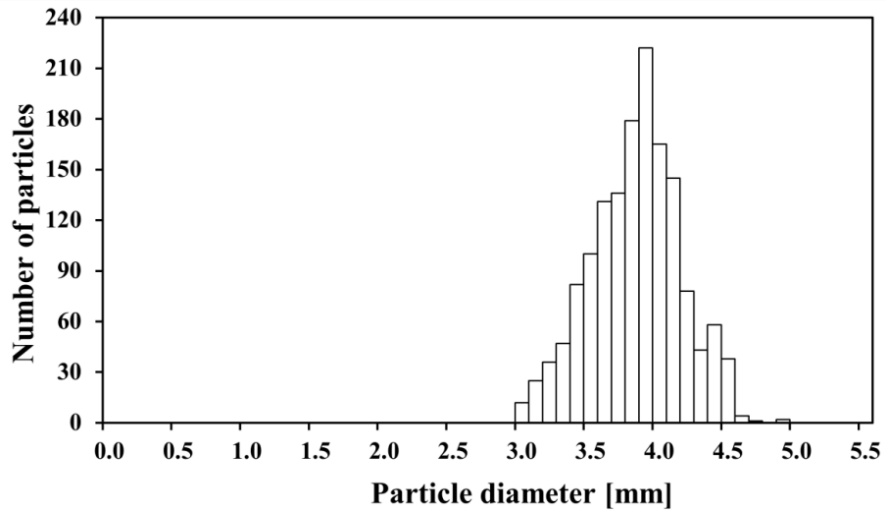

Figure 33: A circular base diameter distribution of LentiKats® used in experiments with uniform particle load.
Slika 33: Distibucija premerov krožnih osnovnih ploskev LentiKats® uporabljenih v eksperimentih z unformnim slojem delcev.

When a single or multiple layers of LentiKats® were placed within the channel, the total height of hydrogel material was compressed to the channel depth defined by a PTFE spacer (Section 3.3.4) and particles base adjusted to the empty space within the channel width and length. However, the change in the particles' volume due to compression has been presumed negligible. Since the native conformation of ω-TA used in this study is tetrameric with a molecular weight between 150 and 200 kDa (Börner et al., 2017a, Supporting Information), the protein could be effectively entrapped in LentiKats®, while the mass transport of substrate molecules to the enzymes' active sites was enabled. Specific activities of immobilized preparations evaluated in batch experiments and expressed per mass of immobilized ATA-wt were 0.50 and 0.73 U $mg_{ATA\text{-}wt}^{-1}$ corresponding to 0.025 and 0.037 U mg_{LK}^{-1}, respectively.

4.2.2 Biotransformation in miniaturized packed bed reactors with LentiKats®

The conversion of (*S*)-*α*-MBA to ACP using PYR as the amino acceptor, which is the reaction frequently used for transaminase activity evaluation (Rehn et al., 2014), was performed in MPBRs with rectangular and hexagonal channels of various sizes (Figures 34a, 34b, and 34c, respectively), using uniformly or randomly packed LentiKats®.

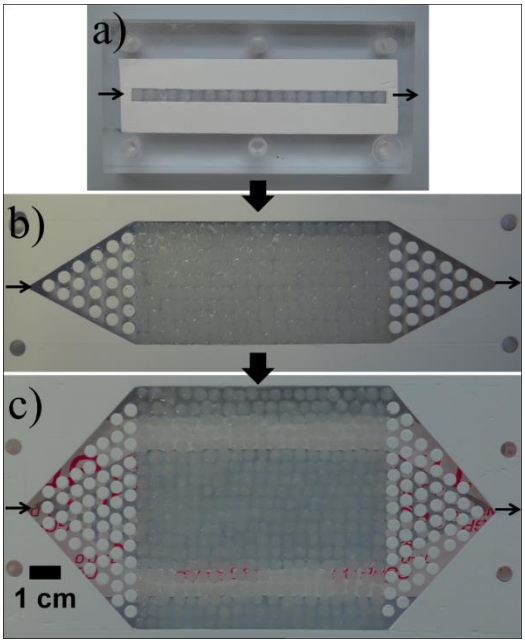

Figure 34: MPBRs presenting the scale-up in channel width, where length and depth were the same: a) an MPBR with cca. 4 mm wide rectangular channel, b) an MPBR with hexagonal channel (rectangular part is cca. 40 mm wide) with triangular inlet and outlet parts containing pillars, and c) an MPBR with hexagonal channel (rectangular part is cca. 80 mm wide) with triangular inlet and outlet parts containing pillars.

Slika 34: Predstavitev povečanja MPBR, na osnovi povečane širine kanala, kje so dolžine in višine enake: a) MPBR s 4 mm širokim pravokotnim kanalom; b) MPBR s šesterokotnim kanalom (pravokotni del je širok približno 40 mm), ki vsebuje trikotni vstopni in izstopni del z stebrički; c) MPBR s šesterokotnim kanalom (pravokotni del je širok približno 80 mm), ki vsebuje trikotni vstopni in izstopni del z stebrički.

As shown in Section 3.3.4, the MPBRs were developed as a sandwich-like structure, which enabled simple and efficient enzyme loading, easy assembly and reusability, as well as a variation of channel dimensions without tedious manufacturing procedures. Characteristics and performances of tested MPBRs are summarized in Table 6.

Table 6: Characteristics and performance of tested MPBRs with LentiKats® at 24 ºC.
Tabela 6: Značilnosti testiranih MPBR z LentiKats® pri 24 ºC.

l **[mm]**	***w*** **[mm]**	***d*** **[mm]**	**No. of layers[b)]**	***V*** **[µL]**	V_v **[µL][c)]**	ε **[c)] [–]**	γ_e **[U mL^{-1}]**	***BPN*** **[d)] [µmol$_{ACP}$ g$_{ATA\text{-}wt}^{-1}$]**
20.00	4.00	0.23	1	18.4	7.4	0.40	65.88	237.4
40.00	4.00	0.23	1	36.8	13.8	0.38	74.28	217.7
60.00	4.00	0.23	1	55.2	20.8	0.38	73.68	257.6
20.00	8.00	0.23	1	36.8	14.5	0.39	68.45	284.2
20.00	12.00	0.23	1	55.2	22.7	0.41	63.66	285.6
81.50	4.00	0.32	1	104.3	60.0	0.58	46.87	485.2
82.80	40.10[a)]	0.32	1	1,062.5	629.4	0.59	43.49	536.2
82.00	79.67[a)]	0.32	1	2,090.5	1,260.8	0.60	43.75	642.4
82.80	40.10[a)]	0.64	2	2,125.0	1,290.6	0.61	42.46	439.9
82.80	40.10[a)]	0.96	3	3,187.5	1,979.0	0.62	40.57	362.7
82.80	40.10[a)]	0.64	2–3	2,125.0	594.0	0.28	167.45	72.1
81.61	4.10	0.32	1	107.1	64.1	0.60	43.28	361.7[e)]

a) The values refer to the width of the rectangular part of the hexagonal channel.

b) Number of LentiKats® layers placed one on top of the other within the channel depth.

c) Estimated from the reactor volume and the volume of particles calculated from their number and average dimensions.

d) Maximal *BPN* calculated at the longest mean residence times tested.

e) Calculated at T = 55 °C and τ = 2.6 min.

4.2.2.1 Miniaturized packed bed reactors of different channel lengths

First, the MPBR with only one row of LentiKats® was tested utilizing a high-pressure pump providing a continuous laminar flow through the channel (Pohar et al., 2012). LentiKats® with the specific enzyme activity of 0.50 U mg$_{ATA\text{-}wt}^{-1}$ were uniformly packed in 20 to 60 mm long, 4 mm wide and 0.23 mm deep rectangular channels with volumes up to 55.2 µL, yielding final enzyme loads between 65.88 and 74.28 U mL^{-1} (Table 6). Bed porosities of tested MPBRs were estimated to be between 0.38 and 0.40 (Table 6), which is close to the

value of 0.395, reported for an MPBR having a total volume of 6.8 mL and randomly packed with PVA particles of 3.5 mm in diameter (Nunes et al., 2014).

When an equimolar aqueous solution of both substrates was pumped through the reactors together with cofactor PLP at flow rates ranging from 2 to 100 µL min^{-1} yielding the mean residence times up to 10.4 min, the laminar flow around uniformly packed particles and short diffusion paths enabled a very efficient biotransformation process. As evident from Figure 35, all three reactors performed equally well at the same mean residence times and above 80% conversion was obtained in less than 5 min.

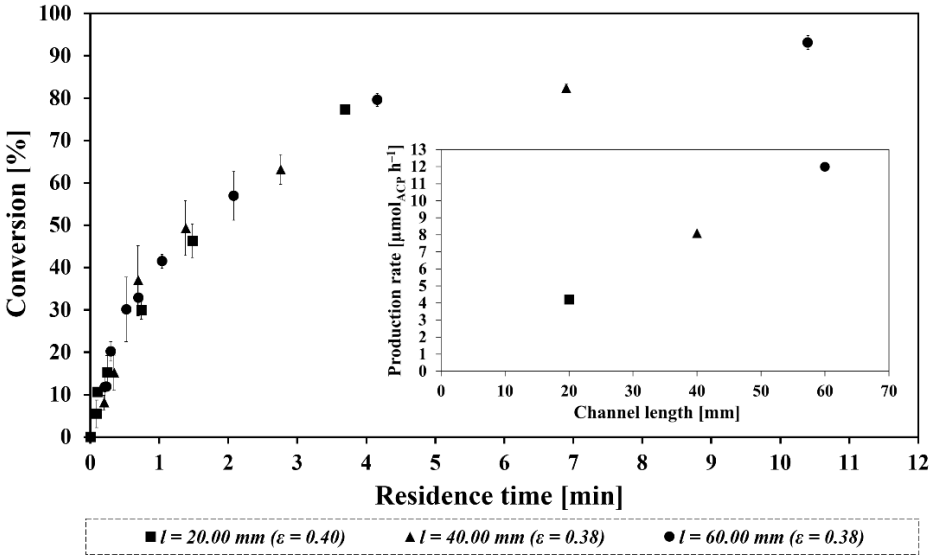

Figure 35: Impact of channel length on substrate conversion at the MPBRs outlets at various flow rates and thereby mean residence times together with production rates estimated at 70% conversion in the MPBRs with rectangular channels uniformly packed with LentiKats® having the specific enzyme activity of 0.50 U $mg_{ATA\text{-}wt}^{-1}$. The reaction was performed by continuous pumping of 40 mM equimolar inlet concentration of (*S*)-*α*-MBA and PYR in 20 mM sodium phosphate buffer (pH 8.0) together with 0.1 mM PLP, at room temperature (*T* = 24 °C). Other characteristics of the MPBRs are presented in Table 6. The relative standard deviations in the inset graph are below 15%.

Slika 35: Vpliv dolžine kanala na konverzijo substrata na izstopu iz MPBR pri različnih pretokih in s tem zadrževalnih časih skupaj s produktivnostjo, ocenjeno pri 70 % konverziji, v MPBR s pravokotnim kanalom z uniformnim slojem LentiKats® s specifično encimsko aktivnostjo 0,50 U $mg_{ATA\text{-}wt}^{-1}$. Reakcijo smo izvedli z kontinuiranim črpanjem 40 mM ekvimolarne vstopne raztopine (*S*)-*α*-MBA in PYR v 20 mM natrijevem fosfatnem pufru (pH 8.0) skupaj z 0,1 mM PLP pri sobni temperaturi (*T* = 24 °C). Ostale značilnosti MPBR so predstavljene v Tabeli 6. Relativne standardne deviacije v notranjem grafu so manjše od 15 %.

The comparison of production rates in reactors of varying channel lengths, estimated at 70% conversions, revealed linear proportionality within tested dimensions (inset graph in Figure 35). *BPN*s between 217.7 and 257.6 µmol_{ACP} $g_{ATA\text{-}wt}^{-1}$ were achieved in these MPBRs (Table 6). This indicates that the scale-up of the channel length allows for increased capacity and simultaneously retained good biocatalyst accessibility due to favorable hydrodynamic conditions.

4.2.2.2 Miniaturized packed bed reactors of different channel widths

Since the scale-up in the direction of channel length would be limited by a pressure drop and undesirable flow conditions at higher flow rates, scaling in the direction of the channel width was further considered. Selected transamination reaction was performed in the MPBRs with 4 to 12 mm wide rectangular channels of 20 mm length and 0.23 mm depth, with uniformly packed LentiKats® having the specific enzyme activity of 0.50 U $mg_{ATA\text{-}wt}^{-1}$, yielding final enzyme loads of 65.88, 68.45 and 63.66 U mL^{-1} (Table 6). Bed porosities between 0.39 and 0.41 (Table 6), similar to longer channels described above, were achieved. The flow rates were ranging from 2 to 100 µL min^{-1} yielding the mean residence times up to 11.4 min. Slightly larger *BPN*s of around 285 μmol_{ACP} $g_{ATA\text{-}wt}^{-1}$ were obtained by scaling-up of the MPBR's width (Table 6).

In contrast, conversions achieved in all three MPBRs were equal at the flow rates leading to the mean residence times below 2 min, while a slight deviation was observed for the widest channel at higher mean residence times/lower flow rates (Figure 36).

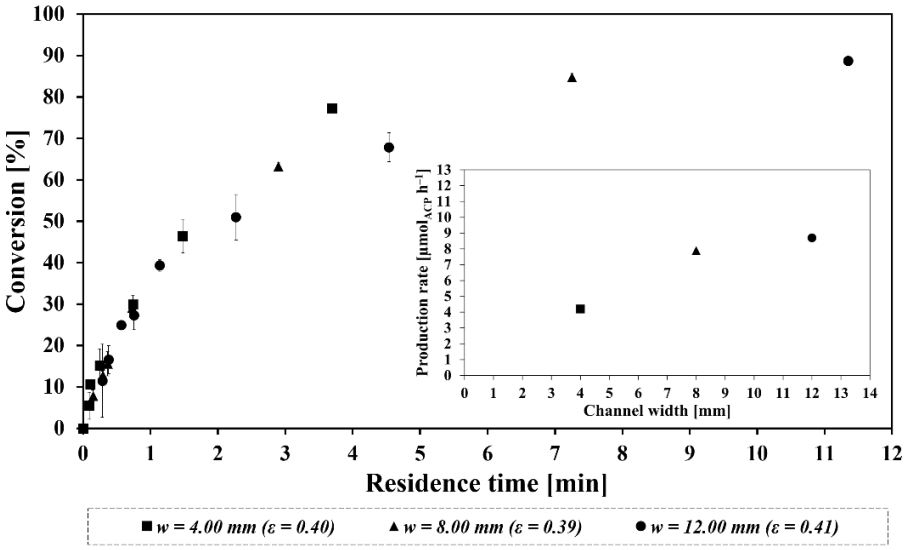

Figure 36: Impact of channel width on substrate conversions at the MPBRs outlets at various flow rates and thereby mean residence times together with production rates estimated at 70% conversion in MPBRs with rectangular channels uniformly packed with LentiKats® having the specific enzyme activity of 0.50 U $mg_{ATA\text{-}wt}^{-1}$. The reaction was performed under the same conditions as described in Figure 35. Other characteristics of the MPBRs are presented in Table 6. The relative standard deviations in the inset graphs are below 10%.

Slika 36: Vpliv širine kanala na konverzijo substrata na izstopu iz MPBR pri različnih pretokih in s tem zadrževalnih časih skupaj s produktivnostjo, ocenjeno pri 70 % konverziji, v MPBR s pravokotnim kanalom z uniformnim slojem LentiKats® s specifično encimsko aktivnostjo 0,50 U $mg_{ATA\text{-}wt}^{-1}$. Reakcijo smo izvedli pod enakimi pogoji kot je opisano na Sliki 35. Ostale značilnosti MPBR so predstavljene v Tabeli 6. Relativne standardne deviacije v notranjem grafu so manjše od 10 %.

This might be a consequence of unfavorable hydrodynamic conditions, since a direct inflow into the widest rectangular channel from the top single point might result in a non-uniform velocity profile along the channel width. The nonlinearity of production rate estimated at 70% conversion for each separate MPBR as a function of channel width also confirmed previous assumptions (inset graph in Figure 36).

In order to allow for sufficient fluid flow distribution along the channel width, a triangular pre-chamber containing pillars was introduced in the reactor design (Figures 34b and 34c), as pillar structures are often used in microchannels to guide the fluid flow (Saha et al., 2009; Amini et al., 2013). At the same time, the pillars placed in the triangular chamber at the channel outlet prevent possible wash-out of LentiKats® from the reactor. Monitoring of colored water flow within the empty channel of the widest dimension with the pre-chamber containing pillars revealed efficient flow distribution (Figure 37).

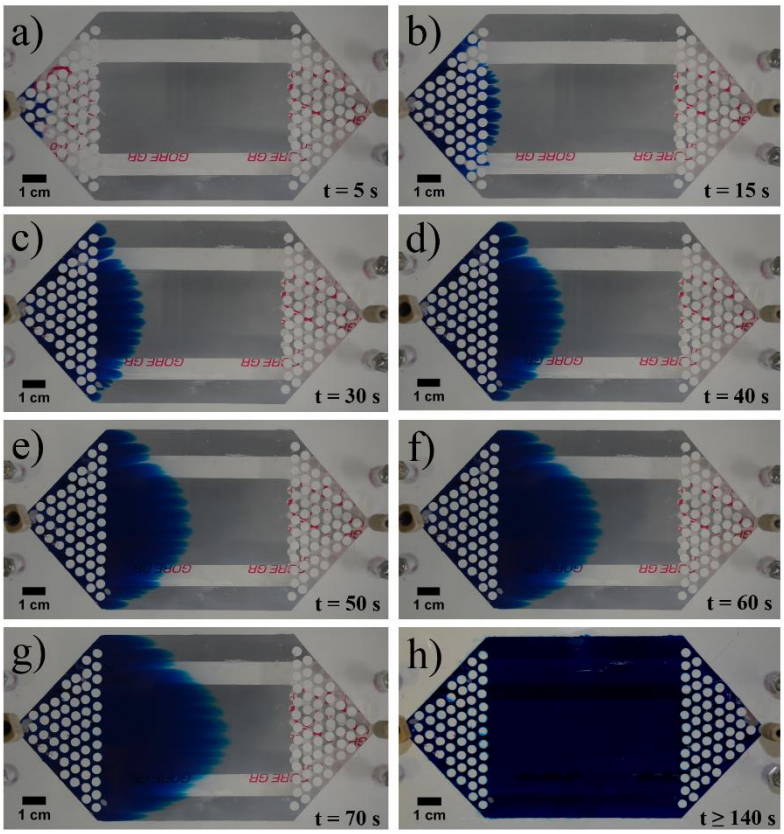

Figure 37: The snapshot image of the time evolution of colored water flow distribution achieved by the inlet pre-chamber containing pillars in the hexagonal channel with the rectangular part of 82.00 mm length, 79.67 mm width and 0.32 mm depth. The channel was filled with water, and colored water was pumped by means of a syringe pump at the flow rate of 1,000 µL min^{-1}. Pictures were taken at: a) 5 s; b) 15 s; c) 30 s; d) 40 s; e) 50 s; f) 60 s; g) 70 s and h) ≥ 140 s after starting the pump.

Slika 37: Posnetek časovnega poteka porazdelitve toka obarvane vode v kanalu s predkomoro, ki vsebuje stebričke za porazdelitev tekočine v šesterokotnem kanalu z 82,00 mm dolgim, 79,67 mm širokim in 0,32 mm globokim pravokotnim delom. Po napolnjenju kanala z vodo smo vanj s pomočjo injekcijske črpalke črpali obarvano vodo s pretokom 1000 µL min^{-1}. Slike smo posneli po času: a) 5 s; b) 15 s; c) 30 s; d) 40 s; e) 50 s; f) 60 s; g) 70 s in h) ≥ 140 s od zagona črpalke.

The MPBRs presented in Figure 34 with 4, 40.10 and 79.67 mm wide channels, where the latter two yielded reactor volumes above 1 mL (Table 6), were tested and compared regarding efficiency. The flow rates ranged from 1.7 to 50.8 µL min^{-1} for the narrowest and from 36.3 to 1,090.0 µL min^{-1} for the widest channel, yielding the mean residence times up to 35.4 min. The amount of packed LentiKats® with the specific enzyme activity of 0.73 U $mg_{ATA\text{-}wt}^{-1}$ yielded final enzyme loads between 43.49 and 46.87 U mL^{-1} and bed porosities between 0.58 and 0.60 (Table 6). As evident from Figure 38, improved fluid flow distribution resulted in the almost equal performance of MPBRs with various channel widths, where proportionally higher flow rates were used to achieve the same mean residence times. Conversions of above 90% were achieved in all tested MPBRs within less than 20 min (Figure 38), while achieved *BPN*s were 485.2, 536.2 and 642.4 μmol_{ACP} $g_{ATA\text{-}wt}^{-1}$ for the three consecutively wider channels, respectively (Table 6).

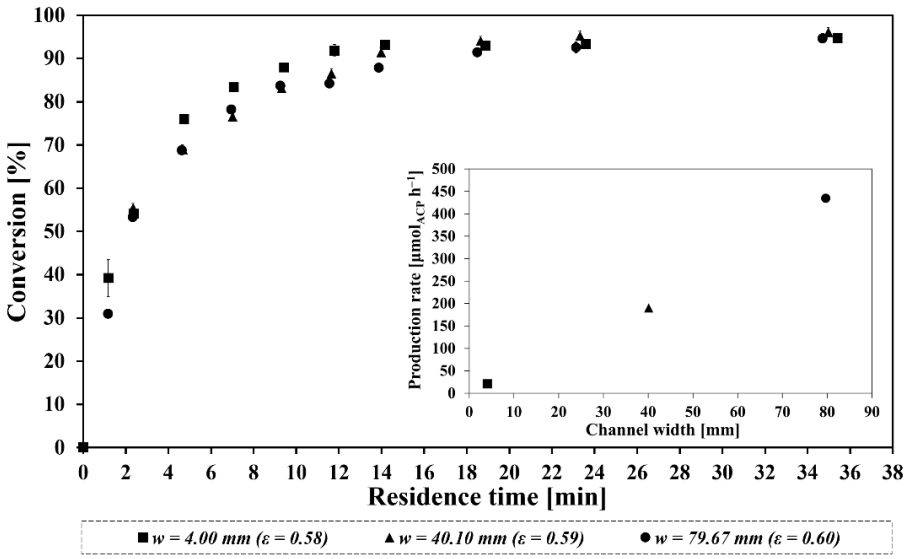

Figure 38: Impact of channel width on substrate conversions at the MPBRs outlets at various flow rates and thereby mean residence times together with production rates estimated at 70% conversion in the MPBRs with rectangular (■) and hexagonal (▲ and ●) channels uniformly packed with LentiKats® having the specific enzyme activity of 0.73 U $mg_{ATA\text{-}wt}^{-1}$. The reaction was performed under the same conditions as described in Figure 35. Other characteristics of the MPBRs are presented in Table 6. The relative standard deviations in the inset graphs are below 10%.

Slika 38: Vpliv širine kanala na konverzijo substrata na izstopu iz MPBR pri različnih pretokih in s tem zadrževalnih časih skupaj s produktivnostjo, ocenjeno pri 70 % konverziji, v MPBR s pravokotnim (■) in šesterokotnim (▲ in ●) kanalom z uniformnim slojem LentiKats® s specifično encimsko aktivnostjo 0,73 U $mg_{ATA\text{-}wt}^{-1}$. Reakcijo smo izvedli pod enakimi pogoji kot je opisano na Sliki 35. Ostale značilnosti MPBR so predstavljene v Tabeli 6. Relativne standardne deviacije v notranjem grafu so manjše od 10 %.

Favorable hydrodynamic conditions within all tested channel widths with pre-chambers containing pillars were further confirmed by linear increases in production rates with channel widths. The widest channel achieved a more than 20-times higher production rate than the MPBR with 4 mm wide channel of the same length (inset graph in Figure 38).

4.2.2.3 Miniaturized packed bed reactors of different channel depths

Further study considered changes in channel depth for increasing the capacity of MPBRs with hexagonal channels having 82.80 mm long, 40.10 mm wide, and 0.32, 0.64, or 0.96 mm deep rectangular parts, where the last two had the reactor volumes above 2 mL (Table 6). The MPBRs were uniformly packed with LentiKats® with the enzyme-specific activity of 0.73 U $mg_{ATA\text{-}wt}^{-1}$ in one, two, or three layers, yielding final enzyme loads between 40.57 and 43.49 U mL^{-1}, and bed porosities between 0.59 and 0.62 (Table 6). The substrate mixture was introduced at different flow rates ranging from 18.0 to 540.0 µL min^{-1} for the MPBR with 0.32 mm deep channel, and from 57.7 to 1,730.7 µL min^{-1} for the MPBR with 0.96 mm deep channel, yielding the mean residence times up to 35 min. It was demonstrated that only the MPBR containing one layer of LentiKats® reached maximal conversion within tested mean residence times, while the MPBRs with more layers of particles one on top of the other achieved significantly lower conversions at the same mean residence times (Figure 39). A decrease of *BPN*s from 536.2 $\mu mol_{ACP}\ g_{ATA\text{-}wt}^{-1}$ achieved in the MPBR with one layer down to 362.7 $\mu mol_{ACP}\ g_{ATA\text{-}wt}^{-1}$ achieved in the MPBR with three layers of LentiKats® (0.96 mm deep channel) was observed despite cca. 3-times increased flow rates (Table 6). This could result from the observed sticking of particles packed in layers, preventing the fluid flow around the particles and leading to the formation of flow channels. Such bypassing prevented substrate molecules from reaching all enzymes packed in more than one layer within the MPBRs. As a consequence, the production rate dropped about 1.8 times in the MPBRs with three layers of LentiKats® compared to the one with only one layer (inset graph in Figure 39).

Significantly lower conversions were obtained in the MPBR with the 0.64 mm deep channel randomly packed with LentiKats® with the enzyme-specific activity of 0.73 U $mg_{ATA\text{-}wt}^{-1}$ in multiple layers yielding the final enzyme load of 167.45 U mL^{-1} and bed porosity of 0.28 (Table 6). *BPN* of 72.1 $\mu mol_{ACP}\ g_{ATA\text{-}wt}^{-1}$ was achieved in this MPBR (Table 6). The less efficient performance of MPBRs with multiple layers of LentiKats® was again a consequence of the squeezing and sticking of hydrogel particles during the packing, resulting in the formation of larger fluid streams through the layer (Fogler, 1999). As a consequence, the production rate of only cca. 20 $\mu mol_{ACP}\ h^{-1}$ was achieved (inset graph in Figure 39).

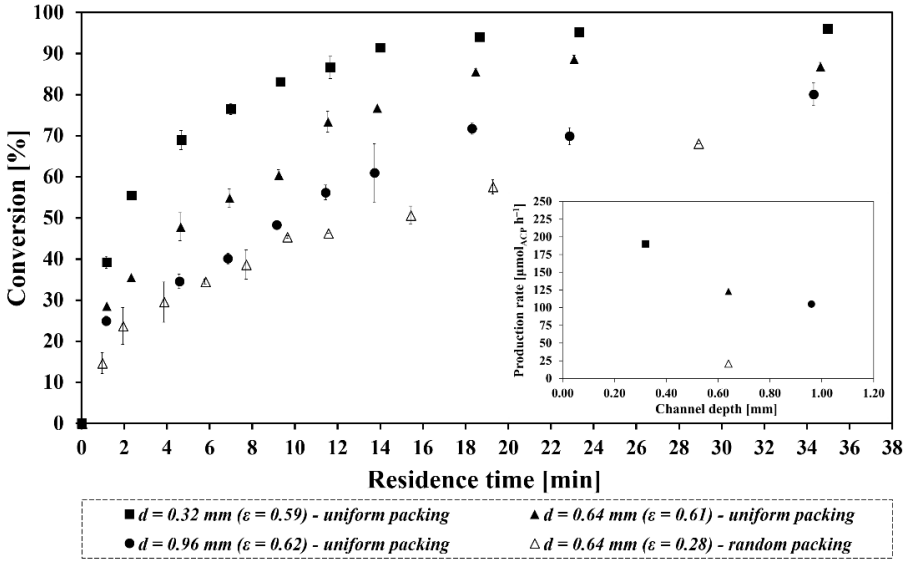

Figure 39: Impact of channel depth and particle distribution on substrate conversions at the MPBR outlets at various flow rates and thereby mean residence times together with production rates estimated at 70% conversion in the MPBRs with hexagonal channels uniformly or randomly packed with LentiKats® having the specific enzyme activity of 0.73 U $mg_{ATA\text{-}wt}^{-1}$. The reaction was performed under the same conditions as described in Figure 35. Other characteristics of the MPBRs are presented in Table 6. The relative standard deviations in the inset graph are below 10%.

Slika 39: Vpliv globine kanala na konverzijo substrata na izstopu iz MPBR pri različnih pretokih in s tem zadrževalnih časih skupaj s produktivnostjo, ocenjeno pri 70 % konverziji, v MPBR s šesterokotnim kanalom z uniformnim ali neuniformnim slojem LentiKats® s specifično encimsko aktivnostjo 0,73 U $mg_{ATA\text{-}wt}^{-1}$. Reakcijo smo izvedli pod enakimi pogoji kot je opisano na Sliki 35. Ostale značilnosti MPBR so predstavljene v Tabeli 6. Relativne standardne deviacije v notranjem grafu so manjše od 10 %.

4.2.2.4 Estimation of temperature effects

Miniaturized devices could be used for a high throughput optimization of the process parameters studied under continuous flow conditions, leading to lower material consumption in comparison to conventional systems (Wohlgemuth et al., 2015). In this study, a temperature effect on transamination was evaluated in the range from 30 to 75 °C at the flow rate of 25 µL min^{-1} yielding the mean residence time of 2.6 min. Experiments were performed in a thermostated MPBR with a rectangular 81.61 mm long, 4.10 mm wide and 0.32 mm deep channel, packed with one layer of LentiKats® with an enzyme-specific activity of 0.73 U $mg_{ATA\text{-}wt}^{-1}$, giving bed porosity of 0.60 and enzyme load of 43.28 U mL^{-1} (Table 6).

As evident from Figure 40, the results revealed 55 °C as the optimal temperature for the studied process using LentiKats® with immobilized ATA-wt. After 2.6 min at 55 °C, *BPN* of 361.7 μmol_{ACP} $g_{ATA\text{-}wt}^{-1}$ and production rate of cca. 31.9 μmol_{ACP} h^{-1} were achieved (Table 6), while MPBR with almost the same reactor geometry yielded *BPN* of 276.8 μmol_{ACP} $g_{ATA\text{-}wt}^{-1}$ and production rate of cca. 27 μmol_{ACP} h^{-1} at similar mean residence time

(τ = 2.4 min) when operated at room temperature. Such result indicates on the enzyme thermostabilization after immobilization since 30 °C was determined as the optimal temperature for the same (non-immobilized) ATA-wt assayed using (*S*)-α-MBA and PYR (Börner et al., 2017a). On the other hand, an assay using isopropylamine and 4-phenyl-2-butanone as a substrate revealed retained activity below 20% after 40 h of incubation at 50 °C as well as decrease of enzyme specific activity at elevated temperatures (Börner et al., 2017a, 2017b).

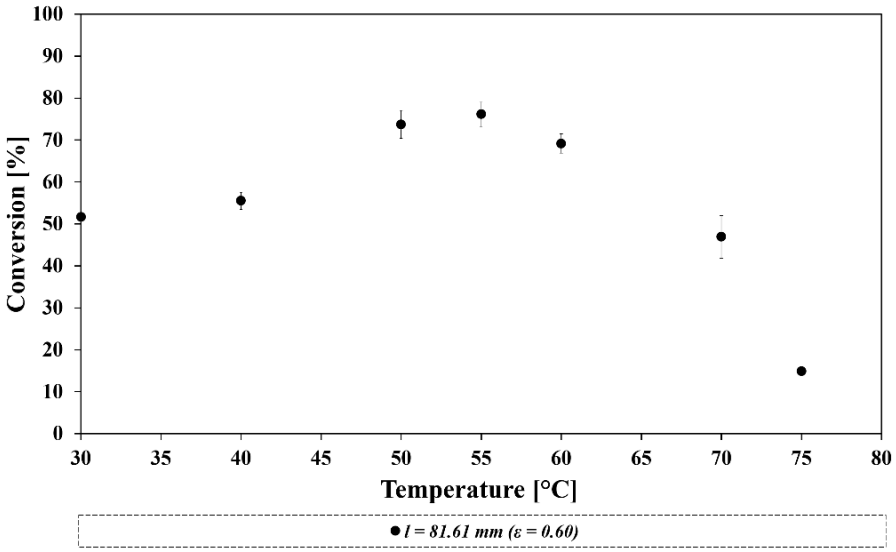

Figure 40: Influence of temperature on conversion at the MPBR outlet at the flow rate of 25 µL min^{-1} (τ = 2.6 min) during the continuous operation of the MPBR uniformly packed with LentiKats® having the specific enzyme activity of 0.73 U $mg_{ATA\text{-}wt}^{-1}$. The reaction was performed at the same conditions as described in Figure 35, except the temperature. Other characteristics of the MPBR are presented in Table 6.

Slika 40: Vpliv temperature na konverzijo na izstopu iz MPBR pri pretoku 25 µL min^{-1} (τ = 2.6 min) ob kontinuirnem obratovanju MPBR z uniformnim slojem LentiKats® s specifično encimsko aktivnostjo 0,73 U $mg_{ATA\text{-}wt}^{-1}$. Reakcijo smo izvedli pod enakimi pogoji kot je opisano na Sliki 35. Ostale značilnosti MPBR so predstavljene v Tabeli 6.

Regarding other transaminases, ATA-117 (Codexis® Inc., Redwood City, USA) immobilized in a sol-gel/Celite 545 shown an optimal temperature between 40 and 50 °C, while the specific activity of non-immobilized enzyme decreased at temperatures above 30 °C (Koszelewski et al., 2010b). This is consistent with reports on the optimal temperatures in the range between 50 °C and 60 °C reported for various immobilized ω-TAs (Schell et al., 2009; Mallin et al., 2014).

4.2.2.5 Estimation of operational stability

In order to evaluate the operational stability of the system, the MPBR with a rectangular 20 mm long, 4 mm wide and 0.23 mm deep channel was tested over the period of 21 days. The

channel was packed with one layer of LentiKats® having enzyme activity of 0.50 U $mg_{ATA\text{-}wt}^{-1}$ and yielding enzyme load of 65.88 U mL^{-1} and bed porosity of 0.40 (Table 6). As evident from Figure 41, the MPBR with ATA-wt immobilized in LentiKats® expressed relative volumetric productivity above 80% within the tested period (volumetric productivity at the beginning was 38.5 $mmol_{ACP}$ L^{-1} min^{-1}).

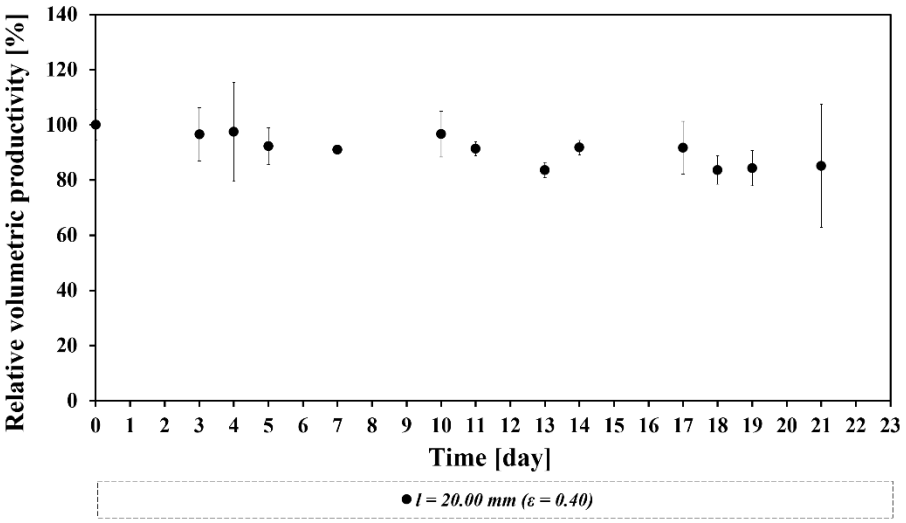

Figure 41: Operational stability of the MPBR uniformly packed with LentiKats® having the specific enzyme activity of 0.50 U $mg_{ATA\text{-}wt}^{-1}$ over the period of 21 days. The reaction in MPBR was performed by continuous pumping of 40 mM equimolar inlet concentration of (*S*)-*α*-MBA and PYR in 20 mM sodium phosphate buffer (pH 8.0) together with 0.1 mM PLP, at the flow rate of 0.5 µL min^{-1} at 24 ºC. Other characteristics of the MPBR are presented in Table 6.

Slika 41: Obratovalna stabilnost MPBR z uniformnim slojem LentiKats® s specifično encimsko aktivnostjo 0,50 U $mg_{ATA\text{-}wt}^{-1}$ v obdobju 21 dni. Reakcijo smo izvedli z kontinuiranim črpanjem 40 mM ekvimolarne mešance (*S*)-*α*-MBA in PYR v 20 mM natrijevem fosfatnem pufru (pH 8,0) z 0,1 mM PLP pri pretoku 0,5 µL min^{-1} in pri 24 °C. Ostale značilnosti MPBR so predstavljene v Tabeli 6.

No changes in the physical or mechanical characteristics of LentiKats® were observed during continuous MPBR operation. Results obtained with LentiKats® in the developed MPBR were much better than reported for MPBR with His_6-tagged ω-TAs immobilized onto Ni-NTA agarose beads, for which the productivity was reduced to 60% after only 8 h of a continuous process (Halim A. A. et al., 2013), and in the study with *E. coli* cells overexpressing ω-TA, immobilized in LentiKats®, which retained around 80% of initial activity in five consecutive batch processes, each running for 3 h (Cárdenas-Fernández et al., 2012). Furthermore, sol-gel/Celite 545 immobilized ATA-117 retained 78% of its initial activity after 8 repetitive uses (total time 8 days) in a batch process for the kinetic resolution of *rac*-4-phenyl-2-butylamine at 30 °C (Koszelewski et al., 2010b). The same ATA-117 entrapped in a sol-gel carrier prepared by PVA and used for the kinetic resolution of racemic MBA retained cca. 82% of its initial activity after 5 days at 30 °C (Päiviö and Kanerva, 2013).

4.2.3 Hydrodynamics in miniaturized packed bed reactors with LentiKats®

The hydrodynamics in MPBRs is categorized as one of the three major topics important for reactor efficiency (together with mass transfer and kinetic studies) and mainly considers flow regime, pressure drop and RTD (Faridkhou et al., 2016). MPBRs have similarities with both macro- as well as micro-scale reactors. The former are similar to the MPBRs regarding the operational and structural point of view, while the latter are similar regarding the scale point of view (Faridkhou et al., 2016). Therefore, this subchapter deals with the hydrodynamics of MPBRs packed with LentiKats®, whereby their characteristics are estimated under the operational conditions (conditions applied during the transamination reaction presented in Sections 4.2.2.2 and 4.2.2.3).

4.2.3.1 Pressure drop

The measurements have revealed moderate and linearly dependent pressure drops in the MPBRs along the applied range of flow rates, which is in accordance with the predictions. The pressure drops were approximately equal among various channel geometries, except in the smallest among the tested MPBR with a rectangular channel of 81.50 mm length, 4.00 mm width and 0.32 mm depth, where the pressure drop of cca. 9 kPa was measured at the flow rate of 100 µL min^{-1} (Figure 42).

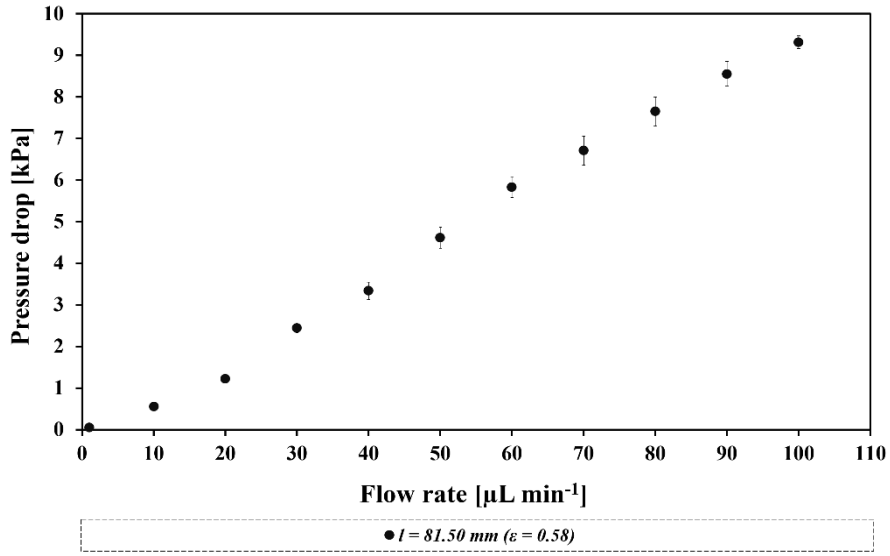

Figure 42: The effect of flow rate on the pressure drop in an MPBR with rectangular channel uniformly packed with LentiKats® in one layer (Q = 10–100 µL min^{-1}; T = 24 ºC). Other characteristics of the MPBR are presented in Table 6.

Slika 42: Vpliv pretoka na padec tlaka v MPBR s pravokotnim kanalom z uniformnim enim slojem LentiKats® (Q = 10–100 µL min^{-1}; T = 24 ºC). Ostale značilnosti MPBR so predstavljene v Tabeli 6.

This is at the same time the MPBR with the longest rectangular channel, so the measured pressure drop is assumed to be maximal compared to the MPBRs with shorter channels of the same geometry described previously (Table 6). Such results are presumed to be a consequence of the reactor's design. Namely, only the MPBR with 81.50 mm long, 4.00 mm wide and 0.32 mm deep rectangular channel had LentiKats® packed directly below the inlet and outlet holes, which could increase the pressure drop, while this was not the case with MPBRs with triangular pre-chambers containing pillars (Figure 34b and 34c). The measured pressure drop was a 3-times higher than that of cca. 3 kPa measured in other MPBRs at the same flow rate (Q = 100 µL min^{-1}) (Figure 43).

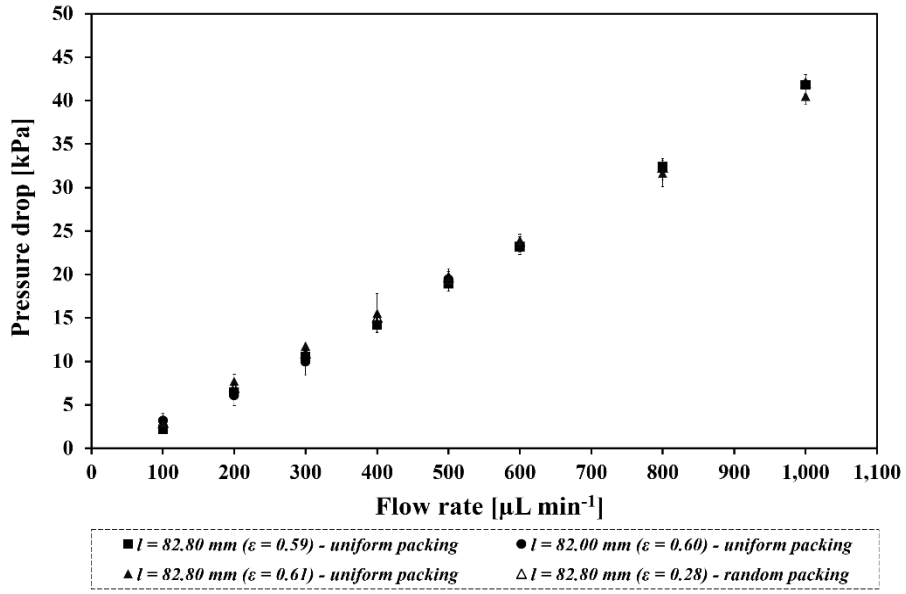

Figure 43: The effect of flow rate on the pressure drop in the MPBRs with hexagonal channels of different widths and depths uniformly or randomly packed with LentiKats® (Q = 100–1,000 µL min^{-1}; T = 24 ºC). Other characteristics of the MPBRs are presented in Table 6.

Slika 43: Vpliv pretoka na padec tlaka v MPBR s šesterokotnimi kanali različnih širin in globin z uniformnim ali neuniformnim slojem LentiKats® (Q = 100–1000 µL min^{-1}; T = 24 ºC). Ostale značilnosti MPBR so predstavljene v Tabeli 6.

The measured pressure drops in the MPBRs with hexagonal channels were higher at elevated flow rates but still moderate, not exceeding 42 kPa at the flow rate of 1,000 µL min^{-1} (Figure 43). For instance, a pressure drop in a microreactor packed with the spherical microparticles (diameter 53–74 µm) was 560 kPa measured by flowing ethanol at the same flow rate (Losey et al., 2001). Ajmera et al. (2002) have been proposed a solution for excessive pressure drops in miniaturized devices, where a cross-flow reactor design capable of minimizing the pressure drop through the bed of microparticles has been reported.

On the other hand, the large-scale packed bed chromatographic columns packed with a gel-type material undergo unforeseeable increase of the pressure drop due to a sudden and

unexpected collapse of the gel beads (Weuster-Botz et al., 2007). In such a way, a preparative-scale chromatographic column packed with the gel-type ion exchange resin (diameter 20–30 μm) had the pressure drop up to 24.9 MPa at flow rate of 500 μL min^{-1} (Ladisch, 2001; Weuster-Botz et al., 2007). Such results once again confirmed ascendancy of the MPBR, and are in accordance with the assertions from the literature that the enzymes are more stable in MPBRs due to lower pressure drop compared with CPBRs (Wohlgemuth et al., 2015).

As evident from Table 7, the MPBRs of different sizes and uniform packing had basically the same Re_p calculated at the maximal flow rates (except the MPBR with three layer of particles, which is expected to be within the similar range), while the MPBR with random packing had slightly larger Re_p. These estimations undoubtedly confirmed the existence of laminar flow (Ribeiro et al., 2010). The unchanged Re_p at proportionally higher flow rates at the inlets of different MPBRs indicates retained hydrodynamic properties.

Table 7: Hydrodynamic characteristics and energy dissipation rate of MPBRs with LentiKats® at 24 °C.
Tabela 7: Hidrodinamske lastnosti in vnos moči v MPBR z LentiKats® pri 24 °C.

l **[mm]**	***w*** **[mm]**	***d*** **[mm]**	**No. of layers[b)]**	***Q*** **[c)] [μL min^{-1}]**	***Re*** **$_p$[d)] [–]**	***P*** **$_1$[e)] [kW m^{-3}]**	**Price[g)] [€ m^{-3} day^{-1}]**
81.50	4.00	0.32	1	50.8	0.66	0.07	0.13
82.80	40.10[a)]	0.32	1	540.0	0.68	0.20[f)]	0.39[f)]
82.00	79.67[a)]	0.32	1	1,090.0	0.68	0.39[f)]	0.74[f)]
82.80	40.10[a)]	0.64	2	1,118.7	0.68	0.47[f)]	0.89[f)]
82.80	40.10[a)]	0.64	2–3	616.4	0.81	0.23[f)]	0.43[f)]

a) The values refer to the width of the rectangular part of the hexagonal channel.

b) Number of LentiKats® layers placed one on top of the other within the channel depth.

c) Maximal flow rate under reaction conditions.

d) Calculated according to Equation 13 at maximal flow rates using the Sauter mean diameter of LentiKats® (d_{32} = 0.52 mm), bed porosities as stated in Table 6 and properties of water as follows: ρ = 997.3 kg m^{-3} and $\eta = 9.11 \times 10^{-4}$ Pa s.

e) Energy dissipation rate estimated from the experimental data for given operational conditions (Sections 4.2.2.2 and 4.2.2.3).

f) Estimated including the void volume in the triangular pre-chambers containing pillars.

g) The price for the operation of the MPBR under given conditions over the period of one day. Estimated based on the average electricity price for industry exclusive of VAT in the Republic of Slovenia (0.079 EUR kWh^{-1}) in the 4th quarter 2016 (SORS, 2016).

The relationships between applied flow rates and pressure drops (Figures 42 and 43) were used to estimate important parameters related to the flow regime, energy dissipation rate and operational costs per single MPBR under the operational conditions used for the biotransformation (Sections 4.2.2.2 and 4.2.2.3) (Table 7). Namely, the energy dissipation rate was up to 0.47 kW m^{-3}, which requires up to 0.89 € m^{-3} to operate the reactor under given conditions over the period of one day. For instance, a batch reactor (V = 1 m^3), static mixer ($V = 1 \times 10^{-5}$ m^3) and packed microchannel ($V = 1 \times 10^{-8}$ m^3) would cause the energy

dissipation rate of 10, 179.5–2,991.9 and 29.9–4,886.8 kW m^{-3} if using water as working fluid, respectively (Su et al., 2010 and ref. therein).

4.2.4 Mass transfer in a miniaturized packed bed reactor with LentiKats®

The influence of fluid flow dynamics on the immobilized transaminase specific activity within LentiKats® was firstly evaluated in a mixing reactor at different stirring speeds. By increasing the stirring speed from 400 rpm to 600, 800 and 1,000 rpm, estimated specific enzyme activities increased from 0.50 to 0.53, 0.54 and 0.59 U $mg_{ATA\text{-}wt}^{-1}$, respectively. It indicates that the outer boundary layer of the fluid at the surface of the particles, acting as a mass transfer barrier, influenced the reaction rate in the batch reactor. Nonetheless, this boundary layer was assumed to be insignificant in the MPBR due to very small scale length, what has already been discussed in the theoretical part (Section 2.3.3.1).

Furthermore, diffusion coefficients for (*S*)-*α*-MBA, PYR, ACP and L-ALA in water (D_{MBA}, D_{PYR}, D_{ACP} and D_{ALA}) were estimated using the Wilke-Chang empirical correlation (Equation 8), while the corresponding effective diffusion coefficients in hydrogel (D_{eMBA}, D_{ePYR}, D_{eACP} and D_{eALA}) were estimated using Equation 16 and taking into accound porosity (ε_{LK}) and tortuosity (ζ_{LK}) of LentiKats® as 0.703 and 1.170, respectively (Schenkmayerová et al., 2014). Estimated values are within the order of magnitude typically reported for various chemical species in water (Introduction to Soil…, 2015), and in hydrogels (Axelsson and Persson, 1988; Ariga et al., 1994; Graham and Jovanovic, 1999) (Table 8).

Table 8: Estimated values of diffusion (D) and effective diffusion (D_e) coefficients for substrates and products of transamination in water and in LentiKats®, respectively.

Tabela 8: Ocenjene vrednosti difuzijskih koeficientov za substrate in produkte transaminacije v vodi (D) in pripadajočih koeficientov efektivne difuzije (D_e) v LentiKats® pripravku.

Parameter	Estimated value	Parameter	Estimated value
D_{MBA}	0.90×10^{-9} m^2 s^{-1}	D_{eMBA}	5.38×10^{-10} m^2 s^{-1}
D_{PYR}	1.13×10^{-9} m^2 s^{-1}	D_{ePYR}	6.82×10^{-10} m^2 s^{-1}
D_{ACP}	0.95×10^{-9} m^2 s^{-1}	D_{eACP}	5.71×10^{-10} m^2 s^{-1}
D_{ALA}	1.22×10^{-9} m^2 s^{-1}	D_{eALA}	7.34×10^{-10} m^2 s^{-1}

Regarding mass transport phenomena in MPBRs, a time-scale analysis was performed based on the example of the MPBR with 81.50 mm long, 4.00 mm wide and 0.32 mm deep rectangular channel uniformly packed with one layer of LentiKats® (Table 6) in order to identify the rate limiting step for the overall process flow. The values of Pe_p, calculated according to Equation 18 and considering diffusivity of (*S*)-*α*-MBA (Table 8), were sufficiently high (from 22.35 to 670.62 at the applied flow rates from 1.7 to 50.8 μL min^{-1}, respectively) to conclude the dominance of the convective mass transport over the diffusive

one along the channel length. Therefore, assuming a uniform fluid distribution across the entire width of the channel, it could be said that the reactant molecules are being transferred rapidly to the surface of the particles and the characteristic diffusion times in the directions of the channel width and depth could be neglected in order to simplify the analysis. So, the relevant characteristic times used in the analysis are the mean residence time, reaction time and diffusion time in a porous LentiKats® approximated as a spherical particle with the Sauter mean diameter of 0.52 mm (Table 9).

Table 9: Characteristic times considered in the time-scale analysis of an MPBR with LentiKats®.
Tabela 9: Značilni časi upoštevani pri časovno-dimenzijski analizi v MPBR z LentiKats® delci.

Characteristic time	**Equation**	**Estimated value**
Mean residence time, τ	Equation 24[a)]	1.2–35.4 min
Reaction time, τ_r	Equation 11[b)]	1.55 min
Diffusion time in the porous particle, τ_p	Equation 17[c)]	2.09 min

a) Parameters: V_V = 60 µL; Q = 1.7–50.8 µL min^{-1}.

b) Parameters: C_{Sin} = 40 mol m^{-3}; C_e = 36.92 g L^{-1}; $v_0 = 7 \times 10^{-4}$ mol g^{-1} min^{-1} (v_0 was experimentally obtained for the non-immobilized enzyme in a batch reactor at 24 °C according to the protocol for enzyme activity determination described in Section 3.3.2).

c) Parameters: d_{32} = 0.52 mm; $D_e = 5.38 \times 10^{-10}$ m^2 s^{-1} (D_e was used for (*S*)-α-MBA, since it was lower than for PYR).

Comparison of estimated characteristic times presented in Table 9 has revealed that $\tau_p > \tau_r$, which indicates the diffusive mass transfer inside LentiKats®, visualized in Figure 44, as the limiting factor for the overall reaction process.

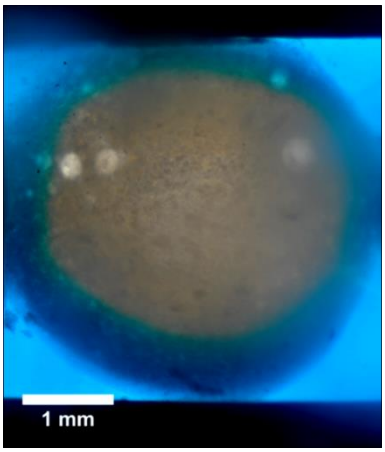

Figure 44: Visualization of diffusion process into LentiKats® using Amidoblau V: the dye diffuses from the brim towards the center of the particle.
Slika 44: Vizualizacija difuzije v LentiKats® z barvo Amidoblau V: barva difundira od roba proti centru delca.

This was not unexpected because the diffusive mass transfer limitation is a common problem when using porous hydrogel particles as biocatalysts carriers (Jovanovic et al., 2015). An opposite situation has been reported for a microreactor with ω-TA immobilized on the inner

walls based on the ionic interactions of positively tagged enzyme and negatively charged surface, wherein the absence of any physical hindrance (e.g. caused by porous carrier material) led to the reaction-limited process (Miložič et al., 2017).

The conclusion of this time-scale analysis also stands for the MPBRs with wider channels, because they had approximately the same hydrodynamic conditions (similar values of Re_p with maximal error of 3.16%, mostly due to the differences in bed porosity).

4.3 MINIATURIZED PACKED BED REACTORS WITH NOVOZYM® 435

4.3.1 Characterization of Novozym® 435

As reported in the literature (Denčić et al., 2013), spherical particles of the immobilized preparation Novozym® 435 have a high polydispersity, which is undesirable for the application in MPBRs. These findings were confirmed through the measurements of the particle diameter performed on a random sample (n = 300) obtained from the commercial preparation. The results revealed a very broad size distribution of particles, with the average diameter of 351.39 ± 132.18 µm. In order to gain a narrower size distribution, the initial sample was sieved through the sieves with the pore size ranging from 500 to 425 µm and from 425 to 300 µm, respectively. The first fraction had the average particle diameter of 462.94 ± 19.60 µm, while the second contained the particles with the average diameter of 372.10 ± 27.05 µm (Figure 45). It was also observed that the fraction below 300 µm contained a lot of debris and dust emanating from the broken particles, so this fraction would not be suitable for the application.

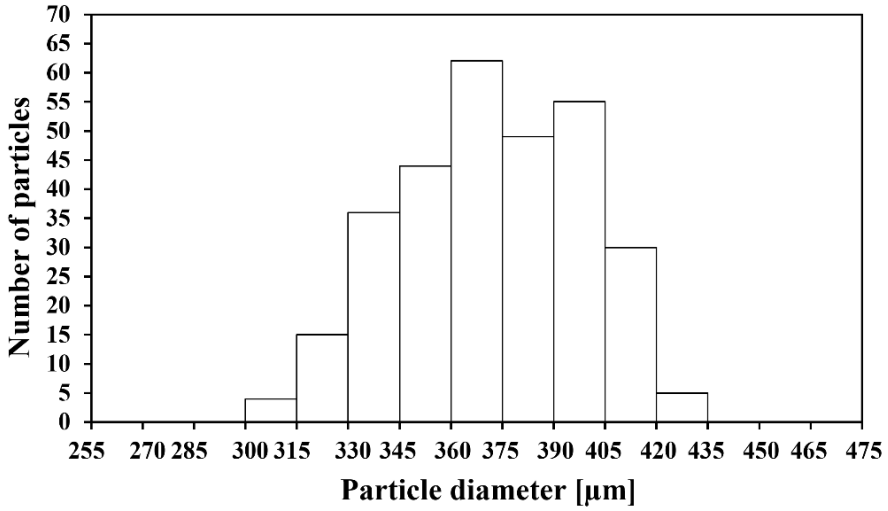

Figure 45: A size distribution of the Novozym® 435 fraction obtained after sieving through the sieves with the pore size from 425 to 300 µm (n = 300).

Slika 45: Porazdelitev velikosti delcev pripravka Novozym® 435 po presejanju skozi sita z velikostjo por od 425 do 300 µm (n = 300).

Therefore, the particles from the second fraction were exclusively used throughout the study. The specific activity of Novozym® 435 from this fraction evaluated in a batch experiment and expressed either per mass of immobilized CaLB or per mass of particles were 133.05 ± 2.71 U mg_{CaLB}^{-1} and 13.31 ± 0.27 U mg_{N435}^{-1}, respectively.

4.3.2 Biotransformation in miniaturized packed bed reactors with Novozym® 435

The second biotransformation, namely transesterification of VB to BB, was successfully performed in the developed MPBRs with rectangular (Figure 46a) and hexagonal (Figure 46b) channels of various sizes randomly packed in one or two layers with immobilized CaLB in the form of commercial preparation Novozym® 435. The scale-up principle was the same as in the case of the MPBRs with LentiKats®, while the design of MPBRs was enriched by embedding an additional layer of the non-compressible PTFE stripe to define the channel depth and a thin double-sided adhesive tape to fix and retain the particles within the reactor.

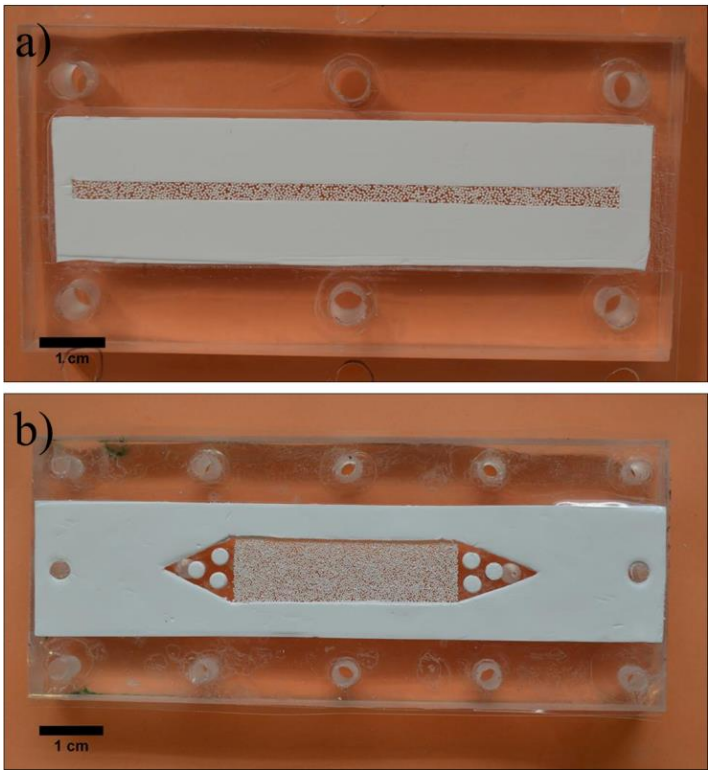

Figure 46: MPBRs, randomly packed with one layer of Novozym® 435 in: a) rectangular channel; b) hexagonal channel with triangular inlet and outlet parts containing pillars.

Slika 46: MPBR z enim slojem Novozym® 435 pripravka v: a) pravokotnem kanalu; b) šesterokotnem kanalu s trikotnim vstopnim in izstopnim delom s stebrički.

Characteristics and performances of tested MPBRs are summarized in Table 10.

Table 10: Characteristics and performance of tested MPBRs with Novozym® 435 at 24 °C.
Tabela 10: Značilnosti testiranih MPBR z Novozym® 435 pri 24 °C.

l [mm]	w [mm]	d [mm]	No. of layers[b)]	V [µL]	V_v[c)] [µL]	ε [–]	γ_e [U µL^{-1}]	BPN[d)] [mmol$_{BB}$ g$_{CaLB}^{-1}$]
23.93	3.12	0.40	1	29.9	17.1	0.57	5.53	13.56
52.19	2.95	0.40	1	61.6	35.3	0.57	5.51	12.72
81.00	2.94	0.40	1	95.3	56.5	0.59	5.06	13.35
50.88	15.80[a)]	0.40	1	321.6	184.0	0.57	5.52	12.18
53.79	29.22[a)]	0.40	1	628.7	363.6	0.58	5.38	12.64
50.88	15.80[a)]	0.80	2	643.1	375.6	0.58	5.26	14.03
23.93	3.12	0.40	1	29.9	17.1	0.57	5.53	11.39[e)]
82.00	2.92	0.40	1	95.8	55.9	0.58	5.28	7.21[f)]

a) The values refer to the width of the rectangular part of the hexagonal channel.

b) Number of Novozym® 435 layers placed one on top of the other within the channel depth.

c) Estimated from the reactor volume and volume of particles calculated from their mass and density.

d) Maximal *BPN* calculated at the longest mean residence time (τ = 1.4 min).

e) Calculated at T = 75 °C and τ = 0.1 min.

f) Calculated at the beginning of the operational stability experiment (Q = 559 µL min^{-1} and τ = 0.1 min).

4.3.2.1 Miniaturized packed bed reactors of different channel lengths

The MPBRs with only one layer of Novozym® 435 with the specific enzyme activity of 133.05 U mg$_{CaLB}^{-1}$ were tested first. The particles (7.1 to 21.5 mg) were randomly packed in 23.93 to 81.00 mm long, cca. 3 mm wide (differences are stemming from the channel cutting; error is less than 3%) and 0.40 mm deep rectangular channels with volumes from 29.9 to 95.3 µL, yielding final enzyme loads between 5.06 and 5.53 U µL^{-1} (Table 10). Bed porosities of tested MPBRs were between 0.57 and 0.59 (Table 10), which is slightly less than the value of 0.64 reported by Pohar et al. (2012) who had a 90 mm long, 5 mm wide and 0.448 mm deep rectangular channel packed with Novozym® 435 with the average diameter of 454 µm. An equimolar 600 mM solution of both substrates in *n*-heptane was pumping through the MPBRs at flow rates ranging from 12.2 to 565.2 µL min^{-1} in order to achieve the mean residence times from 0.1 to 1.4 min.

All three tested MPBRs performed equally well at the same mean residence times and the maximal conversion of cca. 95% was obtained in less than 0.8 min (Figure 47). By comparison, the same reaction performed in an MPBR with the CaLB concentration expressed per reactor volume of 24.80 g$_{CaLB}$ L^{-1} (the MPBRs tested within this part had the CaLB concentrations expressed per reactor volume from 22.57 to 23.77 g$_{CaLB}$ L^{-1}) at 25 °C

using an imidazolium-based ionic liquid as a solvent achieved a 100% conversion in cca. 5 min (Pohar et al., 2012).

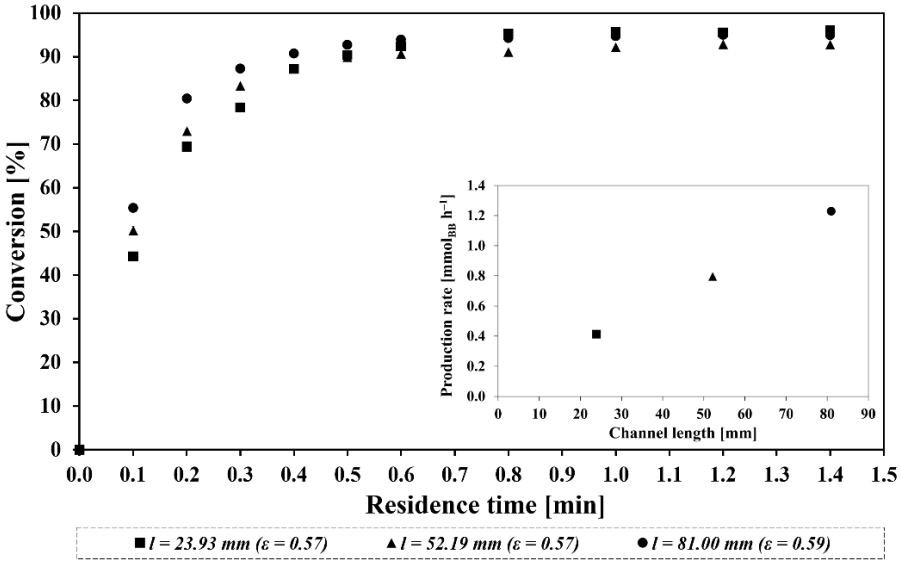

Figure 47: Impact of channel length on substrate conversion at the MPBRs outlets at various flow rates and thereby mean residence times together with production rates estimated at the longest mean residence time (maximal conversion) in the MPBRs with rectangular channels randomly packed in one layer with Novozym® 435 having the specific enzyme activity of 133.05 U mg_{CaLB}^{-1}. The reaction was performed by continuous pumping of 600 mM equimolar inlet concentration of VB and BUT in *n*-heptane, at room temperature (T = 24 °C). Other characteristics of the MPBRs are presented in Table 10. The relative standard deviations in the inset graph are below 2%.

Slika 47: Vpliv dolžine kanala na konverzijo substrata na izstopu iz MPBR pri različnih pretokih in s tem zadrževalnih časih skupaj s produktivnostjo, ocenjeno pri najdaljšem zadrževalnem času (makismalni konverziji). MPBR so imeli pravokotni kanal naključno polnjen v enem sloju z Novozym® 435 pripravkom s specifično encimsko aktivnostjo 133,05 U mg_{CaLB}^{-1}. Reakcijo smo izvedli z kontinuiranim črpanjem 600 mM ekvimolarne vstopne raztopine VB in BUT v *n*-heptanu pri sobni temperaturi (T = 24 °C). Ostale značilnosti MPBR so predstavljene v Tabeli 10. Relativne standardne deviacije v notarnjem grafu so manjše kot 2 %.

The comparison of production rates in MPBRs of varying channel lengths estimated at the longest mean residence time (i.e. maximal conversions) revealed a linear proportionality (inset graph in Figure 47), whereby *BPN*s between 12.72 and 13.56 $mmol_{BB}\ g_{CaLB}^{-1}$ were achieved (Table 10), which confirmed an efficient scale-up by increasing channel length within tested inlet concentrations.

4.3.2.2 Miniaturized packed bed reactors of different channel widths

Selected transesterification was further conducted in the MPBRs with the basic rectangular (Figure 46a) or hexagonal (Figure 46b) channels containing pre-chambers with pillars. The MPBRs had 2.95 to 29.22 mm wide channels of cca. 52.29 mm length (error less than 3%) and 0.40 mm depth, randomly packed with Novozym® 435 (from 14.6 to 147.1 mg) having

the specific enzyme activity of 133.05 U mg_{CaLB}^{-1}, yielding in that way the final enzyme loads of 5.51, 5.52 and 5.38 U μL^{-1}, as shown in Table 10. In addition, bed porosities of 0.57 and 0.58 were achieved (Table 10), which were approximately the same as in the previous set of experiments. The flow rates were set to range from 25.2 to 3,636.4 µL min^{-1} in all three MPBRs in order to achieve the mean residence times from 0.1 to 1.4 min.

The maximal conversion of cca. 95% was again achieved within less than 0.8 min in all tested MPBRs (Figure 48), while the production rate estimated at the longest mean residence time kept its linearity with increasing channel width. The MPBR with the widest channel (29.22 mm) achieved cca. 10-times higher production rate than the MPBR with the narrowest channel (2.95 mm) (inset graph in Figure 48). The achieved *BPN*s were revolving around 12.51 $mmol_{BB}$ g_{CaLB}^{-1} for the three MPBRs with the consecutively wider channels (Table 10).

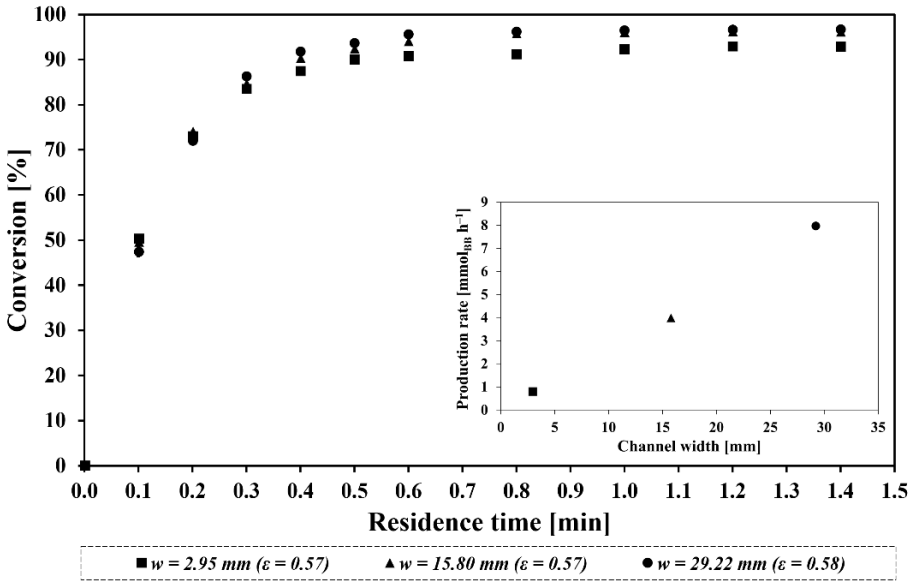

Figure 48: Impact of channel width on substrate conversion at the MPBRs outlets at various flow rates and thereby mean residence times together with production rates estimated at the longest mean residence time (maximal conversion) in the MPBRs with rectangular (■) or hexagonal (▲ and ●) channels randomly packed in one layer with Novozym® 435 having the specific enzyme activity of 133.05 U mg_{CaLB}^{-1}. The reaction was performed under the same conditions as described in Figure 47. Other characteristics of the MPBRs are presented in Table 10. The relative standard deviations in the inset graph are below 2%.

Slika 48: Vpliv širine kanala na konverzijo substrata na izstopu iz MPBR pri različnih pretokih in s tem zadrževalnih časih skupaj s produktivnostjo ocenjeno pri najdaljšem zadržavalnem času (makismalni konverziji) v MPBR s pravokotnim (■) ali šesterokotnim (▲ in ●) kanalom, naključno polnjenim z enim slojem Novozym® 435 pripravka s specifično encimsko aktivnostjo 133,05 U mg_{CaLB}^{-1}. Reakcijo smo izvedli pod enakimi pogoji kot je opisano na Sliki 47. Ostale značilnosti MPBR so predstavljene v Tabeli 10. Relativne standardne deviacije v notranjem grafu so manjše od 2 %.

4.3.2.3 Miniaturized packed bed reactors of different channel depths

The effect of the channel depth on the reactor performance was examined using two MPBRs with the same length and width (50.88 and 15.80 mm), and with channel depths of 0.40 and 0.80 mm, respectively (Table 10). The hexagonal channels with the pre-chambers containing pillars were randomly packed within the rectangular parts of the MPBR in one or two layers with Novozym® 435 (76.3 and 148.4 mg, respectively). Such packing resulted in final enzyme loads of 5.52 and 5.26 U μL^{-1} as well as bed porosities of 0.57 and 0.58, respectively (Table 10). Evaluation of the MPBRs was performed under the flow rates ranging from 131.5 to 3,756.3 µL min^{-1} in order to achieve the mean residence times from 0.1 to 1.4 min.

As evident from Figure 49, the MPBR with two layers achieved slightly higher conversion at mean residence times below 0.6 min than the MPBR with one layer.

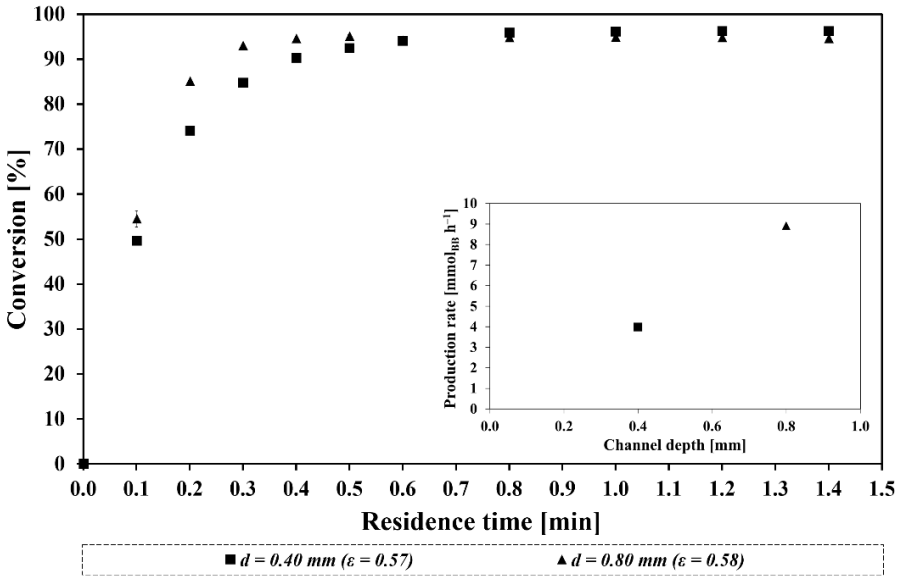

Figure 49: Impact of channel depth on substrate conversion at the MPBRs outlets at various flow rates and thereby mean residence times together with production rates estimated at the longest mean residence time (maximal conversion) in the MPBRs with hexagonal channels randomly packed in one or two layers with Novozym® 435 having the specific enzyme activity of 133.05 U mg_{CaLB}^{-1}. The reaction was performed under the same conditions as described for MPBRs in Figure 47. Other characteristics of the MPBRs are presented in Table 10. The relative standard deviations in the inset graph are below 2%.

Slika 49: Vpliv globine kanala na konverzijo substrata na izstopu iz MPBR pri različnih pretokih in s tem zadrževalnih časih skupaj s produktivnostjo ocenjeno pri najdaljšem zadržavalnem času (makismalni konverziji) v MPBR z šesterokotnim kanalom naključno polnjenim z enim ali dvema slojema Novozym® 435 pripravka s specifično encimsko aktivnostjo 133,05 U mg_{CaLB}^{-1}. Reakcijo smo izvedli pod enakimi pogoji kot je opisano na Sliki 47. Ostale značilnosti MPBR so predstavljene v Tabeli 10. Relativne standardne deviacije v notranjem grafu so manjše od 2 %.

As a consequence, estimated production rates at the longest mean residence time slightly deviate from the linearity but still should allow for the efficiently increased capacity (inset graph in Figure 49). As presented in Table 10, achieved *BPN* in the MPBR with two layers

of particles (14.03 $mmol_{BB}$ g_{CaLB}^{-1}) was slightly higher than that achieved in the MPBR with one layer of particles (12.18 $mmol_{BB}$ g_{CaLB}^{-1}).

4.3.2.4 Estimation of temperature effects

It has been reported that the immobilized CaLB in the form of Novozym® 435 is stable at temperatures up to 80 °C (Denčić et al., 2013; Wang J. et al., 2013, 2014). A temperature effect on the transesterification reaction was evaluated in a thermostated MPBR with 23.93 mm long, 3.12 mm wide and 0.40 mm deep rectangular channel randomly packed in one layer with 7.1 mg of Novozym® 435 with specific enzyme activity of 133.05 U mg_{CaLB}^{-1}, yielding bed porosity of 0.57 and final enzyme load of 5.53 U μL^{-1} (Table 10). An equimolar 600 mM solution of both substrates was continuously pumped through the MPBR at the flow rate of 170.7 µL min^{-1} (τ = 0.1 min). The solvent used in transesterification (*n*-heptane), one substrate (BUT) and the product (BB) have the boiling points at 98.4, 117.6 and 166.7 °C, respectively (NCBI, 2004), so in order to avoid possible problems with the sample evaporation, the temperature range tested was from 24 to 80 °C. It has been shown that 75 °C is the optimal temperature, because the highest conversion of cca. 81% was achieved at the mean residence time of 0.1 min, which is almost 2-times higher than at 24 °C (Figure 50).

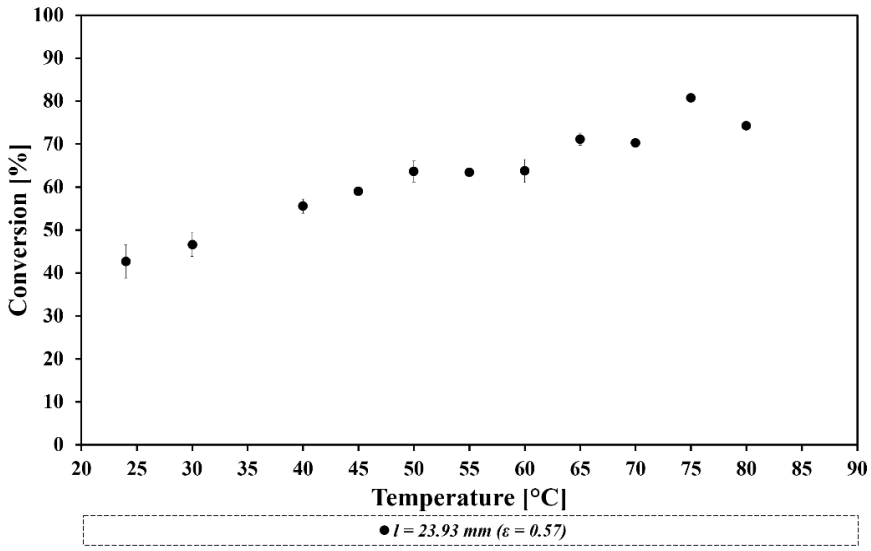

Figure 50: Influence of temperature on conversion at the channel outlet at the flow rate of 170.7 µL min^{-1} (τ = 0.1 min) during the continuous operation of the MPBR randomly packed with Novozym® 435 having the specific enzyme activity of 133.05 U mg_{CaLB}^{-1}. The reaction was performed at the same conditions as described for MPBRs in Figure 47, except the temperature. Other characteristics of the MPBR are presented in Table 10.

Slika 50: Vpliv temperature na konverzijo na izstopu iz kontinuirno delujočega MPBR pri pretoku 170,7 µL min^{-1} (τ = 0,1 min). MPBR je bil naključno polnjen z Novozym® 435 pripravkom s specifično encimsko aktivnostjo 133,05 U mg_{CaLB}^{-1}. Reakcijo smo izvedli pod enakimi pogoji kot je opisano na Sliki 47, razen temperature. Ostale značilnosti MPBR so predstavljene v Tabeli 10.

This equals to *BPN* of 11.39 $mmol_{BB}\ g_{CaLB}^{-1}$ and production rate of 4.85 $mmol_{BB}\ h^{-1}$. Further increase in the temperature resulted in decrease of the reaction rate, since the maximal conversion decreased from cca. 81% at 75 °C to cca. 74% at 80 °C (Figure 50). This was likely caused by irreversible enzyme inactivation. By comparison, the optimal temperature is close to that of 70 °C reported by Wang J. et al. (2014).

4.3.2.5 Estimation of operational stability

The operational stability of the system was evaluated over the period of 53 days using the MPBR with a 82.00 mm long, 2.92 mm wide and 0.40 mm deep rectangular channel randomly packed with 22.2 mg of Novozym® 435, yielding bed porosity of 0.58 and final enzyme load of 5.28 U μL^{-1} (Table 10). The volumetric productivity at the beginning of the experiment was 2,862.79 $mmol_{BB}\ L^{-1}\ min^{-1}$, and it dropped below 50% of the initial one after the period of 53 days (Figure 51).

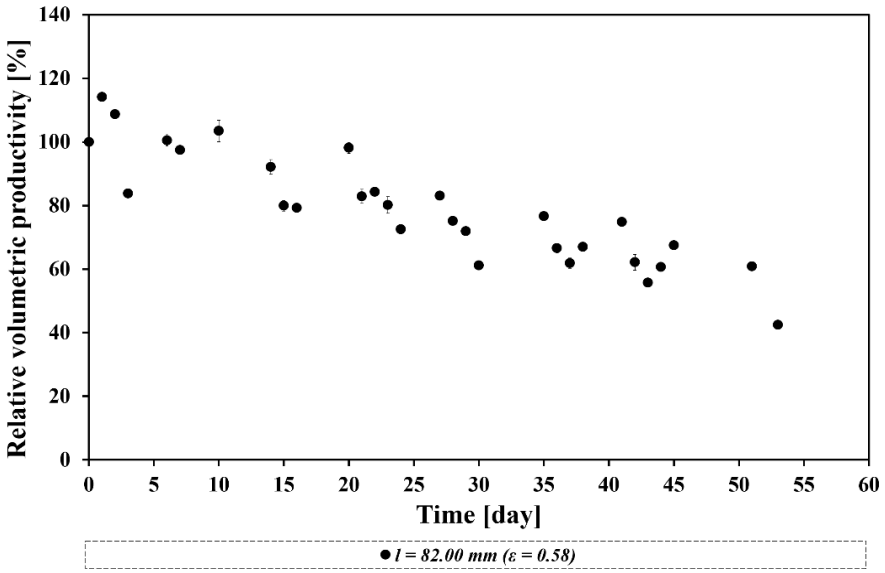

Figure 51: Operational stability of the MPBR randomly packed with Novozym® 435 having the specific enzyme activity of 133.05 U mg_{CaLB}^{-1} over the period of 53 days. The reaction was performed by pumping of 600 mM equimolar inlet concentration of VB and BUT in *n*-heptane (Q = 559 µL min^{-1}, τ = 0.1 min, T = 24 ºC). Other experimental conditions are described in Section 3.4.4.3. Other characteristics of the MPBR are presented in Table 10.

Slika 51: Obratovalna stabilnost MPBR z naključno polnjenim pripravkom Novozym® 435 s specifično encimsko aktivnostjo 133,05 U mg_{CaLB}^{-1} v obdobju 53 dni. Reakcijo smo izvedli s črpanjem 600 mM ekvimolarne vstopne raztopine VB in BUT v *n*-heptanu (Q = 559 µL min^{-1}, τ = 0,1 min, T = 24 ºC). Ostali eksperimentalni pogoji so opisani v poglavju 3.4.4.3. Ostale značilnosti MPBR so predstavljene v Tabeli 10.

By comparison, the activity of the same enzyme preparation dropped to 50% after 11 days of the continuous synthesis of caffeic acid phenethyl ester in 1-butyl-3-methylimidazolium bis(trifluoromethylsulfonyl)imide at 60 °C using an MPBR with 75 mm long, 1 cm wide and

500 µm deep rectangular channel packed with 90 mg of Novozym® 435 (Wang J. et al., 2014).

4.3.3 Hydrodynamics in miniaturized packed bed reactors with Novozym® 435

Hydrodynamics of MPBRs with Novozym® 435 has been considered with the same approach as in the case of MPBRs with LentiKats®. Since the transesterification was performed in *n*-heptane, the ratio of pressure drops caused by flowing water and *n*-heptane was calculated by the Ergun equation using their viscosities and densities as variables, and further used to estimate the pressure drop under the operational conditions (the values which would occur by flowing *n*-heptane under the flow rates applied in Sections 4.3.2.1–4.3.2.3). Moreover, the RTD analysis of the MPBRs with rectangular channels is added to this subchapter.

4.3.3.1 Pressure drop

Similar as in the previous case with MPBRs packed with LentiKats®, the measurements have shown moderate and linearly dependent pressure drops in the MPBRs along the applied range of flow rates. The highest pressure drop of cca. 88 kPa was measured at the flow rate of 1,800 µL min^{-1} in the MPBR with 53.79 mm long and 29.22 mm wide rectangular part (Figure 52).

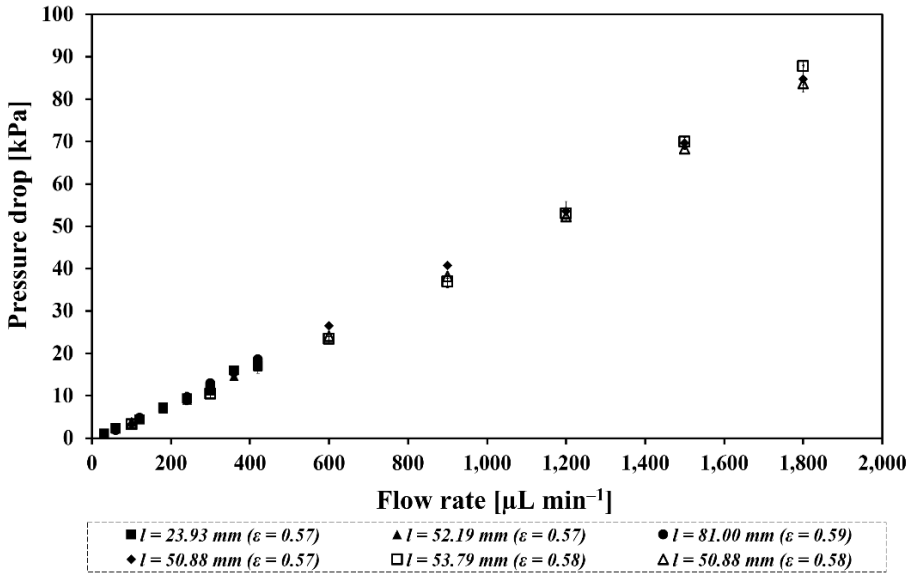

Figure 52: The effect of the flow rate on the pressure drop in the MPBRs with rectangular (■, ▲, ●) and hexagonal (♦, □, ∆) channels randomly packed with Novozym® 435 (Q = 30–1,800 µL min^{-1}; T = 24 ºC). Other characteristics of the MPBRs are presented in Table 10.

Slika 52: Vpliv pretoka na padec tlaka v MPBR s pravokotnimi (■, ▲, ●) in šesterokotnimi (♦, □, ∆) kanalom, naključno polnjenim z Novozym® 435 pripravkom (Q = 30–1800 µL min^{-1}; T = 24 ºC). Ostale značilnosti MPBR so predstavljene v Tabeli 10.

Calculation of Re_p under the reaction conditions (where *n*-heptane was used as the solvent) has revealed completely laminar flow regime, with Re_p calculated at the maximal flow rates varying between 2.47 and 8.37 (Table 11). This is still below the critical value of 10 which assumes the switch to the transitional flow regime (Ribeiro et al., 2010). The ratio of pressure drops caused by flowing two fluids of different viscosities and densities ($\Delta p_{water}/\Delta p_{heptane} \sim 2.2$) calculated applying the Ergun equation (Equation 15) was used for the estimation of pressure drops under the reaction conditions (Sections 4.3.2.1–4.3.2.3), and the obtained data were then used to estimate energy dissipation rate and operational costs per single MPBR (Table 11).

Table 11: Hydrodynamic characteristics and energy dissipation rate of MPBRs with Novozym® 435 at 24 °C.
Tabela 11: Hidrodinamske lastnosti in vnos moči za MPBR z Novozym® 435 pri 24 °C.

l **[mm]**	***w*** **[mm]**	***d*** **[mm]**	**No. of layers[b)]**	***Q*** **[c)] [µL min^{-1}]**	***Re*$_p$** **[d)] [–]**	***P*$_1$** **[e)] [kW m^{-3}]**	**Price[g)] [€ m^{-3} day^{-1}]**
23.93	3.12	0.40	1	170.7	2.47	0.51	0.96
52.19	2.95	0.40	1	352.8	5.39	1.05	1.98
81.00	2.94	0.40	1	565.2	8.37	1.96	3.71
50.88	15.80[a)]	0.40	1	1840.3	5.25	4.60[f)]	8.73[f)]
53.79	29.22[a)]	0.40	1	3,636.4	5.51	8.95[f)]	16.96[f)]
50.88	15.80[a)]	0.80	2	3,756.3	5.27	9.77[f)]	18.52[f)]

a) The values refer to the width of the rectangular part of the hexagonal channel.

b) Number of Novozym® 435 layers placed one on top of the other within the channel depth.

c) Maximal flow rate under reaction conditions.

d) Calculated according to Equation 13 at maximal flow rates using the average diameter of Novozym® 435 (d_{N435} = 372.10 µm), bed porosities as stated in Table 10 and properties of *n*-heptane as follows: ρ = 679.5 kg m^{-3}; $\eta = 4.10 \times 10^{-4}$ Pa s (Smallwood, 1996: 11).

e) Energy dissipation rate estimated from the experimental data for given operational conditions (Sections 4.3.2.1–4.3.2.3).

f) Estimated including the void volume in the triangular pre-chambers containing pillars.

g) The price for the operation of the MPBR under given conditions over the period of one day. Estimated based on the average electricity price for industry exclusive of VAT in the Republic of Slovenia (0.079 EUR kWh^{-1}) in the 4th quarter 2016 (SORS, 2016).

From the obtained results it follows that the maximal energy dissipation rate per single MPBR was up to 9.77 kW m^{-3}, which requires up to 18.52 € m^{-3} to operate the process under given conditions over the period of one day (Table 11).

4.3.3.2 Residence time distribution

RTD for the test loop without connected MPBR was first examined using a pulse-response method with glucose as a non-reactive tracer. A sharp output pulse could be expected in large-scale systems, similar to or approaching a Dirac delta function (Levenspiel, 2012). This

does not necessarily occur in microsystems, where the impulse encounters instant shear gradients in the laminar fluid flow (Coblyn et al., 2016). Therefore, the output profile following Gaussian-like distribution for the test loop displayed in Figure 53 (square marks) was considered as a perfect signal.

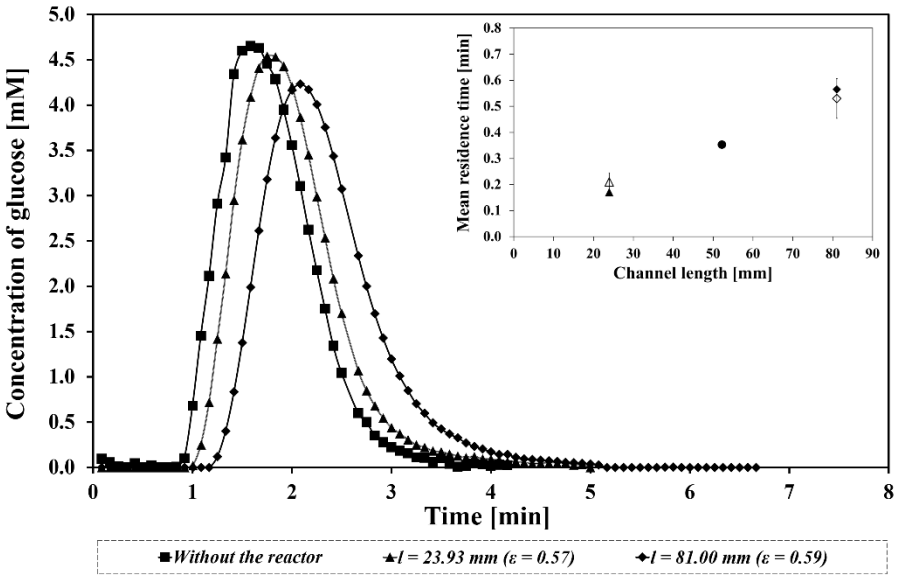

Figure 53: Pulse-response curves obtained in RTD analysis of MPBRs with rectangular channels of different lengths randomly packed with Novozym® 435 in one layer, together with estimated mean residence times (● denotes calculated mean residence time distribution for the MPBR with 52.19 mm long rectangular channel). Filled and empty marks in the inset graph denote calculated ($\tau = V_v/Q$) and experimentally obtained mean residence times for the same MPBRs, respectively. The experiments were performed by pumping 50 mM solution of glucose in 100 mM PBS (pH 7.4) at Q = 100 µm min^{-1} and T = 24 ºC. Other characteristics of the MPBR are presented in Table 10.

Slika 53: Krivulje, pridobljene s pulzno motnjo za RTD analizo MPBR s pravokotnimi kanali različnih dolžin, naključno polnjenih z Novozym® 435 pripravkom v enem sloju, skupaj z ocenjenim povprečnim zadrževalnim časom (● označuje izračunan povprečni zadrževalni čas v MPBR z 52,19 mm dolgim pravokotnim kanalom). Polni in prazni simboli v notranjem grafu označujejo izračunan ($\tau = V_v/Q$) in eksperimentalno pridobljen povprečni zadrževalni čas za isti MPBR. Eksperimente smo izvedli s črpanjem 50 mM raztopine glukoze v 100 mM fosfatnem pufru z NaCl (pH 7,4) pri Q = 100 µm min^{-1} in T = 24 ºC. Ostale značilnosti MPBR so predstavljene v Tabeli 10.

The first (τ), the second (σ^2) and the third (s) moment of $C_{glu}(t)$ distribution show how long the tracer material stays inside the system, [how long]^2 it takes for the curve to pass by the measuring point and the level of (a)symmetry of the distribution, respectively, where $s = 0$ stands for the perfectly symmetrical distribution, while positive and negative values stand for right- and left-sided asymmetry (Levenspiel, 2012; Coblyn et al., 2016). The values of τ, σ^2 and s, calculated from the pulse-response data were 1.78 min, 0.21 min^2 and 0.79, respectively.

The moments of distribution are additive for devices connected in series (like in the case of the test loop and a reactor) and therefore the values for the test loop were subtracted in order to obtain the values for the MPBRs alone (Márquez et al., 2008). The results have revealed

that the experimentally obtained mean residence times converge with the calculated values (V_v/Q) for the given channel lengths, and were 0.21 min (relative error with the respect to the calculated value was 18.6%) and 0.53 min (relative error 6.2%) for the MPBRs with 23.93 mm and 81.00 mm long channels, respectively (inset graph in Figure 53). This indicates that the whole reactors were active, without any dead spaces or fluid bypassing (Levenspiel, 2012). The corresponding variance and skewness were 0.08 min^2 and 0.77 for the MPBR with the shortest channel and 0.14 min^2 and 0.42 for the MPBR with the longest channel.

On the other hand, the profiles for the MPBRs with the shortest and longest rectangular channels shift from left to right on the time scale by increasing the channel length (Figure 53). Such outcome is expected due to an increase in the total volume when the MPBRs were placed in the test loop. Further observation revealed a decrease in the heights of the peaks as well as slight increase in the spread of the distribution (σ^2) characterized by the appearance of right-sided tails caused by the portion of the fluid which stays in the reactor longer than the mean residence time. Similar decrease in the heights of the peaks was observed in the analysis of 7 and 97 cm long columns (2 mm ID) packed with 100 µm spherical particles (Márquez et al., 2008).

Based on this longitudinal spread of the pulse of flowing tracer, Levenspiel (1999, 2012) suggested a dispersion model as the most appropriate one to represent the fluid flow in packed bed reactors, where a diffusion-like process superimposed on plug flow is assumed (Delgado, 2006; Gupta and Bansal, 2013). The relation shown in Equation 36 can be used to calculate the longitudinal or axial dispersion coefficient ($\mathfrak{D}$) which represents the overall spreading process (large $\mathfrak{D}$ means rapid spreading and *vice versa*, while $\mathfrak{D} = 0$ stands for the plug flow) (Levenspiel, 1999).

$$\sigma^2 = 2\frac{\mathfrak{D}\, l}{v^3} \qquad \text{... (36)}$$

σ^2 *variance [s^2]*
$\mathfrak{D}$ *axial dispersion coefficient [$m^2\ s^{-1}$]*

The dispersion coefficient for flowing water with the tracer at the flow rate of 100 µL min^{-1} through the MPBRs with two consecutive channel lengths (Re_p of 0.95 and 0.98) calculated using Equation 36 were 1.42×10^{-5} $m^2\ s^{-1}$ and 0.92×10^{-5} $m^2\ s^{-1}$, respectively. By comparison, Pohar et al. (2012) have reported a diffusion coefficient of 2×10^{-4} $m^2\ s^{-1}$ evaluated by fitting the experimental data obtained using a highly viscous ionic liquid.

A dimensionless parameter called dispersion number ($\mathfrak{D}/v\ l$) which characterizes the spreading rate of flowing material in the reactor (i.e. the extent of axial dispersion) caused by all acting factors ($\mathfrak{D}/v\ l > 0.01$ means significant deviation from plug flow) (Levenspiel,

2012), was calculated to be 0.45 and 0.08. Therefore, the flow of the fluid through the MPBRs with rectangular channels (the longest one 81.00 mm) could be described by the model which incorporates relatively slow but significant axial dispersion, i.e. deviation from the plug flow.

4.3.4 Mass transfer in a miniaturized packed bed reactor with Novozym® 435

The influence of fluid flow dynamics on the immobilized CaLB specific activity was firstly evaluated in a mixing reactor at different stirring speeds ranging from 300 to 1,200 rpm. As evident from Figure 54, the conversions increased at more vigorous agitation (above 300 rpm), and the highest values were achieved at 800 rpm, where the external mass transfer limitations through the stagnant boundary layer of *n*-heptane are assumed to be surmounted. Increasing the degree of conversion along with increasing the stirring speed in batch processes was also reported in several studies utilizing Novozym® 435 (Dong et al., 2010; Yadav and Devendran, 2012; Bansode et al., 2016). Further increase in stirring speed to 1,200 rpm resulted in slight decrease of conversion (Figure 54), which could be attributed to the shearing effect occurring at vigorous agitation (Gharat and Rathod, 2013).

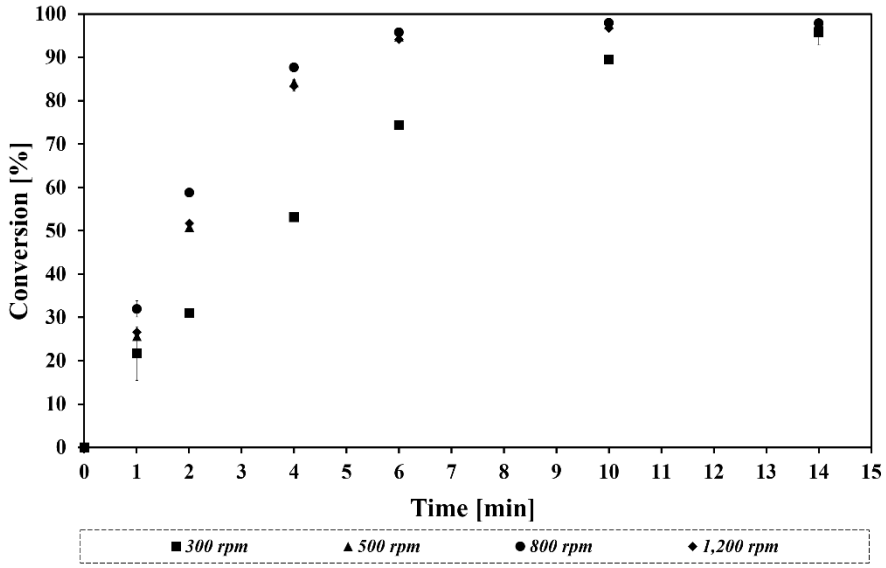

Figure 54: Achieved conversions in a batch process at different mixing speed ranging from 300 to 1,200 rpm. Other experimental conditions were as follows: C_{VB} = C_{BUT} = 500 mM; C_{CaLB} = 1.25 g_{CaLB} L^{-1} and T = 24 °C.

Slika 54: Dosežene konverzije v šaržnem procesu z različno vrtilno hitrostjo od 300 do 1200 min^{-1}. Ostali eksperimentalni pogoji so bili kot sledi: C_{VB} = C_{BUT} = 500 mM; C_{CaLB} = 1,25 g_{CaLB} L^{-1} in T = 24 °C.

However, this boundary layer was assumed to be insignificant in the MPBR, the same as in the case of the MPBR with LentiKats® (Section 4.2.4). In addition to a small length scale of

the reactor, the channel was packed with relatively small spherical particles continuously perfused by *n*-heptane, a fluid with different hydrodynamic properties than that of water.

Table 12 summarizes diffusion coefficients for VB, BUT and BB in *n*-heptane (D_{VB}, D_{BUT}, and D_{BB}) estimated using Equation 8, and the corresponding effective diffusion coefficients in Novozym® 435 (D_{VB}, D_{BUT}, and D_{BB}) estimated using Equation 16 and taking into account porosity (ε_{N435}) and tortuosity (ζ_{N435}) of Novozym® 435 as 0.5 and 6, respectively (Dong et al., 2010).

Table 12: Estimated values of diffusion and effective diffusion coefficients in *n*-heptane and Novozym® 435, respectively.

Tabela 12: Ocenjene vrednosti difuzijskih in efektivno difuzijskih koeficijentov v *n*-heptanu in Novozym® 435 pripravku.

Parameter	**Estimated value**	**Parameter**	**Estimated value**
D_{VB}	2.13×10^{-9} m^2 s^{-1}	D_{eVB}	1.78×10^{-10} m^2 s^{-1}
D_{BUT}	2.59×10^{-9} m^2 s^{-1}	D_{eBUT}	2.16×10^{-10} m^2 s^{-1}
D_{BB}	1.81×10^{-9} m^2 s^{-1}	D_{eBB}	1.51×10^{-10} m^2 s^{-1}

The values of Pe_p (Equation 18), calculated for the MPBR with 81.00 mm long, 2.94 mm wide and 0.40 mm deep rectangular channel randomly packed with one layer of Novozym® 435 (Table 10) using diffusivity of VB (Table 12), were ranging from 169.39 to 2,371.46 at flow rates of *n*-heptane from 40.4 to 562.2 μL min^{-1}, respectively. Such results reveal the dominance of the convective mass transport over diffusive one along the channel length, and assuming a uniform fluid distribution across the entire width of the channel, the characteristic diffusion times in the directions of the channel width and depth could be neglected, as explained in Section 4.2.4. The characteristic times used in the analysis are listed in Table 13.

Table 13: Characteristic times considered in the time-scale analysis of an MPBR with Novozym® 435.

Tabela 13: Značilni časovi upoštevani pri časovno-dimenzijski analizi v MPBR z Novozym® 435 pripravkom.

Characteristic time	**Equation**	**Estimated value**
Mean residence time, τ	Equation 24[a)]	0.1–1.4 min
Reaction time, τ_r	Equation 11[b)]	0.20 min
Diffusion time in the porous particle, τ_p	Equation 17[c)]	3.25 min (for the whole particle) 1.57 min (for δ_{CaLB})

a) Parameters: Vv = 56.5 μL; Q = 40.4–562.2 μL min^{-1}.

b) Parameters: C_{Sin} = 600 mol m^{-3}; C_e = 22.57 g L^{-1}; v_0 = 0.132 mol g^{-1} min^{-1} (v_0 was experimentally obtained for immobilized enzyme in a batch reactor at 24 °C according to the protocol for enzyme activity determination described in Section 3.4.2.2).

c) Parameters: d_{N435} = 372.10 μm; $D_e = 1.78 \times 10^{-10}$ m^2 s^{-1} (D_e was used for VB, since it was lower than for BUT).

Comparison of estimated characteristic times has revealed intra-particle mass transfer limitations as the rate limiting step because $\tau_p > \tau_r$ (Table 13). Since Novozym® 435 is a commercial product, used CaLB is not always available in a non-immobilized form, and therefore the characteristic reaction time was estimated using an initial rate measured for the immobilized enzyme in a batch system under the conditions presuming the absence of the external mass transfer limitations (Figure 54). On the other hand, the characteristic diffusion time was estimated for approx. 90 µm thick external shell containing immobilized CaLB (δ_{CaLB}) (Mei et al., 2003) as well, but also in that case τ_p was significantly higher than τ_r (Table 13). Intra-particle mass transfer limitations in Novozym® 435 used in an MPBR have already been reported in the literature (Denčić et al., 2013), although the reaction step could be the rate-limiting one (Kundu et al., 2011).

4.3.5 Modeling of a miniaturized packed bed reactor with Novozym® 435

A mathematical model comprising convective mass transport in the flow direction, and diffusion-reaction dynamics described by the axial dispersion coefficient obtained by fitting the experimental data, has already been reported for an MPBR used for Novozym® 435-catalyzed transesterification of VB and BUT to BB and ACE in an ionic liquid (Pohar et al., 2012). The differential mass balance equations (Equations 37 to 39) with appropriate boundary conditions (Equations 40 and 41) are as follows.

$$v_x \frac{\mathrm{d}C_{VB}}{\mathrm{d}x} - \mathfrak{D} \frac{\mathrm{d}^2 C_{VB}}{\mathrm{d}x^2} = - \frac{(1-\varepsilon)}{\varepsilon} r_a \quad \ldots (37)$$

$$v_x \frac{\mathrm{d}C_{BUT}}{\mathrm{d}x} - \mathfrak{D} \frac{\mathrm{d}^2 C_{BUT}}{\mathrm{d}x^2} = - \frac{(1-\varepsilon)}{\varepsilon} r_a \quad \ldots (38)$$

$$v_x \frac{\mathrm{d}C_{BB}}{\mathrm{d}x} - \mathfrak{D} \frac{\mathrm{d}^2 C_{BB}}{\mathrm{d}x^2} = \frac{(1-\varepsilon)}{\varepsilon} r_a \quad \ldots (39)$$

$$C_{VB}(0) = C_{VBin};\ C_{BUT}(0) = C_{BUTin};\ C_{VB}(0) = 0 \quad \ldots (40)$$

$$\frac{\mathrm{d}C_{VB}}{\mathrm{d}x}(L) = 0;\ \frac{\mathrm{d}C_{BUT}}{\mathrm{d}x}(L) = 0;\ \frac{\mathrm{d}C_{BB}}{\mathrm{d}x}(L) = 0 \quad \ldots (41)$$

v_x *average fluid velocity in x-direction [m s^{-1}]*
C_{VB} *concentration of vinyl butyrate [mol m^{-3}]*
C_{BUT} *concentration of 1-butanol [mol m^{-3}]*
C_{BB} *concentration of butyl butyrate [mol m^{-3}]*
C_{VBin} *inlet concentration of vinyl butyrate [mol m^{-3}]*
C_{BUTin} *inlet concentration of 1-butanol [mol m^{-3}]*

As stated before, the transesterification is a second-order reaction that follows a ping-pong bi-bi reaction mechanism (Paiva et al., 2002; Ferrario et al., 2015). It has been discussed that lipases may be susceptible to the inhibition by both substrates (Žnidaršič-Plazl and Plazl, 2009), by one (alcohol) substrate (Paiva et al., 2002; Bezbradica et al., 2006), but also may catalyze without any kind of inhibition (Arcos et al., 2001), when used in transesterifications and esterifications performed in various reaction systems. The type of inhibition depends on factors such as agitation of the reaction mixture, kind of immobilization as well as whether the reaction is performed in an organic solvent, ionic liquid or solvent-free system (Bezbradica et al., 2006). Pohar et al. (2012) have reported that the rate of transesterification of VB and BUT to BB and ACE in an ionic liquid can be described considering the inhibition by both substrates (Equation 42).

$$r_a = \frac{V_f\, C_{CaLB}\, C_{BUT}\, C_{VB}}{K_{BUT}\, C_{VB}\left(1 + \frac{C_{VB}}{K_{iVB}}\right) + K_{VB}\, C_{BUT}\left(1 + \frac{C_{BUT}}{K_{iBUT}}\right) + C_{BUT}\, C_{VB}} \quad \ldots (42)$$

V_f	*maximum velocity of the forward reaction [mol g^{-1} s^{-1}]*
C_{CaLB}	*concentration of CaLB [g_{CaLB} m^{-3}]*
K_{VB}	*binding constant of vinyl butyrate [mol m^{-3}]*
K_{BUT}	*binding constant of 1-butanol [mol m^{-3}]*
K_{iVB}	*inhibition constant of vinyl butyrate [mol m^{-3}]*
K_{iBUT}	*inhibition constant of 1-butanol [mol m^{-3}]*

Since the reaction in this study was performed in *n*-heptane, a set of experiments has been performed in well-mixed batch reactors at varaying substrate concentrations in order to confirm the inhibition by both substrates. The binding and inhibition constants were taken from the literature (Pohar et al., 2012), and the maximum rate of forward reaction was obtained by fitting on the experimental points for each set of data using Equation 42, while the mass balances in batch reactors are as demonstrated by Equations 43 to 45, with the initial conditions demonstrated by Equation 46.

$$\frac{\mathrm{d}C_{VB}}{\mathrm{d}t} = -r_a \quad \ldots (43)$$

$$\frac{\mathrm{d}C_{BUT}}{\mathrm{d}t} = -r_a \quad \ldots (44)$$

$$\frac{\mathrm{d}C_{BB}}{\mathrm{d}t} = r_a \quad \ldots (45)$$

$$C_{VB}(0) = C_{VBin};\ C_{BUT}(0) = C_{BUTin};\ C_{VB}(0) = 0 \quad \ldots (46)$$

The results obtained using the kinetic parameters summarized in Table 14 (which stand for the apparent kinetic parameters for immobilized CaLB) have shown that the inhibition by both substrates is also present when using *n*-heptane as the reaction medium, because the modeled lines converged to the experimental points (Figure 55a and 55b). Therefore, it has been confirmed that Equation 42 can be used in the model for an MPBR.

Table 14: Kinetic parameters used to fit Equation 42 on the experimental data.
Tabela 14: Kinetični parametri uporabljeni za prileganje eksperimentalnih podatkov na kruvuljo z enadžbo 42.

Parameter	**Value**
K_{VB} [a)]	469 ± 50.6 mol m^{-3}
K_{BUT} [a)]	190 ± 85.5 mol m^{-3}
K_{iVB} [a)]	196.8 ± 119.1 mol m^{-3}
K_{iBUT} [a)]	106.3 ± 13.9 mol m^{-3}
V_f [b)]	0.90 ± 0.19 mol g_{CaLB}^{-1} s^{-1}

a) Parameters taken from the literature (Pohar et al., 2012).

b) Parameter obtained by fitting on the experimental data (C_{CaLB} = 1.25 g_{CaLB} L^{-1}).

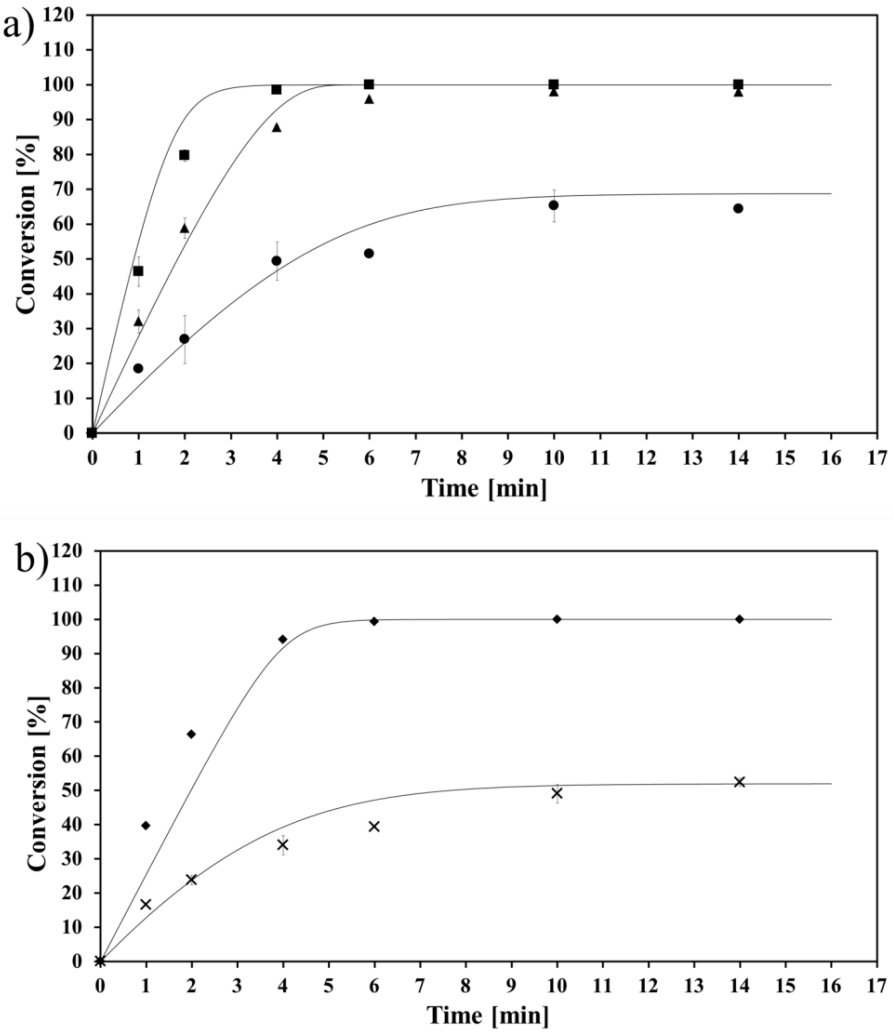

Figure 55: Kinetics of CaLB-catalyzed synthesis of BB at different substrate initial concentrations obtained in a batch process: a) concentration of VB fixed at 600 mM, while concentration of BUT was (■) 300 mM, (▲) 500 mM and (●) 900 mM; b) concentration of BUT fixed at 700 mM, while concentration of VB was (×) 400 mM and (♦) 1,100 mM. Points denote experimental data, while the trendlines denote predictions with the model for inhibition by both substrates calculated using the kinetic parameters summarized in Table 14. Other experimental conditions were as follows: C_{CaLB} = 1.25 g_{CaLB} L^{-1}, T = 24 ºC and mixing 800 rpm.

Slika 55: Kinetika sinteze BB katalizirane z lipazo B iz kvasovke *Candida antarctica* v šaržnem procesu pri različnih začetnih koncentracijah obeh substratov: a) fiksna koncentracija VB 600 mM in koncentracija BUT (■) 300 mM, (▲) 500 mM in (●) 900 mM; b) fiksna koncentracija BUT 700 mM, in koncentracija VB (×) 400 mM in (♦) 1100 mM. Točke označujejo eksperimentalne podatke, dokler trendne črte označujejo napovedi modela ki vključuje inhibicijo z obema substratoma izračunanih s parametri ki so prikazani v Tabeli 14. Drugi eksperimentalni pogoji so bili kot sledi: C_{CaLB} = 1,25 g_{CaLB} L^{-1}, T = 24 ºC in vrtilna hitrost 800 min^{-1}.

5 CONCLUSIONS

The present study primarily focuses on development and evaluation of a two-plate MPBR with immobilized enzymes applicable for biocatalytic processes and the effect of the systematic scale-up on their performance. ω-TA immobilized in poly(vinyl alcohol)-based LentiKats® and CaLB, immobilized on acrylic resin in the form of commercially available preparation Novozym® 435 were used within this study. The enzyme carriers were chosen as representatives of the materials commonly used for enzyme immobilization, lens-shaped LentiKats® as a representative of synthetic polymer-based hydrogels and spherical Novozym® 435 as a commonly used porous resin. In addition to that, a naturally occurring polymer alginate was used to develop a microfluidic-based method for the immobilization of *E. coli* cells overexpressing ω-TA into microparticles which could be used in an MPBR. The model reactions used in this study, namely ω-TA-catalyzed synthesis of ACP in an aqueous solution and CaLB-catalyzed synthesis of BB in *n*-heptane are very frequently used as assay/model reactions. The latter is also important because BB is a highly demanded industrial fragrance.

Reusable MPBRs of different channel sizes and designs enabling simple and efficient enzyme loading in the form of uniformly or randomly packed LentiKats® were developed and tested using ω-TA-catalyzed synthesis of ACP as the model reaction. A systematic scale-up study of a two-plate MPBR revealed that for the increased capacity enabling efficient use of LentiKats® containing ω-TA, a single layer of uniformly packed particles within a wide channel with a triangular inlet pre-chamber with pillars should be considered. In contrast, increasing the depth of an MPBR with particle loading in layers one on top of the other resulted in decreased production rates presumably due to the fluid maldistribution within the reactor with stuck-together hydrogel particles. This study revealed an efficient scale-up from a microliter to the milliliter scale reactor, while a numbering-up concept is suggested for further increase in production capacity. Furthermore, developed MPBRs were used as a tool for process parameters optimization using ω-TA in LentiKats® under continuous flow conditions. Optimal temperature of 55 °C for ω-TA-catalyzed synthesis of ACP and satisfactory operational stability over the period of 21 days at 24 °C (retained more than 80% of the initial productivity) were evaluated with low-material and time consumption, confirming the importance of implementation of microreactor technology in bioprocess development studies. Such operational stability is assumed to be at least partly a consequence moderate pressure drops of up to 42 kPa measured in MPBRs using the piezoresistive pressure sensor. Estimation of mass transfer phenomena in the MPBRs has revealed an operation under the internal mass transfer limitations within the hydrogel material.

Furthermore, MPBRs utilizing Novozym® 435 were developed and evaluated using CaLB-catalyzed synthesis of BB as the model reaction. The results of systematic scale-up study were similar to performance of MPBRs with LentiKats®, except that the increase in

the channel depth by random packing with two layers of Novozym® 435 resulted in favorable hydrodynamic conditions and consequently reactor efficiency. Further investigations revealed an optimal temperature of 75 °C for CaLB-catalyzed synthesis of BB as well as satisfactory operational stability over the period of 53 days at 24 °C (retained more than 40% of the initial productivity). Pressure drops up to 88 kPa were measured in the MPBRs with different channel shapes and dimensions. Evaluation of mass transfer phenomena also revealed operation under the intra-particle mass transfer limitations. This study confirmed that the inhibition with both substrates is also present when using *n*-heptane as the reaction medium for CaLB-catalyzed synthesis of BB.

A separate part of the study refers to the microfluidic-based method for the immobilization of *E. coli* cells overexpressing ω-TA in alginate microparticles. This method was developed as a proof-of-concept confirming feasibility of using a microfluidic device for an efficient and rapid production of immobilized biocatalysts which would be small enough to be easily applied in MPBRs. In this respect, alginate microparticles containing immobilized cells were successfully obtained and tested in a batch process using ω-TA-catalyzed synthesis of ACP as the model reaction, where a conversion higher than 90% was achieved after the period of 47 h. This confirmed the possibility of biocatalyst production by this method and its further application in biocatalytic processes.

6 SUMMARY (POVZETEK)

6.1 SUMMARY

Chemical industry is facing with the high demands towards the implementation of the environment-friendly production, known as 'Green Chemistry' or 'Sustainable Technology', where biocatalysis has emerged as a technology which perfectly fits this concept, and besides can be merged with MPBRs as powerful tools for process intensification. Therefore, the purpose of the work was the development, systematic scale-up and characterization of MPBRs with rectangular and hexagonal channels of various lengths, widths, and depths utilizing ω-TA entrapped in LentiKats® and *Candida antarctica* lipase B adsorbed on acrylic resin (Novozym® 435). A proof-of-concept of a microfluidic-based method suitable for entrapment of *E. coli* cells overexpressing ω-TA in alginate microparticles was among the aims as well.

After the comprehensive review of the literature and the theoretical background of this work have been presented throughout the fields of biocatalysis and biocatalytic processes, biocatalysts immobilization as well as miniaturization and microsystems, a set of experiments performed in order to fulfill previously declared aims have been shown. The experimental part contained the protocols for determination of the enzyme specific activity in batch processes (for both immobilized and non-immobilized biocatalysts in the case of *E. coli* and ω-TA), but also microfluidic-based method for the immobilization of *E.coli* cells in alginate microparticles and their characterization as well as characterization of LentiKats® and Novozym® 435. Subsequently, the main principles of MPBRs assembly, operation and evaluation were also presented. The results are summarized in the three main parts considering the immobilization of *E. coli* cells as well as development and evaluation of the aforementioned MPBRs.

Firstly, an aqueous solution of alginate and an edible sunflower oil were emulsified under the laminar conditions in a glass microchip with a T-junction. Produced alginate-containing aqueous microdroplets were afterwards successfully solidified resulting in the formation of tail-shaped alginate microparticles having a spherical body with the average diameter of 446.21 ± 36.54 μm. The same method was applied for the immobilization of *E. coli* cells, where alginate-containing aqueous microdroplets with suspended cells were solidified resulting in the formation of spherical, tail-free alginate microparticles with the average diameter of 932.72 ± 115.30 μm. Obtained microparticles with immobilized *E. coli* cells were thereafter successfully tested regarding their storage stability and efficiency, reavealing that the activity decreased below 40% of the initial one after 4 days of storage in 20 mM Tris-HCl buffer (pH 8.0) at 4 °C, while approximately 90% conversion was achieved within less than 30 h when immobilized *E. coli* cells were used for ω-TA-catayzed synthesis of ACP in a batch process.

The next big part deals with the development, systematic scale-up and evaluation of MPBRs with LentiKats® containing immobilized ω-TAs. Firstly, the continuously operated MPBRs with only one row of LentiKats® packed in rectangular channels were subjected to the systematic scale-up in the direction of the channel length (max. 60 mm long channel) and tested regarding their productivity. The laminar flow around uniformly packed LentiKats® enabled a very efficient biotransformation process where all tested MPBRs performed equally well at the same mean residence times, and above 80% conversion was obtained in less than 5 min. The comparison of production rates estimated at 70% conversions in the MPBRs of varying channel lengths revealed a linear proportionality within tested dimensions as well as *BPN*s up to 257.6 $\mu mol_{ACP}\ g_{ATA\text{-}wt}^{-1}$. This indicated that the scale-up of the channel length allowed for increased capacity and simultaneously retained favorable hydrodynamic conditions. Further on, scaling in the direction of the channel width was done on the MPBRs with rectangular channels (max. 12 mm wide channels) uniformly packed with one layer of LentiKats®. The results revealed slightly larger *BPN*s than in the previous case (cca. 285 $\mu mol_{ACP}\ g_{ATA\text{-}wt}^{-1}$) as well as nonlinearity of production rate estimated at 70% conversion, which was a consequence of unfavorable hydrodynamic conditions. Therefore, a triangular pre-chamber containing pillars was introduced in the reactor design in order to improve fluid flow distribution along the channel width. Such MPBRs with hexagonal channels of significantly increased widths (max. 79.67 mm wide rectangular part of the channel) packed with one layer of LentiKats® were tested and compared. These MPBRs shown almost equal performance, with conversions of above 90% achieved within less than 20 min, and *BPN*s up to 642.4 $\mu mol_{ACP}\ g_{ATA\text{-}wt}^{-1}$. Favorable hydrodynamic conditions within all tested channel widths with pre-chambers containing pillars were further confirmed by linear increases in production rates with channel widths up to 435 $\mu mol_{ACP}\ h^{-1}$. Evaluation of the MPBRs having hexagonal channels with pre-chambers containing pillars subjested to systematic scale-up in the direction of the channel depth (max. 0.96 mm deep channels) uniformly packed with one to three layers of LentiKats® revealed that only the MPBR with one layer of LentiKats® reached maximal conversion, while the MPBRs with more layers of particles achieved significantly lower conversions at the same mean residence times. A decrease of *BPN*s from 536.2 $\mu mol_{ACP}\ g_{ATA\text{-}wt}^{-1}$ achieved in the MPBR with one layer down to 362.7 $\mu mol_{ACP}\ g_{ATA\text{-}wt}^{-1}$ achieved in the MPBR with three layers of LentiKats® was a consequence of observed sticking of particles packed in layers leading to the appearance of bypassing and preventing a favorable enzyme accessibility. On the other hand, significantly lower conversions were obtained in the MPBR with the 0.64 mm deep channel randomly packed with LentiKats® in multiple layers, where *BPN* of 72.1 $\mu mol_{ACP}\ g_{ATA\text{-}wt}^{-1}$ and production rate of cca. 20 $\mu mol_{ACP}\ h^{-1}$ were achieved, which was again a consequence of the squeezing and sticking of hydrogel particles. A temperature effect on transamination was evaluated in the range from 30 to 75 °C uisng an MPBR with rectangular channel, where the results revealed 55 °C as the optimal temperature for the studied process. On the other hand,

another MPBR with one row of uniformly packed LentiKats® revealed a good operational stability, with above 80% relative volumetric productivity expressed within the tested period of 21 days at 24 °C. The measurements of pressure drop in the developed MPBRs with LentiKats® revealed moderate and linearly dependent values of up to 42 kPa at the flow rates up to 1,000 µL min^{-1} among the MPBRs with various channel geometries, except in the smallest one where the pressure drop of cca. 9 kPa was measured at the flow rate of 100 µL min^{-1}. Re_p was cca. 0.68 for all MPBRs with uniform packing, which confirmed the existence of laminar flow. Furthermore, the time-scale analysis performed based on the example of an MPBR with a rectangular channel uniformly packed with one layer of LentiKats® revealed the dominance of the convective mass transport over diffusive one (Pe_p from 22.35 to 670.62 at different flow rates from 1.7 to 50.8 µL min^{-1}, respectively) as well as the diffusive mass transfer inside LentiKats® as the limiting factor for the overall reaction process.

The next big part deals with the evaluation of developed and systematically scaled-up MPBRs randomly packed in one or two layers with Novozym® 435 having the average diameter of 372.10 ± 27.05 µm and the specific activity evaluated in a batch experiment of 133.05 ± 2.71 U mg_{CaLB}^{-1} (13.31 ± 0.27 U mg_{N435}^{-1}). On the beginning, the MPBRs with only one row of randomly packed Novozym® 435 were subjected to the systematic scale-up in the direction of the channel length (max. 81.00 mm long rectangular channels) and evaluated. All tested MPBRs performed equally well at the same mean residence times and the maximal conversion of cca. 95% was obtained in less than 0.8 min, while the production rates estimated at the longest mean residence time revealed a linear proportionality. The *BPN*s up to 13.56 $mmol_{BB}$ g_{CaLB}^{-1} were achieved, which allowed for an efficient scale-up process. Selected transesterification was further conducted in the MPBRs with the basic rectangular or hexagonal channels of various widths (max. 29.22 mm wide rectangular part of the channel) randomly packed with one layer of Novozym® 435. The evaluation revealed maximal conversion of cca. 95% achieved within less than 0.8 min in all tested MPBRs, linearly increased production rate estimated at the longest mean residence time, and *BPN*s revolving around 12.51 $mmol_{BB}$ g_{CaLB}^{-1}. The effect of the channel depth on the reactor performance was examined using two MPBRs of different channel depths (0.40 and 0.80 mm deep channels), whereby the MPBR with two layers achieved a slightly higher conversion at the mean residence times below 0.6 min. Consequently, estimated production rates at the longest mean residence time slightly deviated from the linearity but still allowed for efficiently increased capacity. The achieved *BPN* in the MPBR with two layers of particles (14.03 $mmol_{BB}$ g_{CaLB}^{-1}) was slightly higher than that achieved in the MPBR with one layer of particles (12.18 $mmol_{BB}$ g_{CaLB}^{-1}).A temperature effect on transesterification reaction was evaluated using an MPBR with a rectangular channel randomly packed with one layer of Novozym® 435 over the temperature range from 24 to 80 °C. It was shown that 75 °C is an optimal temperature, where the conversion of cca. 81%, *BPN* of 11.39

$mmol_{BB}\ g_{CaLB}^{-1}$ and production rate of 4.85 $mmol_{BB}\ h^{-1}$ were achieved. On the other hand, an operational stability evaluated over the period of 53 days at 24 °C using another MPBR with a rectangular channel randomly packed with one layer of Novozym® 435 revealed the relative volumetric productivity droped below 50% of the initial one after this period. The measurements of pressure drop in the MPBRs with Novozym® 435 revealed a moderate and linearly dependent trend, with the highest pressure drop of cca. 88 kPa at the flow rate of 1,800 µL min^{-1}. Calculated Re_p under reaction conditions revealed completely laminar flow regime. The RTD analysis performed on the MPBRs with two consecutive channel lengths (23.93 and 81.00 mm, respectively) shown that the experimentally obtained values for the mean residence time converge with the calculated values for the given channel lengths (0.21 and 0.53 min, respectively) which indicated that the whole reactors were active, without any dead spaces or fluid bypassing. The corresponding σ^2 and s were 0.08 min^2 and 0.77 for the MPBR with shorter and 0.14 min^2 and 0.42 for the MPBR with longer channel, respectively. Such results could be represented by a dispersion model characterized by the axial dispersion coefficients of $1.42 \times 10^{-5}\ m^2\ s^{-1}$ and $0.92 \times 10^{-5}\ m^2\ s^{-1}$, calculated for the MPBRs with 23.93 and 81.00 mm long channels, respectively. Moreover, the analysis of an MPBR with rectangular channel randomly packed with one layer of Novozym® 435 revealed the dominance of the convective mass transport over diffusive one, while further comparison of estimated characteristic times shown intra-particle mass transfer limitations as the rate limiting step. Finally, an inhibition by both substrates was confirmed for the selected transesterification by evaluating a set of experimental data obtained in a batch process.

Taking all into account, it can be concluded that the reusable MPBRs of different channel sizes and designs enabling simple and efficient enzyme loading in the form of uniformly or randomly packed LentiKats®, as well as randomly packed Novozym® 435, were developed and tested using ω-TA-catalyzed synthesis of ACP and CaLB-catalyzed synthesis of BB as the model reactions, respectively. In the case of the MPBRs with LentiKats®, a systematic scale-up study of a two-plate MPBR revealed that for the increased capacity enabling efficient use of LentiKats® containing ω-TA, a single layer of uniformly packed particles within a wide channel with a triangular inlet pre-chamber with pillars should be considered. In contrast, increasing the depth of an MPBR with particle loading in layers one on top of the other resulted in decreased production rates presumably due to the fluid maldistribution within the reactor with stuck-together gel particles. The results of systematic scale-up study of the MPBRs utilizing Novozym® 435 were similar to performance of MPBRs with LentiKats®, except that the increase in the channel depth by random packing with two layers of Novozym® 435 resulted in favorable, hydrodynamic conditions and consequently reactor efficiency. This study reported an efficient scale-up, while a numbering-up concept is suggested for further increase in production capacity. Furthermore, developed MPBRs were used as a tool for process parameters optimization evaluated with low-material and time consumption, confirming the importance of implementation of microreactor technology in

bioprocess development studies. A microfluidic-based method for immobilization of *E. coli* cells in alginate microparticles was developed as a proof-of-concept confirming feasibility of using a microfluidic device for an efficient and rapid production of immobilized biocatalysts which could be applied in MPBRs.

6.2 POVZETEK

Kemična industrija se sooča z visokimi zahtevami za postavitev okolju prijazne proizvodnje, ki je znana kot ‘zelena kemija’ ali ‘trajnostna tehnologija’. Biokataliza uporablja različne neimobilizirane in imobilizirane encime ali cele celice kot zelo učinkovite katalizatorje, in se je pojavila kot tehnologija, ki se popolnoma prilega na omenjeni koncept in zaradi tega postaja močna alternativa kemični katalizi. Sinergija med biokatalizo in miniaturizacijo reaktorja oz. obratovalne enote se je izkazala kot učinkovito orodje za hiter razvoj biokatalitskih procesov, saj so miniaturni sistemi pokazali številne prednosti pred klasičnimi. Med različnimi vrstami mikroreaktorjev veliko pozornosti zavzemajo miniaturizirani kontinuirno delujoči reaktorji s strnjenim slojem (MPBR) z imobiliziranimi encimi ali celimi celicami, vendar pa se v industriji še ne uporabljajo veliko, predvsem zaradi svoje majhnosti. Zato je za njihovo uporabo na industrijski ravni ključno najti rešitev za učinkovito povečevanje zmogljivosti MPBR in hkrati obdržati koristi miniaturizacije. Matematično modeliranje MPBR z imobiliziranimi biokatalizatorji je tudi lahko v veliko pomoč pri praktičnem delu njihovega razvoja in optimizacije. Iskanje ustreznih nosilcev, ki se uporabljajo za imobilizacijo biokatalizatorjev in njihovo nadaljnjo uporabo v MPBR, in ki bi se lahko hitro proizvajali s pomočjo mikrofluidnih naprav, je tudi korak več k začrtanemu cilju.

Namen tega dela sta razvoj in karakterizacija MPBR z imobiliziranimi biokatalizatorji, in sicer ω-transaminaze (ω-TA) ujete v polivinil alkohol (PVA) delce v obliki leč (LentiKats®) in lipaze B iz kvasovke *Candida antarctica* (CaLB) adsorbirane na akrilno smolo (Novozym® 435) v obliki kroglic. Sistematično povečevanje MPBR, ki smo jih uporabili za katalitske procese s pomočjo imobiliziranih transaminaz in lipaz, smo izvedli z namenom povečevanja zmogljivosti reaktorjev in hkrati omogočanjem učinkovite uporabe biokatalizatorja. S primerjavo produktivnosti reaktorjev smo preučili vpliv oblike (pravokotni in šesterokotni kanali) ter dolžine, širine in globine kanala na delovanje MPBR. Preučili smo tudi vpliv temperature na imobilizirane encime in oceno obratovalne stabilnosti MPBR. Med cilji raziskave sta bila tudi merjenje padca tlaka in analiza porazdelitve zadrževalnih časov v MPBR. Poleg tega smo razvili metodo za imobilizacijo *E. coli* celic s prekomerno izraženo ω-TA v alginatne mikrodelce, ki temelji na mikrofluidiki. Tako smo predstavili nov pristop k uporabi miniaturiziranih naprav za imobilizacijo biokatalizatorjev z možnostjo uporabe v MPBR.

V celovitem pregledu literature so v teoretičnem ozadju tega dela predstavljeni pomen biokatalize in biokatalitskih procesov, imobilizacija biokatalizatorjev ter miniaturizacija in mikroreaktorski sistemi. Podpoglavje o biokatalizi in biokatalitskih procesih obravnava glavne prednosti (visoka specifičnost, visoka aktivnost pod blagimi pogoji, visoko pretvorbeno število in biorazgradljivost ter naraven izvor) in slabosti (visoka molekulska kompleksnost, visoki proizvodni stroški in nestabilnost) encimov kot biokatalizatorjev. V podpoglavje so vključene tudi glavne lastnosti in uporaba encimov ω-TA in CaLB ter opis modelnih reakcij ω-TA-katalizirane sinteze acetofenona (ACP) in s CaLB katalizirane sinteze butil butirata (BB) skupaj z ping-pong bi-bi mehanizmom obeh reakcij.

Podpoglavje, ki obravnava imobilizacijo biokatalizatorjev, podaja definicijo imobilizacije kot "metode, ki se uporablja za fizično ali kemično fiksacijo celic, organelov, encimov ali drugih proteinov na trdnem nosilcu, v trdnih matrikah ali v membranah, da bi povečali njihovo stabilnost in omogočili večkratno ali kontinuirno uporabo". V tem delu so opisane tudi glavne prednosti (izboljšanje katalitskih funkcij, boljša stabilnost in selektivnost biokatalizatorjev, kot tudi njihova olajšana separacija, čiščenje in ponovna uporaba) in slabosti (možne omejitve prenosa snovi) imobilizacije z ujetjem in z adsorpcijo na nosilcu. Biokatalizatorji, uporabljeni v tej raziskavi, so imobilizirani v polimernih matrikah ali na nosilcih na osnovi akrilne smole z uporabo zgoraj omenjenih konceptov. ω-TA je imobilizirana v LentiKats® PVA hidrogel, medtem ko so bile celice *E. coli* z vstavljenim genom za ekspresijo ω-TA imobilizirane v alginatno matriko z uporabo v tem delu razvite metode, ki temelji na mikrofluidiki. Po drugi strani pa je bil encim CaLB adsorbiran na akrilne sferične delce, kjer je lokaliziran v 80–100 μm debelem zunanjem sloju, in uporabljen v obliki komercialno dostopnega pripravka Novozym® 435.

Podpoglavje, ki se ukvarja z miniaturizacijo in mikrosistemi, poudarja mikro nivo kot glavno značilnost miniaturiziranih reaktorjev, in jih definira kot naprave pretežno izdelane z uporabo mikroinženirstva, z vsaj eno karakteristično dimenzijo manjšo od 1 mm in razmerjem med površino in volumnom precej višjim od tradicionalnih reaktorjev. Kot glavne značilnosti miniaturiziranih naprav so poudarjeni kontinuirno obratovanje v pogojih laminarnega toka, zelo učinkovit prenos snovi in toplote, ki vodi do intenziviranja procesov, ter dober prostorski in časovni nadzor, zmanjšane okoljske, finančne in varnostne obremenitve. Transportni pojavi so na mikro nivoju predstavljeni v kratkem pregledu najpomembnejših brezdimenzijskih števil povezanih z dinamiko tekočin (*Re, Bo, Oh* in *Ca*) in prenosom snovi (*Da* in *Pe*) ter primerjavi njihovih vrednosti med različnimi nivoji velikosti reaktorjev. Hidrodinamika reaktorjev je na splošno podana v teoretičnem ozadju analize porazdelitve zadrževalnih časov (RTD). Poleg tega so v kratkem predgovoru k eksperimentalnemu delu, ki se ukvarja z imobilizacijo celic *E. coli*, podana glavna načela tvorjenja kapljic in proizvodnje alginatnih mikrodelcev z uporabo visoko pretočih mikrofluidnih naprav (s poudarkom na uporabi geometrije T-križišča). Kratkemu vpogledu v najbolj pomembne značilnosti MPBR, kot so sposobnost zagotavljanja relativno majhnih

padcev tlaka, velike površine za kontakt med tekočino in nosilcem, ponovna uporaba biokatalizatorja brez predhodne ločitve, velike koncentracije biokatalizatorja in dolgoročne obratovalne stabilnosti, skupaj z brezdimenzijskimi števili, pomembnimi za hidrodinamiko in prenos snovi v MPBR (Re_p in Pe_p), sledi pregled biotransformacij v MPBR in njihovega opisa z matematičnimi modeli. Na koncu podpoglavja je predstavljeno povečevanje biokatalitskih procesov iz laboratorijskega na industrijski nivo kot ključen korak k vzpostavljanju praktičnega, gospodarsko konkurenčnega in trajnostno uporabnega biokatalitskega procesa.

V pričujočem delu smo izvedli niz eksperimentov z uporabo nepatogenega seva rekombinantnih celic *E. coli* BL21 (DE3) z vstavljenim genom za intracelularno ekspresijo ω-TA (divji tip oz. 'wild type' aminske transaminaze, ATA-wt). Poleg tega smo uporabili ω-TA v izolirani obliki, imobilizirano v LentiKats®, in CaLB v obliki komercialnega pripravka Novozym® 435. Najprej smo nagojili celice *E. coli* z uporabo gojišča ZYM-505, ki vsebuje kanamicin sulfat iz bakterije *Streptomyces kanamyceticus*, nato smo celice imobilizirali v alginatne mikrodelce. Proizvodnjo alginatnih mikrodelcev in imobilizacijo celic *E. coli* smo izvedli z metodo, ki temelji na mikrofluidiki, z uporabo steklenega mikročipa s T-križiščem za tvorbo mikrokapljic, ki ima hidrofobni premaz primeren za tvorbo reverznih emulzij. Proizvodnjo vodnih mikrokapljic, ki vsebujejo alginat, smo izvedli s pomočjo emulzifikacije vode v olju z uporabo jedilnega olja kot zvezne faze (pretok 100 µL min^{-1}) in vodne raztopine alginata (2 g L^{-1}) kot faze ki tvori kapljice (pretok 50 µL min^{-1}). Nato smo vodne mikrokapljice z alginatom solidificirali *ex situ* oz. z njihovim zbiranjem v dvofazni želirni kopeli, ki je vsebovala Ca^{2+} ione. Za karakterizacijo kapljičastega toka v sistemu smo določili gostoto in viskoznost obeh kapljevin skupaj z medfazno napetostjo med njima. Velikost in porazdelitev velikosti proizvedenih alginatnih mikrodelcev (bodisi praznih ali z imobiliziranimi celicami) smo analizirali z uporabo svetlobnega mikroskopa, foto kamere in ustrezno kalibrirane programske opreme za analizo slik. Alginatne mikrodelce z imobiliziranimi celicami *E. coli* smo z uporabo ω-TA-katalizirane sinteze ACP kot modelne reakcije testirali glede učinkovitosti in njihove stabilnosti pri skladiščenju.

Izoliran encim ω-TA je bil imobiliziran v LentiKats®, kar so izvedli v podjetju LentiKat's a. s. po standardnem postopku. Delcem z imobiliziranim encimom smo določili porazdelitev velikosti in aktivnost ter jih uporabili za testiranje razvitih MPBR. MPBR, narejeni iz dveh polimetilmetakrilatnih plošč, ekspandiranega politetrafluoroetilena (uporabljen za izdelavo kanalov in stebrov za distribucijo kapljevine) in nestisljivega politetrafluoroetilenskega traka (uporabljen za zunanji distančnik, ki zagotavlja fiksno globino kanala), so bili naključno ali enakomerno polnjeni v enega, dva ali tri sloje z različnimi količinami LentiKats® (od 19,5 do 2725,1 mg). Prvotni MPBR s pravokotnom kanalom smo sistematično povečevali tako glede dolžine, širine, kot globine kanalov, pri čemer smo držali drugi dve dimenziji konstantni. Reaktorje različnih velikosti in oblik (poleg pravokotne smo vpeljali še

šesterokotno, ki je omogočala boljšo porazdelitev tekočine z vstopnim delom s stebrički) smo testirali glede njihove produktivnosti. Vpliv temperature na proces transaminacije smo ocenili z vstavitvijo kontinuirno delujočega MPBR v termostatirano kopel postavljeno na magnetno mešalo z nadzorom temperature, prav tako pa smo testirali obratovalno stabilnost MPBR v obdobju 21 dni pri 24 °C. Hidrodinamiko v MPBR z LentiKats® smo analizirali z merjenjem padca tlaka na v reaktorju z uporabo silicijevega piezouporovnega senzorja tlaka z obratovalnim območjem od 0 do 100 kPa, pri konstantnem pretoku vode v območju od 10 do 1000 µL min^{-1}.

Enaka načela sistematičnega povečevanja dimenzij smo uporabili tudi za MPBR, naključno polnjene z enim do dvema slojema sferičnih delcev Novozym® 435. Razviti MPBR so bili prav tako kot pri LentiKats® modularnega tipa, z nekaterimi manjšimi spremembami, uvedenim z namenom prilagoditve globine kanalov (dodaten sloj nestisljivega politetrafluoroetilenskega traka, uporabljen kot distančnik) in zadrževanja delcev znotraj kanalov (v ta namen je bil dodan tanek dvostranski poliesterski lepilni trak). Da bi dobili čim bolj uniformne delce, primerne za uporabo v MPBR, smo komercialni pripravek Novozym® 435 s pomočjo sistema sejalnih sit (velikost por 300–425 µm in 425–500 µm) ločili na frakcije. Po analizi velikosti in porazdelitve velikosti delcev, smo primerno frakcijo pripravka Novozym® 435 (300–425 µm) uporabili za nadaljnje raziskave – najprej smo jim določili encimsko aktivnost ter vpliv vrtilne hitrosti (v razponu od 300 do 1200 min^{-1}) na konverzijo substrata v šaržnem reaktorju, nato pa še za izvedbo s CaLB katalizirane sinteze BB v *n*-heptanu v kontinuirno delujočem MPBR s pravokotnimi ali šesterokotnimi kanali naključno polnjenimi z različnimi količinami delcev Novozym® 435 (od 7,1 do 148,4 mg). Vpliv temperature na proces transesterifikacije smo ocenili s postavitvijo kontinuirno delujočega MPBR z enim slojem Novozym® 435 v termostatirano kopel z avtomatskim nadzorom temperature, medtem ko smo obratovalno stabilnost MPBR testirali v obdobju 53 dni pri 24 °C. Poleg tega smo MPBR z Novozym® 435 analizirali z merjenjem padca tlaka v reaktorju z uporabo zgoraj opisanega senzorja tlaka, pri konstantnem pretoku vode v območju od 30 do 1800 µL min^{-1}. Tudi smo izvedli analizo RTD za MPBR s pravokotnima kanaloma dolžine 23,93 in 81,00 mm, naključno polnjenima z Novozym® 435 delci v enem sloju. Za to smo izvedli eksperiment s pulzno motnjo, kjer smo kot inertni sledilec uporabili glukozo (50 mM) raztopljeno v fosfatnem pufru z NaCl (pH 7,4). Koncentracijo glukoze na izhodu MPBR smo merili z uporabo ustrezno kalibriranega biosenzorja z imobilizirano glukoza-oksidazo iz glive *Aspergillus niger* VII S, ki smo ga integrirali v mikrofluidni čip. Reaktante in produkte obeh modelnih reakcij smo spremljali z uporabo analiznih metod HPLC in/ali GC.

Rezultati so povzeti v treh glavnih poglavjih, ki se ukvarjajo tako z imobilizacijo celic *E. coli* kot tudi razvojem in ovrednotenjem MPBR z LentiKats® in Novozym® 435. Z uporabo sistema, sestavljenega iz steklenega mikročipa s T-križiščem in cevke submilimetrskega premera, sta dve nemešljivi tekočini s površinsko napetostjo 10,5

mN m^{-1}, in sicer vodna raztopina alginata (gostota 1008,70 ± 0,30 kg m^{-3} in viskoznost 18,01 ± 0,10 mPa s) in sončnično olje (gostota 916,04 ± 1,20 kg m^{-3} in viskoznost 70,19 ± 1,90 mPa s), pod laminarnimi pogoji (največji *Re* v sistemu je bil 0,233) tvorili sferične monodisperzne vodne mikrokapljice z alginatom. Mikrokapljice so dosegle premer izstopne cevi (500 µm), iz katere smo jih s hitrostjo približno 25 s^{-1} vodili v želirno kopel, kjer je potekalo *ex situ* želiranje. Pridobljeni v vodi netopni alginatni mikrodelci z 'repkom' so imeli sferično telo s povprečnim premerom 446,21 ± 36,54 µm. Z enako metodo smo imobilizirali celice *E. coli* z izraženo ω-TA, kjer so vodne mikrokapljice z alginatom in suspendiranimi celicami (0,39 mg_{dry} mL^{-1}) po želiranju tvorile sferične mikrodelce brez 'repkov' in s povprečnim premerom 932,72 ± 115,30 µm. Pridobljene mikrodelce z imobiliziranimi celicami *E. coli* s specifično aktivnostjo 4,46 ± 0,47 U mg_{dry}^{-1} smo nato testirali glede stabilnosti pri skladiščenju ter učinkovitosti v šaržnem procesu. Rezultati so pokazali, da se je aktivnost znižala pod 40 % začetne vrednosti po 4 dneh skladiščenja v 20 mM Tris-HCl pufru (pH 8,0) pri 4 °C.

Naslednje poglavje se ukvarja z ocenjevanjem razvitih in sistematično povečanih MPBR polnjenih z LentiKats® povprečnega premera krožne osnove 3,87 ± 0,33 mm, višine 0,35 ± 0,10 mm, ter Sauterjevega premera 0,52 mm. Uporabljenemu imobiliziranemu pripravku LentiKats® z ω-TA smo določili specifično aktivnost 0,50 in 0,73 U $mg_{ATA\text{-}wt}^{-1}$ oz. 0,025 in 0,037 U mg_{LK}^{-1}. Sintezo ACP, katalizirano z ω-TA, smo izvedli v enostavno sestavljivih in modularno strukturiranih MPBR s pravokotnimi in šesterokotnimi kanali različnih velikosti, enakomerno ali naključno polnjenih z LentiKats® v enem do treh slojih.

Najprej smo osnovnemu MPBR z eno vrsto LentiKats® sistematično povečali dolžino kanala na 20 do 60 mm, tako da smo dobili dolge pravokotne kanale z volumni do 55,2 µL, koncentracijo encima do 74,28 U mL^{-1} in poroznostjo do 0,40, ki smo jim določili produktivnost. Ko smo ekvimolarno vodno raztopino obeh substratov (oz. (*S*)-(–)-α-metilbenzilamina in natrijevega piruvata) črpali skozi MPBR pri pretokih v razponu od 2 do 100 µL min^{-1} (povprečni zadrževalni čas do 10,4 min), je laminarni tok okrog enakomerno nasutih delcev omogočil zelo učinkovito biotransformacijo. Vsi testirani MPBR so obratovali približno enako dobro pri enakih povprečnih zadrževalnih časih, pri čemer so dosegli več kot 80 % konverzijo v manj kot 5 min. Nadaljnja primerjava reakcijskih hitrosti (*PR*), ocenjenih pri 70 % konverziji v MPBR različnih dolžin kanalov, je pokazala linearno sorazmernost znotraj testiranih dimenzij in produktivnost biokatalizatorja (*BPN*) do 257,6 μmol_{ACP} $g_{ATA\text{-}wt}^{-1}$. Tako se je izkazalo, da smo s sistematičnim povečevanju dolžine kanalov hkrati dosegli povečano zmogljivost reaktorja in učinkovito dostopnost biokatalizatorja zaradi ugodnih hidrodinamiskih pogojev.

Povečanje velikosti smo nadalje izvedli v smeri širine kanala (od 4 do 12 mm široki pravokotni kanali z volumni do 55,2 µL, koncentracijo encima do 68,45 U mL^{-1} in poroznostjo 0,41), kjer smo MPBR enakomerno polnili z eno plastjo LentiKats®. Pri uporabi

pretokov v razponu od 2 do 100 µL min^{-1} (povprečni zadrževalni čas do 11,4 min) so rezultati pokazali nekoliko večje *BPN* kot v prejšnjem primeru (okrog 285 μmol_{ACP} $g_{ATA\text{-}wt}^{-1}$) ter nelinearno sorazmernost pri zvišanju reakcijskih hitrosti ocenjenih pri 70 % konverziji, kar je lahko posledica neugodnih hidrodinamiskih pogojev. Da bi zagotovili ustreznejšo porazdelitev tekočine vzdolž širine kanala smo uvedli trikotni vstopni in izstopni del kanala s stebrički. MPBR s kanali občutno povečanih širin (od 4 do 79,67 mm, z volumni pravokotnega dela kanala do 2090,5 µL, koncentracijo encima do 46,87 U mL^{-1} in poroznostjo do 0,60), polnjenih z eno plastjo LentiKats®, smo testirali in primerjali glede njihove produktivnosti. Pri pretokih od 1,7 do 1090,0 µL min^{-1} (povprečni zadrževalni čas do 35,4 min) so MPBR z izboljšano porazdelitvijo toka tekočine pokazali skoraj enako učinkovitost pri istih povprečnih zadrževalnih časih, pri čemer so dosegli konverzije nad 90 % v manj kot 20 min, vrednosti *BPN* pa so znašale do 642,4 μmol_{ACP} $g_{ATA\text{-}wt}^{-1}$. Ugodne hidrodinamske pogoje smo v nadaljevanju potrdili pri MPBR z vsemi testiranimi širinami kanalov s trikotnimi deli s stebrički.

V nadaljevanju smo na osnovi različnega nasutja LentiKats® v enega, dva ali tri sloje preučili še vpliv povečanja globine kanalov na učinkovitost MPBR s šesterokotnimi kanali s trikotnimi vstopnimi in izstopnimi deli s stebrički, pri čemer smo dosegli globine od 0,32 do 0,96 mm z volumni pravokotnega dela do 3187,5 µL, koncentracijo ecima do 43,49 U mL^{-1} in poroznostjo do 0,62. Pri uporabi pretokov v razponu od 18,0 do 1730,7 µL min^{-1} (povprečni zadrževalni čas do 35 min) je samo MPBR z enim slojem LentiKats® pri najdaljših povprečnih zadrževalnih časih dosegel maksimalno konverzijo, medtem ko so MPBR z več sloji delcev dosegli bistveno nižje konverzije pri enakih povprečnih zadrževalnih časih. Zmanjšanje vrednosti *BPN* iz 536,2 μmol_{ACP} $g_{ATA\text{-}wt}^{-1}$, dosežene v MPBR z enim slojem, na 362,7 μmol_{ACP} $g_{ATA\text{-}wt}^{-1}$, dosežene v MPBR s tremi sloji LentiKats®, smo pripisali opaženemu lepljenju delcev pakiranih v sloje, kar je preprečilo vzpostavitev homogenega toka tekočine okoli delcev in je vodilo do nastanka kanalov, ki so preprečili molekulam substrata dostop do encimov. Reakcijska hitrost v MPBR s tremi sloji LentiKats® se je zmanjšala za 1,8-krat v primerjavi z vrednostjo pri MPBR z enim slojem. Še bistveno nižje konverzije smo pridobili v MPBR z 0,64 mm globokim kanalom, naključno polnjenim z LentiKats® v več slojih (koncentracija encima 167,45 U mL^{-1} in poroznost 0,28), kjer je bila vrednost *BPN* 72,1 μmol_{ACP} $g_{ATA\text{-}wt}^{-1}$. Manjša učinkovitost MPBR z več sloji LentiKats® je bila spet posledica stiskanja in lepljenja delcev hidrogela v kanalu, kar je vodilo v tvorbo kanalov tekočine skozi sloje in posledično reakcijske hitrosti le do 20 μmol_{ACP} h^{-1}.

Z razvitimi MPBR smo ocenili tudi vpliv temperature na transaminacijo v razponu od 30 do 75 °C pri pretoku od 25 µL min^{-1} (povprečni zadrževalni čas 2,6 min). Rezultati so pokazali, da je 55 °C optimalna temperatura za obravnavano reakcijo z LentiKats® z imobilizirano ω-TA. Po 2,6 min pri 55 °C je MPBR dosegel *BPN* in reakcijsko hitrost 361,7 μmol_{ACP} $g_{ATA\text{-}wt}^{-1}$ in približno 31,9 μmol_{ACP} h^{-1}. Po drugi strani pa je MPBR z eno vrsto in enim

slojem enakomerno nasutih LentiKats® pokazal dobro obratovalno stabilnost, saj je v obdobju 21 dni pri 24 °C zadržal več kot 80 % začetne volumetrične produktivnosti.

Meritve padca tlaka v razvitih MPBR z LentiKats® so pokazale zmerno in linearno odvisne vrednosti, ki so znašale do 42 kPa pri pretokih do 1000 µL min^{-1}. Padci tlaka so bili približno enaki pri različnih geometrijah kanalov, razen pri MPBR z najmanjšim pravokotnim kanalom, kjer je bil pri pretoku 100 µL min^{-1} izmerjen padec tlaka 9 kPa. Izračunani Re_p za delce je znašal blizu 0,68 za vse MPBR z enakomernim nasutjem, kar nedvomno potrjuje obstoj laminarnega toka in zadržanih ugodnih hidrodinamskih lastnosti.

Časovno dimenzijska analiza MPBR s pravokotnim kanalom enakomerno nasutega z enim slojem LentiKats® je pokazala prevlado konvektivnega prenosa snovi nad prenosom z difuzijo (Pe_p od 22,35 do 670,62 pri pretokih od 1,7 do 50,8 µL min^{-1}) in s tem difuzijski prenos snovi znotraj LentiKats® kot omejitveni dejavnik celotnega procesa.

V nadaljevanju smo preučevali MPBR naključno polnjene z enim ali dvema slojema Novozym® 435 s povprečnim premerom 372,10 ± 27,05 µm in s specifično aktivnostjo 133,05 ± 2,71 U mg_{CaLB}^{-1} (13,31 ± 0,27 U mg_{N435}^{-1}).

MPBR, naključno polnjene z eno vrsto in enim slojem Novozym® 435, smo sistematično podaljšali od 23,93 do 81,00 mm in s tem pridobili dolge pravokotne kanale z volumni do 95,3 µL, koncentracijo encima do 5,53 U $µL^{-1}$ in poroznostjo do 0,59, ki smo jim določili produktivnost s črpanjem ekvimolarne raztopine obeh substratov (oz. vinil butirata in 1-butanola) v *n*-heptanu pri pretokih v razponu od 12,2 do 565,2 µL min^{-1} (povprečni zadrževalni čas do 1,4 min). Vsi trije preizkušeni MPBR so obratovali enako ugodno pri enakih povprečnih zadževalnih časih, pri čemer smo dosegli maksimalno konverzijo približno 95 % v manj kot 0,8 min. Reakcijske hitrosti, ocenjene pri najdaljšem povprečnem zadrževalnem času (oz. pri maksimalni konverziji), so pokazale linearno sorazmernost z dolžino kanalov ob isti širini in globini. Dosežene vrednosti *BPN* do 13,56 $mmol_{BB}$ g_{CaLB}^{-1} so dokazovale, da je bilo povečanje kapacitete reaktorja na osnovi njegovega podaljšanja učinkovito.

Sintezo BB, katalizirano s CaLB, smo v nadaljevanju izvedli še v MPBR s pravokotnimi ali šesterokotnimi kanali (s trikotnimi vstopni in izstopnimi deli s stebrički) različnih širin (od 2,95 do 29,22 mm široki kanali z volumni pravokotnega dela do 628,7 µL, koncentracijo encima do 5,38 U $µL^{-1}$ in poroznostjo do 0,58), naključno polnjenimi z enim slojem Novozym® 435. Evalvacija pri pretokih v razponu od 25,2 do 3636,4 µL min^{-1} (povprečni zadrževalni čas do 1,4 min) je pokazala maksimalno konverzijo okrog 95 % doseženo v manj kot 0,8 min v vseh testiranih MPBR, linearno povečanje reakcijskih hitrosti ocenjenih pri najdaljših zadrevalnih časih v odvisnosti od širine kanala ter vrednosti *BPN* okrog 12,5 $mmol_{BB}$ g_{CaLB}^{-1}.Vpliv globine kanala na učinkovitost reaktorja smo raziskali z uporabo MPBR z dvema različnima globinama šesterokotnih kanalov (0,40 in 0,80 mm globoka kanala z volumni pravokotnega dela do 643,1 µL, koncentracijo encima do 5,52 U $µL^{-1}$ in

poroznostjo do 0,58) najključno polnjenima z Novozym® 435, ki delujeta pri pretokih v razponu od 131,5 do 3756,3 µL min^{-1} (povprečni zadrževalni čas do 1,4 min). MPBR z dvema slojema je dosegel nekoliko višjo konverzijo pri povprečnih zadrževalnih časih manjših od 0,6 min. Posledica tega je, da reakcijska hitrost, ocenjena pri najdaljšem povprečnem zadrževalnem času, neznatno odstopa od linearnosti, vendar še vedno zagotavlja učinkovito povečanje zmogljivosti MPBR. Dosežen *BPN* v MPBR z dvema slojema delcev (14,03 $mmol_{BB}$ g_{CaLB}^{-1}) je bil višji od tistega, ki smog a dosegli v MPBR z enim slojem delcev (12,18 $mmol_{BB}$ g_{CaLB}^{-1}).

Vpliv temperature na sintezo BB, katalizirano s CaLB, smo ocenili v temperaturnem območju od 24 do 80 °C v termostatiranem in kontinuirno delujočem MPBR s pravokotnim kanalom, naključno polnjenim z enim slojem Novozym® 435 (koncentracija encima 5,53 U $µL^{-1}$ in poroznost 0,57) pri pretoku 170,7 µL min^{-1} (povprečni zadrževalni čas 0,1 min). Kot optimalna temperatura se je izkazala 75 °C, kjer smo dosegli konverzijo okrog 81 %, *BPN* je znašal 11,39 $mmol_{BB}$ g_{CaLB}^{-1}, *PR* pa 4,85 $mmol_{BB}$ h^{-1}. Po drugi strani smo obratovalno stabilnost ovrednotili v obdobju 53 dni pri 24 °C z uporabo MPBR s pravokotnim kanalom, naključno polnjenim z enim slojem Novozym® 435 (koncentracija encima 5,28 U $µL^{-1}$ in poroznost 0,58). V tem času je relativna volumetrična produktivnost padla pod 50 % začetne vrednosti. Meritve padca tlaka v MPBR z Novozym® 435 so pokazale zmeren in linearno odvisen trend z višanjem pretoka, z največjim padcem tlaka okrog 88 kPa pri pretoku od 1800 µL min^{-1}. Izračunano Re_p število je izkazalo popolnoma laminarni tok tekočine (Re_p pri maksimalnih pretokih so znašali do 8,37).

Analiza porazdelitve zadrževalnih časov, ki smo jo najprej preučili na eksperimentalni postavitvi zanke brez priključenega MPBR z uporabo glukoze kot inertnega sledilca, je pokazala vrednosti povprečnega zadrževalnega časa od 1,78 min, variance 0,21 min^2 in asimetrije 0,79. Nato smo izvedli analizo RTD na MPBR z dolžinama pravokotnih kanalov 23,93 in 81,00 mm. Rezultati so pokazali, da se eksperimentalno določene vrednosti povprečnih zadrževalnih časov (0,21 min za krajši in 0,53 min za daljši kanal) ujemajo z izračunanimi idealnimi vrednostmi za podane dolžine kanalov. Na ta način smo dokazali, da so bili celotni reaktorji izkoriščeni oziroma da so bili brez neaktivnih prostornin ali obvoda tekočine. Za MPBR s krajšim kanalom je znašala vrednost variance 0,08 min^2 in asimetrije 0,77 ter aksialni koeficient disperzije $1{,}42 \times 10^{-5}$ m^2 s^{-1}, medtem ko je bila za MPBR z daljšim kanalom vrednost variance 0,14 min^2, asimetrije 0,42 in aksialni koeficient disperzije $0{,}92 \times 10^{-5}$ m^2 s^{-1}.

Tudi pri MPBR s pravokotnim kanalom, naključno polnjenim z enim slojem Novozym® 435, je časovno dimenzijska analiza pokazala prevlado konvektivnega prenosa snovi nad difuzijskim prenosom (vrednosti za Pe_p število so bile v območju od 169,39 do 2371,46 pri pretokih od 40,4 do 562,2 µL min^{-1}) in omejitve prenosa snovi znotraj delcev kot omejitveni dejavnik za celotno reakcijo.

Za izbrano transesterifikacijo vinil butirata in 1-butanola smo z ovrednotenjem niza eksperimentalnih podatkov, pridobljenih v šaržnem procesu, potrdili inhibicijo z obema substratoma. Potrdili smo, da se lahko matematični model, ki je že predstavljen v literaturi, z uporabo pridobljenih parametrov uporablja tudi za opis MPBR z Novozym® 435, razvitim v tej študiji.

V zaključku ugotavljamo, da so razviti MPBR omogočali enostavno in učinkovito polnjenje z imobiliziranimi encimi v obliki hidrogelov ali sferičnih poroznih delcev ter večkratno uporabo, uspešno pa smo jih evalvirali na primeru sinteze ACP katalizirane z ω-TA ter sinteze BB, katalizirane s CaLB. V primeru MPBR z LentiKats® je sistematična študija povečevanja reaktorja, narejenega iz dveh plošč, pokazala, da je za povečanje zmogljivosti in hkrati učinkovito uporabo LentiKats®, ki vsebuje ω-TA, najbolj učinkovit en sloj enakomerno nasutih delcev v širokem kanalu s trikotnimi deli s stebrički. V nasprotju s tem pa ima povečanje globine kanalov v MPBR z višanjem nasutja delcev kot posledico zmanjšanje reakcijske hitrosti ter posledično zmanjšano učinkovitost, kar pripisujemo neugodnim hidrodinamskim pogojem v takšni konfiguraciji MPBR. Rezultati študije sistematičnega povečanja MPBR z Novozym® 435 so bili podobni kot pri LentiKats®, razen tega, da je povečanje globine kanalov, naključno polnjenih z dvema slojema Novozym® 435, izkazalo zadržano dobro učinkovitost reaktorja, kar kaže na ugodne hidrodinamske pogoje v reaktorju. S to študijo smo predstavili učinkovito sistematično povečevanje naprav, pri čemer bi za nadaljnje povečanje proizvodne zmogljivosti predlagali koncept povečanja števila enot oz. angl. ‘numbering-up’. Poleg tega smo razvite MPBR uporabili kot orodje za optimizacijo procesnih parametrov, pri čemer smo zagotovili nizko porabo materiala in časa, kaj potrjuje prednost uporabe mikroreaktorske tehnologije pri razvoju bioprocesov. Končno, razvili smo postopek za imobilizacijo celic *E. coli* v alginatne mikrodelce, ki temelji na mikrofluidiki, s čimer smo nakazali možnost uporabe mikrofluidnih naprav za učinkovito in hitro pripravo imobiliziranih biokatalizatorjev, ki jih lahko uporabljamo v MPBR.

7 REFERENCES

Adlercreutz P. 2013. Immobilisation and Application of Lipases in Organic Media. Chemical Society Reviews, 42, 15: 6406–6436

Aehle W. 2004. Enzymes in Industry: Production and Applications. 2nd ed. Weinheim, Wiley-VCH, Verlag GmbH & Co. KGaA: 484 p.

Ahmed E. M. 2015. Hydrogel: Preparation, Characterization, and Applications: A Review. Journal of Advanced Research, 6, 2: 105–121

Ajmera S. K., Delattre C., Schmidt M. A., Jensen K. F. 2002. Microfabricated Cross-Flow Chemical Reactor for Catalyst Testing. Sensors and Actuators, B: Chemical, 82, 2–3: 297–306

Akbari S., Pirbodaghi T. 2014. Microfluidic Encapsulation of Cells in Alginate Particles via an Improved Internal Gelation Approach. Microfluidics and Nanofluidics, 16, 4: 773–777

Al-Mayah A. M. R. 2012. Simulation of Enzyme Catalysis in Calcium Alginate Beads. Enzyme Research, 2012, Article ID 459190, doi:10.1155/2012/459190: 13 p.

Allain F., Dixon A. G. 2010. Modeling of Transport and Reaction in a Catalytic Bed Using a Catalyst. In: Proceedings of the COMSOL Conference. COMSOL Conference 2010, Boston, October 7-October 9: 7 p. https://www.comsol.com/paper/download/101925/allain_paper.pdf (8th April 2017)

Allen K. G., von Backström T. W., Kröger D. G. 2013. Packed Bed Pressure Drop Dependence on Particle Shape, Size Distribution, Packing Arrangement and Roughness. Powder Technology, 246: 590–600

Amici E., Tetradis-Meris G., de Torres C. P., Jousse F. 2008. Alginate Gelation in Microfluidic Channels. Food Hydrocolloids, 22, 1: 97–104

Amini H., Sollier E., Masaeli M., Xie Y., Ganapathysubramanian B., Stone H. A., Di Carlo D. 2013. Engineering Fluid Flow Using Sequenced Microstructures. Nature Communications, 4, 1826, doi: 10.1038/ncomms2841: 8 p.

Amsden B. 1998. Solute Diffusion Within Hydrogels. Mechanisms and Models. Macromolecules, 31, 23: 8382–8395

Anderson E. M., Larsson K. M., Kirk O. 1998. One Biocatalyst Many Applications: The Use of *Candida antarctica* B-Lipase in Organic Synthesis. Biocatalysts and Biotransformations, 16, 3: 181–204

Andrade L. H., Kroutil W., Jamison T. F. 2014. Continuous Flow Synthesis of Chiral Amines in Organic Solvents: Immobilization of *E. coli* Cells Containing Both ω-Transaminase and PLP. Organic Letters, 16, 23: 6092–6095

AppliChem. 2008. Biological Buffers. Darmstadt, AppliChem GmbH: 18 p. https://www.applichem.com/fileadmin/Broschueren/BioBuffer.pdf (3rd February 2017)

Arcos J. A., Hill Jr. C. G., Otero C. 2001. Kinetics of the Lipase-Catalyzed Synthesis of Glucose Esters in Acetone. Biotechnology and Bioengineering, 73, 2: 104–110

Ariga O., Kubo T., Sano Y. 1994. Effective Diffusivity of Glucose in PVA Hydrogel. Journal of Fermentation and Bioengineering, 78, 2: 200–201

Aris R. 1999. Mathematical Modeling: A Chemical Engineer's Perspective. San Diego, Academic Press: 479 p.

Atencia J., Beebe D. J. 2005. Controlled Microfluidic Interfaces. Nature, 437: 648–655

Axelsson A., Persson B. 1988. Determination of Effective Diffusion Coefficients in Calcium Alginate Gel Plates With Varying Yeast Cell Content. Applied Biochemistry and Biotechnology, 18, 1: 231–250

Azevedo A. M., Cabral J. M. S., Gibson T. D., Fonseca L. P. 2004a. Operation and Performance of Analytical Packed-Bed Reactors With an Immobilized Alcohol Oxidase. Journal of Molecular Catalysis B: Enzymatic, 28, 2–3: 45–53

Azevedo A.M., Vojinović V., Cabral J.M.S., Gibson T.D., Fonseca L.P. 2004b. Operational Stability of Immobilized Horseradish Peroxidase in Mini-Packed Bed Bioreactors. Journal of Molecular Catalysis B: Enzymatic, 28, 2–3: 121–128

Babich L., Hartog A. F., van der Horst M. A., Wever R. 2012. Continuous-Flow Reactor-Based Enzymatic Synthesis of Phosphorylated Compounds on a Large Scale. Chemistry - A European Journal, 18, 21: 6604–6609

Bai L., Fu Y., Zhao S., Cheng Y. 2016. Droplet Formation in a Microfluidic T-junction Involving Highly Viscous Fluid Systems. Chemical Engineering Science, 145: 141–148

Bailey J. E. 1998. Mathematical Modeling and Analysis in Biochemical Engineering: Past Accomplishments and Future Opportunities. Biotechnology Progress, 14, 1: 8–20

Bajić M., Žnidaršič-Plazl P., Michael Rayappan M. K., Hessel V. 2017. General Aspects of Immobilized Biocatalysts and Their Application in Flow. In: Science of Synthesis Knowledge Updates. Rademann J., Schaumann E. (Vol. eds.). Stuttgart, Georg Thieme Verlag KG. In press.

Bansode S. R., Hardikar M. A., Rathod V. K. 2016. Evaluation of Reaction Parameters and Kinetic Modelling for Novozym 435 Catalyzed Synthesis of Isoamyl Butyrate. Journal of Chemical Technology and Biotechnology, doi: 10.1002/jctb.5125: 9 p.

Basso A., Braiuca P., Cantone S., Ebert C., Linda P., Spizzo P., Caimi P., Hanefeld U., Degrassi G., Gardossi L. 2007. In Silico Analysis of Enzyme Surface and Glycosylation Effect as a Tool for Efficient Covalent Immobilisation of CaLB and PGA on Sepabeads®. Advanced Synthesis and Catalysis, 349, 6: 877–886

Berthier J., Silberzan P. 2010. Microfluidics for Biotechnology. 2nd ed. Norwood, Artech House: 483 p.

Bezbradica D., Mijin D., Siler-Marinkovic S., Knezevic Z. 2006. The *Candida rugosa* Lipase Catalyzed Synthesis of Amyl Isobutyrate in Organic Solvent and Solvent-Free System: A kinetic study. Journal of Molecular Catalysis B: Enzymatic, 38, 1: 11–16

Bieringer T., Buchholz S., Kockmann N. 2013. Future Production Concepts in the Chemical Industry: Modular – Small-Scale – Continuous. Chemical Engineering and Technology, 36, 6: 900–910

Bisswanger H. 2014. Enzyme Assays. Perspectives in Science, 1, 1–6: 41–55

Bisswanger H. 2002. Enzyme Kinetics: Principles and Methods. Weinheim, Wiley-VCH Verlag GmbH: 256 p.

Boccardo G., Augier F., Haroun Y., Ferré D., Marchisio D. L. 2015. Validation of a Novel Open-Source Work-Flow for the Simulation of Packed-Bed Reactors. Chemical Engineering Journal, 279: 809–820

Bodla V. K., Seerup R., Krühne U., Woodley J. M., Gernaey K. V. 2013. Microreactors and CFD as Tools for Biocatalysis Reactor Design: A Case Study. Chemical Engineering and Technology, 36, 6: 1017–1026

Bolivar J. M., Nidetzky B. 2012. Positively Charged Mini-Protein Z_{basic2} as Highly Efficient Silica Binding Module: Opportunities for Enzyme Immobilization on Unmodified Silica Supports. Langmuir, 28, 26: 10040–10049

Bolivar J. M., Nidetzky B. 2013. Multiphase Biotransformations in Microstructured Reactors: Opportunities for Biocatalytic Process Intensification and Smart Flow Processing. Green Processing and Synthesis, 2, 6: 541–559

Bolivar J. M., Tribulato M. A., Petrasek Z., Nidetzky B. 2016. Let the Substrate Flow, Not the Enzyme: Practical Immobilization of D-Amino Acid Oxidase in a Glass Microreactor for Effective Biocatalytic Conversions. Biotechnology and Bioengineering, 113,1: 2342–2349

Bolivar J. M., Wiesbauer J., Nidetzky B. 2011. Biotransformations in Microstructured Reactors: More Than Flowing With the Stream? Trends in Biotechnology, 29, 7: 333–342

Bommarius A. S., Riebel B. R. 2004. Biocatalysis: Fundamentals and Applications. Weinheim, Wiley-VCH, Verlag GmbH & Co. KGaA: 634 p.

Börner T., Grey C., Adlercreutz P. 2016. Generic HPLC Platform for Automated Enzyme Reaction Monitoring: Advancing the Assay Toolbox for Transaminases and Other PLP-Dependent Enzymes. Biotechnology Journal, 11, 8: 1025–1036

Börner T., Rämisch S., Bartsch S., Vogel A., Adlercreutz P., Grey C. 2017b. Three In One Go: Thermo-, Solvent and Catalytic Stability by Engineering the Cofactor-Binding Element of Amine Transaminases. ChemBioChem, doi: 10.1002/cbic.201700236: 8 p.

Börner T., Rämisch S., Reddem E. R., Bartsch S., Vogel A., Thunnissen A.-M. W. H., Adlercreutz P., Grey C. 2017a. Explaining Operational Instability of Amine Transaminases: Substrate-Induced Inactivation Mechanism and Influence of Quaternary Structure on Enzyme–Cofactor Intermediate Stability. ACS Catalysis, 7, 2: 1259–1269

Börner T., Rehn G., Grey C., Adlercreutz P. 2015. A Process Concept for High-Purity Production of Amines by Transaminase-Catalyzed Asymmetric Synthesis: Combining Enzyme Cascade and Membrane-Assisted ISPR. Organic Process Research and Development, 19, 7: 793–799

Bošković D., Loebbecke S., Gross G. A., Koehler J. M. 2011. Residence Time Distribution Studies in Microfluidic Mixing Structures. Chemical Engineering and Technology, 34, 3: 361–370

Bosley J. 1997. Turning Lipases into Industrial Biocatalysts. Biochemical Society Transactions, 25, 1: 174–178

Boušková A., Mrákota J., Stloukal R., Trögl J., Pilařová V., Křiklavová L., Lederer T. 2011. Three Examples of Nitrogen Removal From Industrial Wastewater Using Lentikats Biotechnology. Desalination, 280, 1–3: 191–196

Bozzano G., Dente M., Manenti F., Corna P., Masserdotti F. 2014a. Fluid Distribution in Packed Beds. Part 1. Literature and Technology Overview. Industrial and Engineering Chemistry Research, 53, 8: 3157–3164

Bozzano G., Dente M., Manenti F., Corna P., Masserdotti F. 2014b. Fluid Distribution in Packed Beds. Part 2. Experimental and Phenomenological Assessment of Distributor and Packing Interactions. Industrial and Engineering Chemistry Research, 53, 8: 3165–3183

Braccini I., Pérez S. 2001. Molecular Basis of Ca^{2+}-Induced Gelation in Alginates and Pectins: The Egg-Box Model Revisited. Biomacromolecules, 2, 4: 1089–1096

Buchholz K., Kasche V., Bornscheuer U. T. 2012. Biocatalysts and Enzyme Technology. 2nd ed. Weinheim, Wiley-VCH Verlag & Co. KGaA: 626 p.

Buchholz K. B., Poulsen P. B. 2005. Introduction. In: Applied Biocatalysis. Straathof A. J. J., Adlercreutz P. (eds.). 2nd ed. Amsterdam, Taylor & Francis e-Library: 1–17

Buenrostro-Figueroa J., Huerta-Ochoa S., Prado-Barragán A., Ascacio-Valdés J., Sepúlveda L., Rodríguez R., Aguilera-Carbó A., Aguilar C. N. 2014. Continuous Production of Ellagic Acid in a Packed-Bed Reactor. Process Biochemistry, 49, 10: 1595–1600

Butt H.-J., Karlheinz G., Kappl M. 2003. Physics and chemistry of interfaces. Weinheim, Wiley-VCH Verlag GmbH & Co. KGaA: 361 p.

Cabral J. M.S., Tramper J. 2005. Bioreactor Design. In: Applied Biocatalysis. Straathof A. J. J., Adlercreutz P. (eds.). 2nd ed. Amsterdam, Taylor & Francis e-Library: 392–440

Cantone S., Ferrario V., Corici L., Ebert C., Fattor D., Spizzo P., Gardossi L. 2013. Efficient Immobilisation of Industrial Biocatalysts: Criteria and Constraints for the Selection of Organic Polymeric Carriers and Immobilisation Methods. Chemical Society Reviews, 42, 15: 6262–6276

Cantu-Perez A., Bi S., Barrass S., Wood M., Gavriilidis A. 2011. Residence Time Distribution Studies in Microstructured Plate Reactors. Applied Thermal Engineering, 31, 5: 634–639

Cao L. 2005. Carrier-Bound Immobilized Enzymes: Principles, Applications and Design. Weinheim, Wiley-VCH Verlag GmbH & Co. KGaA: 578 p.

Capretto L., Mazzitelli S., Balestra C., Tosi A., Nastruzzi C. 2008. Effect of the Gelation Process on the Production of Alginate Microbeads by Microfluidic Chip Technology. Lab on a Chip, 8, 4: 617–621

Capretto L., Mazzitelli S., Luca G., Nastruzzi C. 2010. Preparation and Characterization of Polysaccharidic Microbeads by a Microfluidic Technique: Application to the Encapsulation of Sertoli Cells. Acta Biomaterialia, 6, 2: 429–435

Cárdenas-Fernández M., Neto W., López C., Álvaro G., Tufvesson P., Woodley J. M. 2012. Immobilization of *Escherichia coli* Containing ω-Transaminase Activity in LentiKats®. Biotechnology Progress, 28, 3: 693–698

Carvalho F., Fernandes P. 2015. Packed Bed Enzyme Microreactor: Application in Sucrose Hydrolysis as Proof-of-Concept. Biochemical Engineering Journal, 104: 74–81

Casablancas A., Cárdenas-Fernández M., Álvaro G., Benaiges M. D., Caminal G., de Mas C., González G., López C., López-Santín J. 2013. New Ammonia Lyases and Amine Transaminases: Standardization of Production Process and Preparation of Immobilized Biocatalysts. Electronic Journal of Biotechnology, 16, 3, doi: 10.2225/vol16-issue3-fulltext-4: 13 p.

Casas A., Ramos M. J., Pérez A. 2013. Production of Biodiesel Through Interesterification of Triglycerides with Methyl Acetate. In: Acetate: Versatile Building Block of Biology and Chemistry. Sanders D. A. (ed.). Hauppauge, Nova Science Pub.: 244 p.

Chart H., Smith H. R., La Ragione R. M., Woodward M. J. 2000. An Investigation into the Pathogenic Properties of *Escherichia coli* strains BLR, BL21, DH5α and EQ1. Journal of Applied Microbiology, 89, 6: 1048–1058

Chen B., Hu J., Miller E. M., Xie W., Cai M., Gross R. A. 2008. *Candida antarctica* Lipase B Chemically Immobilized on Epoxy-Activated Micro- and Nanobeads: Catalysts for Polyester Synthesis. Biomacromolecules, 9, 2: 463–471

Chen B., Li G., Wang W., Wang P. 2015. 3D Numerical Simulation of Droplet Passive Breakup in a Micro-Channel T-junction Using the Volume-of-Fluid Method. Applied Thermal Engineering, 88: 94–101

Chen H.-C., Ju H.-Y., Wu T.-T., Liu Y.-C., Lee C.-C., Chang C., Chung Y.-L., Shieh C.-J. 2011. Continuous Production of Lipase-Catalyzed Biodiesel in a Packed-Bed Reactor: Optimization and Enzyme Reuse Study. Journal of Biomedicine and Biotechnology, 2011, Article ID 950725, doi:10.1155/2011/950725: 6 p.

Chen S., Liu K., Liu C., Wang D., Ba D., Xie Y., Du G., Ba Y., Lin Q. 2016. Effects of Surface Tension and Viscosity on the Forming and Transferring Process of Microscale Droplets. Applied Surface Science, 388: 196–202

Chen W., Kim J.-H., Zhang D., Lee K.-H., Cangelosi G. A, Soelberg S. D., Furlong C. E., Chung J.-C., Shen A. Q. 2013. Microfluidic One-Step Synthesis of Alginate Microspheres Immobilized With Antibodies. Journal of the Royal Society Interface, 10, 88, doi: 10.1098/rsif.2013.0566: 8 p.

Cheng Y., Terrell J., Luo X., Betz J., Wu H.-C., Payne G. F., Bentley W. E., Rubloff G. W. 2011. Immobilization and Culturing of Mammalian Cells With Biocompatible Electrodeposition of Calcium Alginate Gel in Microfluidic Devices. 15th International Conference on Miniaturized Systems for Chemistry and Life Sciences, Seattle, October 2-October 6: 121–123 https://pdfs.semanticscholar.org/c4b9/a53933527b9c9289fa6f65b2fc3a0cdb6ee8.pdf (8th April 2017)

Cho B.-K., Park H.-Y., Seo J.-H., Kim J., Kang T.-J., Lee B.-S., Kim B.-G. 2008. Redesigning the Substrate Specificity of ω-Aminotransferase for the Kinetic Resolution of Aliphatic Chiral Amines. Biotechnology and Bioengineering, 99, 2: 275–284

Choi C.-H., Jung J.-H., Rhee Y. W., Kim D.-P., Shim S.-E., Lee C.-S. 2007. Generation of Monodisperse Alginate Microbeads and *in situ* Encapsulation of Cell in Microfluidic Device. Biomedical Microdevices, 9, 6: 855–862

Choi J.-M., Han S.-S., Kim H.-S. 2015. Industrial Applications of Ezyme Biocatalysis: Current Status and Future Aspects. Biotechnology Advances, 33, 7: 1443–1454

Chuah A. M., Kuroiwa T., Kobayashi I., Zhang X., Nakajima M. 2009. Preparation of Uniformly Sized Alginate Microspheres Using the Novel Combined Methods of Microchannel Emulsification and External Gelation. Colloids and Surfaces A: Physicochemical and Engineering Aspects, 351, 1–3: 9–17

Coblyn M., Truszkowska A., Jovanovic G. 2016. Characterization of Microchannel Hemodialyzers Using Residence Time Distribution Analysis. Journal of Flow Chemistry, 6, 1: 53–61

Csajági C., Szatzker G., Rita Tőke E., Ürge L., Darvas F., Poppe L. 2008. Enantiomer Selective Acylation of Racemic Alcohols by Lipases in Continuous-Flow Bioreactors. Tetrahedron Asymmetry, 19, 2: 237–246

Cussler E. L. 2009. Diffusion: Mass Transfer in Fluid Systems. 3rd ed. Cambridge, Cambridge University Press: 647 p.

Cvjetko M., Vorkapić-Furač J., Žnidaršič-Plazl P. 2012. Isoamyl Acetate Synthesis in Imidazolium-Based Ionic Liquids Using Packed Bed Enzyme Microreactor. Process Biochemistry, 47, 9: 1344–1350

Daegelen P., Studier F. W., Lenski R. E., Cure S., Kim J. F. 2009. Tracing Ancestors and Relatives of *Escherichia coli* B, and the Derivation of B Strains REL606 and BL21(DE3). Journal of Molecular Biology, 394, 4: 634–643

Dang T. D., Joo S. W. 2013. Preparation of Tadpole-Shaped Calcium Alginate Microparticles with Sphericity Control. Colloids and Surfaces B: Biointerfaces, 102: 766–771

Das S., Deen N. G., Kuipers J. A. M. 2017. A DNS Study of Flow and Heat Transfer Through Slender Fixed-Bed Reactors Randomly Packed with Spherical Particles. Chemical Engineering Science, 160: 1–19

Datta S., Christena L. R., Rajaram Y. R. S. 2012. Enzyme Immobilization: An Overview on Techniques and Support Materials. 3 Biotech, 3, 1: 1–9

Delaplace G., Loubière K., Ducept F., Jeantet R. 2015. Dimensional Analysis of Food Processes. London, ISTE Press Ltd: 356 p.

De los Ríos A. P., Hernández-Fernández F. J., Martínez F. A., Rubio M., Víllora G. 2007. The Effect of Ionic Liquid Media on Activity, Selectivity and Stability of *Candida antarctica* Lipase B in Transesterification Reactions. Biocatalysis and Biotransformation, 25, 2–4: 151–156

De los Ríos A. P., Hernández-Fernández F. J., Tomás-Alonso F., Gómez D., Víllora G. 2008. Synthesis of Esters in Ionic Liquids: The Effect of Vinyl Esters and Alcohols. Process Biochemistry, 43, 8: 892–895

De Miranda A. S., Miranda L. S. M., de Souza R. O. M. A. 2015. Lipases: Valuable Catalysts for Dynamic Kinetic Resolutions. Biotechnology Advances, 33, 5: 372–393

Delgado J. M. P. Q. 2006. A Critical Review of Dispersion in Packed Beds. Heat and Mass Transfer, 42, 4: 279–310

Delgado J.M.P.Q., Alves M.A., Guedes de Carvalho J.R.F. 2005. A Simple and Inexpensive Technique to Measure Molecular Diffusion Coefficients. Journal of Phase Equilibria and Diffusion, 26, 5: 447-451

Denčić I., De Vaan S., Noë T., Meuldijk J., de Croon M., Hessel V. 2013. Lipase-Based Biocatalytic Flow Process in a Packed-Bed Microreactor. Industrial and Engineering Chemistry Research, 52, 32: 10951–10960

Dendukuri D., Doyle P. S. 2009. The Synthesis and Assembly of Polymeric Microparticles Using Microfluidics. Advanced Materials, 21, 41: 4071–4086

DiCosimo R., McAuliffe J., Poulose A. J., Bohlmann G. 2013. Industrial Use of Immobilized Enzymes. Chemical Society Reviews, 42, 15: 6437–6474

Ding W.A., Vorlop K.D. 1995. Gel aus Polyvinylalkohol und Verfahren zu seiner Herstellung. DE patent application, DE 4327923 A1: 4 p.

Dixon A. G., Macdonald B., Olm A. 2014. Modeling of Packed Bed Reactors: Hydrogen Production by the Steam Reforming of Methane and Glycerol. In: Proceedings of the COMSOL Conference. COMSOL 2014, Boston, October 8-October 10: 6 p. https://www.comsol.com/paper/download/194125/dixon_paper.pdf (8th April 2017)

Dolomite Product Datasheet. Droplet Junction Chips. Royston, The Dolomite Centre: 9 p. http://www.dolomite-microfluidics.com/images/stories/PDFs/datasheets/droplet_junction_chips_product_datasheet.pdf (23rd February 2017)

Dong H.-P., Wang Y.-J., Zheng Y.-G. 2010. Enantioselective Hydrolysis of Diethyl 3-Hydroxyglutarate to Ethyl (*S*)-3-Hydroxyglutarate by Immobilized *Candida antarctica* Lipase B. Journal of Molecular Catalysis B: Enzymatic, 66, 1–2: 90–94

Doran P. M. 2013. Bioprocess Engineering Principles. 2nd ed. Oxford, Academic Press: 919 p.

Dorn M., Hekmat D. 2016. Simulation of the Dynamic Packing Behavior of Preparative Chromatography Columns via Discrete Particle Modeling. Biotechnology Progress, 32, 2: 363–371

Dreyfus R., Tabeling P., Willaime H. 2003. Ordered and Disordered Patterns in Two-Phase Flows in Microchannels. Physical Review Letters, 90, 14, 144505, doi: https://doi.org/10.1103/PhysRevLett.90.144505: 4 p.

Du Noüy P. L. 1919. A New Apparatus for Measuring Surface Tension. The Journal of General Physiology, 1, 5: 521–524

Du Noüy P. L. 1925. An Interfacial Tensiometer for Universal Use. The Journal of General Physiology, 7, 5: 625–631

Du W., Quan N., Lu P., Xu J., Wei W., Zhang L. 2016. Experimental and Statistical Analysis of the Void Size Distribution and Pressure Drop Validations in Packed Beds. Chemical Engineering Research and Design, 106: 115–125

Duduković M. P., Mills P. L. 2015. Scale-Up and Multiphase Reaction Engineering. Current Opinion in Chemical Engineering, 9: 49–58

Dwivedi P. N., Upadhyay S. N. 1977. Particle-Fluid Mass Transfer in Fixed and Fluidized Beds. Industrial and Engineering Chemistry Process Design and Development, 16, 2, 157–165

Ehrfeld W., Hessel V., Löwe H. 2000. Microreactors. Weinheim, Wiley-VCH, Verlag GmbH & Co. KGaA: 288 p.

Engelmark Cassimjee K., Manta B., Himo F. 2015. A Quantum Chemical Study of the ω-Transaminase Reaction Mechanism. Organic and Biomolecular Chemistry, 13, 31: 8453–8464

Ergun S., Orning A. A. 1949. Fluid Flow Through Randomly Packed Columns and Fluidized Beds. Industrial and Engineering Chemistry, 41, 6: 1179–1184

Eş I., Vieira J. D. G., Amaral A. C. 2015. Principles, Techniques, and Applications of Biocatalyst Immobilization for Industrial Application. Applied Microbiology and Biotechnology, 99, 5: 2065–2082

Faber K. 2011. Biotransformations in Organic Chemistry. 6th ed. Berlin Heidelberg, Springer-Verlag GmbH: 423 p.

Falus P., Boros Z., Hornyánszky G., Nagy J., Ürge L., Darvas F., Poppe L. 2010. Synthesis and Lipase Catalyzed Kinetic Resolution of Racemic Amines. Studia Universitatis Babes-Bolyai Chemia, 4: 289–296

Fan T. 2001. Viscosity Measurement Using Cannon-Fenske Viscometers. 2 p. (Instructions) http://www.prrc.nmt.edu/groups/petrophysics/media/pdf/viscometer.pdf (3rd February 2017)

Fang A., Cathala B. 2011. Smart Swelling Biopolymer Microparticles by a Microfluidic Approach: Synthesis, *in situ* Encapsulation and Controlled Release. Colloids and Surfaces B: Biointerfaces, 82, 1: 81–86

Faridkhou A., Hamidipour M., Larachi F. 2013. Hydrodynamics of Gas-Liquid Micro-Fixed Beds: Measurement Approaches and Technical Challenges. Chemical Engineering Journal, 223: 425–435

Faridkhou A., Larachi F. 2014. Two-Phase Flow Hydrodynamic Study in Micro-Packed Beds – Effect of Bed Geometry and Particle Size. Chemical Engineering and Processing: Process Intensification, 78: 27–36

Faridkhou A., Tourvieille J.-N., Larachi F. 2016. Reactions, Hydrodynamics and Mass Transfer in Micro-Packed Beds – Overview and New Mass Transfer Data. Chemical Engineering and Processing: Process Intensification, 110: 80–96

Fate G., Lynn D. G. 1990. Molecular Diffusion Coefficients: Experimental Determination and Demonstration. Journal of Chemical Education, 67, 6: 536–538

Fernandes P., Marques M. P. C., Carvalho F., Cabral J. M. S. 2009. A Simple Method for Biocatalyst Immobilization Using PVA-Based Hydrogel Particles. Journal of Chemical Technology and Biotechnology, 84, 4: 561–564

Ferrario V., Ebert C., Nitti P., Pitacco G., Gardossi L. 2015. Modelling and Predicting Enzyme Enantioselectivity: The Aid of Computational Methods for the Rational Use of Lipase B from *Candida antarctica*. Current Biotechnology, 4, 2: 87–99

Fesko K., Steiner K., Breinbauer R., Schwab H., Schürmann M., Strohmeier G. A. 2013. Investigation of One-Enzyme Systems in the ω-Transaminase-Catalyzed Synthesis of Chiral Amines. Journal of Molecular Catalysis B: Enzymatic, 96: 103–110

Fessner W.-D., Anthonsen T. 2009. Modern Biocatalysis: Stereoselective and Environmentally Friendly Reactions. Weinheim, Wiley-VCH Verlag GmbH & Co. KGaA: 375 p.

Fischer J., Guidini C. Z., Santana L. N. S., de Resende M. M., Cardoso V. L., Ribeiro E. J. 2013. Optimization and Modeling of Lactose Hydrolysis in a Packed Bed System Using Immobilized β-Galactosidase From *Aspergillus oryzae*. Journal of Molecular Catalysis B: Enzymatic, 85–86: 178–186

Fogler H. S., 1999. Elements of Chemical Reaction Engineering. 3rd ed. New Jersey, Prentice Hall International Editions: 967 p.

Fourati M., Roig V., Raynal L. 2012. Experimental Study of Liquid Spreading in Structured Packings. Chemical Engineering Science, 80: 1–15

Fraga M. A., Koberstein L. L. 2012. An Overview on the Modeling of Silicon Piezoresistive Pressure Microsensors. 2012 Workshop on Engineering Applications, Bogota, May 2-May 4, doi: 10.1109/WEA.2012.6220091: 6 p.

Froment G. F., Bischoff K. B., De Wilde J. 2011. Chemical Reactor Analysis and Design. 3rd ed. Hoboken, John Wiley & Sons, Inc.: 900 p.

Fu H., Denčić I., Tibhe J., Sanchez Pedraza C. A., Wang Q., Noel T., Meuldijk J., de Croon M., Hessel V., Weizenmann N., Oeser T., Kinkeade, T., Hyatt D., Van Roy S., Dejonghe W., Diels L. 2012. Threonine Aldolase Immobilization on Different Supports for Engineering of Productive, Cost-Efficient Enzymatic Microreactors. Chemical Engineering Journal, 207–208: 564–576

Fuchs C. S., Simon R. C., Riethorst W., Zepeck F., Kroutil W. 2014. Synthesis of (*R*)- or (*S*)-Valinol Using ω-Transaminases in Aqueous and Organic Media. Bioorganic and Medicinal Chemistry, 22, 20: 5558–5562

Fuchs M., Farnberger J. E., Kroutil W. 2015. The Industrial Age of Biocatalytic Transamination. European Journal of Organic Chemistry, 2015, 32: 6965–6982

Ganetsos G., Barker P. E. 1991. Large-Scale Chromatography in Industrial Processing. Journal of Chemical Technology and Biotechnology, 50, 1: 101–108

Ganjalikhany M. R., Ranjbar B., Taghavi A. H., Moghadam T. T. 2012. Functional Motions of *Candida antarctica lipase* B: A Survey Through Open-Close Conformations. PLoS ONE, 7, 7, e40327, doi:10.1371/journal.pone.0040327: 11 p.

Gåserød O. 1998. Microcapsules of Alginate-Chitosan: A Study of Capsule Formation and Functional Properties. PhD thesis, Trondheim, Norwegian Univeristy of Science and Technology

Georget E., Sauvageat J. L., Burbidge A., Mathys A. 2013. Residence Time Distributions in a Modular Micro Reaction System. Journal of Food Engineering, 116, 4: 910–919

Gharat N., Rathod V. K. 2013. Ultrasound Assisted Enzyme Catalyzed Transesterification of Waste Cooking Oil With Dimethyl Carbonate. Ultrasonics Sonochemistry, 20, 3: 900–905

Glazyrina J., Materne E.-M., Dreher T., Storm D., Junne S., Adams T., Greller G., Neubauer P. 2010. High Cell Density Cultivation and Recombinant Protein Production With *Escherichia coli* in a Rocking-Motion-Type Bioreactor. Microbial Cell Factories, 9, 42, doi: 10.1186/1475-2859-9-42: 11 p.

Goto S, Sugiyama J., Iizuka H. 1969. A Taxonomic Study of Antarctic Yeasts. Mycologia, 61, 4: 748–774

Graham L. J., Jovanovic G. 1999. Dechlorination of *p*-Chlorophenol on a Pd/Fe Catalyst in a Magnetically Stabilized Fluidized Bed; Implications for Sludge and Liquid Remediation. Chemical Engineering Science, 54, 15–16: 3085–3093

Green A. P., Turner N. J., O'Reilly E. 2014. Chiral Amine Synthesis Using ω-Transaminases: An Amine Donor That Displaces Equilibria and Enables High-Throughput Screening. Angewandte Chemie International Edition, 53, 40: 10714–10717

Green D. W., Perry R. H. 2008. Perry's Chemical Engineers' Handbook. 8th ed. New York, McGraw-Hill Companies, Inc.: 2700 p.

Gruber P., Marques M. P. C., O'Sullivan B., Baganz F., Wohlgemuth R., Szita N. 2017. Conscious Coupling: The Challenges and Opportunities of Cascading Enzymatic Microreactors. Biotechnology Journal, 12, 1700030, doi: 10.1002/biot.201700030: 13 p.

Grunwald P. 2015. Biocatalysts: Global Market, Industrial Applications, Aspects of Biotransformation Design, and Societal Challenges. In: Industrial Biocatalysis. Grunwald P. (ed.). Boca Raton, Taylor & Francis Group: 1–32

Gundersen M. T., Abu R., Schürmann M., Woodley J. M. 2015. Amine Donor and Acceptor Influence on the Thermodynamics of ω-Transaminase Reactions. Tetrahedron: Asymmetry, 26, 10–11: 567–570

Gupta R., Bansal A. 2013. Axial Dispersion in Packed Bed Reactors Involving Viscoinelastic and Viscoelastic Non-Newtonian Fluids. Bioprocess and Biosystems Engineering, 36, 8: 1011–1018

Gustavsson M., Muraleedharan M. N., Larsson G. 2014. Surface Expression of ω-Transaminase in *Escherichia coli*. Applied and Environmental Microbiology, 80, 7: 2293–2298

Halim A. A., Szita N., Baganz F. 2013. Characterization and Multi-Step Transketolase-ω-Transaminase Bioconversions in an Immobilized Enzyme Microreactor (IEMR) With Packed Tube. Journal of Biotechnology, 168, 4: 567–575

Halim M., Rios-Solis L., Micheletti M., Ward J. M., Lye G. J. 2014. Microscale Methods to Rapidly Evaluate Bioprocess Options for Increasing Bioconversion Yields: Application to the ω-Transaminase Synthesis of Chiral Amines. Bioprocess and Biosystems Engineering, 37, 5: 931–941

Halim S. F. A., Kamaruddin A. H., Fernando W. J. N. 2009. Continuous Biosynthesis of Biodiesel From Waste Cooking Palm Oil in a Packed Bed Reactor: Optimization Using Response Surface Methodology (RSM) and Mass Transfer Studies. Bioresource Technology, 100, 2: 710–716

Han Q., Li J., Li J. 2004. pH Dependence, Substrate Specificity and Inhibition of Human Kynurenine Aminotransferase I. European Journal of Biochemistry, 271, 23–24: 4804–4814

Han Q., Robinson H., Cai T., Tagle D. A., Li J. 2009. Structural Insight into the Inhibition of Human Kynurenine Aminotransferase I/Glutamine Transaminase K. Journal of Medicinal Chemistry, 52, 9: 2786–2793

Hanefeld U., Gardossi L., Magner E. 2009. Understanding Enzyme Immobilisation. Chemical Society Reviews, 38, 2: 453–468

Hartman R. L., McMullen J. P., Jensen K. F. 2011. Deciding Whether To Go with the Flow: Evaluating the Merits of Flow Reactors for Synthesis. Angewandte Chemie International Edition, 50, 33: 7502–7519

Hay I. D., Rehman Z. U., Moradali M. F., Wang Y., Rehm B. H. A. 2013. Microbial Alginate Production, Modification And Its Applications. Microbial Biotechnology, 6: 637–650

Hayduk W., Laudie H. 1974. Prediction of diffusion coefficients for nonelectrolytes in dilute aqueous solutions. AIChE Journal, 20, 3: 611–615

Heinsman N. W. J. T., Schroën C. G. P. H., van der Padt A., Franssen M. C. R., Boom R. M., van't Riet K. 2003. Substrate Sorption into the Polymer Matrix of Novozym 435® and Its Effect on the Enantiomeric Ratio Determination. Tetrahedron Asymmetry, 14, 18: 2699–2704

Heintz S., Börner T., Ringborg R. H., Rehn G., Grey C., Nordblad M., Krühne U., Gernaey K. V., Adlercreutz P., Woodley J. M. 2016b. Development of *in situ* Product Removal Strategies in Biocatalysis Applying Scaled-Down Unit Operations. Biotechnology and Bioengineering, 114, 3: 600–609

Heintz S., Mitic A., Ringborg R. H., Krühne U., Woodley J. M., Gernaey K. V. 2016a. A Microfluidic Toolbox for the Development of *in-situ* Product Removal Strategies in Biocatalysis. Journal of Flow Chemistry, 6, 1: 18–26

Hessel V. 2009. Novel process windows – Gate to Maximizing Process Intensification Via Flow Chemistry. Chemical Engineering and Technology, 32, 11: 1655–1681

Hessel V., Hardt S., Löwe H. 2004. Chemical Micro Process Engineering: Fundamentals, Modelling and Reactions. Weinheim, Wiley: 674 p.

Hessel V., Kralisch D., Kockmann N., Noël T., Wang Q. 2013. Novel Process Windows for Enabling, Accelerating, and Uplifting Flow Chemistry. ChemSusChem, 6, 5: 746–789

Hessel V., Tibhe J., Noël T., Wang Q. 2014. Biotechnical Micro-Flow Processing at the EDGE – Lessons to Be Learnt for a Young Discipline. Chemical and Biochemical Engineering Quarterly, 28, 2: 167–188

Hessel V., Vural Gürsel I., Wang Q., Noël T., Lang J. 2012. Potential Analysis of Smart Flow Processing and Micro Process Technology for Fastening Process Development: Use of Chemistry and Process Design as Intensification Fields. Chemical Engineering and Technology, 35, 7: 1184–1204

Honda T., Miyazaki M., Nakamura H., Maeda H. 2006. Facile Preparation of an Enzyme-Immobilized Microreactor Using a Cross-Linking Enzyme Membrane on a Microchannel Surface. Advanced Synthesis and Catalysis, 348, 15: 2163–2171

Hong J., deMello A. J., Jayasinghe S. N. 2010. Bio-Electrospraying and Droplet-Based Microfluidics: Control of Cell Numbers Within Living Residues. Biomedical Materials, 5, 2, doi: 10.1088/1748-6041/5/2/021001: 6 p.

Hu Y., Azadi G., Ardekani A. M. 2015. Microfluidic Fabrication of Shape-Tunable Alginate Microgels: Effect of Size and Impact Velocity. Carbohydrate Polymers, 120: 38–45

Hu Y., Wang Q., Wang J., Zhu J., Wang H., Yang Y. 2012. Shape Controllable Microgel Particles Prepared By Microfluidic Combining External Ionic Crosslinking. Biomicrofluidics, 6, 2, 026502, doi: 10.1063/1.4720396: 9 p.

Huang K.-S., Lai T.-H., Lin Y.-C. 2006. Manipulating The Generation of Ca-Alginate Microspheres Using Microfluidic Channels as a Carrier of Gold Nanoparticles. Lab on a Chip, 6, 7: 954–957

Huang K.-S., Lin Y.-S., Yang C.-H., Tsai C.-W., Hsu M.-Y. 2011. *In situ* Synthesis of Twin Monodispersed Alginate Microparticles. Soft Matter, 7, 14: 6713–6718

Huang K.-S., Liu M.-K., Wu C.-H., Yen Y.-T., Lin Y.-C. 2007. Calcium Alginate Microcapsule Generation on a Microfluidic System Fabricated Using the Optical Disk Process. Journal of Micromechanics and Microengineering, 17, 8: 1428–1434

Huang S.-B., Wu M.-H., Lee G.-B. 2010. Microfluidic Device Utilizing Pneumatic Micro-Vibrators to Generate Alginate Microbeads for Microencapsulation of Cells. Sensors and Actuators, B: Chemical, 147, 2: 755–764

Hussain A., Kangwa M., Abo-Elwafa A. G., Fernandez-Lahore M. 2015. Influence of Operational Parameters on the Fluid-Side Mass Transfer Resistance Observed in a Packed Bed Bioreactor. AMB Express, 5, 25, doi: 10.1186/s13568-015-0111-x: 9 p.

Idris A., Bukhari A. 2012. Immobilized *Candida antarctica* lipase B: Hydration, Stripping off and Application in Ring Opening Polyester Synthesis. Biotechnology Advances, 30, 3: 550–563

Illanes A. 2008. Introduction. In: Enzyme Biocatalysis: Principles and Applications. Illanes A. (ed.). Dordrecht, Springer Science + Business Media: 1–56

Illanes A., Wilson L., Vera C. 2014. Problem Solving in Enzyme Biocatalysis. Chichester, John Wiley & Sons, Ltd: 318 p.

Introduction to Soil Remediation Standards Guidance. 2015. Chemical Properties for Calculation of Impact to Ground Water Soil Remediation Standards: 3 p. http://www.nj.gov/dep/srp/guidance/rs/chemproperties.pdf (22nd February 2017)

Inoue T., Adachi J., Ohtaki K., Lu M., Murakami S., Sun X., Wang D. F. 2015. Direct Hydrogen Peroxide Synthesis Using Glass Microfabricated Reactor – Paralleled Packed Bed Operation. Chemical Engineering Journal, 278: 517–526

Iordanidis A. A. 2002. Mathematical Modeling Of Catalytic Fixed Bed Reactors. PhD thesis, Twente, University of Twente, 195 p.

Jakovetić Tanasković S., Jokić B., Grbavčić S., Drvenica I., Prlainović N., Luković N., Knežević-Jugović Z. 2016. Immobilization of *Candida antarctica* Lipase B on Kaolin and Its Application in Synthesis of Lipophilic Antioxidants. Applied Clay Science, 135: 103–111

Jensen K. F. 2017. Flow Chemistry–Microreaction Technology Comes of Age. AIChE Journal, 63, 3: 858–869

Jensen K. F., Reizman B. J., Newman S. G. 2014. Tools for Chemical Synthesis in Microsystems. Lab on a Chip, 14, 17: 3206–3212

Jeong H., Barbe V., Lee C. H., Vallenet D., Yu D. S., Choi S.-H., Couloux A., Lee S.-W. Yoon S. H., Cattolico L., Hur C.-G., Park H.-S., Ségurens B., Kim S. C., Oh T. K., Lenski R. E., Studier F. W., Daegelen P., Kim J. F. 2009. Genome Sequences of *Escherichia coli* B Strains REL606 and BL21(DE3). Journal of Molecular Biology, 394, 4: 644–652

Jiang J., Chen X., Feng J., Wu Q., Zhu D. 2014. Substrate Profile of an ω-Transaminase from *Burkholderia vietnamiensis* and Its Potential for the Production of Optically Pure Amines and Unnatural Amino Acids. Journal of Molecular Catalysis B: Enzymatic, 100: 32–39

José C., Austic G. B., Bonetto R. D., Burton R. M., Briand L. E. 2013. Investigation of the Stability of Novozym® 435 in the Production of Biodiesel. Catalysis Today, 213: 73–80

Jovanovic G. N., Atwater J. E., Žnidaršič-Plazl P., Plazl I. 2015. Dechlorination of Polychlorinated Phenols on Bimetallic Pd/Fe Catalyst in a Magnetically Stabilized Fluidized Bed. Chemical Engineering Journal, 274; 50–60

Kang A., Park J., Ju J., Jeong G. S., Lee S.-H. 2014. Cell Encapsulation via Microtechnologies. Biomaterials, 35, 9: 2651–2663

Kapoor M., Gupta M. N. 2012. Lipase Promiscuity and Its Biochemical Applications. Process Biochemistry, 47, 4: 555–569

Karande R., Schmid A., Buehler K. 2016. Applications of Multiphasic Microreactors for Biocatalytic Reactions. Organic Process Research and Development, 20, 2: 361–370

Kashani M. N., Elekaei H., Zivkovic V., Zhang H., Biggs M. J. 2016. Explicit Numerical Simulation-Based Study of the Hydrodynamics of Micro-Packed Beds. Chemical Engineering Science, 145: 71–79

Kashid M. N., Gupta A., Renken A., Kiwi-Minsker L. 2010. Numbering-Up and Mass Transfer Studies of Liquid–Liquid Two-Phase Microstructured Reactors. Chemical Engineering Journal, 158, 2: 233–240

Kashid M. N., Renken A., Kiwi-Minsker L. 2015. Microstructured Devices for Chemical Processing. Weinheim, Wiley-VCH Verlag GmbH & Co. KGaA, 384 p.

Kaulmann U., Smithies K., Smith M. E. B., Hailes H. C., Ward J. M. 2007. Substrate Spectrum of ω-Transaminase from *Chromobacterium violaceum* DSM30191 and Its Potential for Biocatalysis. Enzyme and Microbial Technology, 41, 5: 628–637

KEM Kyoto Electronics. Water Content of Hydrocarbons. KEM application note: 4 p. http://www.kyoto-kem.com/en/pdf/industry/OrganicIndustrialProduct/EKVX-01201.pdf (22nd February 2017)

Kerby M. B., Legge R. S., Tripathi A. 2006. Measurements of Kinetic Parameters in a Microfluidic Reactor. Analytical Chemistry, 78, 24: 8273–8280

Kim C. 2015. Droplet-Based Microfluidics for Making Uniform-Sized Cellular Spheroids in Alginate Beads With the Regulation of Encapsulated Cell Number. BioChip Journal, 9, 2: 105–113

Kim C., Chung S., Kim Y. E., Lee K. S., Lee S. H., Oh K. W., Kang J. Y. 2011. Generation of Core-Shell Microcapsules With Three-Dimensional Focusing Device for Efficient Formation of Cell Spheroid. Lab on a Chip, 11, 2: 246–252

Kim C., Lee K. S., Kim Y. E., Lee K.-J., Lee S. H., Kim T. S., Kang J. Y. 2009. Rapid Exchange of Oil-Phase in Microencapsulation Chip to Enhance Cell Viability. Lab on a Chip, 9, 9: 1294–1297

Kim C., Park J., Kang J. Y. 2014. A Microfluidic Manifold With a Single Pump System to Generate Highly Mono-Disperse Alginate Beads for Cell Encapsulation. Biomicrofluidics, 8, 6, 066504, doi: 10.1063/1.4902943: 10 p.

Klähn M., Lim G. S., Seduraman A., Wu P. 2011. On the Different Roles of Anions and Cations in the Solvation of Enzymes in Ionic Liquids. Physical Chemistry Chemical Physics: 13, 4: 1649–1662

Kockmann N. 2008. Transport Phenomena in Micro Process Engineering. Berlin Heidelberg, Springer-Verlag GmbH: 365 p.

Koch K., van den Berg R.J.F., Nieuwland P.J., Wijtmans R., Schoemaker H. E., van Hest J.C.M., Rutjes F. P. J. T. 2008. Enzymatic Enantioselective C–C-Bond Formation in Microreactors. Biotechnology and Bioengineering, 99, 4: 1028–1033

Kockmann N., Gottsponer M., Roberge D. M. 2011. Scale-Up Concept Of Single-Channel Microreactors From Process Development to Industrial Production. Chemical Engineering Journal, 167, 2–3: 718–726

Koekemoer A., Luckos A. 2015. Effect of Material Type and Particle Size Distribution on Pressure Drop in Packed Beds of Large Particles: Extending the Ergun equation. Fuel, 158: 232–238

Kohls H., Steffen-Munsberg F., Höhne M. 2014. Recent Achievements in Developing the Biocatalytic Toolbox for Chiral Amine Synthesis. Current Opinion in Chemical Biology, 19: 180–192

Kolev N. 2006. Packed Bed Columns For Absorption, Desorption, Rectification and Direct Heat Transfer. Amsterdam, Elsevier B. V.: 708 p.

Kolfschoten R. C., Swarts J. W., Janssen A. E. M., Boom R. M. 2011. Guidelines for Optimal Design of Coflow Enzyme Microreactors. Chemical Engineering Journal, 172, 2–3: 1072–1077

Koszelewski D., Müller N., Schrittwieser J. H., Faber K., Kroutil W. 2010b. Immobilization of ω-Transaminases by Encapsulation in a Sol–Gel/Celite Matrix. Journal of Molecular Catalysis B: Enzymatic, 63, 1–2: 39–44

Koszelewski D., Tauber K., Faber K., Kroutil W. 2010a. ω-Transaminases for the Synthesis of Non-Racemic α-Chiral Primary Amines. Trends in Biotechnology, 28, 6: 324–332

Kramer M., Cruz J. C., Pfromm P. H., Rezac M. E., Czermak P. 2010. Enantioselective Transesterification by *Candida antarctica* Lipase B Immobilized on Fumed Silica. Journal of Biotechnology, 150, 1: 80–86

Krasňan V., Stloukal R., Rosenberg M., Rebroš M. 2016. Immobilization of Cells and Enzymes to LentiKats®. Applied Microbiology and Biotechnology, 100, 6: 2535–2553

Krenkova J., Svec F. 2009. Less Common Applications of Monoliths: IV. Recent Developments in Immobilized Enzyme Reactors for Proteomics and Biotechnology. Journal of Separation Science, 32, 5–6: 706–718

Kroutil W., Fischereder E.-M., Fuchs C. S., Lechner H., Mutti F. G., Pressnitz D., Rajagopalan A., Sattler J. H., Simon R. C., Siirola E. 2013. Asymmetric Preparation of prim-, sec-, and tert-Amines Employing Selected Biocatalysts. Organic Process Research and Development, 17, 5: 751–759

Krühne U., Heintz S., Ringborg R., Rosinha I. P., Tufvesson P., Gernaey K. V., Woodley J. M. 2014. Biocatalytic Process Development Using Microfluidic Miniaturized Systems. Green Processing and Synthesis, 3, 1: 23–31

Krüss user manual. 2002. Tensiometer K6. Vol. 2. Hamburg, Krüss GmbH: 17 p.

Kuhnert P., Hacker J., Mühldorfer I., Burnens A. P., Nicolet J., Frey J. 1997. Detection System for *Escherichia coli*-Specific Virulence Genes: Absence of Virulence Determinants in B and C Strains. Applied and Environmental Microbiology, 63, 2: 703–709

Kumacheva E., Garstecki P. 2011. Microfluidic Reactors for Polymer Particles. Chichester, John Wiley & Sons, Ltd: 223 p.

Kumar A., Dhar K., Kanwar S. S., Arora P. K. 2016. Lipase Catalysis in Organic Solvents: Advantages and Applications. Biological Procedures Online, 18, 2, doi: 10.1186/s12575-016-0033-2: 11 p.

Kundu S., Bhangale A. S., Wallace W. E., Flynn K. M., Guttman C. M., Gross R. A., Beers K. L. 2011. Continuous Flow Enzyme-Catalyzed Polymerization in a Microreactor. Journal of the American Chemical Society, 133, 15: 6006–6011

Ladisch M. R. 2001. Bioseparations Engineering: Principles, Practice, and Economics. New York, John Wiley & Sons, Inc.: 760 p.

Laurenti E., dos Santos Vianna Jr. A. 2016. Enzymatic Microreactors in Biocatalysis: History, Features, and Future Perspectives. Biocatalysis, 1, 1: 148–165

Lee K. Y., Mooney D. J. 2012. Alginate: Properties and Biomedical Applications. Progress in Polymer Science, 37, 1: 106–126

Leskovac V. 2003. Comprehensive Enzyme Kinetics, New York, Kluwer Academic Publishers: 438 p.

Levenspiel O. 1999. Chemical Reaction Engineering. 3rd ed. New York, John Wiley & Sons, Inc. 668 p.

Levenspiel O. 2012. Tracer Technology: Modeling the Flow Of Fluids. New York, Springer Science+Business Media: 137 p.

Levic S., Djordjevic V., Rajic N., Milivojevic M., Bugarski B., Nedovic V. 2013. Entrapment of Ethyl Vanillin in Calcium Alginate and Calcium Alginate/Poly(vinyl alcohol) Beads. Chemical Papers, 67, 2: 221–228

Li C., Tan T., Zhang H., Feng W. 2010. Analysis of the Conformational Stability and Activity of *Candida antarctica* lipase B in Organic Solvents: Insight From Molecular Dynamics and Quantum Mechanics/Simulations. The Journal of Biological Chemistry, 285, 37: 28434–28441

Li J., Carr P. W. 1997. Accuracy of Empirical Correlations for Estimating Diffusion Coefficients in Aqueous Organic Mixtures. Analytical Chemistry, 69, 13: 2530–2536

Li X.-B., Li F.-C., Yang J.-C., Kinoshita H., Oishi M., Oshima M. 2012. Study on the Mechanism of Droplet Formation in T-junction Microchannel. Chemical Engineering Science, 69, 1: 340–351

Li Y., Yan B., Xu X., Deng C., Yang P., Shen X, Zhang X. 2007. On-Column Tryptic Mapping of Proteins Using Metal-Ion-Chelated Magnetic Silica Microspheres by Matrix-Assisted Laser Desorption/Ionization Time-of-Flight Mass Spectrometry. Rapid Communications in Mass Spectrometry, 21: 2263–2268

Liese A., Seelbach K., Wandrey C. 2006. Industrial Biotransformations. Weinheim, Verlag GmbH & Co. KGaA: 556 p.

Lin Y.-S., Yang C.-H., Hsu Y.-Y., Hsieh C.-L. 2013. Microfluidic Synthesis of Tail-Shaped Alginate Microparticles Using Slow Sedimentation. Electrophoresis, 34, 3: 425–431

Liu J., Lin S., Qi D., Deng C., Yang P., Zhang X. 2007. On-Chip Enzymatic Microreactor Using Trypsin-Immobilized Superparamagnetic Nanoparticles for Highly Efficient Proteolysis. Journal of Chromatography A, 1176, 1–2: 169–77

Liu K., Ding H.-J., Liu J., Chen Y., Zhao X.-Z. 2006. Shape-Controlled Production of Biodegradable Calcium Alginate Gel Microparticles Using a Novel Microfluidic Device. Langmuir, 22, 22: 9453–9457

Liu L., Wu F., Ju X.-J., Xie R., Wang W., Niu C. H., Chu L.-Y. 2013. Preparation of Monodisperse Calcium Alginate Microcapsules via Internal Gelation in Microfluidic-Generated Double Emulsions. Journal of Colloid and Interface Science, 404: 85–90

Lloret L., Eibes G., Feijoo G., Moreira M. T., Lema J. M., Hollmann F. 2011. Immobilization of Laccase by Encapsulation in a Sol-Gel Matrix and Its Characterization and use for the Removal of Estrogens. Biotechnology Progress, 27, 6: 1570–1579

Lloret L., Hollmann F., Eibes G., Feijoo G., Moreira M. T., Lema J. M. 2012. Immobilisation of Laccase on Eupergit Supports and Its Application for the Removal of Endocrine Disrupting Chemicals in a Packed-Bed Reactor. Biodegradation, 23, 3: 373–386

Losey M. W., Schmidt M. A, Jensen K. F. 2001. Microfabricated Multiphase Packed-Bed Reactors: Characterization of Mass Transfer and Reactions, 40, 12: 2555–2562

Lozinsky V. I. 1998. Cryotropic Gelation of Poly(vinyl alcohol) Solutions. Russian Chemical Reviews, 67, 7: 573–586

Lubej M., Novak U., Liu M., Martelanc M., Franko M., Plazl I. 2015. Microfluidic Droplet-Based Liquid–Liquid Extraction: Online Model Validation. Lab on a Chip, 15, 10: 2233–2239

Lusis M. A., Ratcliff C. A. 1968. Diffusion in binary liquid mixtures at infinite dilution. The Canadian Journal of Chemical Engineering, 46, 5: 385–387

Machsun A. L., Gozan M., Nasikin M., Setyahadi S., Yoo Y. J. 2010. Membrane Microreactor in Biocatalytic Transesterification of Triolein for Biodiesel Production. Biotechnology and Bioprocess Engineering, 15, 6: 911–916

Madarász J., Németh D., Bakos J., Gubicza L., Bakonyi P. 2015. Solvent-Free Enzymatic Process for Biolubricant Production in Continuous Microfluidic Reactor. Journal of Cleaner Production, 93: 140–144

Malik M. S., Park E.-S., Shin J.-S. 2012a. Features and Technical Applications of ω-Transaminases. Applied Microbiology and Biotechnology, 94, 5: 1163–1171

Malik M. S., Park E.-S., Shin J.-S. 2012b. ω-Transaminase-Catalyzed Kinetic Resolution of Chiral Amines Using L-Threonine as an Amino Acceptor Precursor. Green Chemistry, 14, 8: 2137–2140

Mallin H., Höhne M., Bornscheuer U. T. 2014. Immobilization of (*R*)- and (*S*)-Amine Transaminases on Chitosan Support and Their Application for Amine Synthesis Using Isopropylamine as Donor. Journal of Biotechnology, 191: 32–37

Manojlovic V., Djonlagic J., Obradovic B., Nedovic V., Bugarski B. 2006. Investigations of Cell Immobilization in Alginate: Rheological and Electrostatic Extrusion Studies. Journal of Chemical Technology and Biotechnology, 81, 4: 505–510

Manojlovic V., Rajic N., Djonlagic J., Obradovic B., Nedovic V., Bugarski B. 2008. Application of Electrostatic Extrusion – Flavour Encapsulation and Controlled Release. Sensors, 8, 3: 1488–1496

Marques M. P. C., Cabral J. M. S., Fernandes P. 2010. Bioprocess Scale-Up: Quest for the Parameters to be Used as Criterion to Move From Microreactors to Lab-Scale. Journal of Chemical Technology and Biotechnology, 85, 9: 1184–1198

Marques M. P. C., Fernandes P. 2011. Microfluidic Devices: Useful Tools for Bioprocess Intensification. Molecules, 16, 10: 8368–8401

Marques M. P. C., Fernandes P., Cabral J. M. S., Žnidaršič-Plazl P., Plazl I. 2012. Continuous Steroid Biotransformations in Microchannel Reactors. New Biotechnology, 29, 2: 227–234

Márquez N., Castaño P., Makkee M., Moulijn J. A., Kreutzer M. T. 2008. Dispersion and Holdup in Multiphase Packed Bed Microreactors. Chemical Engineering and Technology, 31, 8: 1130–1139

Marquis M., Davy J., Cathala B., Fang A., Renard D. 2015. Microfluidics Assisted Generation of Innovative Polysaccharide Hydrogel Microparticles. Carbohydrate Polymers, 116: 189–199

Martin A. R., Shonnard D., Pannuri S., Kamat S. 2007. Characterization of Free and Immobilized (*S*)-Aminotransferase for Acetophenone Production. Applied Microbiology and Biotechnology, 76, 4: 843–851

Martinelle M., Holmquist M., Hult K. 1995. On the Interfacial Activation of *Candida antarctica* Lipase A and B as Compared With *Humicola lanuginosa* lipase. Biochimica et Biophysica Acta – Lipids and Lipid Metabolism, 1258, 3: 272–276

Martinez C. J., Kim J. W., Ye C., Ortiz I., Rowat A. C., Marquez M., Weitz D. 2012. A Microfluidic Approach to Encapsulate Living Cells in Uniform Alginate Hydrogel Microparticles. Macromolecular Bioscience, 12, 7: 946–951

Mashaghi S., Abbaspourrad A., Weitz D. A., van Oijen A. M. 2016. Droplet Microfluidics: A Tool for Biology, Chemistry and Nanotechnology. Trends in Analytical Chemistry, 82: 118–125

Matcham G. W., Bowen A. R. S. 1996. Biocatalysis for Chiral Intermediates: Meeting Commercial and Technical Challenges. Chimica Oggi, 14, 6: 20–24

Mathew S., Yun H. 2012. ω-Transaminases for the Production of Optically Pure Amines and Unnatural Amino Acids. ACS Catalysis, 2, 6: 993–1001

Matosevic S., Lye G. J., Baganz F. 2011a. Immobilized Enzyme Microreactor for Screening of Multi-Step Bioconversions: Characterisation of a *de novo* Transketolase-ω-Transaminase Pathway to Synthesise Chiral Amino Alcohols. Journal of Biotechnology, 155, 3: 320–329

Matosevic S., Szita N., Baganz F. 2011b. Fundamentals and Applications of Immobilized Microfluidic Enzymatic Reactors. Journal of Chemical Technology and Biotechnology, 86, 3: 325–334

Mazzitelli S., Capretto L., Quinci F., Piva R., Nastruzzi C. 2013. Preparation of Cell-Encapsulation Devices in Confined Microenvironment. Advanced Drug Delivery Reviews, 65, 11–12: 1533–1555

Matyka M., Khalili A., Koza Z. 2008. Tortuosity-Porosity Relation in Porous Media Flow. Physical Review E, 78, 026306, doi: https://doi.org/10.1103/PhysRevE.78.026306: 8 p.

McKinley G. H., Renardy M. 2011. Wolfgang von Ohnesorge. Physics of Fluids, 23, 12, 127101, doi: 10.1063/1.3663616: 6 p.

Mehta P. K., Hale T. I., Christen P. 1993. Aminotransferases: Demonstration of Homology and Division into Evolutionary Subgroups. European Journal of Biochemistry, 214, 2: 549–561

Mei Y., Miller L., Gao W., Gross R. A. 2003. Imaging the Distribution and Secondary Structure of Immobilized Enzymes Using Infrared Microspectroscopy. Biomacromolecules, 4, 1: 70–74

Melvik J. E., Dornish, M. 2004. Alginate as a Carrier for Cell Immobilisation. In: Fundamentals of Cell Immobilisation Biotechnology. Nedović V., Willaert, R. (eds.). Dordrecht, Springer Science+Business Media: 33–51

Miložič N., Lubej M., Lakner M., Žnidaršič-Plazl P., Plazl I. 2017. Theoretical and Experimental Study of Enzyme Kinetics in a Microreactor System With Surface-Immobilized Biocatalyst. Chemical Engineering Journal, 313: 374–381

Miložič N., Lubej M., Novak U., Žnidaršič-Plazl P., Plazl I. 2014. Evaluation of Diffusion Coefficient Determination Using a Microfluidic Device. Chemical and Biochemical Engineering Quarterly, 28, 2: 215–223

Mohanty R., Mohanty S., Mishra B. K. 2016. Study of Flow Through a Packed Bed Using Discrete Element Method and Computational Fluid Dynamics. Journal of the Taiwan Institute of Chemical Engineers, 63: 71–80

Morchain J. 2017. Numerical Tools for Scaling Up Bioreactors. In: Current Developments in Biotechnology and Bioengineering: Bioprocesses, Bioreactors and Controls. Larroche, C., Sanromán M. A., Du G., Pandey A. (eds.). Amsterdam, Elsevier B.V.: 495–523

Morimoto Y., Tan W.-H., Tsuda Y., Takeuchi S. 2009. Monodisperse Semi-Permeable Microcapsules for Continuous Observation of Cells. Lab on a Chip, 9, 15: 2217–2223

Moshaverinia A., Xu X., Chen C., Akiyama K., Snead M. L., Shi S. 2013. Dental Mesenchymal Stem Cells Encapsulated in an Alginate Hydrogel Co-Delivery Microencapsulation System for Cartilage Regeneration. Acta Biomaterialia, 9, 12: 9343–9350

Mukherjee T., Hanes J., Tews I., Ealick S. E., Begley T. P. 2011. Pyridoxal Phosphate: Biosynthesis and Catabolism. Biochimica et Biophysica Acta (BBA) - Proteins and Proteomics, 1814, 11: 1585–1596

Munirathinam R., Huskens J., Verboom W. 2015. Supported Catalysis in Continuous-Flow Microreactors. Advanced Synthesis and Catalysis, 357, 6: 1093–1123

Murakami S., Ohtaki K., Matsumoto S., Inoue T. 2012. Parallelization of Catalytic Packed-Bed Microchannels With Pressure-Drop Microstructures for Gas-Liquid Multiphase Reactions. Japanese Journal of Applied Physics, 51, 06FK11, doi: 10.1143/JJAP.51.06FK11: 2 p.

Mutti F. G., Fuchs C. S., Pressnitz D., Sattler J. H., Kroutil W. 2011. Stereoselectivity of Four (*R*)-Selective Transaminases for the Asymmetric Amination of Ketones. Advanced Synthesis and Catalysis, 353, 17: 3227–3233

Mutti F. G., Kroutil W. 2012. Asymmetric Bio-Amination of Ketones in Organic Solvents. Advanced Synthesis and Catalysis, 354, 18: 3409–3413

Nagel B., Dellweg H., Gierasch L. M. 1992. Glossary for Chemists of Terms Used in Biotechnology (IUPAC Recommendations 1992). In: Pure and Applied Chemistry, 64, 1: 143–168

Najafpour G. 2015. Biochemical Engineering and Biotechnology. 2nd ed. Amsterdam, Elsevier B.V.: 668 p.

NCBI. 2004. PubChem Compound Database. Bethesda, National Center for Biotechnology Information (database)
https://pubchem.ncbi.nlm.nih.gov/ (23rd February 2017)

Nedović V., Willaert, R. 2004. Fundamentals of Cell Immobilisation Biotechnology. Dordrecht, Springer Science+Business Media: 555 p.

Nelson J. M., Griffin E. G. 1916. Adsorption of Invertase. Journal of the American Chemical Society, 38, 5: 1109–1115

Nestl B. M., Hammer S. C., Nebel B. A., Hauer B. 2014. New Generation of Biocatalysts for Organic Synthesis. Angewandte Chemie - International Edition, 53, 12: 3070–3095

Neto W., Schürmann M., Panella L., Vogel A., Woodley J. M. 2015. Immobilisation of ω-Transaminase for Industrial Application: Screening and Characterisation of Commercial Ready to Use Enzyme Carriers. Journal of Molecular Catalysis B: Enzymatic, 117: 54–61

Nicoletti G., Cipolatti E. P., Valério A., Gamba Carbonera N. T., Spillere Soares N., Theilacker E., Ninow J. L., de Oliveira D. 2015. Evaluation of Different Methods for Immobilization of *Candida antarctica* Lipase B (CalB Lipase) in Polyurethane Foam and Its Application in the Production of Geranyl Propionate. Bioprocess and Biosystems Engineering, 38, 9: 1739–1748

Nielsen T. B., Ishii M., Kirk O. 1999. Lipases A and B from the Yeast *Candida antarctica*. In: Biotechnological Applications of Cold-Adapted Organisms. Margesin R., Schinner F. (eds.). Berlin Heidelberg, Springer-Verlag GmbH: 339 p.

NIH Guidelines. 2016. NIH Guidelines for Research Involving Recombinant or Synthetic Nucleic Acid Molecules. Bethesda, National Institutes of Health
http://osp.od.nih.gov/sites/default/files/NIH_Guidelines.html (23rd February, 2017)

Novak U., Lavric D., Žnidaršič-Plazl P. 2016. Continuous Lipase B-Catalyzed Isoamyl Acetate Synthesis in a Two-Liquid Phase System Using Corning® AFRTM Module Coupled With a Membrane Separator Enabling Biocatalyst Recycle. Journal of Flow Chemistry, 6, 1: 33–38

Novak U., Žnidaršič-Plazl P. 2013. Integrated Lipase-Catalyzed Isoamyl Acetate Synthesis in a Miniaturized System With Enzyme and Ionic Liquid Recycle. Green Processing and Synthesis, 2, 6: 561–568

Nunes M. A. P., Fernandes P. C. B., Ribeiro M. H. L. 2012. High-Affinity Water-Soluble System for Efficient Naringinase Immobilization in Polyvinyl Alcohol-Dimethyl Sulfoxide Lens-Shaped Particles. Journal of Molecular Recognition, 25, 11: 580–594

Nunes M. A. P., Rosa M. E., Fernandes P. C. B., Ribeiro M. H. L. 2014. Operational Stability of Naringinase PVA Lens-Shaped Microparticles in Batch Stirred Reactors and Mini Packed Bed Reactors-One Step Closer to Industry. Bioresource Technology, 164: 362–370

Obradovic B., Nedovic V. A., Bugarski B., Willaert R. G., Vunjak-Novakovic G. 2004. Immobilized Cell Bioreactors. In: Fundamentals of Cell Immobilisation Biotechnology. Nedović V., Willaert, R. (eds.). Dordrecht, Springer Science+Business Media: 411–436

Oliveira E. F., Cerqueira N. M. F. S. A., Fernandes P. A., Ramos M. J. 2011. Mechanism of Formation of the Internal Aldimine in Pyridoxal 5'-Phosphate-Dependent Enzymes. Journal of the American Chemical Society, 133, 39: 15496–15505

Onoe H., Inamori K., Takinoue M., Takeuchi S. 2014. Centrifuge-Based Cell Encapsulation in Hydrogel Microbeads Using Sub-Microliter Sample Solution. RSC Advances, 4, 58: 30480–30484

Ozahi E., Gundogdu M. Y., Carpinlioglu M. Ö. 2008. A Modification on Ergun's Correlation for Use in Cylindrical Packed Beds With Non-Spherical Particles. Advanced Powder Technology, 19, 4: 369–381

Özdural A. R., Alkan-Sungur A., Boyaci I. H., Webb C. 2008. Determination of Immobilized Enzyme Apparent Kinetic Parameters in Packed-Bed Reactors: Presentation of a New Methodology. Food and Bioproducts Processing, 86, 2: 104–108

Paiva A. L., van Rossum D., Malcata F. X. 2002. Kinetics of Lipase-Mediated Synthesis of Butyl Butyrate in *n*-Hexane. Biocatalysis and Biotransformation, 20, 1: 43–51

Päiviö M., Kanerva L. T. 2013. Reusable ω-Transaminase Sol–Gel Catalyst for the Preparation of Amine Enantiomers. Process Biochemistry, 48, 10: 1488–1494

Pang Y., Liu Z., Zhao F. 2016. Downstream Pressure and Elastic Wall Reflection of Droplet Flow in a T-junction Microchannel. Acta Mechanica Sinica, 32, 4: 579–587

Park E.-S., Dong J.-Y., Shin J.-S. 2013. ω-Transaminase-Catalyzed Asymmetric Synthesis of Unnatural Amino Acids Using Isopropylamine as an Amino Donor. Organic and Biomolecular Chemistry, 11, 40: 6929–6933

Park E.-S., Dong J.-Y., Shin J.-S. 2014. Active Site Model of (*R*)-Selective ω-Transaminase and Its Application to the Production of D-Amino Acids. Applied Microbiology and Biotechnology, 98, 2: 651–660

Park E.-S., Shin J.-S. 2013. ω-Transaminase from *Ochrobactrum anthropi* is Devoid of Substrate and Product Inhibitions. Applied and Environmental Microbiology, 79, 13: 4141–4144

Park E.-S., Shin J.-S. 2014. Deracemization of Amino Acids by Coupling Transaminases of Opposite Stereoselectivity. Advanced Synthesis and Catalysis, 356, 17: 3505–3509

Park H. J., Joo J. C., Park K., Kim Y. H., Yoo Y. J. 2013. Prediction of the Solvent Affecting Site and the Computational Design of Stable *Candida antarctica* Lipase B in a Hydrophilic Organic Solvent. Journal of Biotechnology, 163, 3: 346–352

Petera J., Nowicki L., Ledakowicz S. 2013. New Numerical Algorithm for Solving Multidimensional Heterogeneous Model of the Fixed Bed Reactor. Chemical Engineering Journal, 214: 237–246

Pleiss J., Fischer M., Schmid R. D. 1998. Anatomy of lipase binding sites: The Scissile Fatty Acid Binding Site. Chemistry and Physics of Lipids, 93, 1–2: 67–80

Pohar A., Belavič D., Dolanc G., Hočevar S. 2014. Modeling of Methanol Decomposition on $Pt/CeO_2/ZrO_2$ Catalyst in a Packed Bed Microreactor. Journal of Power Sources, 256: 80–87

Pohar A., Plazl I. 2009. Process Intensification Through Microreactor Application. Chemical and Biochemical Engineering Quarterly, 23, 4: 537–544

Pohar A., Plazl I., Žnidaršič-Plazl P. 2009. Lipase-Catalyzed Synthesis of Isoamyl Acetate in an Ionic Liquid/*n*-Heptane Two-Phase System at the Microreactor Scale. Lab on a Chip, 9, 23: 3385–3390

Pohar A., Žnidaršič-Plazl P., Plazl I. 2012. Integrated System of a Microbioreactor and a Miniaturized Continuous Separator for Enzyme Catalyzed Reactions. Chemical Engineering Journal, 189–190: 376–382

Polyanin A. D., Manzhirov A. V. 2007. Handbook of Mathematics for Engineers and Scientists. Boca Raton, Taylor & Francis Group: 1509 p.

Poojari Y., Clarson S. J. 2013. Thermal Stability of *Candida antarctica* Lipase B Immobilized on Macroporous Acrylic Resin Particles in Organic Media. Biocatalysis and Agricultural Biotechnology, 2, 1: 7–11

Prileszky T. A., Ogunnaike B. A., Furst E. M. 2016. Statistics of Droplet Sizes Generated by a Microfluidic Device. AIChE Journal, 62, 8: 2923–2928

Rathore S., Desai P. M., Liew C. V., Chan L. W., Heng P. W. S. 2013. Microencapsulation of Microbial Cells. Journal of Food Engineering, 116, 2: 369–381

Rebroš M., Rosenberg M., Mlichová Z., Krištofíková L. 2007. Hydrolysis of Sucrose by Invertase Entrapped in Polyvinyl Alcohol Hydrogel Capsules. Food Chemistry, 102, 3: 784–787

Reddy K. A., Doraiswamy L. K. 1967. Estimating Liquid Diffusivity, Industrial and Engineering Chemistry Fundamentals, 6, 1: 77–79

Rehn G., Adlercreutz P., Grey C. 2014. Supported Liquid Membrane as a Novel Tool for Driving the Equilibrium of ω-Transaminase Catalyzed Asymmetric Synthesis. Journal of Biotechnology, 179, 1: 50–55

Reis P., Holmberg K., Watzke H., Leser M. E., Miller R. 2009. Lipases at Interfaces: A Review. Advances in Colloid and Interface Science, 147–148: 237–250

Renken A., Kiwi-Minsker L. 2010. Microstructured Catalytic Reactors. In: Advances in Catalysis. Vol. 53. Gates B., Knözinger H., Jentoft F. (eds.). San Diego, Academic Press: 47–122

Ribeiro A. M., Neto P., Pinho C. 2010. Mean Porosity and Pressure Drop Measurements in Packed Beds of Monosized Spheres: Side Wall Effects. International Review of Chemical Engineering, 2, 1: 40–46

Ricci F., Amine A., Palleschi G., Moscone D. 2002. Prussian Blue Based Screen Printed Biosensors With Improved Characteristics of Long-Term Lifetime and pH Stability. Biosensors and Bioelectronics, 18, 2–3: 165–174

Ricci F., Amine A., Tuta C. S., Ciucu A. A., Lucarelli F., Palleschi G., Moscone D. 2003. Prussian Blue and Enzyme Bulk-Modified Screen-Printed Electrodes for Hydrogen Peroxide and Glucose Determination With Improved Storage and Operational Stability. Analytica Chimica Acta, 485, 1: 111–120

Riddle K. W., Mooney D. J. 2004. Biomaterials for Cell Immobilization. In: Fundamentals of Cell Immobilisation Biotechnology. Nedović V., Willaert, R. (eds.). Dordrecht, Springer Science+Business Media: 15–32

Roberge D. M., Gottsponer M., Eyholzer M., Kockmann N. 2009. Industrial Design, Scale-Up, and Use of Microreactors. Chimica Oggi, 27, 4: 8–11

Rong L. W., Dong K. J., Yu A. B. 2013. Lattice-Boltzmann Simulation of Fluid Flow Through Packed Beds of Uniform Spheres: Effect of Porosity. Chemical Engineering Science, 99: 44–58

Rosinha Grundtvig I. P., Daugaard A. E., Woodley J. M., Gernaey K. V., Krühne U. 2017. Shape Optimization as a Tool to Design Biocatalytic Microreactors, Chemical Engineering Journal, 322: 215–223

Roy B., Das T., Maiti T. K., Chakraborty S. 2011. Effect of Fluidic Transport on the Reaction Kinetics in Lectin Microarrays. Analytica Chimica Acta, 701, 1: 6–14

Saber M., Commenge J. M., Falk L. 2010. Microreactor Numbering-Up in Multi-Scale Networks for Industrial-Scale Applications: Impact of Flow Maldistribution on the Reactor Performances. Chemical Engineering Science, 65, 1: 372–379

Saha A. A., Mitra S. K., Tweedie M., Roy S., McLaughlin J. 2009. Experimental and Numerical Investigation Of Capillary Flow in SU8 and PDMS Microchannels With Integrated Pillars. Microfluidics and Nanofluidics, 7, 4: 451–465

Saunders P., Brask J. 2010. Improved Immobilization Supports for *Candida Antarctica* Lipase B. In: Biocatalysis in Polymer Chemistry. Loos K. (ed.). Weinheim, Wiley-VCH Verlag & Co. KGaA: 65–82

Šalić A., Pindrić K., Podrepšek G. H., Leitgeb M., Zelić B. 2013. NADH Oxidation in a Microreactor Catalyzed by ADH Immobilized on γ-Fe_2O_3 Nanoparticles. Green Processing and Synthesis, 2, 6: 569–578

Šalić A., Pindrić K., Podrepšek G. H., Novosel N., Leitgeb M., Zelić B. 2016. NADH Oxidation in a Microreactor With an Oscillating Magnetic Field. Journal of Flow Chemistry, 6, 1: 27–32

Šalić A., Tušek A., Kurtanjek Ž., Zelić B. 2011. Biotransformation in a Microreactor: New Method for Production of Hexanal. Biotechnology and Bioprocess Engineering, 16, 3: 495–504

Salihu A., Alam M. Z. 2015. Solvent Tolerant Lipases: A Review. Process Biochemistry, 50, 1: 86–96

Sangster J. 1989. Octanol-Water Partition Coefficients of Simple Organic Compounds. Journal of Physical and Chemical Reference Data, 18, 3: 1111–1229

Santos J. C., De Castro H. F. 2006. Optimization of Lipase-Catalyzed Synthesis of Butyl Butyrate Using a Factorial Design. World Journal of Microbiology and Biotechnology, 22, 10: 1007–1011

Scheibel E. G. 1954. Correspondence. Liquid Diffusivities. Viscosity of Gases. Industrial and Engineering Chemistry, 46, 9: 2007–2008

Schell U., Wohlgemuth R., Ward J. M. 2009. Synthesis of Pyridoxamine 5′-Phosphate Using an MBA:Pyruvate Transaminase as Biocatalyst. Journal of Molecular Catalysis B: Enzymatic, 59, 4: 279–285

Schenk R., Hessel V., Hofmann C., Kiss J., Löwe H., Ziogas A. 2004. Numbering-Up of Micro Devices: A First Liquid-Flow Splitting Unit. Chemical Engineering Journal, 101, 1–3: 421–429

Schenkmayerová, A., Bučko M., Gemeiner P., Trel'ová D., Lacík I., Chorvát D. Jr., Ačai P., Polakovič M., Lipták L., Rebroš M., Rosenberg M., Štefuca V., Neděla V., Tihlaříková E. 2014. Physical and Bioengineering Properties of Polyvinyl Alcohol Lens-Shaped Particles Versus Spherical Polyelectrolyte Complex Microcapsules as Immobilisation Matrices for a Whole-Cell Baeyer-Villiger Monooxygenase. Applied Biochemistry and Biotechnology, 174, 5: 1834–1849

Schilke K. F., Wilson K. L., Cantrell T., Corti G., McIlroy D. N., Kelly C. 2010. A Novel Enzymatic Microreactor With *Aspergillus oryzae* β-Galactosidase Immobilized on Silicon Dioxide Nanosprings. Biotechnology Progress, 26, 6: 1597–1605

Sen P., Nath A., Bhattacharjee C. 2017. Packed-Bed Bioreactor and Its Application in Dairy, Food, and Beverage Industry. In: Current Developments in Biotechnology and Bioengineering: Bioprocesses, Bioreactors and Controls. Larroche, C., Sanromán M. A., Du G., Pandey A. (eds.). Amsterdam, Elsevier B.V.: 235–277

Sen P., Nath A., Bhattacharjee C., Chowdhury R., Bhattacharya P. 2014. Process Engineering Studies of Free and Micro-Encapsulated β-Galactosidase in Batch and Packed Bed Bioreactors for Production of Galactooligosaccharides. Biochemical Engineering Journal, 90: 59–72

Seong G. H., Heo J., Crooks R. M. 2003. Measurement of Enzyme Kinetics Using a Continuous-Flow Microfluidic System. Analytical Chemistry, 75, 13: 3161–3167

Sezonov G., Joseleau-Petit D., D'Ari R. 2007. *Escherichia coli* Physiology in Luria-Bertani Broth. Journal of Bacteriology, 189, 23: 8746–8749

Sharma S., Kanwar S. S. 2014. Organic Solvent Tolerant Lipases and Applications. The Scientific World Journal, 2014, Article ID 625258, doi: http://dx.doi.org/10.1155/2014/625258: 15 p.

Sheldon R. A. 2007. Enzyme Immobilization: The Quest for Optimum Performance. Advanced Synthesis and Catalysis, 349, 8–9: 1289–1307

Sheldon R. A., Arends I., Hanefeld U. 2007. Green Chemistry and Catalysis. Weinheim, Wiley-VCH, Verlag GmbH & Co. KGaA: 433 p.

Sheldon R. A., van Pelt S. 2013. Enzyme Immobilisation in Biocatalysis: Why, What and How. Chemical Society Reviews, 42, 15: 6223–6235

Shin G., Mathew S., Shon M., Kim B.-G., Yun H. 2013. One-Pot One-Step Deracemization of Amines Using ω-Transaminases. Chemical Communications, 49, 77: 8629–8631

Shin G., Mathew S., Yun H. 2015. Kinetic Resolution of Amines by (*R*)-Selective Omega-Transaminase From *Mycobacterium vanbaalenii*. Journal of Industrial and Engineering Chemistry, 23: 128–133

Shin J.-S., Kim B.-G. 1997. Kinetic Resolution of *α*-Methylbenzylamine With ω-Transaminase Screened From Soil Microorganisms: Application of a Biphasic System to Overcome Product Inhibition. Biotechnology and Bioengineering, 55, 2: 348–358

Shin J.-S., Kim B.-G. 1998. Kinetic Modeling of ω-Transamination for Enzymatic Kinetic Resolution of *α*-Methylbenzylamine. Biotechnology and Bioengineering, 60, 5: 534–540

Shin J.-S., Kim B.-G. 1999a. Asymmetric Synthesis of Chiral Amines With ω-Transaminase. Biotechnology and Bioengineering, 65, 2: 206–211

Shin J.-S., Kim B.-G. 1999b. Modeling of the Kinetic Resolution of *α*-Methylbenzylamine With ω-Transaminase in a Two-Liquid-Phase System. Enzyme and Microbial Technology, 25, 3–5: 426–432

Shin J.-S., Kim B.-G., Liese A., Wandrey C. 2001a. Kinetic Resolution of Chiral Amines With ω-Transaminase Using an Enzyme-Membrane Reactor. Biotechnology and Bioengineering, 73, 3: 179–187

Shin J.-S., Kim B.-G., Shin D.-H. 2001b. Kinetic Resolution of Chiral Amines Using Packed-Bed Reactor. Enzyme and Microbial Technology, 29, 4–5: 232–239

Shintaku H., Kuwabara T., Kawano S., Suzuki T., Kanno I., Kotera H. 2007. Micro Cell Encapsulation and its Hydrogel-Beads Production Using Microfluidic Device. Microsystem Technologies, 13, 8–10: 951–958

Simon R. C., Richter N., Busto E., Kroutil W. 2014. Recent Developments of Cascade Reactions Involving ω-Transaminases. ACS Catalysis, 4, 1: 129–143

Singhal A., Cloete S., Radl S., Quinta-Ferreira R., Amini S. 2016. Heat Transfer to a Gas From Densely Packed Beds of Monodisperse Spherical Particles. Chemical Engineering Journal, 314: 27–37

Smallwood, I. M. 1996. Handbook of Organic Solvent Properties. London, Arnold: 306 p.

Smidsrød O., Skjåk-Bræk G. 1990. Alginate as Immobilization Matrix for Cells. Trends in Biotechnology, 8, 3: 71–78

Smithies K., Smith M. E. B., Kaulmann U., Galman J. L., Ward J. M., Hailes H. C. 2009. Stereoselectivity of an ω-Transaminase-Mediated Amination of 1,3-Dihydroxy-1-phenylpropane-2-one. Tetrahedron Asymmetry, 20, 5: 570–574

Soh G. Y., Yeoh G. H., Timchenko V. 2016. Numerical Investigation on the Velocity Fields During Droplet Formation in a Microfluidic T-junction. Chemical Engineering Science, 139: 99–108

SORS. 2016. Prices of Energy Sources, Slovenia, 1st quarter 2016. Statistical Office of the Republic of Slovenia http://www.stat.si/StatWeb/en/Field/Index/2/30 (25th December 2016)

Sotowa K.-I., Miyoshi R., Lee C.-G., Kang Y., Kusakabe K. 2005. Mixing and Enzyme Reactions in a Microchannel Packed With Glass Beads. Korean Journal of Chemical Engineering, 22, 4: 552–555

Stauch B., Fisher S. J., Cianci M. 2015. Open and Closed States of *Candida antarctica* Lipase B: Protonation and the Mechanism of Interfacial Activation. Journal of Lipid Research, 56, 12: 2348–2358

Stergiou P.-Y., Foukis A., Filippou M., Koukouritaki M., Parapouli M., Theodorou L. G., Hatziloukas E., Afendra A., Pandey A., Papamichael E. M. 2013. Advances in Lipase-Catalyzed Esterification Reactions. Biotechnology Advances, 31, 8: 1846–1859

Stirling D. I., Zeitlin A. L., Matcham G. W. 1990. Enantiomeric Enrichment and Stereoselective Synthesis of Chiral Amines. United States Patent application 4 950 606: 10 p.

Stojkovič G., Krivec M., Vesel A., Marinšek M., Žnidaršič-Plazl P. 2014. Surface Cell Immobilization Within Perfluoroalkoxy Microchannels. Applied Surface Science, 320: 810–817

Stojkovič G., Plazl I., Žnidaršič-Plazl P. 2011. L-Malic Acid Production Within a Microreactor With Surface Immobilized Fumarase. Microfluidics and Nanofluidics, 10, 3: 627–635

Stojkovič G., Žnidaršič-Plazl P. 2012. Continuous Synthesis of L-Malic Acid Using Whole-Cell Microreactor. Process Biochemistry, 47, 7: 1102–1107

Straathof A. J. J., Adlercreutz P. 2005. Applied Biocatalysis. 2nd ed. Amsterdam, Taylor & Francis e-Library: 533 p.

Studier F. W. 2005. Protein Production by Auto-Induction in High-Density Shaking Cultures. Protein Expression and Purification, 41, 1: 207–234

Su Y., Kuijpers K., Hessel V., Noël T. 2016. A Convenient Numbering-Up Strategy for the Scale-Up of Gas–Liquid Photoredox Catalysis in Flow. Reaction Chemistry and Engineering, 1, 1: 73–81

Su Y., Zhao Y., Chen G., Yuan Q. 2010. Liquid-Liquid Two-Phase Flow and Mass Transfer Characteristics in Packed Microchannels. Chemical Engineering Science, 65, 13: 3947–3956

Sugiura S., Oda T., Izumida Y., Aoyagi Y., Satake M., Ochiai A., Ohkohchi N., Nakajima M. 2005. Size Control of Calcium Alginate Beads Containing Living Cells Using Micro-Nozzle Array. Biomaterials, 26, 16: 3327–3331

Swarts J. W., Kolfschoten R. C., Jansen M. C. A. A., Janssen A. E. M., Boom R. M. 2010. Effect of Diffusion on Enzyme Activity in a Microreactor. Chemical Engineering Journal, 162, 1: 301–306

Tan W.-H., Takeuchi S. 2007. Monodisperse Alginate Hydrogel Microbeads for Cell Encapsulation. Advanced Materials, 19, 18: 2696–2701

Tang D., Jess A., Ren X., Bluemich B., Stapf S. 2004. Axial Dispersion and Wall Effects in Narrow Fixed Bed Reactors: A Comparative Study Based on RTD and NMR Measurements. Chemical Engineering and Technology, 27, 8: 866–873

Teh S.-Y., Lin R., Hung L.-H., Lee A. P. 2008. Droplet Microfluidics. Lab on a Chip, 8, 2: 198–220

Tendulkar S., Mirmalek-Sani S. H., Childers C., Saul J., Opara E. C., Ramasubramanian M. K. 2012. A Three-Dimensional Microfluidic Approach to Scaling Up Microencapsulation of Cells. Biomedical Microdevices, 14, 3: 461–469

Tepe O., Dursun A. Y. 2008. Combined Effects of External Mass Transfer and Biodegradation Rates on Removal of Phenol by Immobilized *Ralstonia eutropha* in a Packed Bed Reactor. Journal of Hazardous Materials, 151, 1: 9–16

Thorsen T., Roberts R. W., Arnold F. H., Quake S. R. 2001. Dynamic Pattern Formation in a Vesicle-Generating Microfluidic Device. Physical Review Letters, 86, 18: 4163–4166

Tibhe J. D., Fu H., Noël T., Wang Q., Meuldijk J., Hessel V. 2013. Flow Synthesis of Phenylserine Using Threonine Aldolase Immobilized on Eupergit Support. Beilstein Journal of Organic Chemistry, 9: 2168–2179

Tidona B., Desportes S., Altheimer M., Ninck K., von Rohr P. R. 2012. Liquid-to-Particle Mass Transfer in a Micro Packed Bed Reactor. International Journal of Heat and Mass Transfer, 55, 4: 522–530

Tišma M., Zelić B., Vasić-Rački Đ., Žnidaršič-Plazl P., Plazl I. 2009. Modelling of Laccase-Catalyzed L-DOPA Oxidation in a Microreactor. Chemical Engineering Journal, 149, 1–3: 383–388

Tomin A., Hornyánszky G., Kupai K., Dorkó Z., Ürge L., Darvas F., Poppe L. 2010. Lipase-Catalyzed Kinetic Resolution of 2-Methylene-Substituted Cycloalkanols in Batch and Continuous-Flow Modes. Process Biochemistry, 45, 6: 859–865

Toney M. D. 2005. Reaction Specificity in Pyridoxal Phosphate Enzymes. Archives of Biochemistry and Biophysics, 433, 1: 279–287

Tonkovich A. L. Y., Daymo E. A. 2009. Microreaction Systems for Large-Scale Production. In: Microchemical Engineering in Practice. Dietrich T. R. (ed.). Hoboken, John Wiley & Sons, Inc.: 299–323

Tonkovich A. L. Y., Kuhlmann D. J., Rogers A., Mcdaniel J. S., Fitzgerald S. P., Arora R., Yuschak T. D. 2005. Microchannel Technology Scale-Up to Commercial Capacity. Chemical Engineering Research and Design, 83, 6: 634–639

Trachsel F., Günther A., Khan S., Jensen K. F. 2005. Measurement of Residence Time Distribution in Microfluidic Systems. Chemical Engineering Science, 60, 21: 5729–5737

Tran D.-T., Lin Y.-J., Chen C.-L., Chang J.-S. 2014. Modeling the Methanolysis of Triglyceride Catalyzed by Immobilized Lipase in a Continuous-Flow Packed-Bed Reactor. Applied Energy, 126: 151–160

Trodler P., Pleiss J. 2008. Modeling Structure and Flexibility of *Candida antarctica* Lipase B in Organic Solvents. BMC Structural Biology, 8, 9, doi: 10.1186/1472-6807-8-9: 10 p.

Trubiano G., Borio D., Errazu A. 2006. Influence of the Operating Conditions and the External Mass Transfer Limitations on the Synthesis of Fatty Acid Esters Using a *Candida antarctica* Lipase. Enzyme and Microbial Technology, 40, 4: 716–722

Truppo M. D., Strotman H., Hughes G. 2012. Development of an Immobilized Transaminase Capable of Operating in Organic Solvent. ChemCatChem, 4, 8: 1071–1074

Tufvesson P., Bach C., Woodley J. M. 2014. A Model to Assess the Feasibility of Shifting Reaction Equilibrium by Acetone Removal in the Transamination of Ketones Using 2-Propylamine. Biotechnology and Bioengineering, 111, 2: 309–319

Tufvesson P., Fu W., Jensen J. S., Woodley J. M. 2010. Process Considerations for the Scale-Up and Implementation of Biocatalysis. Food and Bioproducts Processing, 88, 1: 3–11

Tufvesson P., Jensen J. S., Kroutil W., Woodley J. M. 2012. Experimental Determination of Thermodynamic Equilibrium in Biocatalytic Transamination. Biotechnology and Bioengineering, 109, 8: 2159–2162

Tufvesson P., Lima-Ramos J., Jensen J. S., Al-Haque N., Neto W., Woodley J. M. 2011. Process Considerations for the Asymmetric Synthesis of Chiral Amines Using Transaminases. Biotechnology and Bioengineering, 108, 7: 1479–1493

Tufvesson P., Nordblad M., Krühne U., Schürmann M., Vogel A., Wohlgemuth R., Woodley J. M. 2015. Economic Considerations for Selecting an Amine Donor in Biocatalytic Transamination. Organic Process Research and Development, 19, 6: 652–660

Um E., Lee D.-S., Pyo H.-B., Park J.-K. 2008. Continuous Generation of Hydrogel Beads and Encapsulation of Biological Materials Using a Microfluidic Droplet-Merging Channel. Microfluidics and Nanofluidics, 5, 4: 541–549

Uppenberg J., Hansen M. T., Patkar S., Jones T. A. 1994. The Sequence, Crystal Structure Determination and Refinement of Two Crystal Forms of Lipase B From *Candida antarctica*. Structure, 2, 4: 293–308

Uppenberg J., Ohrner N., Norin M., Hult K., Kleywegt G. J., Patkar S., Waagen V., Anthonsen T., Jones T. A. 1995. Crystallographic and Molecular-Modeling Studies of Lipase B from *Candida antarctica* Reveal a Stereospecificity Pocket for Secondary Alcohols. Biochemistry, 34, 51: 16838–16851

Valinger D., Vrsalović Presečki A., Kurtanjek Ž., Pohl M., Findrik Blažević Z., Vasić-Rački Đ. 2014. Continuous Enzymatic Carboligation of Benzaldehyde and Acetaldehyde in an Enzyme Ultrafiltration Membrane Reactor and Laminar Flow Microreactors. Journal of Molecular Catalysis B: Enzymatic, 102: 132–137

Van Daele T., Fernandes del Pozo D., Van Hauwermeiren D., Gernaey K. V., Wohlgemuth R., Nopens I. 2016. A Generic Model-Based Methodology for Quantification of Mass Transfer Limitations in Microreactors. Chemical Engineering Journal, 300: 193–208

Vasic-Racki D. 2006. History of Industrial Biotransformations – Dreams and Realities. In: Industrial Biotransformations. Liese A., Seelbach K., Wandrey C. (eds.). Weinheim, Verlag GmbH & Co. KGaA: 1–36

Veny H., Aroua M. K., Sulaiman N. M. N. 2014. Kinetic Study of Lipase Catalyzed Transesterification of Jatropha Oil in Circulated Batch Packed Bed Reactor. Chemical Engineering Journal, 237: 123–130

Voet D., Voet J. G. 2011. Biochemistry. 4th ed. Danvers, John Wiley & Sons Inc.: 1428 p.

Walter S., Malmberg S., Schmidt B., Liauw M. A. 2005. Mass Transfer Limitations in Microchannel Reactors. Catalysis Today, 110, 1–2: 15–25

Wan J. 2012. Microfluidic-Based Synthesis of Hydrogel Particles for Cell Microencapsulation and Cell-Based Drug Delivery. Polymers, 4, 2: 1084–1108

Wang D., Fan L.-S. 2013. Particle Characterization and Behavior Relevant to Fluidized Bed Combustion and Gasification Systems. In: Fluidized Bed Technologies for Near-Zero Emission Combustion and Gasification. Scala F. (ed.). Cambridge, Woodhead Publishing: 42–76

Wang H.-H., Shyr T.-W., Hu M.-S. 1999. The Elastic Property of Polyvinyl Alcohol Gel With Boric Acid as a Crosslinking Agent. Journal of Applied Polymer Science, 74, 13: 3046–3052

Wang J., Gu S.-S., Cui H.-S., Wu X.-Y., Wu F.-A. 2014. A Novel Continuous Flow Biosynthesis of Caffeic Acid Phenethyl Ester from Alkyl Caffeate and Phenethanol in a Packed Bed Microreactor. Bioresource Technology, 158: 39–47

Wang J., Gu S.-S., Cui H.-S., Yang L.-Q., Wu X.-Y. 2013. Rapid Synthesis of Propyl Caffeate in Ionic Liquid Using a Packed Bed Enzyme Microreactor Under Continuous-Flow Conditions. Bioresource Technology, 149: 367–374

Wang J.-T., Wang J., Han J.-J. 2011. Fabrication of Advanced Particles and Particle-Based Materials Assisted by Droplet-Based Microfluidics. Small, 7, 13: 1728–1754

Wang Q., Liu S., Wang H., Zhu J., Yang Y. 2015. Alginate Droplets Pre-Crosslinked in Microchannels to Prepare Monodispersed Spherical Microgels. Colloids and Surfaces A: Physicochemical and Engineering Aspects, 482: 371–377

Warmerdam A., Benjamins E., de Leeuw T. F., Broekhuis T. A., Boom R. M., Janssen A. E. M. 2014. Galacto-Oligosaccharide Production With Immobilized β-Galactosidase in a Packed-Bed Reactor vs. Free β-Galactosidase in a Batch Reactor. Food and Bioproducts Processing, 92, 4: 383–392

Warnock J.N., Bratch K., Al-Rubeai M. 2005. Packed Bed Bioreactors. In: Bioreactors for Tissue Engineering: Principles, Design and Operation. Chaudhuri J., Al-Rubeai M. (eds.). Dordrecht, Springer Science+Business Media: 87–113

Weber H. K., Stecher H., Faber K. 1995. Sensitivity of Microbial Lipases to Acetaldehyde Formed by Acyl-Transfer Reactions from Vinyl Esters. Biotechnology Letters, 17, 8: 803–808

Wegner J., Ceylan S., Kirschning A. 2011. Ten Key Issues in Modern Flow Chemistry. Chemical Communications, 47, 16: 4583–4592

Weuster-Botz D., Hekmat D., Puskeiler R., Franco-Lara E. 2007. Enabling Technologies: Fermentation and Downstream Processing. In: Advances in Biochemical Engineering/Biotechnology. Vol. 105. Ulber R., Sell D. (eds.). Berlin Heidelberg, Springer-Verlag: 205–247

Wiemann L. O., Nieguth R., Eckstein M., Naumann M., Thum O., Ansorge-Schumacher M. B. 2009a. Composite particles of Novozyme 435 and silicone: Advancing Technical Applicability of Macroporous Enzyme Carriers. ChemCatChem, 1, 4: 455–462

Wiemann L. O., Weisshaupt P., Nieguth R., Thum O., Ansorge-Schumacher M. B. 2009b. Enzyme Stabilization by Deposition of Silicone Coatings. Organic Process Research and Development, 13, 3: 617–620

Wiles C., Hammond M. J., Watts P. 2009. The Development and Evaluation of a Continuous Flow Process for the Lipase-Mediated Oxidation of Alkenes. Beilstein Journal of Organic Chemistry, 5, 27, doi: 10.3762/bjoc.5.27: 12 p.

Wilke C. R., Chang P. 1955. Correlation of Diffusion Coefficients in Dilute Solutions. AIChE Journal, 1, 2: 264–270

Willaert, R., Baron G. V., Nedović V. 2004. Diffusive Mass Transfer in Immobilized Cell Systems. In: Fundamentals of Cell Immobilisation Biotechnology. Nedović V., Willaert, R. (eds.). Dordrecht, Springer Science+Business Media: 359–387

Wirth, T. 2013. Microreactors in Organic Chemistry and Catalysis. 2nd ed. Weinheim, Wiley-VCH Verlag GmbH & Co. KGaA: 478 p.

Wittlich P., Capan E., Schlieker M., Vorlop K.-D., Jahnz U. 2004. Entrapment in LentiKats®. In: Fundamentals of Cell Immobilisation Biotechnology. Nedović V., Willaert, R. (eds.). Dordrecht, Springer Science+Business Media: 53–63

Wohlgemuth R. 2010. Biocatalysis-Key to Sustainable Industrial Chemistry. Current Opinion in Biotechnology, 21, 6: 713–724

Wohlgemuth R., Plazl I., Žnidaršič-Plazl P., Gernaey K. V., Woodley J. M. 2015. Microscale Technology and Biocatalytic Processes: Opportunities and Challenges for Synthesis. Trends in Biotechnology, 33, 5: 302–314

Woitalka A., Kuhn S., Jensen K. F. 2014. Scalability of Mass Transfer in Liquid-Liquid Flow. Chemical Engineering Science, 116: 1–8

Woodcock L. L., Wiles C., Greenway G. M., Watts P., Wells A., Eyley S. 2008. Enzymatic Synthesis of a Series of Alkyl Esters Using Novozyme 435 in a Packed-Bed, Miniaturized, Continuous Flow Reactor. Biocatalysis and Biotransformation, 26, 6: 466–472

Workman V. L., Dunnett S. B., Kille P., Palmer D. 2007. Microfluidic Chip-Based Synthesis of Alginate Microspheres for Encapsulation of Immortalized Human Cells. Biomicrofluidics, 1, 1, 014105, doi: 10.1063/1.2431860: 9 p.

Workman V. L., Dunnett S. B., Kille P., Palmer D. D. 2008. On-Chip Alginate Microencapsulation of Functional Cells. Macromolecular Rapid Communications, 29, 2: 165–170

Wu M.-H., Pan W.-C. 2010. Development of Microfluidic Alginate Microbead Generator Tunable by Pulsed Airflow Injection for the Microencapsulation of Cells. Microfluidics and Nanofluidics, 8, 6: 823–835

Xu J. H., Li S. W., Tan J., Luo G. S. 2008. Controllable Preparation of Monodispersed Calcium Alginate Microbeads in a Novel Microfluidic System. Chemical Engineering and Technology, 31, 8: 1223–1226

Xu J. H., Li S. W., Tan J., Wang Y. J., Luo G. S. 2006a. Controllable Preparation of Monodisperse O/W and W/O Emulsions in the Same Microfluidic Device. Langmuir, 22, 19: 7943–7946

Xu J. H., Luo G. S., Li S. W., Chen G. G. 2006b. Shear Force Induced Monodisperse Droplet Formation in a Microfluidic Device by Controlling Wetting Properties. Lab on a Chip, 6, 1: 131–136

Xu S., Nie Z., Seo M., Lewis P., Kumacheva E., Stone H. A., Garstecki P., Weibel D. B., Gitlin I., Whitesides G. M. 2005. Generation of Monodisperse Particles by Using Microfluidics: Control Over Size, Shape, and Composition. Angewandte Chemie - International Edition, 44, 5: 724–728

Yadav G. D., Devendran S. 2012. Lipase Catalyzed Synthesis of Cinnamyl Acetate via Transesterification in Non-Aqueous Medium. Process Biochemistry, 47, 3: 496–502

Yagodnitsyna A. A., Kovalev A. V., Bilsky A. V. 2016. Flow Patterns of Immiscible Liquid-Liquid Flow in a Rectangular Microchannel With T-junction. Chemical Engineering Journal, 303: 547–554

Yang H., Zhou Q., Fan L.-S. 2013. Three-Dimensional Numerical Study on Droplet Formation and Cell Encapsulation Process in a Micro T-junction. Chemical Engineering Science, 87: 100–110

Yeh C.-H., Chen Y.-C., Lin Y.-C. 2011. Generation of Droplets With Different Concentrations Using Gradient-Microfluidic Droplet Generator. Microfluidics and Nanofluidics, 11, 3: 245–253

Yeh C.-H., Zhao Q., Lee S.-J., Lin Y.-C. 2009. Using a T-junction Microfluidic Chip for Monodisperse Calcium Alginate Microparticles and Encapsulation Of Nanoparticles. Sensors and Actuators A: Physical, 151, 2: 231–236

Yeh W.-K., Yang H.-C., McCarthy. 2010. Enzyme technologies: Metagenomics, Evolution, Biocatalysis, and Biosynthesis. New Jersey, John Wiley & Sons, Inc.: 368 p.

Yi S.-S., Lee C.-won, Kim J., Kyung D., Kim B.-G., Lee Y.-S. 2007. Covalent Immobilization of ω-Transaminase from *Vibrio fluvialis* JS17 on Chitosan Beads. Process Biochemistry, 42, 5: 895–898

Yu L., Chen M. C. W., Cheung K. C. 2010. Droplet-Based Microfluidic System for Multicellular Tumor Spheroid Formation and Anticancer Drug Testing. Lab on a Chip, 10, 18: 2424–2432

Zamora-Mora V., Velasco D., Hernández R., Mijangos C., Kumacheva E. 2014. Chitosan/Agarose Hydrogels: Cooperative Properties and Microfluidic Preparation. Carbohydrate Polymers, 111: 348–355

Zhang H., Tumarkin E., Peerani R., Nie Z., Sullan R. M. A., Walker G. C., Kumacheva E. 2006. Microfluidic Production of Biopolymer Microcapsules With Controlled Morphology. Journal of the American Chemical Society, 128, 37: 12205–12210

Zhang H., Tumarkin E., Sullan R. M. A., Walker G. C., Kumacheva E. 2007. Exploring Microfluidic Routes to Microgels of Biological Polymers. Macromolecular Rapid Communications, 28, 5: 527–538

Zhao C.-X., Middelberg A. P. J. 2011. Two-Phase Microfluidic Flows. Chemical Engineering Science, 66, 7: 1394–1411

Zisis T., Freddolino P. L., Turunen P., van Teeseling M. C. F., Rowan A. E., Blank K. G. 2015. Interfacial Activation of *Candida antarctica* Lipase B: Combined Evidence from Experiment and Simulation. Biochemistry, 54, 38: 5969–5979

Zlokarnik M. 2006. Scale-Up in Chemical Engineering. 2nd ed. Weinheim, Wiley-VCH Verlag GmbH & Co. KGaA: 271 p.

Žnidaršič-Plazl P. 2014. Enzymatic Microreactors Utilizing Non-Aqueous Media. Chimica Oggi, 32, 1: 54–60

Žnidaršič-Plazl P., Plazl I. 2009. Modelling and Experimental Studies on Lipase-Catalyzed Isoamyl Acetate Synthesis in a Microreactor. Process Biochemistry, 44, 10: 1115–1121

Žnidaršič-Plazl P., Plazl I. 2011. Microbioreactors. In: Comprehensive Biotechnology. Moo-Young M. (ed.). 2nd ed. Amsterdam, Elsevier B.V.: 289–301

ACKNOWLEDGEMENTS

Foremost, I would like to express sincere and warm gratefulness to my mentor Prof. Dr. Polona Žnidaršič Plazl for giving me a great opportunity for the cooperation over the past three and a half years. Her personal, professional and scientific support as well as immense knowledge and patience were of immeasurable importance on the way to the success.

I would also like to express my deepest personal appreciation to all people who gave their contribution and enormous added value to this work, each one by its own way. A special thanks to Prof. Dr. Igor Plazl for a bunch of great ideas and valuable scientific discussions. My warmest gratitude to Anže Belovič, Uroš Novak, Anja Pajntar, Martin Lubej, Nataša Miložič and Mojca Seručnik for their generous help in the experimental work, friendship and great moments we spent together. Peter Panjan, Borut Pečar and Danilo Vrtačnik are acknowledged for an outstanding cooperation as well as for providing sensors used in the experimental work. All colleagues from the Chair of Chemical Process, Environmental and Biochemical Engineering (Faculty of Chemistry and Chemical Technology, University of Ljubljana) are gratefully acknowledged for the enjoyable time during my research work.

The financial support provided by the Slovene Human Resources Development and Scholarship Fund (Grant No. 11011–73/2013) is greatly acknowledged.

The enzyme ATA-wt was kindly provided by c-LEcta (Leipzig, Germany), and immobilized by LentiKat's a.s. (Stráž pod Ralskem, Czech Republic), whereby the special gratitude is devoted to Radek Stloukal. Preparation Novozym® 435 and adhesive tape ARcare® 90445 were kindly donated by Novozymes A/S (Bagsværd, Denmark) and Adhesives Research Inc. (Glen Rock, USA), respectively. The EU FP7 Projects BIOINTENSE – Mastering Bioprocess Integration and Intensification Across Scales and EUROMBR – European Network for Innovative Microbioreactor Applications in Bioprocess Development are gratefully acknowledged as well.

The last but not least, a special thanks to my beloved family and friends for being endlessly supportive and encouraging on the way towards the aim.

ANNEX A

Proposed mathematical model for a miniaturized packed bed reactor with LentiKats®

A 3D mathematical model for an MPBR with equally-sized and uniformly packed LentiKats® (in one row and one layer) used for the ω-TA-catalyzed synthesis of ACP is proposed here. The model has been established as a continuum-based heterogeneous model, that is to say the physical domain is separated into two parts: the fluid phase comprising convective and diffusive transport of species around the particle in all spatial directions along with velocity profile (domain 1), and hydrogel phase (domain 2) comprising only diffusive transport occurring in all spatial dimensions as well (Supplementary Figure 1).

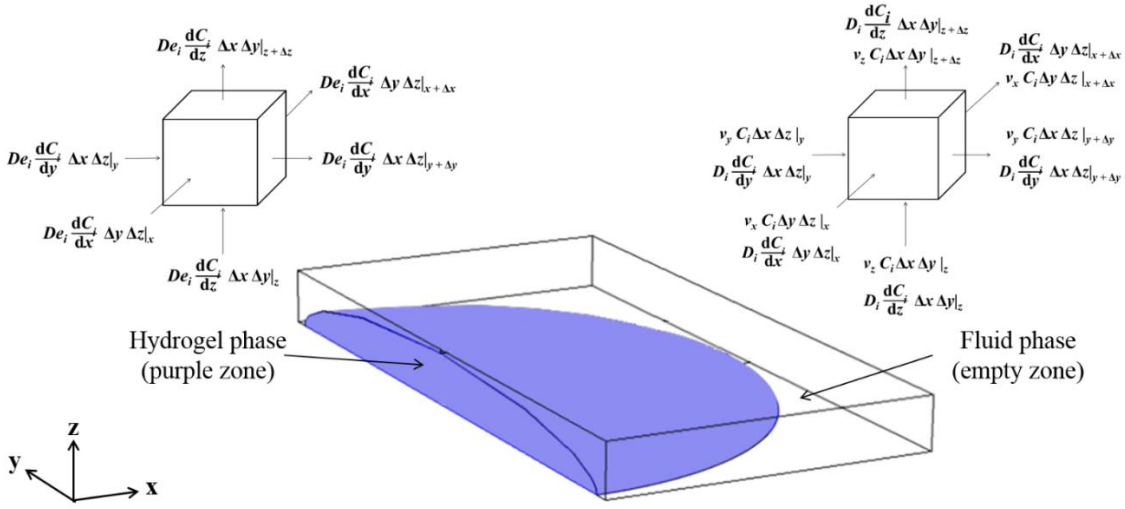

Supplementary Figure 1: An intersection of the lens-shaped particle packed in a rectangular channel with appropriate macroscopic mass balance equations for both physical domains.

Dopolnilna slika 1: Presečišče delca v obliki leče pakiranega v pravokotni kanal z ustreznimi makroskopskimi enačbami za masne bilance v obeh fizičnih domenah.

The developed model equations are based on several assumptions. Firstly, the process is isothermal and operates under the steady state conditions. Secondly, diffusion in the hydrogel (Supplementary Figure 1) can be described using the constant effective diffusivities of the reacting species. And thirdly, the reaction takes place in the hydrogel where a uniform distribution of enzymes is assumed. Taking this into account, the continuum-based macroscopic mass balance equations for all reacting species at steady state conditions were derived for domain 1 (Supplementary Equations 1 to 4) and domain 2 (Supplementary Equations 5 to 8). The Supplementary Equations from 1 to 8 were derived as explained below in the text.

$$\vec{v}\,\nabla C_{MBA} + D_{MBA}\,\nabla^2 C_{MBA} = 0 \quad \ldots (1)$$

$$\vec{v}\,\nabla C_{PYR} + D_{PYR}\,\nabla^2 C_{PYR} = 0 \quad \ldots (2)$$

$$\vec{v}\,\nabla C_{ACP} + D_{ACP}\,\nabla^2 C_{ACP} = 0 \quad \ldots (3)$$

$$\vec{v}\,\nabla C_{ALA} + D_{ALA}\,\nabla^2 C_{ALA} = 0 \quad \ldots (4)$$

$$D_{eMBA}\,\nabla^2 C_{MBA} = -r_a \quad \ldots (5)$$

$$D_{ePYR}\,\nabla^2 C_{PYR} = -r_a \quad \ldots (6)$$

$$D_{eACP}\,\nabla^2 C_{ACP} = r_a \quad \ldots (7)$$

$$D_{eALA}\,\nabla^2 C_{ALA} = r_a \quad \ldots (8)$$

$\vec{v}$	*velocity vector [m s^{-1}]*
C_{MBA}	*concentration of (S)-(–)-α-methylbenzylamine [mol m^{-3}]*
C_{PYR}	*concentration of pyruvate [mol m^{-3}]*
C_{ACP}	*concentration of acetophenone [mol m^{-3}]*
C_{ALA}	*concentration of L-alanine [mol m^{-3}]*
D_{MBA}	*diffusion coefficient of (S)-(–)-α-methylbenzylamine in water [m^2 s^{-1}]*
D_{eMBA}	*effective diffusion coefficient of (S)-(–)-α-methylbenzylamine in LentiKats® [m^2 s^{-1}]*
D_{PYR}	*diffusion coefficient of pyruvate in water [m^2 s^{-1}]*
D_{ePYR}	*effective diffusion coefficient of pyruvate in LentiKats® [m^2 s^{-1}]*
D_{ACP}	*diffusion coefficient of acetophenone in water [m^2 s^{-1}]*
D_{eACP}	*effective diffusion coefficient of acetophenone in LentiKats® [m^2 s^{-1}]*
D_{ALA}	*diffusion coefficient of L-alanine in water [m^2 s^{-1}]*
D_{eALA}	*effective diffusion coefficient of L-alanine in LentiKats® [m^2 s^{-1}]*
r_a	*reaction rate [mol m^{-3} s^{-1}]*

The physical domains are coupled over the interfacial surface using interdependent boundary conditions. The continuity of flux by diffusion normal to the interfacial surface was used as a boundary condition at one side of the interface (Supplementary Equations 9 to 12), while the equality of concentrations of reacting species in both phases was assumed to be a boundary condition at another side of the interface. The boundary conditions at all other surfaces of domains are described by zero concentration gradients.

$$-\vec{n} \cdot \vec{N}_{MBA,1} = -\vec{n} \cdot \vec{N}_{MBA,2} \quad \ldots (9)$$

$$-\vec{n} \cdot \vec{N}_{PYR,1} = -\vec{n} \cdot \vec{N}_{PYR,2} \quad \ldots (10)$$

$$-\vec{n} \cdot \vec{N}_{ACP,1} = -\vec{n} \cdot \vec{N}_{ACP,2} \quad \ldots (11)$$

$$-\vec{n} \cdot \vec{N}_{ALA,1} = -\vec{n} \cdot \vec{N}_{ALA,2} \quad \ldots (12)$$

$$C_{MBA,1} = C_{MBA,2} \quad \ldots (13)$$

$$C_{PYR,1} = C_{PYR,2} \quad \ldots (14)$$

$$C_{ACP,1} = C_{ACP,2} \quad \ldots (15)$$

$$C_{ALA,1} = C_{ALA,2} \quad \ldots (16)$$

$\vec{n}$ *flux vector normal to the interfacial surface [–]*

$\vec{N}_{MBA}$ *molar flux of (S)-(–)-α-methylbenzylamin normal to the interfacial surface [mol m^{-2} s^{-1}]*

$\vec{N}_{PYR}$ *molar flux of pyruvate normal to the interfacial surface [mol m^{-2} s^{-1}]*

$\vec{N}_{ACP}$ *molar flux of acetophenone normal to the interfacial surface [mol m^{-2} s^{-1}]*

$\vec{N}_{ALA}$ *molar flux of L-alanine normal to the interfacial surface [mol m^{-2} s^{-1}]*

The enzymatic transamination reaction is a second-order reversible reaction that follows a ping-pong bi-bi reaction mechanism, and hence the reaction rate term (r_a) can be obtained as discussed in the theoretical part.

A simultaneous numerical solution of the given differential equations (Supplementary Equations 1 to 8) with the associated boundary conditions (Supplementary Equations 9 to 16) could be performed using an appropriate numerical method. The fluid flow velocity profile in domain 1 could be obtained by solving the well-known Navier-Stokes equations, and considering no-slip boundary conditions at the particle surface and at the walls of the channel. This task may be done using some of the best-known computational fluid dynamics tools such as MATLAB®, COMSOL Multiphysics®, OpenFOAM®, simFlow®, etc.

1. Differential mass balance in the fluid phase physical domain

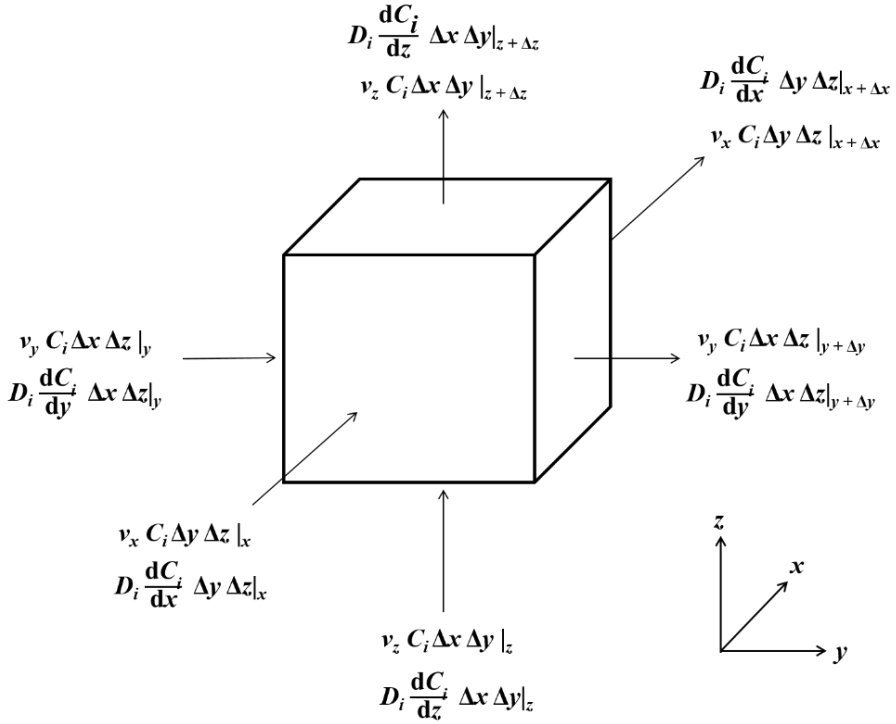

Supplementary Figure 2: A differential element from the fluid phase.
Dopolnilna slika 2: Diferencialni element iz tekoče faze.

$$v_x C_i \Delta y \Delta z|_x - v_x C_i \Delta y \Delta z|_{x+\Delta x} + v_y C_i \Delta x \Delta z|_y - v_y C_i \Delta x \Delta z|_{y+\Delta y} + v_z C_i \Delta x \Delta y|_z -$$

$$- v_z C_i \Delta x \Delta y|_{z+\Delta z} + D_i \frac{dC_i}{dx} \Delta y \Delta z|_x - D_i \frac{dC_i}{dx} \Delta y \Delta z|_{x+\Delta x} + D_i \frac{dC_i}{dy} \Delta x \Delta z|_y - D_i \frac{dC_i}{dy} \Delta x \Delta z|_{y+\Delta y}$$

$$+ D_i \frac{dC_i}{dz} \Delta x \Delta y|_z - D_i \frac{dC_i}{dz} \Delta x \Delta y|_{z+\Delta z} = 0$$

Dividing the whole equation by $\Delta x \Delta y \Delta z$ we get:

$$\frac{v_x C_i|_x - v_x C_i|_{x+\Delta x}}{\Delta x} + \frac{v_y C_i|_y - v_y C_i|_{y+\Delta y}}{\Delta y} + \frac{v_z C_i|_z - v_z C_i|_{z+\Delta z}}{\Delta z} + \frac{D_i \frac{dC_i}{dx}|_x - D_i \frac{dC_i}{dx}|_{x+\Delta x}}{\Delta x} +$$

$$+ \frac{D_i \frac{dC_i}{dy}|_y - D_i \frac{dC_i}{dy}|_{y+\Delta y}}{\Delta y} + \frac{D_i \frac{dC_i}{dz}|_z - D_i \frac{dC_i}{dz}|_{z+\Delta z}}{\Delta z} = 0$$

To develop an equation that stands to any point, we take the limit by shrinking Δx, Δy and Δz to zero:

$$\lim_{\Delta x \to 0} \frac{v_x C_i|_x - v_x C_i|_{x+\Delta x}}{\Delta x} + \lim_{\Delta y \to 0} \frac{v_y C_i|_y - v_y C_i|_{y+\Delta y}}{\Delta y} + \lim_{\Delta z \to 0} \frac{v_z C_i|_z - v_z C_i|_{z+\Delta z}}{\Delta z} +$$

$$+ \lim_{\Delta x \to 0} \frac{D_i \frac{\mathrm{d}C_i}{\mathrm{d}x}|_x - D_i \frac{\mathrm{d}C_i}{\mathrm{d}x}|_{x+\Delta x}}{\Delta x} + \lim_{\Delta y \to 0} \frac{D_i \frac{\mathrm{d}C_i}{\mathrm{d}y}|_y - D_i \frac{\mathrm{d}C_i}{\mathrm{d}y}|_{y+\Delta y}}{\Delta y} + \lim_{\Delta z \to 0} \frac{D_i \frac{\mathrm{d}C_i}{\mathrm{d}z}|_z - D_i \frac{\mathrm{d}C_i}{\mathrm{d}z}|_{z+\Delta z}}{\Delta z} = 0$$

to get:

$$v_x \frac{\mathrm{d}C_i}{\mathrm{d}x} + v_y \frac{\mathrm{d}C_i}{\mathrm{d}y} + v_z \frac{\mathrm{d}C_i}{\mathrm{d}z} + D_i \frac{\mathrm{d}}{\mathrm{d}x}\left(\frac{\mathrm{d}C_i}{\mathrm{d}x}\right) + D_i \frac{\mathrm{d}}{\mathrm{d}y}\left(\frac{\mathrm{d}C_i}{\mathrm{d}y}\right) + D_i \frac{\mathrm{d}}{\mathrm{d}z}\left(\frac{\mathrm{d}C_i}{\mathrm{d}z}\right) = 0$$

The final equation is:

$$\vec{v} \nabla C_i + D_i \nabla^2 C_i = 0$$

where C_i and D_i denote concentrations and diffusivities in aqueous solution of reacting species (*S*)-(–)-*α*-methylbenzylamine, sodium pyruvate, acetophenone and L-alanine, respectively.

2. Differential mass balance in the hydrogel phase physical domain

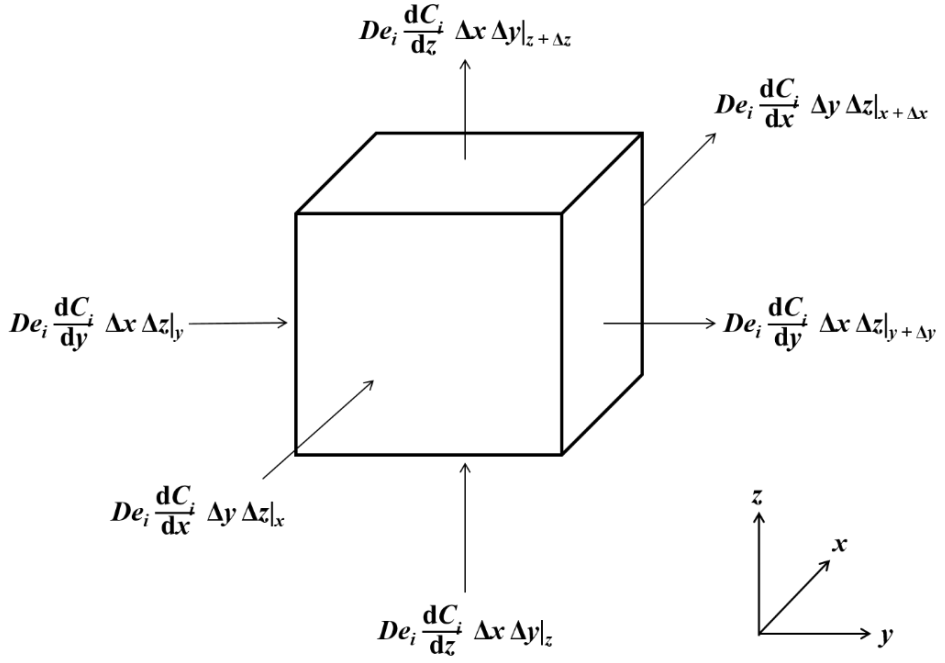

Supplementary Figure 3: A differential element from the hydrogel phase.
Dopolnilna slika 3: Diferencialni element iz hidrogela.

$$D_{ei} \frac{dC_i}{dx} \Delta y \, \Delta z \,|_x - D_{ei} \frac{dC_i}{dx} \Delta y \, \Delta z \,|_{x+\Delta x} + D_{ei} \frac{dC_i}{dy} \Delta x \, \Delta z \,|_y - D_{ei} \frac{dC_i}{dy} \Delta x \, \Delta z \,|_{y+\Delta y} + D_{ei} \frac{dC_i}{dz} \Delta x \, \Delta y \,|_z -$$

$$- D_{ei} \frac{dC_i}{dz} \Delta x \, \Delta y \,|_{z+\Delta z} - r_a \, \Delta x \, \Delta y \, \Delta z = 0$$

Dividing the whole equation by $\Delta x \, \Delta y \, \Delta z$ we get:

$$\frac{D_{ei} \frac{dC_i}{dx}|_x - D_{ei} \frac{dC_i}{dx}|_{x+\Delta x}}{\Delta x} + \frac{D_{ei} \frac{dC_i}{dy}|_y - D_{ei} \frac{dC_i}{dy}|_{y+\Delta y}}{\Delta y} + \frac{D_{ei} \frac{dC_i}{dz}|_z - D_{ei} \frac{dC_i}{dz}|_{z+\Delta z}}{\Delta z} = r_a$$

To develop an equation that stands to any point, we take the limit by shrinking Δx, Δy and Δz to zero:

$$\lim_{\Delta x \to 0} \frac{D_{ei} \frac{\mathrm{d}C_i}{\mathrm{d}x}|_x - D_{ei} \frac{\mathrm{d}C_i}{\mathrm{d}x}|_{x+\Delta x}}{\Delta x} + \lim_{\Delta y \to 0} \frac{D_{ei} \frac{\mathrm{d}C_i}{\mathrm{d}y}|_y - D_{ei} \frac{\mathrm{d}C_i}{\mathrm{d}y}|_{y+\Delta y}}{\Delta y} +$$

$$+ \lim_{\Delta z \to 0} \frac{D_{ei} \frac{\mathrm{d}C_i}{\mathrm{d}z}|_z - D_{ei} \frac{\mathrm{d}C_i}{\mathrm{d}z}|_{z+\Delta z}}{\Delta z} = r_a$$

to get:

$$D_{ei} \frac{\mathrm{d}}{\mathrm{d}x}\left(\frac{\mathrm{d}C_i}{\mathrm{d}x}\right) + D_{ei} \frac{\mathrm{d}}{\mathrm{d}y}\left(\frac{\mathrm{d}C_i}{\mathrm{d}y}\right) + D_{ei} \frac{\mathrm{d}}{\mathrm{d}z}\left(\frac{\mathrm{d}C_i}{\mathrm{d}z}\right) = r_a$$

The final equation is:

$$D_{ei} \nabla^2 C_i = r_a$$

where C_i an D_{ei} denote concentrations and effective diffusivities in hydrogel of reacting species (*S*)-(–)-*α*-methylbenzylamine, sodium pyruvate, acetophenone and L-alanine, respectively.

ANNEX B

Chemical compounds with corresponding molecular formulas and PubChem CID numbers

Compound	*Molecular formula*	*Molecular weight [g mol^{-1}]*	*PubChem CID*
Acetonitrile	C_2H_3N	41.053	6342
Acetophenone	C_8H_8O	120.151	7410
Ammonium chloride	NH_4Cl	53.489	25517
Butyl butyrate	$C_8H_{16}O_2$	144.214	7983
Calcium acetate	$C_4H_6CaO_4$	158.166	6116
Calcium chloride	$CaCl_2$	110.978	5284359
Glucose	$C_6H_{12}O_6$	180.156	79025
Glycerol	$C_3H_8O_3$	92.094	753
Hydrochloric acid	HCl	36.458	313
β-D-1-thiogalactopyranoside	$C_9H_{18}O_5S$	238.298	656894
Kanamycin sulfate	$C_{18}H_{38}N_4O_{15}S$	582.575	32943
L-alanine	$C_3H_7NO_2$	89.094	5950
Magnesium sulfate	$MgSO_4$	120.361	24083
n-heptane	C_7H_{16}	100.205	8900
Potassium phosphate monobasic	KH_2PO_4	136.084	516951
Pyridoxal-5'-phosphate	$C_8H_{10}NO_6P$	247.143	1051
Sodium hydroxide	NaOH	39.997	14798
Sodium phosphate dibasic	Na_2HPO_4	141.957	24203
Sodium phosphate monobasic	NaH_2PO_4	119.976	23672064
Sodium pyruvate	$C_3H_3NaO_3$	110.044	23662274
Sodium sulfate	Na_2SO_4	142.036	24436
Tris(hydroxymethyl)aminomethane	$C_4H_{11}NO_3$	121.136	6503
Vinyl butyrate	$C_6H_{10}O_2$	114.144	31247
(*S*)-α-methylbenzylamine	$C_8H_{11}N$	121.183	7408
1-butanol	$C_4H_{10}O$	74.123	263